TAMPEREEN TEKNILLINEN YLIOPISTO
TAMPERE UNIVERSITY OF TECHNOLOGY
Julkaisu 605 • Publication 605

Olli Kerokoski

Soil-Structure Interaction of Long Jointless Bridges with Integral Abutments

Tampere 2006

Tampereen teknillinen yliopisto. Julkaisu 605
Tampere University of Technology. Publication 605

Olli Kerokoski

Soil-Structure Interaction of Long Jointless Bridges with Integral Abutments

Thesis for the degree of Doctor of Technology to be presented with due permission for public examination and criticism in Rakennustalo Building, Auditorium RG202, at Tampere University of Technology, on the 25th of August 2006, at 12 noon.

Tampereen teknillinen yliopisto - Tampere University of Technology
Tampere 2006

Supervisor (until 31.7.2005):

Professor, Dr. Tech. Jorma Hartikainen
Institute of Earth and Foundation Structures
Tampere University of Technology
Tampere, Finland

Supervisor (from 1.8.2005) and Custos:

Professor, Dr. Ing. Tim Länsivaara
Institute of Earth and Foundation Structures
Tampere University of Technology
Tampere, Finland

Preliminary assessors:

Professor / Bridge Manager, Dr. Tech. Peter Collin
Ramboll Ltd
Luleå, Sweden

Dr. Tech. Mauri Koskinen
VR-Track Ltd
Helsinki, Finland

Professor, Lic. Tech. Olli Ravaska
Laboratory of Soil Mechanics and Foundation Engineering
Helsinki University of Technology
Espoo, Finland

Opponents:

Dr. Tech. Vesa Järvinen
A-Insinöörit Oy
Tampere, Finland

Professor, Lic. Tech. Olli Ravaska
Laboratory of Soil Mechanics and Foundation Engineering
Helsinki University of Technology
Espoo, Finland

ISBN 952-15-1620-8 (printed)
ISBN 952-15-1830-8 (PDF)
ISSN 1459-2045

Tampere University of Technology
Publication 605

Olli Kerokoski:
Soil-Structure Interaction of Long Jointless Bridges with Integral Abutments

ERRATA 23.8.2006

Page 66:
… cell) increased 0.59 kN/m^2 while the deck moved 0.55 mm against the embankment. =>
… cell) decreased 0.59 kN/m^2 while the deck moved 0.55 mm against the opposite embankment.

Page 132:
Kerokoski, Olli. 2005 a. Soil–structure interaction of jointless bridges. Literarture research. =>
Kerokoski, Olli. 2005 a. Soil–structure interaction of jointless bridges. Literature research.

Page 133:
Kerokoski, Olli. 2005 c. Soil–… railway bridges. Literature search. =>
Kerokoski, Olli. 2005 c. Soil–… railway bridges. Literature research.

In decimal numbers dot (.) instead of comma (,) in figures 4.7, 4.12, 4.14, 4.32, 4.40 – 4.43, 5.2, 5.5 – 5.8, 5.12, 5.13, 5.18, 6.10, 7.5, 7.7 and in equations in page 67 (0.366) and in appendix 3.

ERRATA 28.8.2006

Page 12: Reference in Table 2.2: (Finnra 1999a). Reference in the paragraph just below Table 2.2: (Finnra 2002).

Page 45 and 109: In figures 4.30 and 7.6 the bottom of pier pile should be fixed also in horizontal direction.

Page 67: Please, ignore text and equations below title: ‘Longitudinal track stiffness’ and see the revised reference (Laaksonen 2005, version after 25.8.2006).

Page 108: unit 1/t => 1/h , unit mm/t => mm/h , unit t => h (time in hours (or in seconds)).

ABSTRACT

More than 1000 jointless bridges have been built in Finland during recent decades. The maximum length of a symmetrical road bridge has been 70 meters, that is, 35 m + 35 m from the centre of thermal movements.

Integral abutment bridges are best suited for locations providing enough space to build a sufficiently long deck with a low-gradient slope where the embankment is stable and its settlements are small.

As a wall supporting earth moves horizontally towards the earth, earth pressure increases non-linearly from at-rest pressure to the ultimate pressure called passive earth pressure. The horizontal displacements presented in research reports and design manuals required to create passive earth pressure vary considerably. Generally it is estimated that a relative displacement magnitude of 0.005–0.050 times H is adequate, where H is the height of the wall. In Finland passive earth pressure on an integral abutment is estimated to be mobilised by just a small abutment displacement.

In the presented empirical study, the main subjects of interest were: earth pressures after cyclic abutment displacements, behaviour of pavement near the abutments and applicability of Finnish bridge construction practice to integral abutment bridges. The instrumentation of Haavistonjoki Bridge along the Tampere–Jyväskylä highway was completed in autumn 2003. The data were collected by monitoring altogether 191 gauges installed in the bridge structures during construction. The instrumentation was used to measure, for instance, the abutment's horizontal displacement, abutment rotation, abutment pile strains, earth pressure behind abutments, pier strains, concrete deck strains, transition slab strains, superstructure displacements, frost depth, air temperature as well as thermal gradients in the superstructure next to abutment piles and in the approach embankment. Haavistonjoki Bridge is a 56 m long continuous 3-span slab bridge. The bridge is unskewed and totally jointless. The instrumentation showed, for example, that the behaviour of large steel pipe piles under an integral abutment can be sufficiently predicted by structural calculations.

Haavistonjoki Bridge with its transition slabs was modelled with a 2D FEM model considering nine construction stages and the effect of all the separate stages on forces exerted against the structures. The bridge was modelled also with a general 3D FEM model code with three different values for the springs modelling the behaviour of the soil around the piles and behind the abutment. The measured earth pressures on the bridge abutments were quite high because the backfill was well compacted and the values calculated with a soil modulus of elasticity E_d = 250,000 kPa corresponded best to the measured values.

Tekemäjärvenoja Railway Bridge is a continuous slab bridge with integral abutments. The ballasted slab carries a double-track structure. At the time of instrumentation in 2004, it was part of an unfinished railway track, a direct line from Kerava to Lahti in southern Finland that is to be completed in autumn 2006. The railway bridge was tested by special arrangements with four heavily loaded wagons on the bridge with the focus on horizontal forces and displacements.

The horizontal displacement–earth pressure and rotation–earth pressure relations of a wall moving within soil were modelled with a 2D FEM model. The studied earth pressures were active and passive pressures as well as all intermediate pressures and corresponding shear stresses on the surface of the transferring structure. Traditional earth pressure theories

corresponded to the calculated results in the case of the upper parts of the horizontally transferring wall only if the friction angle between the structure and the soil was correctly considered. The effects of cyclic horizontal wall displacements were also evaluated with several different soil input values. According to the calculation results, large non-reversible deformations develop inside the approach embankment soil and earth pressures increase the most during the first five cycles.

Frozen soil is plastic and the mechanical properties of the soil depend, for instance, on the loading rate, temperature and stress state. The horizontal displacement of bridge piers due to temperature change is very slow compared to the general strain rates measured in tri-axial and compression tests. The analysis of a long jointless bridge in frozen soil was made with a 3D FEM spring model. The abutment with its piles and lateral springs as well as the deck of an imaginary 120 m long jointless bridge were modelled on the basis of the Haavistonjoki Bridge. By varying the stiffness of the upper level pile springs below the piers in calculations, it was possible to recommend the lateral spring coefficient for frozen soil.

Besides axial loading, cyclic abutment displacement and rotation and deformations in the embankment exert forces on abutment piles. As the integral abutment and the embankment move simultaneously, the horizontal resistance of soil against the piles is smaller than the resistance of individual piles. Therefore, it is easier for the pile top connected to the abutment to move horizontally within soil compared to an individual pile.

The forces exerted against an individual pile transferring horizontally within soil were evaluated with a 2-dimensional FEM model. The displacement–force relation corresponded to the Finnish design practice satisfactorily with ordinary pile sizes.

FOREWORD

This research has been conducted at the Institute of Earth and Foundation Structures of Tampere University of Technology in 2002–2005. The Finnish Road Administration (Finnra; Tiehallinto in Finnish) commenced research on the area already in 2001 with a short literary review by the Finnish Road Enterprise (Tieliikelaitos).

The thesis deals with the development of long jointless bridges with a focus on soil–structure interaction. Jointless bridges have been quite widely studied in many countries, but so far both the Nordic practice and soil–structure interaction have received little attention.

The main content and results of this research project have already been published in several research reports in Finnish as well as some conference papers in English.

I would like to express my appreciation to the members of the supervisory group of the financier of the road bridge research project for their valuable guidance during the entire project. The members were Juhani Vähäaho, Matti Piispanen, Esko Palmu, and Timo Tirkkonen from the Finnish Road Administration, Matti Manelius from the Finnish Road Enterprise and Jorma Hartikainen, Anssi Laaksonen, and Olli Kerokoski from Tampere University of Technology. The members of the railway bridge research project also provided valuable guidance. The members were Ilkka Sinisalo and Mauri Koskinen from VR-Track Ltd (VR-Rata), Harri Yli-Villamo from the Finnish Rail Administration (Ratahallintokeskus, RHK), and Jorma Hartikainen, Anssi Laaksonen, and Olli Kerokoski from Tampere University of Technology. The personal scholarship I received from the association of Finnish Civil Engineers (Suomen rakennusinsinöörien liitto) also contributed to the completion of my dissertation, for which I express my gratitude.

The staff of the Institute of Earth and Foundation Structures at Tampere University of Technology carried out the field and laboratory tests. Laboratory Engineer Kauko Sahi and Researcher Anssi Laaksonen deserve special thanks for their valuable and persistent work on the extensive field test programme over several years.

I wish to thank all my colleagues for the assistance I have received. I am particularly indebted to the pre-examiners of my thesis, Dr. Peter Collin, Dr. Mauri Koskinen and Professor Olli Ravaska. I also wish to express my special gratitude to Professor Jorma Hartikainen (deceased 9.5.2006) for his guidance and supervision of this work and the research project related to my thesis. This year my work continued mainly under the supervision of Professor Tim Länsivaara, and I thank him for his invaluable contribution. Ms. Sari Merontausta I thank for her kind assistance in processing the graphs. Mr. Jorma Tiainen I wish to thank for checking the English of my thesis.

Finally, I want to express my gratitude to my wife Elina and my daughters Anna, Katriina and Tuuli for their love and understanding during this project.

Tampere, May 2006

Olli Kerokoski

TABLE OF CONTENTS

NOTATION

c	cohesion
d	pile diameter
e_{init}	initial void ratio
e_{max}	maximum void ratio
k	spring constant
k_r	longitudinal plastic strength between rails and deck
k_s	modulus of lateral subgrade reaction
m	power for stress level dependency of stiffness
n_h	coefficient of lateral subgrade reaction
p_m	ultimate lateral resistance of piles
p_a	active earth pressure
p_p	passive earth pressure
p_o	at-rest earth pressure
p_{ref}	reference pressure in calculations using input values from laboratory tests
s	distance between individual springs
s_u	undrained shear strength of cohesive soil
t	thickness of the pipe wall
t	time
u	relative longitudinal displacement of rail
y	horizontal deflection or displacement of pile
y_m	displacement corresponding to ultimate lateral resistance
z	depth
A	area
B	width of abutment
E_c	modulus of elasticity of concrete
E_d	modulus of elasticity of drained soil
E_s	modulus of elasticity of steel
E_{50}	confining stress dependent stiffness modulus
E_{ur}	unloading–reloading modulus
G	shear modulus
H	height of abutment
I	moment of inertia
K	lateral earth pressure coefficient
K_a	active earth pressure coefficient
K_p	passive earth pressure coefficient
K_0	coefficient of earth pressure at-rest
L	length of bridge
L_0	length of separate spans
M	bending moment
M	modulus of compressibility
P_d	force corresponding earth pressure, drained
Q	shear force
R_{inter}	factor defining the ratio of tangent of wall friction angle ($\tan\delta$) to tangent of soil internal friction angle ($\tan\phi$)
T	temperature
α	coefficient of thermal expansion
ε	normal strain
δ	horizontal displacement of abutment

δ	angle of wall friction (the friction angle between the structure and the soil)
ϕ	soil internal friction angle
γ'	effective unit weight of soil
γ / γ_{sat}	unit weight of soil, unsaturated / saturated
γ	shear strain
ν	Poisson's ratio
σ	normal stress
τ	shear stress
ψ	angle of dilatation (dilatancy angle)
$\Delta\sigma$	normal stress change
ΔT	temperature change

1 INTRODUCTION

Definition of jointless bridges with integral abutments

Integral bridges are defined as bridges with no expansion joints between the superstructure and the supporting abutments. Use of such structures was first considered after observing the successful performance of old bridges with inoperative joints (e.g. Mourad et al 1999). Hence, because of several problems resulting from the traditional practice, the jointless bridge has been adopted in several countries.

The structural elements of the typical abutment of an integral bridge usually consist of an abutment wall, two wing walls, and two or more supporting piles, as shown in Figure 1.1. The abutment walls and wing walls are usually of reinforced concrete. The piles are either of structural steel or reinforced concrete.

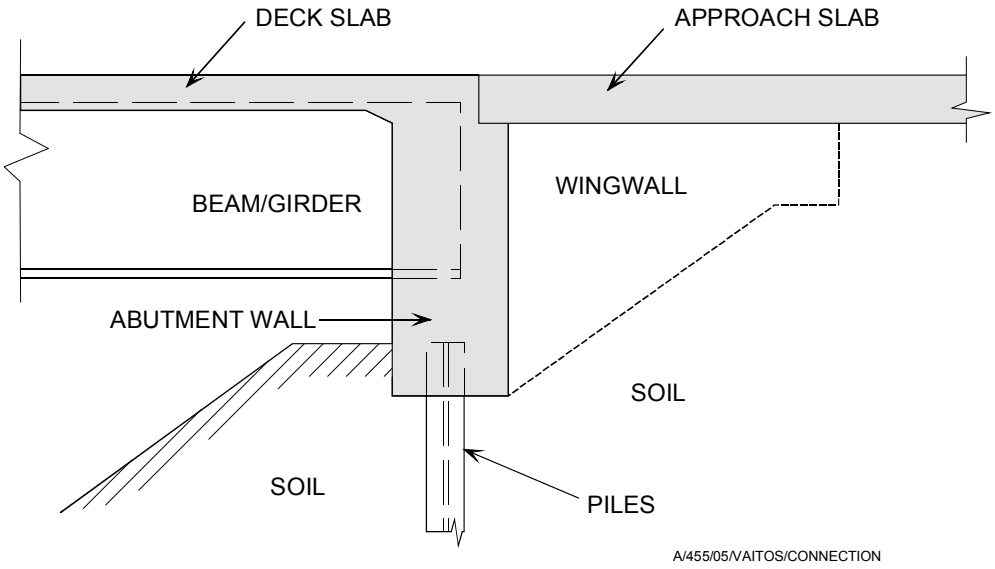

Figure 1.1 Typical connection detail of integral abutment of a composite bridge in USA.

The superstructure of jointless bridges with integral abutments is cast integrally with their substructure. The superstructure is permitted to expand and contract without joints. Thermal movements affect also the behaviour of the substructure and the soil around intermediate piers and abutments.

Advantages and limitations

The increasing interest in jointless bridges derives from the fact that deck joints have proven a permanent problem in existing bridges (Mourad et al 1999). Joints are not a problem just because of their failure and maintenance problems but also because of the significant amount of corrosion damage to girders and underlying substructures from run-off water containing corrosive de-icing salts leaking in through the joints in the deck.

Traditionally, long bridges have been built with bearings and expansion joints. Joints and bearings are expensive in both initial and maintenance costs and can get filled with debris, freeze up, and fail in their task to allow expansion and contraction of the superstructure (Thippeswamy et al. 2002).

Integral abutment bridges are usually economical due to the use of fewer piles, elimination of bearings and expansion joints, and utilisation of non-battered piles. Other advantages of integral bridges include simplified construction procedures, substantial reserve strength capacity, better seismic performance, and aesthetics. Currently, standards in many countries impose some limitations on the geometry of integral bridges. For example, there are limits on total bridge length, skew angle, vertical grade, and horizontal alignment.

Evaluation of the suitability of a long integral bridge for a certain bridge site requires investigating the properties of the ground there. The embankments have to be stable, and the ground below the embankments has to be well consolidated (Burke 1993). It is preferable to build the embankment before the bridge structures in order to let the soil under the structures consolidate and stabilise before the driving of piles. The embankment is not allowed to settle considerably even after the construction of the bridge.

Integral abutment bridges are best suited for locations where there is enough space to build a sufficiently long deck and low-gradient slopes. The longer slopes and deck can be built to compensate for the traditional high vertical structures at the bridge ends (Burke 1993). In many cases the cost of a little longer structure is low compared with the cost of the traditional bridge abutment.

It must be emphasised that generally the most important advantage of integral abutment bridges is the potential reduction in both initial and maintenance costs. The maintenance and occasional replacement of bearings and expansion joints are expensive.

General principles of integral bridge design

An integral bridge designer should take into account the following factors that affect bridge performance and displacements (Card, Carder 1993):

- Temperature and moisture changes in concrete sections
- Elastic shortening and lengthening of the bridge
- Creep of concrete sections
- Displacements and rotations of skewed and curved bridges due to eccentric loading

The greatest contributor to stresses are thermally induced cyclic displacements.

In integral bridge design real material and structural stiffnesses have to be used in structural calculations.

Forces are exerted against the integral abutments by (Card, Carder 1993):

- Dead and live loads
- Temperature changes and gradients in the superstructure
- Moisture content and shrinkage of concrete bridge decks
- Differential settlement of foundations
- Earth pressures
- Pavement pressures
- Embankment translation and consolidation

The piles below the abutment are subject to displacements and bending moments because of the displacements of the surrounding soil (Finnra 2002). At the same time, they are supported horizontally by that same soil. Consequently, they make a special case considering the evaluation of the behaviour of the structure. If the abutments are used to transfer horizontal loads to the embankment, the same phenomenon has to be considered.

Earth pressure and friction at the bridge abutment can prevent developing thermal movements only minimally. For example, if the displacements from a temperature change of 30°C in concrete class K40 were to be limited to zero, the axial stress in the deck structure would be $\sigma = \alpha * \Delta T * E_c = 10 * 10^{-6} * 30 * 31{,}600$ MPa = 9.5 MPa.

Special features of jointless railway bridges

Many national railways around the world have used continuous welded rails (CWRs) for several decades. CWRs cannot expand or compress axially on a railway embankment. A railway bridge is a discontinuous part of the track supporting system due to thermal expansion and structural shrinkage.

Due to large changes in traffic volume and temperature, the soil–structure interaction between the deck and the rails is a particularly complex issue. In some cases special devices are required in order to prevent excessive stresses from being exerted by the expanding deck on the rails. Examples of such special devices are rail expansion devices and so-called zero longitudinal restraint (ZLR) fastenings, that is fastenings with sliding facilities, which do not deliver longitudinal forces between the sleeper and the rail (NBS I19 1988).

The track and ballast on the deck are to be constructed the same way as on a standard railway embankment to attain uniform rail performance and facilitate maintenance.

Development process

The Finnish Road Administration started research on this area in 2001 in the form of a preliminary literature search by the Finnish Road Enterprise together with Tampere University of Technology (TUT). The search yielded promising results, and the Finnish Road Administration decided to continue the project and commissioned the research from the Institute of Earth and Foundation Structures at TUT under the title "Jointless Bridge–Soil Interaction" to be completed in 2002–2008. The work comprises a literature survey (Kerokoski 2005a) and structural calculations (Kerokoski 2005b) in 2003–2006 and short-term (Laaksonen 2004) and long-term field tests at Haavistonjoki Bridge in 2003–2008. The supervisory group checked and approved the research plan (Kerokoski 2003) before it was implemented. Road bridge field tests on a skewed bridge are planned for the summer of 2006.

Finnra is going to give revised design guidelines for long jointless bridges based on the research results.

The railway bridge research programme was carried out in 2004–2005. It comprised a literature survey (Kerokoski 2005c), field tests at Tekemäjärvenoja Railway Bridge (Laaksonen 2005), and comparative calculations by VR-Track Ltd (Koskinen et al 2005).

2 BACKGROUND OF THE STUDY

2.1 Present state of design and construction in Finland

2.1.1 Road bridges

More than 1000 jointless bridges have been built in Finland in recent decades. According to Finnish Road Administration statistics, there were altogether 11,016 road bridges in January 2004. The number of jointless bridges with integral abutments was 796 or 7.2 per cent of the total (see Table 2.1). The majority of the jointless bridges in Finland are of reinforced concrete.

Table 2.1 Jointless bridges with integral abutments owned by Finnra.

Year of construction	Reinforced concrete	Steel	Wood	Pre- or post-stressed concrete	Weather-resistant steel	Total	% of all bridges
bef. 1984	264	4	0	10	1	279	3.6
1985–1989	112	3	0	15	0	130	15.3
1990–1994	164	7	0	29	1	201	16.1
1995–1999	97	6	2	6	0	111	14.4
2000–2004	67	1	2	5	0	75	17.6
Total	704	21	4	65	2	796	7.2

According to Finnish bridge design guidelines, the maximum expanding length of a jointless bridge with integral abutments is 35 m in the case of a normal road bridge and 45 m in the case of a light traffic bridge. The respective maximum bridge lengths are 70 m and 90 m in a totally symmetric case.

Passive earth pressure on an integral abutment is estimated to develop after a quite small abutment displacement, at least in dense non-cohesive soil, according to Table 2.2.

Table 2.2 Horizontal displacement required for passive earth pressure. H = abutment height (Finnra 2002).

Soil	Horizontal displacement
Dense sand	0.002 * H
Loose sand	0.006 * H
Stiff clay	0.02 * H
Soft clay	0.04 * H

If passive earth pressure is used to support the structure and backfill material in dense sand, the required horizontal displacement is assumed to be 0.01 * H (Finnra 1999a). The given internal friction angle for dense sand is $\varphi = 38°$, consequently $K_p = 4.2$.

Bridge pier performance in frozen soil has to be examined also. Frozen soil is modelled by adding a completely rigid horizontal support at the groundwater level (Finnra 2002).

The bridge has to be designed to withstand soil–structure interaction forces caused by superstructure expansion due to a 30°C rise in temperature (Finnra 2002). The structure has to be examined also when there is a gap between the abutment wall and the embankment due to a horizontal superstructure shortening after a 20°C drop in temperature.

If the backfill soil is sufficiently permeable, there is no need for drainage behind the abutment wall (Finnra 1999b).

2.1.2 Railway bridges

In Finland all new railway bridges must be provided with ballast (RHK 2000). Ballasted bridges with an expansion length of over 120 m must be provided with a rail expansion device. Therefore, particularly long bridges have to be divided into segments with expansion joints. The cumulative total displacement of expansion joints must be less than 50 mm. The latter requirement is often decisive.

According to Finnish guidelines, longitudinal forces in rails develop from temperature changes, train braking or acceleration, hill climbing and the rails' resistance to a moving train (RHK 2002).

In Finland the transition slab is omitted in earth pressure and lateral subgrade reaction calculations. The full passive earth pressure against the abutment wall can be calculated based on Rankine's earth pressure theory. The corresponding horizontal displacement is assumed to be 0.002 * H (RHK 1997). In the case of active earth pressure, the required horizontal displacement is assumed to be 0.0005 * H.

The abutment backfill below the track's structural soil layers must be constructed of gravel, crushed rock or blasted rock (< 300 mm) that fulfil the sub-base material requirements (RHK 2003). Compaction has to be performed by layers the same way as with the frost-resistant fill under foundations. The fill must not damage concrete surfaces and the maximum grain size near the abutment is 64 mm.

2.2 Present state of design and construction outside Finland

2.2.1 Road bridges

Practice in North America

In the United States of America and Canada thousands of long jointless and integral bridges have been built. Typically, the concrete surface of the deck serves as pavement for the road structure. Transition slabs, also called approach slabs, are built onto the approach embankment at the bridge deck level. They are connected horizontally to the bridge abutment to prevent cyclic horizontal movement from separating the deck and the transition slab. Typically one row of steel H-piles supports shallow abutments. In North America, integral bridges are normally built as a composite structure consisting of steel, reinforced concrete or pre-tensioned concrete beams, and a reinforced concrete deck. The longest integral bridge in the USA is over 300 meters. According to valid state manuals, the longest permitted length of reinforced concrete bridges is typically 100–150 m but, for instance, in Tennessee it is 244 meters.

In the design of integral abutments, the thermal strains related to casting closure joints need to be considered. Daily variations in girder length can present difficulties, especially

for longer steel girders. To minimise the danger of girders being pulled out of the freshly cast integral abutment closure joint in the Vancouver Island Highway Project, the concrete was placed in the morning, when the weather was overcast and temperature change was expected to be small (Harvey et al 2001). Hence, successful implementation requires attention to the construction sequence by the designer and proper guidance for the contractor in the contract documents.

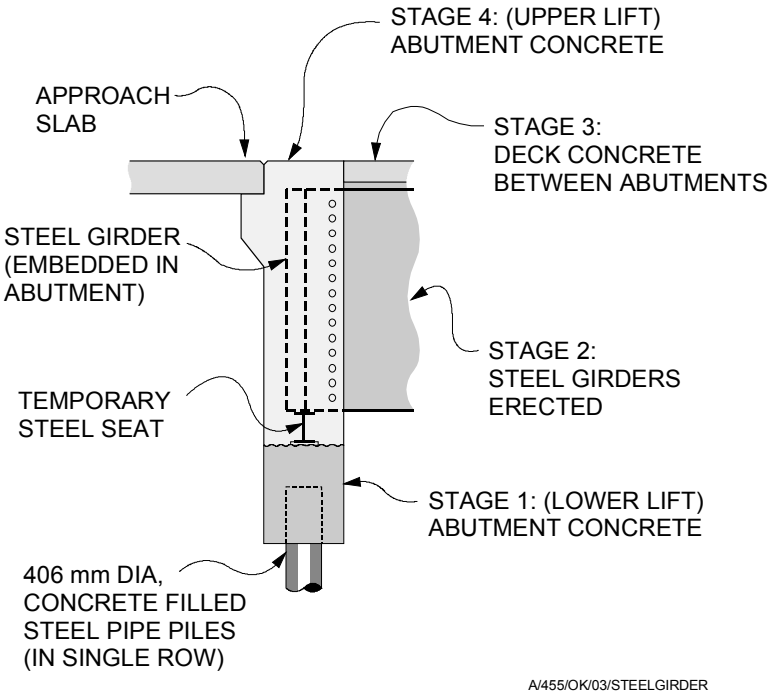

Figure 2.1 Typical cross section and construction sequence of steel girder bridge abutment in Vancouver Island Highway Project (Harvey et al 2001).

Practice in some European countries

In northern Europe, concrete slab bridges and concrete slab-beam bridges are typical. In northern Europe and Great Britain the allowable bridge length is approximately the same, about 60–90 meters. The effect of temperature fluctuation and the corresponding cyclic abutment displacement on earth pressures is considered in Swedish and in British standards.

Practice in Sweden

In Sweden jointless bridges are generally so-called ‘end screen bridges’ where the end screen is connected to the deck without joints and does not transfer considerable vertical forces to the embankment soil (see Figure 2.2). The end of the deck and the end screen form a cantilever structure, and vertical forces are transmitted to the foundations through separate piers or a wall. Often there is also a bearing at the upper part of a vertical structural member, which is founded high enough so that the foundations can be built on dry ground, for instance, for bridges over rivers (see Figure 2.3).

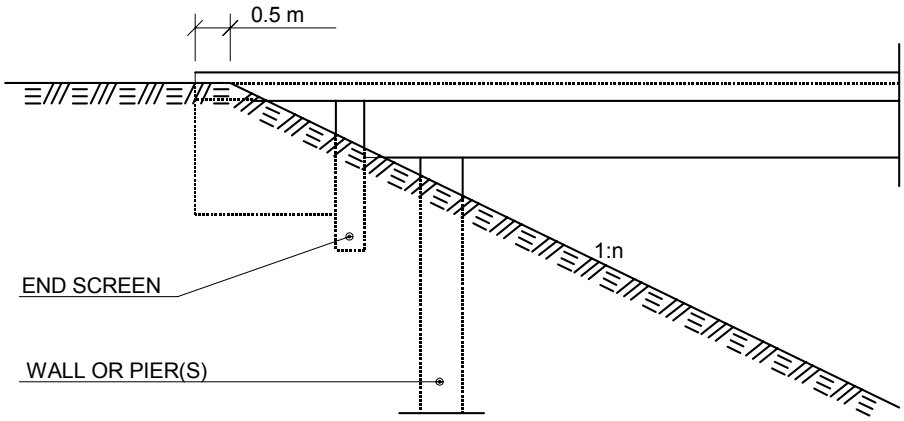

Figure 2.2 Example of Swedish end screen bridge (Vägverket 1996).

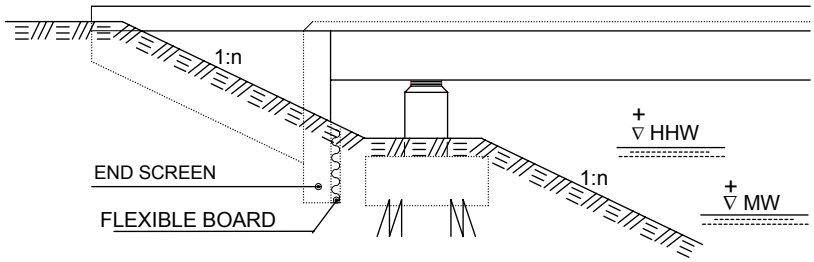

Figure 2.3 Swedish jointless bridge with bearings and high-built foundation on piles (Vägverket 1996).

According to the Swedish code of practice, the maximum bridge length is 60–90 m for concrete bridges and 40–60 m for steel–concrete composite bridges. The exact allowed length depends on how far up north the bridge is located. The limit values have been estimated on the basis of acceptable pavement cracks in approach embankments (Rosell 2003).

The approach embankment is supposed to be well drained. Therefore, the freezing of the embankment is assumed not to change its properties significantly.

In Sweden transition slabs are used only if the probability of large settlements is high on the basis of a ground survey report and bridge structure type. Transition slabs are built according to standard drawings (see Figure 2.4).

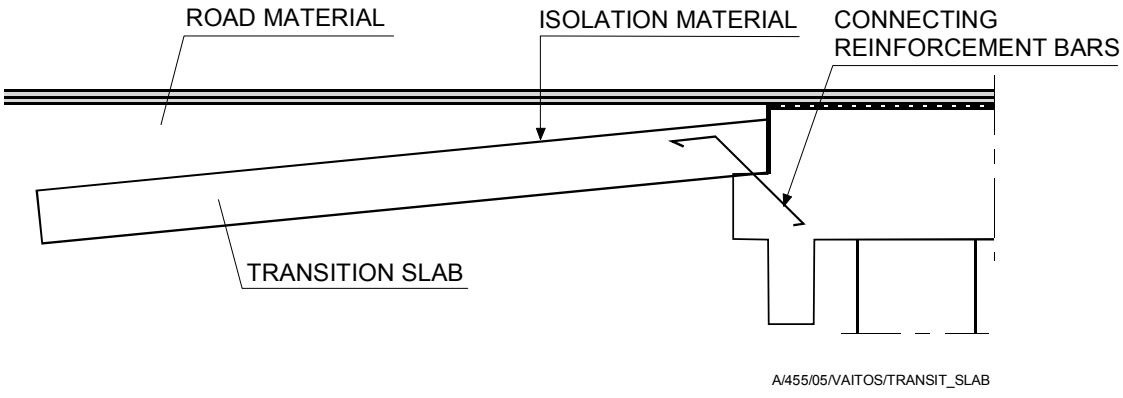

Figure 2.4 Typical transition slab according to Swedish standard drawing 584:3G - g.

Earth pressure against the abutment, which is moving horizontally towards the embankment, is calculated from equations (Vägverket 2002):

$P = P_o$, if $\delta = 0$

$P = P_o + c_1 * \delta * 200/H * (P_p - P_o)$, if $0 < \delta < H/200$

$P = P_o + c_1 * (P_p - P_o)$, if $\delta > H/200$

$c_1 = 1$ in case of unfavourable earth pressure (e.g. forces from temperature changes)
$c_1 = 0.5$ in case of favourable earth pressure (e.g. forces from braking vehicle)
P_o = at-rest pressure
P_p = passive earth pressure
H = abutment height
δ = horizontal abutment displacement towards the embankment.

Hence, passive earth pressure is fully developed after horizontal displacement $\delta = 0.005 * H$.

Practice in Norway

The Norwegian Public Roads Administration (Statens vegvesen) has published precise design guidelines for cast-in-place slab bridges in a manual called Bruhåndbok (Statens vegvesen 2000). According to the guidelines, the length of a three-span bridge may vary between 22–52 m and the middle span length should be 10–20 meters. Bridges not meeting the limit values are designed according to the ordinary code of practice.

The method of the manual is a semi-integral solution where the end screen and wing walls are cast together with the deck to create a uniform structure. Because of the bearings, the horizontal expansion from temperature changes does not transfer remarkable forces to bridge foundations (see Figure 2.5). The 70 mm thick flexible board between the end screen and the vertical support is to be removed after the placing of concrete.

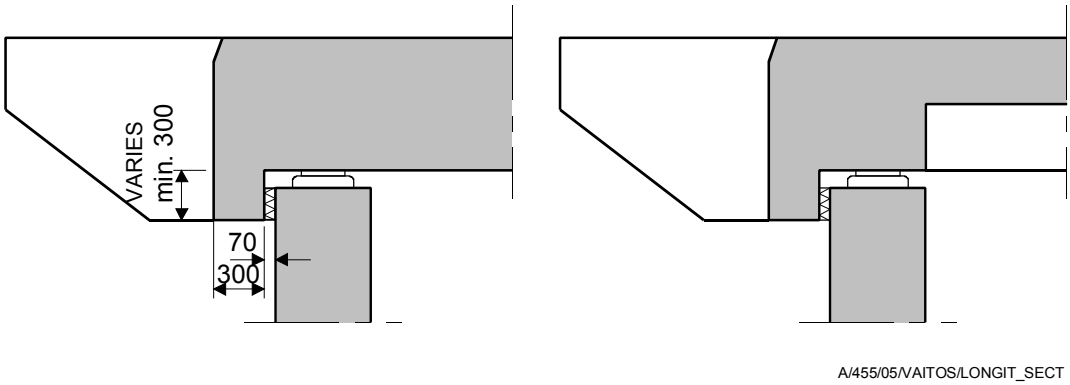

Figure 2.5 Longitudinal section of a Norwegian slab bridge and a slab–beam bridge. Optional transition slab is not shown (Statens vegvesen 2000).

Practice in England

BA 42/96 is a British design manual covering the design of integral highway bridges without expansion joints. According to the manual, all bridges are, in principle, to be

continuous over intermediate piers and bridges with overall lengths not exceeding 60 m and skews not exceeding 30° are to be integral with their abutments. Lengths over 60 m are not allowed.

Resistance to longitudinal thermal movements and braking loads is provided by the stiffness of the soil abutting the end supports and, in some cases, by the stiffness of the intermediate piers.

The typical height of an end screen abutment is about 3 meters, and it is assumed that full passive pressures will apply (BA42 1996).

Bridge engineers in the UK have tended not to use piled abutments in order to avoid the bridge becoming a hard spot as the embankments settle.

Practice in Germany

In Germany there are no specific standards for integral bridges, but related research and development has been going on in recent years and several integral bridges have been constructed; particularly, if the length of the bridge is less than 50 m (Engelsmann 1998). So far, design has been based on publication DAfStb Heft 461 (Pötzl et al 1996).

Field tests outside Finland

Three recent field test reports and their results are presented in Appendix 9 (Huang et al 2004 / Abendroth & Greimann 2005 / Hoppe 2005). The results support the conclusions of the tests presented in this thesis in many respects.

2.2.2 Railway bridges

In the Nordic countries the practice concerning the analysis and design of railway bridge–track interaction varies.

The deck–track interaction is not allowed to present any risk of rail buckling due to the longitudinal forces developed by the expanding deck. According to Nordic practice, the maximum expansion length of a railway bridge with ballast is limited to 120–160 meters. The lower limit applies to areas with especially low air temperatures. The bridge abutment should be perpendicular to the track. The 3–5 m long transition slabs have to be constructed within the approach embankments in the case of poor subsoil especially for high-speed tracks (NBS I25 1991).

In the Swedish and Norwegian codes, the share of the forces from train braking and acceleration on the bridge through rails and bridge structures straight to the embankment is determined.

In Sweden, bridges with more than 80 mm longitudinal displacement must be provided with a rail expansion device and a ballast expansion joint. Generally, if the expansion length of a concrete bridge is more than 150 meters, or if the expansion length of a steel–concrete composite bridge or a steel bridge is more than 100 meters, the rails must be provided with expansion devices (Banverket 2002).

The Norwegian load models 71, SW/0 and SW/2 for horizontal loads and braking and traction are the same as in Eurocode EN 1991-2 (2003). The SW load models concern

heavy traffic. The principles of creating a structural model for calculating longitudinal forces (see Figure 2.6) and thermal excitation stresses also derive from the Eurocode.

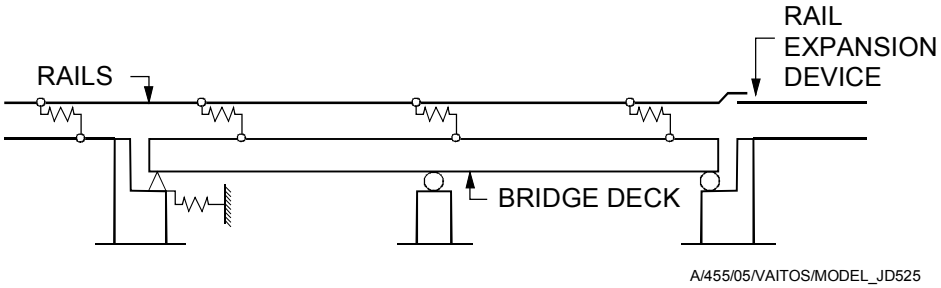

Figure 2.6 Structural model of Norwegian code of practice JD 525 in class a (Jernbaneverket 2002).

In the case of a continuously welded rail (CWR), expansion length is limited as follows:

- Less than 90 m on ballasted railway bridge with steel structures,
- Less than 120 m on ballasted railway bridge with steel–concrete composite structures or concrete structures.

In the Eurocode, the maximum expansion lengths are smaller than in the Norwegian code.

In Norway, the starting value for temperature changes on structures is 10°C. The changes from the starting value are ±35°C for deck and ±50°C for rails. The temperature difference between the deck and the rails is not assumed to be more than 20°C.

In most European railways transition slabs within the approach embankments are not generally used. The practice is based on the principle that large embankment settlements are not permitted at all. Precise evaluation of embankment settlements and strict settlement limits are essential factors in ensuring track behaviour.

The Eurocode offers general guidelines for track–bridge interaction evaluation. Detailed guidelines for parameters left open for national choice can be defined in national annexes. In the case of rails on the bridge and the adjacent abutment, the permissible additional rail stresses due to the combined response of the structure and track to variable actions should be limited to the following design values according to Eurocode EN 1991-2 (2003) and UIC 774-3 (2001):

- Compression: 72 N/mm^2,
- Tension: 92 N/mm^2.

The limiting values for rail stresses given above are valid for track:

- UIC 60 rail with a tensile strength of at least 900 N/mm^2,
- Straight track or track radius r ≥ 1500 m,
- For ballasted tracks with heavy concrete sleepers with a maximum spacing of 0.65 m or equivalent track construction,
- For ballasted tracks with at least 0.3 m consolidated ballast under the sleepers.

The resistance of the track to longitudinal displacements is a function of the displacement of the rail relative to its supporting structure. This resistance increases rapidly while the displacement remains low, but remains virtually constant once the displacement has reached a certain magnitude (see Figure 2.7).

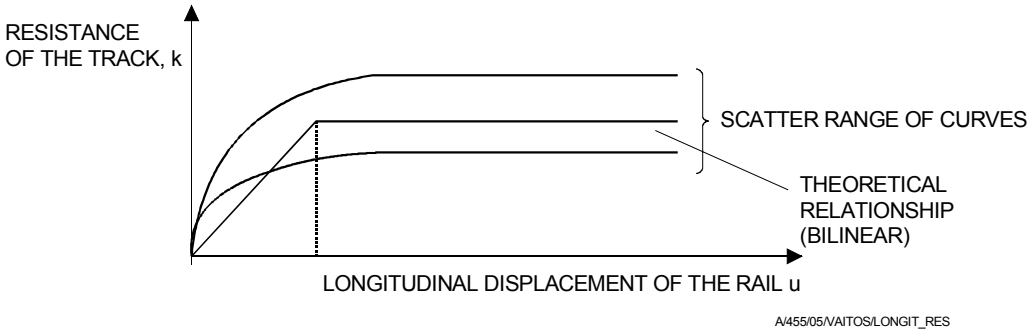

Figure 2.7 Longitudinal resistance of the track as a function of relative longitudinal displacement (UIC 774-3 2001).

Resistance to longitudinal displacement is higher on a loaded track than on an unloaded one.

Conventional values assumed for displacement, u_0, between elastic and plastic zones for a ballasted track are as follows:

- $u_0 = 0.5$ mm for resistance of the rail to sliding relative to the sleeper,
- $u_0 = 2$ mm for resistance of the sleeper in the ballast.

Some railways adopt other values for u_0 for the ballast alone; for example, NS in Netherlands uses 2.8 mm.

Current values of resistance, k_r, in the plastic zone (UIC 774-3 2001):

- Resistance of sleeper in ballast (unloaded track), moderate maintenance: $k_r = 12$ kN/m,
- Resistance of sleeper in ballast (unloaded track), good maintenance: $k_r = 20$ kN/m,
- Resistance of loaded track or track with frozen ballast: $k_r = 60$ kN/m.

Actions to be taken into account

The phenomena that could lead to interactions are ones that cause relative displacement between the track and the deck (UIC 774-3 2001). They are the following:

1. Thermal expansion of the deck only, in the case of continuously welded rail, or thermal expansion of the deck and the rail whenever a rail expansion device is present.
2. Horizontal braking and acceleration forces.
3. Rotation of the deck on its supports as a result of the deck bending under vertical traffic loads.
4. Deformation of the concrete structure due to creep and shrinkage.
5. Longitudinal displacement of the supports under the influence of thermal gradient.
6. Deformation of the structure due to a vertical temperature gradient.

In most cases, the first three actions are of major importance for bridge design.

3 DEFINITION OF THE RESEARCH PROBLEM

An integral bridge is not a new bridge type in Finland, and certainly not, for instance, in the U.S.A. In the Nordic countries, the circumstances and construction methods differ from many other countries. Hence, there is need for comprehensive research on long jointless and integral road and railway bridges. The bridges and the approach embankments should serve the users of all vehicles reliably for many decades with only minor maintenance.

Focus of the study

This research concentrates on unskewed reinforced concrete structures and approach embankments. It studies the forces and stresses from temperature fluctuation and train braking on railway bridges. Earth pressures against the abutment and backfill behaviour are also discussed. The behaviour of the abutment and abutment piles is also looked into, as is the behaviour of the pier nearest to the abutment.

The aim of the study is to find out whether long jointless bridges with integral abutments can be used in Finnish conditions with typical Finnish construction methods to build a bridge superstructure and substructure that behave satisfactorily. The approach embankment and transition slab also have to behave satisfactorily and large bumps are not allowed.

Consequently, answers were sought for the following questions:

- Which criteria should apply to the maximum length of an integral bridge?
- What length limits would they lead to in Finnish conditions?
- Are there any obvious alternatives to “Finnish construction methods”, the bridge design procedure, and the estimation of soil-structure interaction?

A jointless bridge refers here to a continuous deck structure without longitudinal expansion joints between adjacent spans. Finnish conditions mean here low air temperature and frozen soil in wintertime. Finnish construction methods mean using large-diameter steel pipe piles, a cast-in-place concrete superstructure and a transition slab constructed within an approach embankment.

4 RESEARCH MATERIAL AND FIELD TESTS

4.1 Finite element method software

4.1.1 2D FEM software

Plaxis 2D version 8 is a finite element package intended for two-dimensional analysis of deformation and stability in geotechnical engineering. There are elements for modelling walls, plates, anchors, geotextiles, beams, circular tunnels and soil–structure interface units. Automatic load stepping and five different soil models are included as well. Staged construction enables realistic simulation of the building process.

Hardening-Soil model of Plaxis 2D FEM software (isotropic hardening)

In contrast to an elastic perfectly-plastic model, the yield surface of a hardening plasticity model is not fixed in principal stress space, but it can expand due to plastic straining. Distinction can be made between two main types of hardening, namely shear hardening and compression hardening. Shear hardening is used to model irreversible strains due to primary deviatoric loading. Compression hardening is used to model irreversible plastic strains due to primary compression in oedometer loading and isotropic loading. Both types of hardening are contained in Hardening-Soil (HS) model.

The basic idea behind the HS model is the hyperbolic relationship between the vertical strain, ε_1, and the deviatoric stress, q, in primary tri-axial loading. The stress–strain relations based on the HS model and moduli E_{50} and E_{ur} are illustrated in Figure 4.1. E_{ur} is the modulus of elasticity for unloading and reloading corresponding to reference pressure p_{ref}.

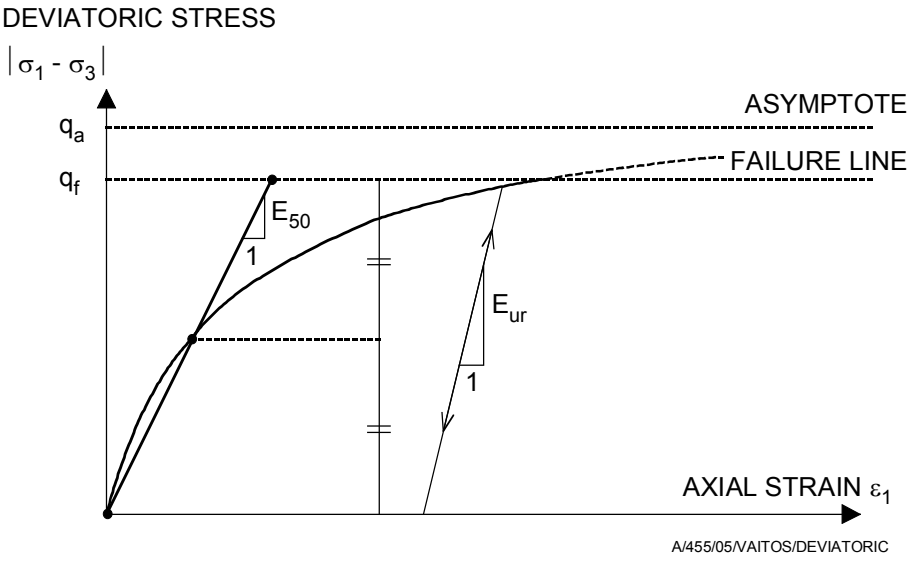

Figure 4.1 Hyperbolic stress–strain relation in primary loading for a standard drained tri-axial test according to HS model recommended by Plaxis.

The default values are $q_f = R_f * q_a = 0.9 * q_a$ and $E_{ur} = 3 * E_{50}$
, where q_f = ultimate deviatoric stress, R_f = failure ratio and q_a = asymptotic value of shear strength.

The elastoplastic Hardening-Soil model does not involve a fixed relationship between the (drained) tri-axial modulus, $E_{50,}$ and the modulus of compressibility, M, for one-dimensional compression. The experimental determination of the modulus of compressibility, M_{ref}, is illustrated in Figure 4.2.

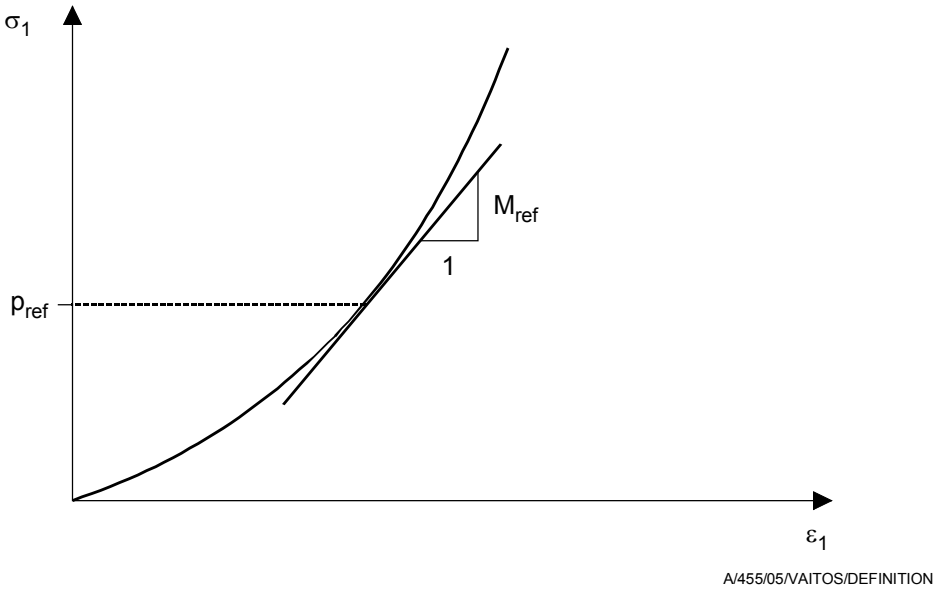

Figure 4.2 Definition of M_{ref} from oedometer test results as a tangent stiffness at a vertical stress of $\sigma'_1 = p_{ref}$.

The stress-level dependency of stiffness modules E_{50} and M is described with the following equations as with Janbu's well-known corresponding equations:

$E_{50} = E_{50ref} * ((c*\cos\phi + \sigma'_3 \sin\phi) / (c*\cos\phi + p_{ref} \sin\phi))^m$,

$E_{50} = E_{50ref} * (\sigma'_3 / p_{ref})^m$, as cohesion c = 0,

$M = M_{ref} * (\sigma_1 / p_{ref})^m$,

where m = power for stress-level dependency of stiffness. ("ref" in p_{ref} refers to reference pressure)

4.1.2 3D FEM software

Abaqus/Standard software code provides a wide variety of finite element solution techniques to simulate a wide variety of linear and non-linear engineering simulations (Abaqus 2001).

4.2 Haavistonjoki Bridge

4.2.1 Superstructure and substructure

Haavistonjoki Bridge in Finland is a 56 m long continuous 3-span slab bridge. Total length of the three spans is 50 meters. Total width of the lanes is 11 m and the thickness of the deck slab is 860 mm. The bridge is unskewed and totally jointless. The approach slab, called a transition slab, is located within the approach embankment. The 5 m long

transition slab is attached horizontally to the abutment with dowels, which allow horizontal movements.

Four piers and two abutments support the reinforced concrete deck according to Figure 4.3–Figure 4.5. Eight steel pipe piles of diameter d = 711 mm and wall thickness t = 14 mm support the piers and the abutments. The piles are filled with reinforced concrete.

Figure 4.3 Haavistonjoki Bridge immediately after construction.

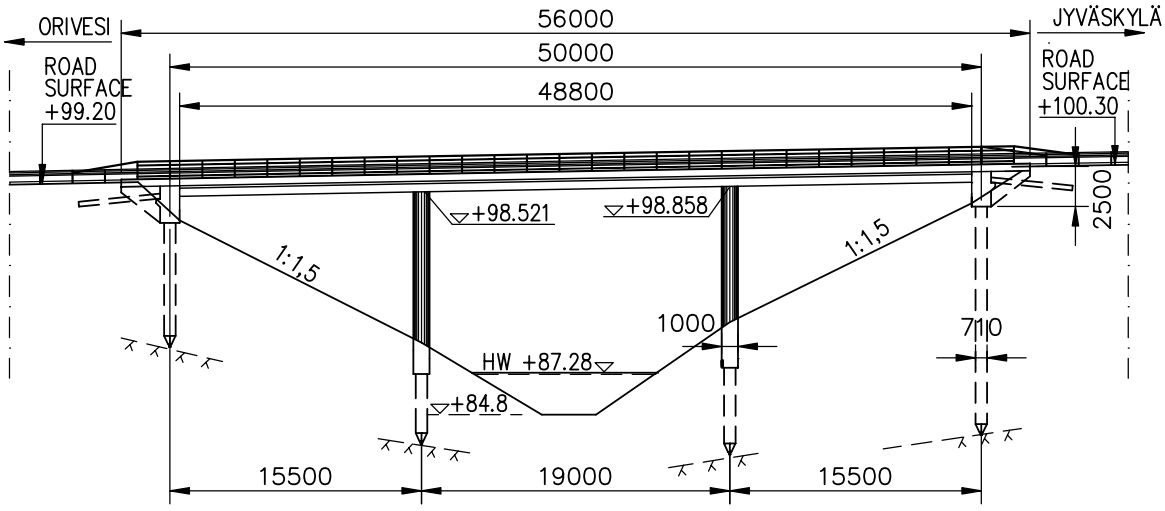

Figure 4.4 Haavistonjoki Bridge on Highway number 9 between Tampere and Jyväskylä. Side view. The transition slab is within the embankment. The support labels beginning from the Orivesi or western end were T1–T4 (Laaksonen 2004).

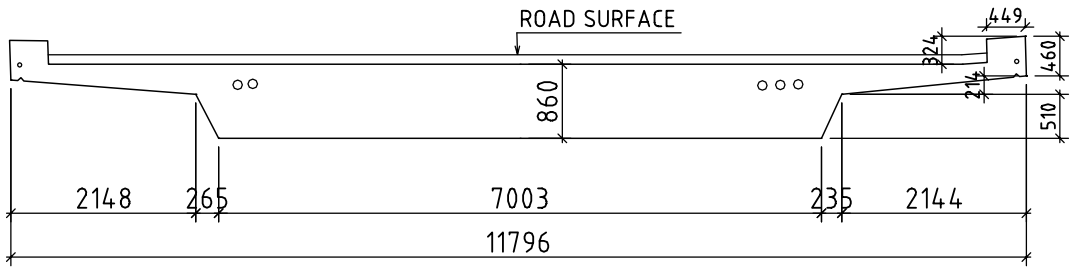

Figure 4.5 Haavistonjoki Bridge. Cross-section.

The connection between the abutment and the transition slab was implemented with vertical dowels on the upper surface of the supporting cantilever according to Finnish type drawing R15/DL 2 (Finnra 1999d). The dimensions of the steel dowels were: diameter 25 mm at 1000 mm intervals, length 570 mm. The dimensions of the recesses for the dowels made with plastic tubes were: diameter 40 mm, length the same as the thickness of the transition slab. Theoretically, the dowels permitted 8 mm movement in both longitudinal directions.

4.2.2 Eastern embankment backfill and site investigation results

The consept of resilient modulus is introduced for example in reference (Kolisoja 1997). For example in the loading condition of the cyclic loading tri-axial test, the resilient modulus is described with the following equation:

$$M_r = \Delta q / \Delta e^e_a$$

, where M_r = resilient modulus, Δq = cyclic deviatoric stress, and Δe^e_a = recoverable axial strain.

The backfill material is well-compacted # 0–60 mm crushed rock. The material has been tested at the geotechnical laboratory of Tampere University of Technology.The resilient modulus was 200,000–250,000 kPa after 100 loading cycles, when the sum of principal stresses was about 100–150 kPa according to Figure 4.6.

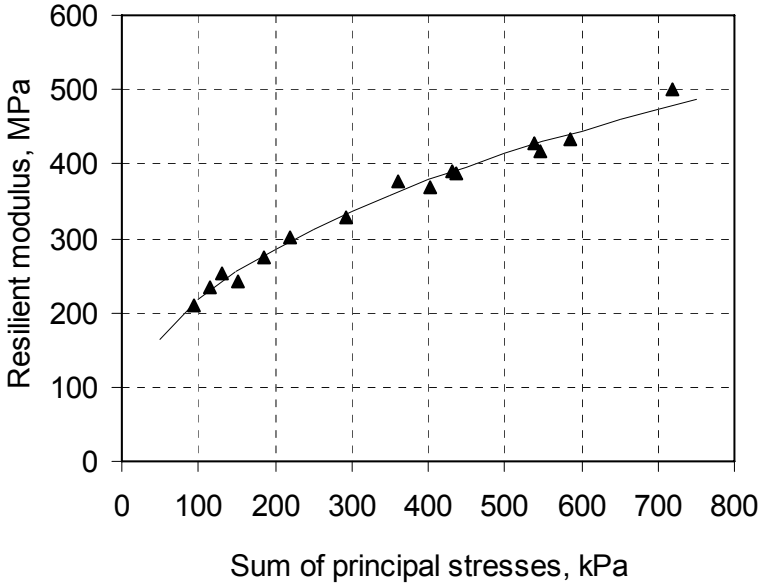

Figure 4.6 Results of large-scale cyclic tri-axial test with Haavistonjoki backfill material. Resilient modulus at various stress levels.

From Figure 4.7 it can be estimated that with a cell pressure of 30 kPa the secant modulus of elasticity was E_d = 373 kPa / (0.00378-0.002) = 210,000 kPa at about 50 per cent compression level. In another test the corresponding result was E_d = 290 kPa / (0.0030-0.0013) = 170,000 kPa.

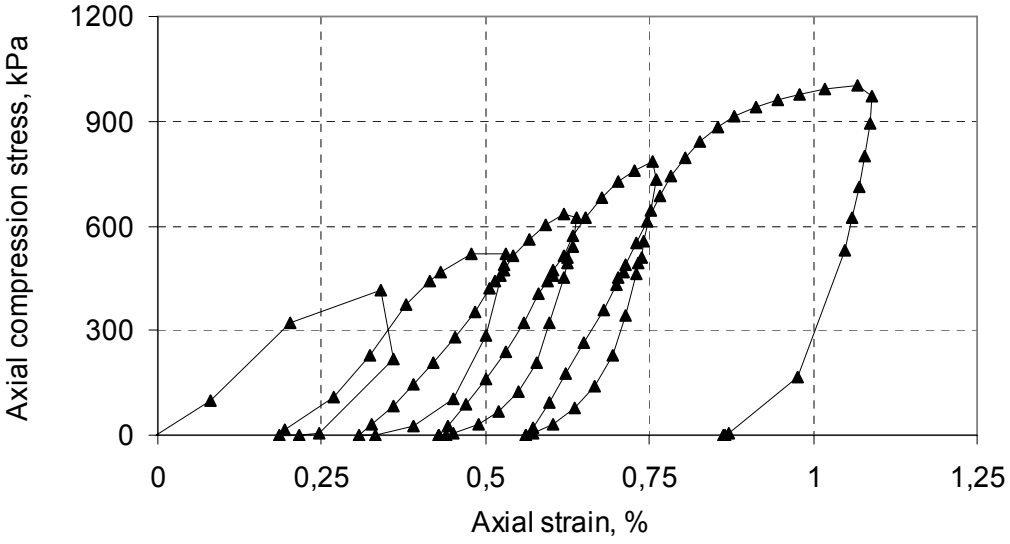

Figure 4.7 Results of large-scale static tri-axial test on Haavistonjoki backfill. Cell pressures were 15, 30, 60, 100 and 150 kPa.

With a cell pressure of 60 kPa, the average secant modulus of elasticity was E_d = 215,000 kPa in two separate tests.

The friction angle and cohesion values of the soil were also measured under laboratory conditions from samples taken from the bridge site. The results were: $\phi = 45°$ and c = 0 kPa.

Plate bearing tests were performed on the compacted eastern embankment fill prior to the construction of the transition slab. The average values of two test results were:

$E_1 = (154 + 180)/2 = 167$ MPa = 167,000 kPa
$E_2 = (390 + 415)/2 = 402$ MPa = 402,000 kPa

The replacement fill area and some site investigation results are illustrated in Figure 4.8. The properties of the silt have been evaluated based on weight sounding test (SGY 1980) results (see App. 7).

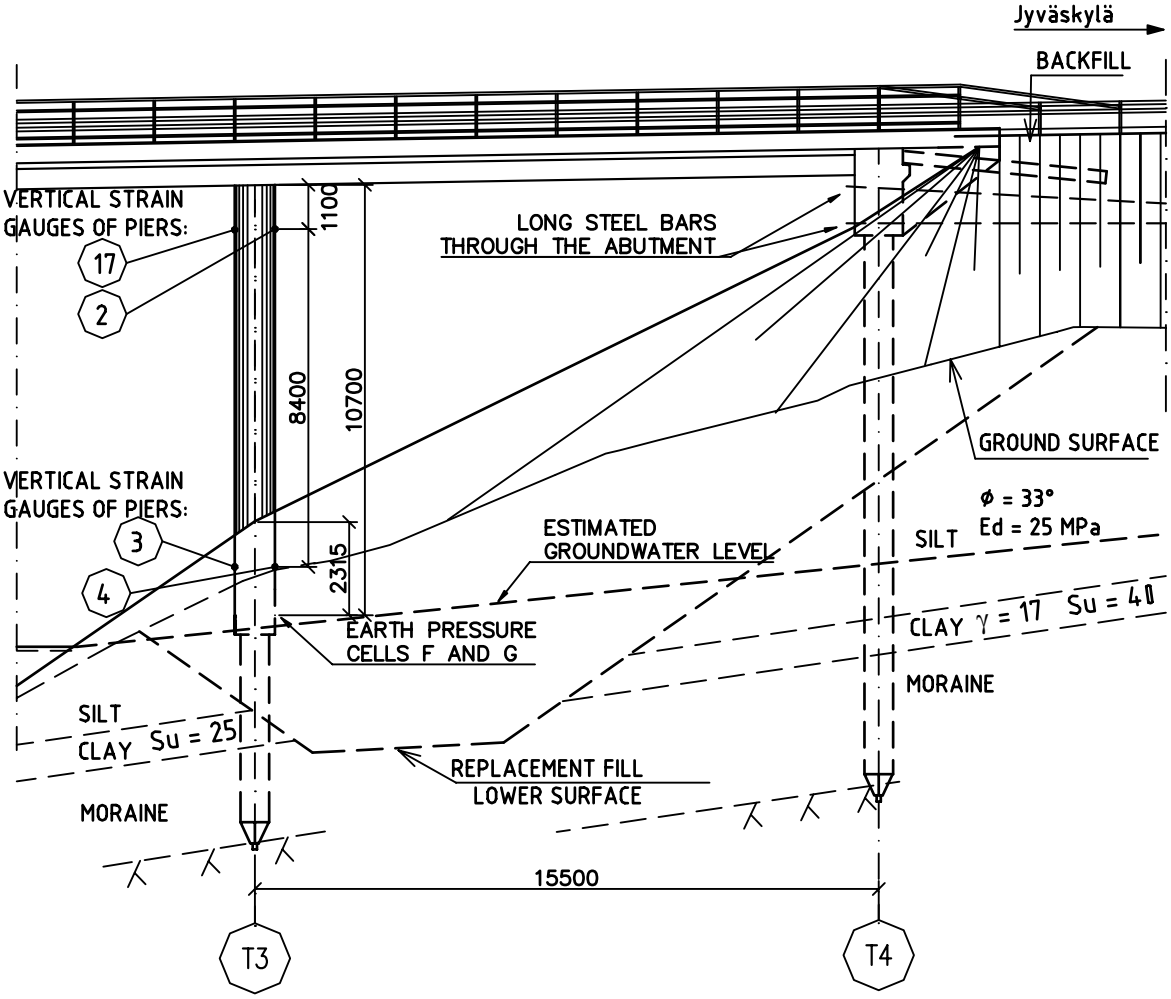

Figure 4.8 Basic soil material data. Replacement fill area: proposed unit weight γ = 20 kN/m^3 and friction angle φ = 42°. Also shown: earth pressure cells and strain gauges of Haavistonjoki bridge pier T3. Location of long steel bars in approach embankment.

According to tested soil samples the soil to the east of Haavistonjoki River below the ground surface consists mainly of clayey silt (see App. 7). The height of the clayey silt layer is about 5 meters. Below that there is a shallow layer of clay, then a moraine layer and rock (see Figure 4.8). According to the soil samples the water content of the clayey silt varied between w = 21 %–36 % and remoulding index F = 28 %–50 %. The friction angle ϕ and modulus of elasticity E_d of the clayey silt was estimated from weight sounding tests and the results are presented in Appendix 7 (see also Figure 4.8).

The groundwater level was not observed, but was estimated and is also presented in Figure 4.8.

Soil samples were not taken from the western river embankment. According to the weight sounding, the soil layers were shallower and the rock was nearer to the ground surface than at eastern river embankment.

Vane test results

Vane tests were performed by Geopalvelu on 15.04.2003 at the eastern embankment of Haavistonjoki River (see App. 2). The shear strength values, s_s, under the approach embankment based on vane test results (see Table 4.1) represented the actual undrained shear strength of the soil, s_u. As the liquid limit, w_L, of the silt was less than 40 per cent, no reduction in shear strength was needed.

Table 4.1 Haavistonjoki Bridge vane test results [kPa]. s_s = shear strength, s_{sh} = remoulded shear strength.

Point 16 at site. Ground surface level: + 90.1		
Depth from ground surface [m]	s_s	s_{sh}
4.3	20.7	5.6
5	23.9	4

Point 21 at site. Ground surface level: + 94.7		
Depth from ground surface [m]	s_s	s_{sh}
7.5	44.6	8

Soil properties based on soil samples and static sounding tests.

Part of the soil sample and weight sounding test (SGY 1980) results are presented along with several figures in Appendix 7.

4.2.3 Field test programme

Overview

The field test programme for Haavistonjoki Bridge was composed at Tampere University of Technology under the name ‘Haavistonjoen silta: Koeohjelma 28.4.2003’. The designed research equipment was manufactured at the TUT laboratory by the staff of the Institute of Earth and Foundation Structures or at nearby engineering workshops. The staff of the same institute also installed all the gauges and data loggers.

The bridge was constructed and instrumented in the summer of 2003. The test programme included 191 gauges, from which the data-logger automatically collects data to a computer every 15 minutes for at least the years 2003–2008.

Displacements

One of the most important reasons for instrumenting Haavistonjoki Bridge was to study the cyclic displacements of the whole bridge and the longitudinal changes in bridge length. The plan was to monitor them and pier displacements by a tacheometer at the bridge site.

The changes in bridge length were also measured by installing laser distance-meter equipment between the opposite abutments (Laaksonen 2004).

Abutment displacements and rotations were observed by installing ten long steel bars at three levels through the eastern abutment (see Figure 4.8 and Figure 4.11) and at two levels through the western abutment. These bars were anchored to the embankment.

The displacement between abutment and transition slab was measured with typical displacement gauges.

Earth pressures

Twelve earth pressure cells were installed on the outer surface of the abutments to measure the earth pressures in the interface between the abutment and the embankment. The cells were embedded in the concrete facing outward. The eastern abutment had ten earth pressure cells and the western abutment two. The earth pressure cell locations are presented in Figure 4.9 and in Figure 4.10.

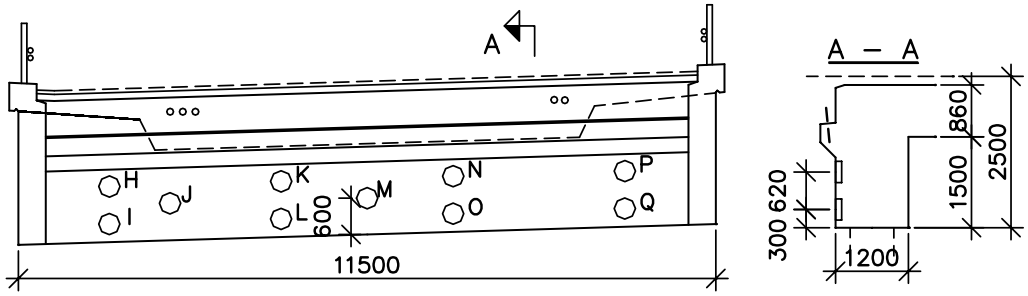

Figure 4.9 Earth pressure cells and their labels on eastern bridge abutment (T4). The western abutment (T1) had cells at locations J (labeled V) and M (labeled W).

Figure 4.10 Installation of abutment earth pressure cells prior to approach fill construction.

Earth pressures at the interface between the pier and the surrounding soil were also measured in the direction of the bridge at two piers.

Strains

The following structural strains were measured with strain gauges:

- Strains within the piers were measured in the direction of the bridge in the upper and lower parts at both surfaces of the pier.
- Strains at the top and bottom surface of the bridge deck slab and the eastern transition slab.
- Strains on the surface of the abutment piles and at the reinforcement level of the eastern abutment in the vertical direction.

Temperatures

Several temperature gauges were installed to measure concrete temperatures, embankment temperatures and air temperatures.

4.2.4 Installation of gauges

Displacement measuring devices

The anchor bars that penetrate horizontally through the abutment were 13.5 m long and their diameter was 20 mm. Each bar was installed into a 25 mm tube to prevent the bar from getting stuck in the surrounding backfill soil. The anchor plate at the end of the bar was 350 mm wide and 15 mm thick, and it was installed in the embankment about 12 m from the abutment.

Four tacheometer target prisms were attached on the edge of the deck at supports T1 to T4 and four prisms on the piers at supports T2 and T3. The tacheometer type was WILD T2002.

The type of the laser distance-meter was Leica DISTO. The precision according to the manufacturer was better than ±1 mm over a 50 m distance. The laser device was installed on the eastern abutment and a smooth board to reflect the laser beam on the western abutment (see Figure 4.11).

Figure 4.11 Laser distance-meter on the inner surface of the abutment.

The potential gap between the backfill soil and the abutment was checked manually with a special measuring device (see Figure 4.12 and Figure 4.13). Research staff at Tampere University of Technology developed and manufactured six of these devices. The inner steel plate of the device can be pushed against the backfill to check if there is a gap during wintertime. Grains from the soil cannot fill the gap between two plates due to a textile sheet between the outer plate and soil.

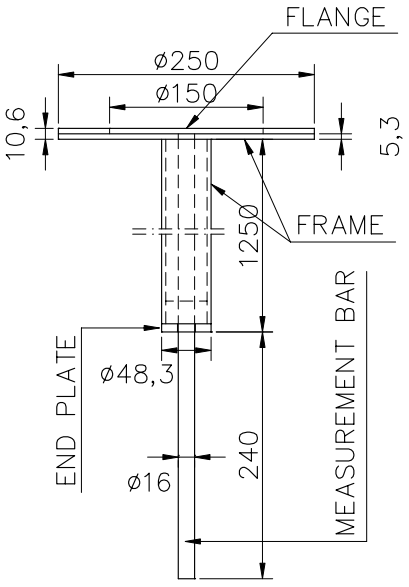

Figure 4.12 Gauge to measure gap width between abutment and backfill. Dimensions (Laaksonen 2004).

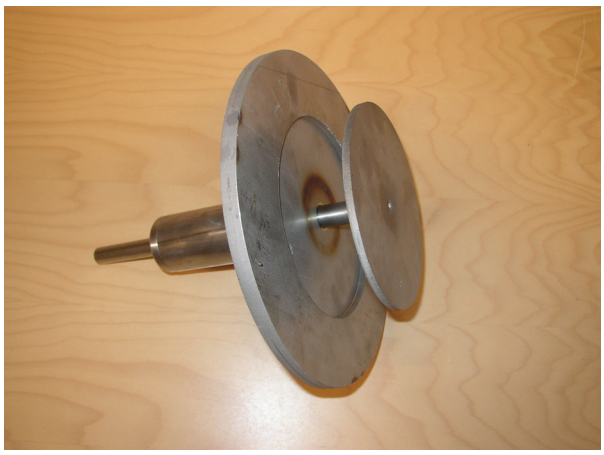

Figure 4.13 Gauge to measure the gap width between abutment and backfill. The pipe and the inner bar have been shortened for this photograph.

The gap between the eastern abutment and the transition slab on both sides of the slab was measured with distance gauges installed between a steel rod in the slab and the wing wall. The wing wall is a monolithic part of the abutment. The gauge and the other equipment were covered to ensure their long-lasting performance.

Earth pressure measuring devices

The earth pressure cells were developed, designed and assembled at Tampere University of Technology. Their structure and main dimensions are illustrated in Figure 4.14. The cells on the piers were similar, only the diameter was smaller. The functional idea was to use strain gauges to measure strains from the 3 mm thick inner steel pipe (see Figure 4.15). Each cell was calibrated separately in laboratory conditions before the installation.

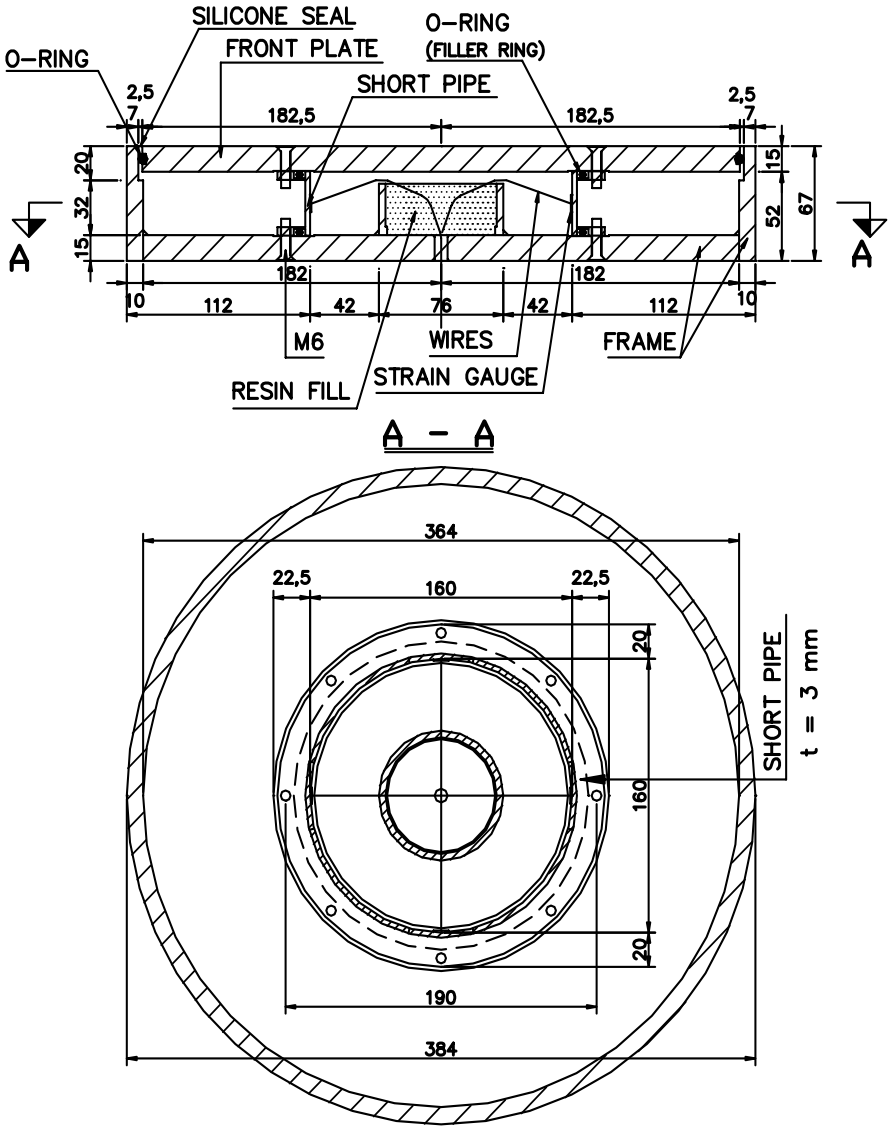

Figure 4.14 Abutment earth pressure cell (Laaksonen 2004).

Figure 4.15 Assembly of earth pressure cell. The cell is shown without a front plate.

Strain gauge bars

Strains were measured with a special strain gauge device manufactured at Tampere University of Technology. The basic setup of the device is the following:

- Reinforcement bar, diameter 16 mm and length 2 m.
- Strain gauges were installed to the smoothed centre of the bar (see Figure 4.16)
- To shelter the strain gauges they were covered with many separate layers of adhesive tape, sheet metal and silicon.

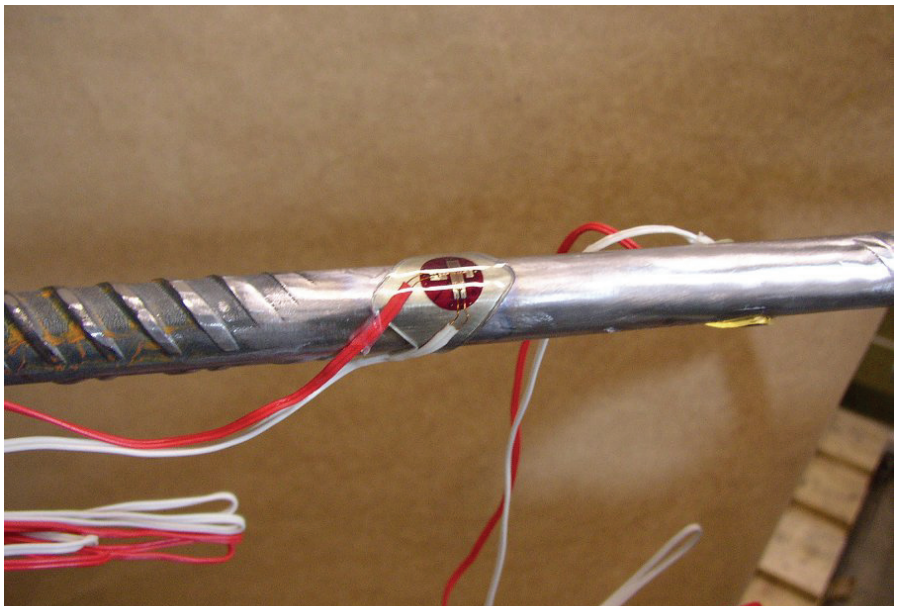

Figure 4.16 Strain gauge on the surface of a reinforcement bar.

Strain gauge bars were installed in the pier formwork outside the reinforcement (see Figure 4.17).

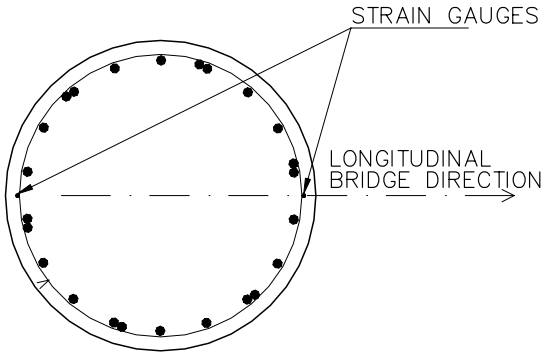

Figure 4.17 Strain gauge bars within the piers near the main reinforcement bars (Laaksonen 2004).

Strain gauge bars for the top and bottom of the deck slab were installed at support T3 and at the free span between supports T3 and T4 about 6 m from the abutment centre.

Strain gauges were installed on the surface of steel pipe piles under the eastern abutment at four levels. Distance between the levels was 2.5 meters. The highest strain gauge level was about 1.5 m below the abutment bottom. The strain gauges were sheltered by a horizontal L-shape steel profile (see Figure 4.18).

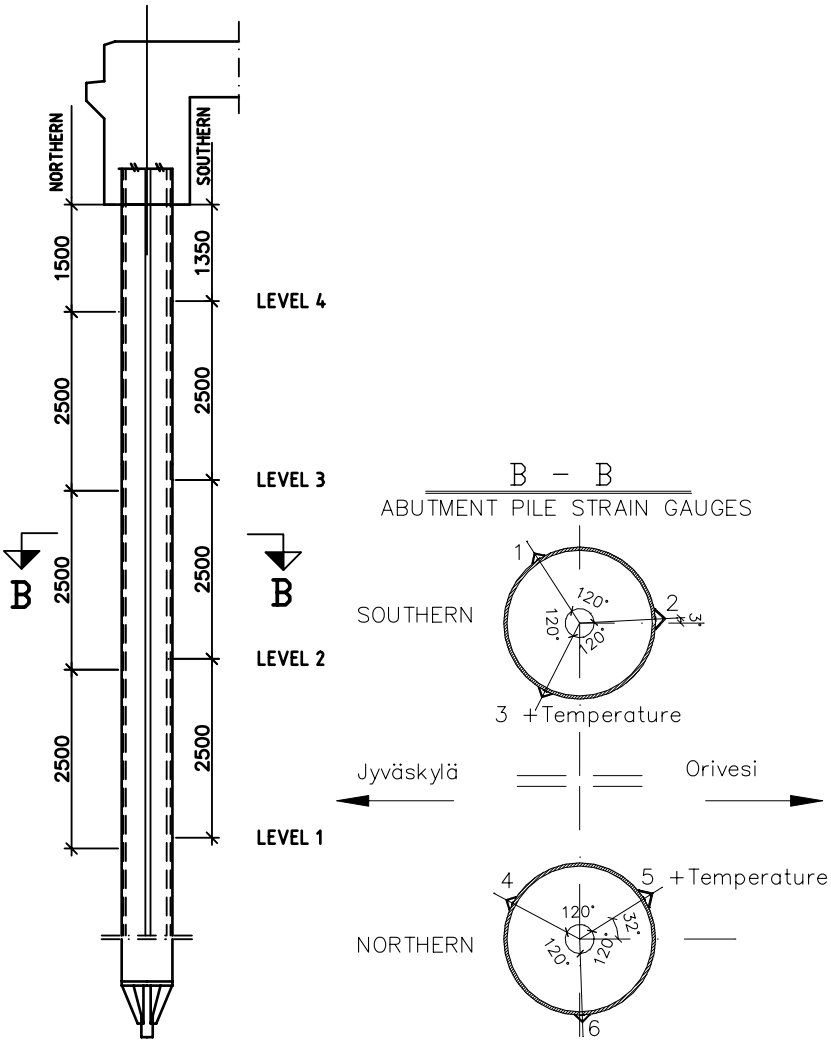

Figure 4.18 Strain gauges at four levels on the surface of steel pipe piles and temperature gauges under the eastern abutment (Laaksonen 2004).

Temperatures

Temperature gauges were installed in 150 mm long plastic tubes 10 mm in diameter. Each tube was filled with resin to shelter the gauge. Several temperature gauges were installed at the top, centre and bottom of the deck slab. Temperature gauges were installed also in the soil near the instrumented abutment piles and within the backfill behind both abutments in several layers (see Figure 4.19).

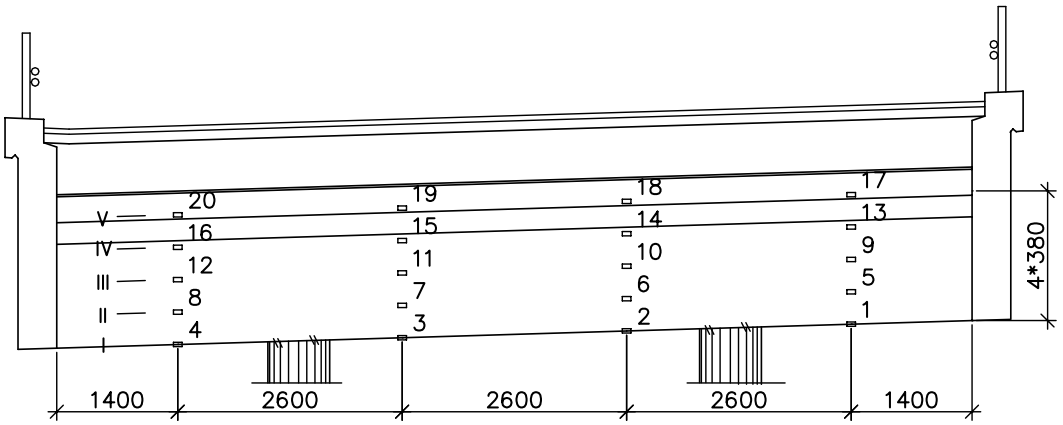

Figure 4.19 Temperature gauges 1–20 in embankment 2.4 m from the eastern abutment. The western embankment had eight temperature gauges (Laaksonen 2004).

Pre-processing of data

Altogether 191 channels are used to automatically collect data every 15 minutes. Some of the channels are used to check the voltage during the measuring.

All data are collected with data loggers to a computer at the bridge site. The data can be transferred automatically to a computer at the university through mobile phone equipment. For the analysis of the large database, a special Excel datasheet was prepared.

4.2.5 Field test results

The main results of the Haavistonjoki Bridge field tests are illustrated in the following figures. The focus is on the period between 11.2.–15.2.2004 when the greatest changes in bridge behaviour took place due to a large air temperature increase.

Figure 4.20 shows the measured earth pressure changes and measuring points.

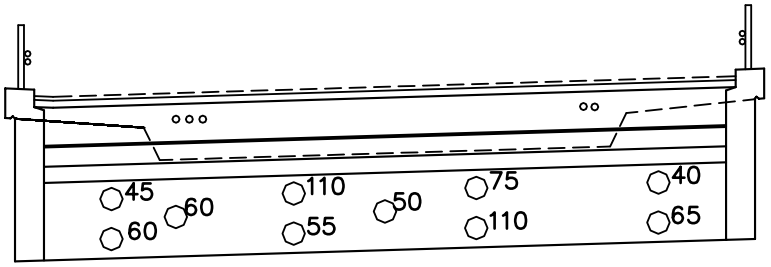

Figure 4.20 Measured earth pressure changes for bridge abutment T4 between 11.2.–15.2.2004 at earth pressure cells H–Q [kPa] (Kerokoski et al 2005a).

The average earth pressure change according to the five cells at the abutment centre was 80 kPa. The height of the vertical part of the abutment under the transition slab is only about 1.2 meters. There is a point of discontinuity both under the cells and directly above the cells. The bottom of the transition slab support is inclined. The bottom of the transition slab adjacent to the abutment is at a depth of 0.75 meters.

Observed earth pressures were smaller at the cells near the wing walls than at the centre of the abutment. The embankment is less stiff at the edges. In addition, the wing walls as rigid abutment members transferred part of the deformations and stresses into the embankment.

The distance from the earth pressure cells H, P, I, and Q to the inner surface of the wing wall is about 1 meter.

During the coldest period, all the earth pressures against the centre of abutment T4 were zero, and non-zero earth pressures were measured only at abutment T1 and near the wing walls at abutment T4. The probable reason for the observed lack of earth pressure was a gap at the abutment–soil interface during the coldest winter days. The gap was also verified manually with the movable steel plate and bar through the abutment. The movement of the plate between the soil and the abutment was observable but not large, that is, less than 1 mm.

Obviously, the general variation between individual earth pressure cells was a result of variations in soil density.

Figure 4.21 shows the earth pressure changes and deck temperatures during 10.2.–16.2.2004. The earth pressures during these six days followed temperature changes, increasing as temperature rose.

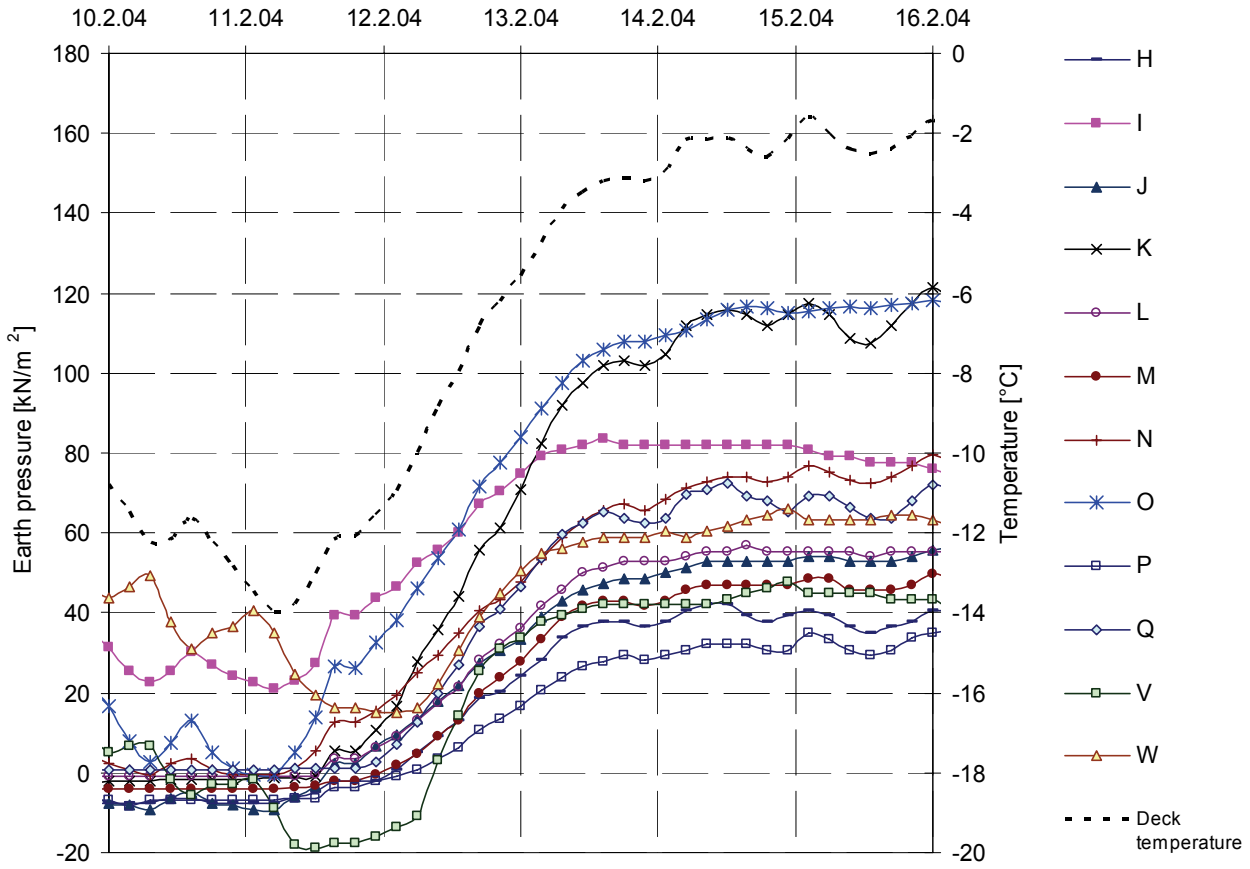

Figure 4.21 Measured changes in average deck temperature and earth pressures on bridge abutment between 10.2.–16.2.2004 at earth pressure cells H–W [kPa]. Cells V and W are located at abutment T1 (Kerokoski et al 2005a).

The average modulus of lateral subgrade reaction based on average earth pressure change and abutment behaviour during 11.2.–15.2.2004 at the five earth pressure cells in the centre of abutment T4 was k_{sT4} = 80 kN/m^2 / 5.2 mm = 15 MN/m^3. Correspondingly, the average modulus of lateral subgrade reaction at the abutment T1 was k_{sT1} = 57 kN/m^2 / 0.3

mm = 190 MN/m^3, which distinctly shows the difference between the stiffnesses at the opposite approach embankments.

Earth pressures were quite small during the first autumn after the construction of the bridge. According to Figure 4.22, earth pressure amplitude due to thermal displacement cycles increased clearly only after the coldest period of the winter in December 2003. The probable causes for the large earth pressure changes after that were the non-reversible deformations within the approach embankment. The observed temperatures in the abutment embankment, 2.4 meters from the abutment, were below zero (°C) only down to a depth of 1 meter from the surface on 1.2.2004 (see Figure 7.5). Certainly, the temperatures next to the earth pressure cells have been lower than the temperatures inside the massive embankment soil, and frozen soil has been stiffer than unfrozen soil.

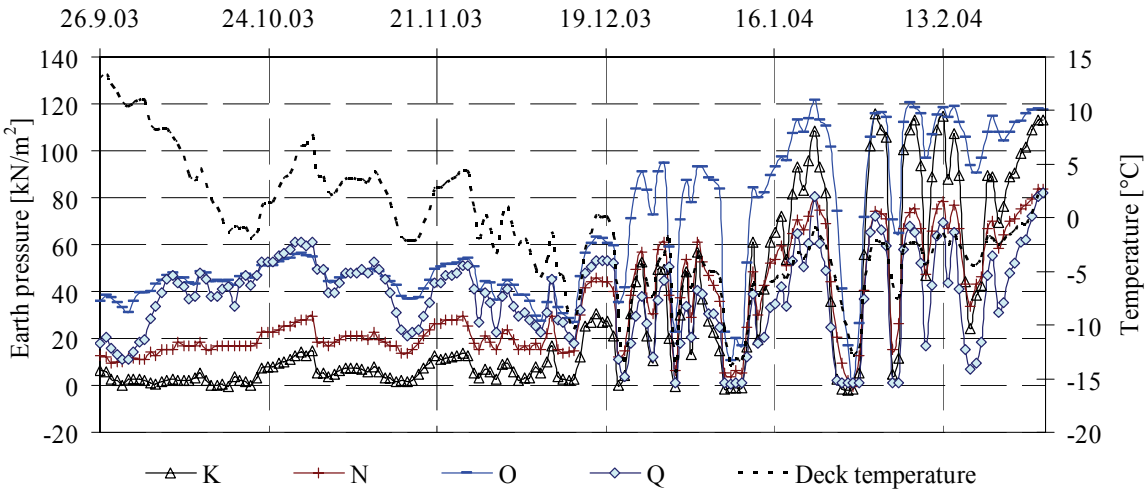

Figure 4.22 Measured changes in average deck temperature and earth pressures on bridge abutment at support T4 during 26.9.2003–29.2.2004.

According to Figure 4.23, earth pressure changes at support T1 remained small also during 1.3.2004–31.8.2004, and the observed pressure level was quite steady. Yet, the lateral subgrade reaction coefficient at abutment T1 was greater due to the much smaller longitudinal abutment displacement. At support T4 after 1.4.2004 the adjacent earth pressure cells L and O at the lower centre of the abutment began to act similarly. The lowest earth pressures during the summertime at support T4 were at the edges of the abutment, that is, at earth pressure cells H, I, P and Q. The highest earth pressures did not develop in the middle of the summer of 2004 but in May and August. Pressure was higher even in the middle of March before the embankment started to warm up than in mid-summer (see also App. 3).

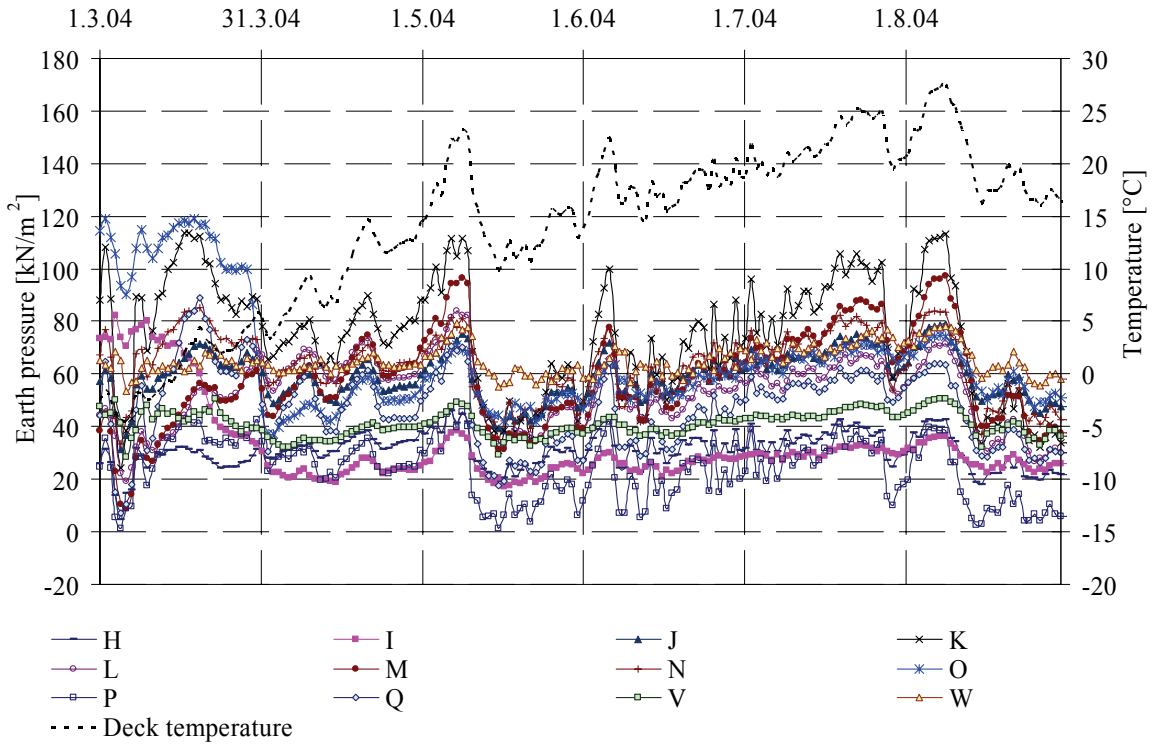

Figure 4.23 Measured changes in average deck temperature and earth pressures on bridge abutments at midnight during 1.3.2004–31.8.2004. Cells V and W are located at abutment T1.

During winter 2004/2005, the observed earth pressure changes during large deck temperature changes were a little smaller than a year before. Consequently, the embankment soil under the transition slab did not get more compacted and stiffer after the cyclic movement of the soil nor did the soil return completely to its original location. That can be stated based on the observations of the abutment movement and the corresponding earth pressures.

The starting point for all the measured values was 3.10.2003 at 00.00 hours, and all the measured changes after that are compared to values of that date. Consequently, the absolute values from the presented measurement periods may be negative or especially high compared to the values at 3.10.2003. In those cases only the variations are relevant. The observations revealed some drift in strain gauges on steel pipe piles and some reinforcement bars. Consequently, only the short time observations are reliable, not the exact values over long time periods.

Figure 4.24 illustrates the measured horizontal abutment displacements at support T4 below the transition slab and the corresponding earth pressure changes at pier T3. The earth pressure increase varied between 16–20 kPa at cells F and G during 11.2.–15.2.2004.

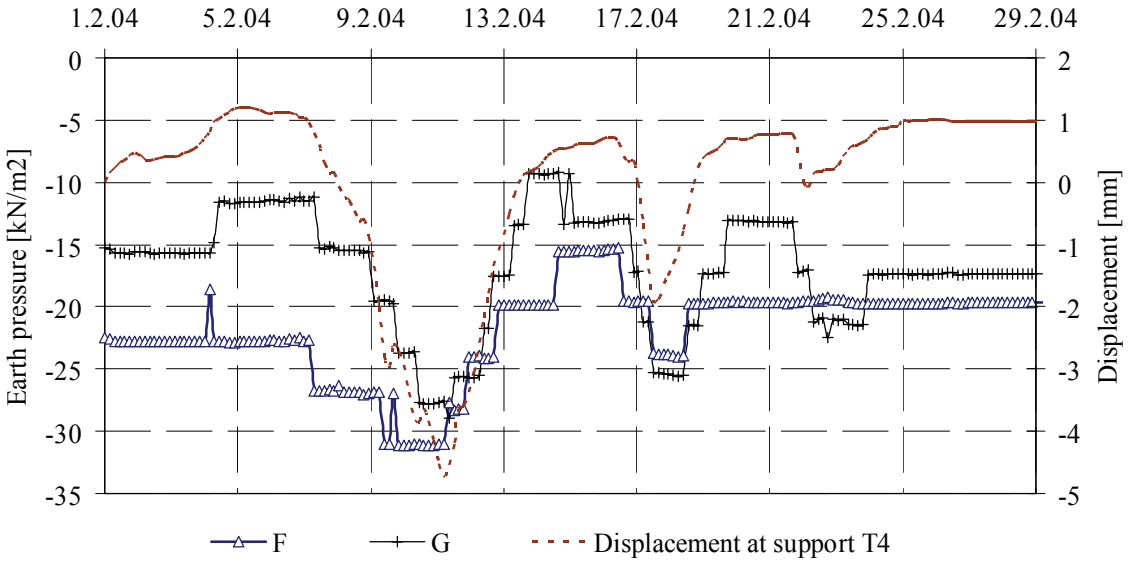

Figure 4.24 Measured horizontal abutment displacements at support T4 under the transition slab and corresponding earth pressure changes at Haavistonjoki bridge pier T3 in February 2004 (Kerokoski et al 2005a).

Figure 4.25 illustrates the measured stress variation on the surface of the steel pipe pile during February 2004 at support T4. The absolute stress values must be disregarded. The pile was the northern one. Level III was located 4 meters under the abutment bottom (cf. Figure 4.18). The observed stress change in steel pipe pile during 11.2.–15.2.2004 was $\Delta\sigma$ = 14 MPa.

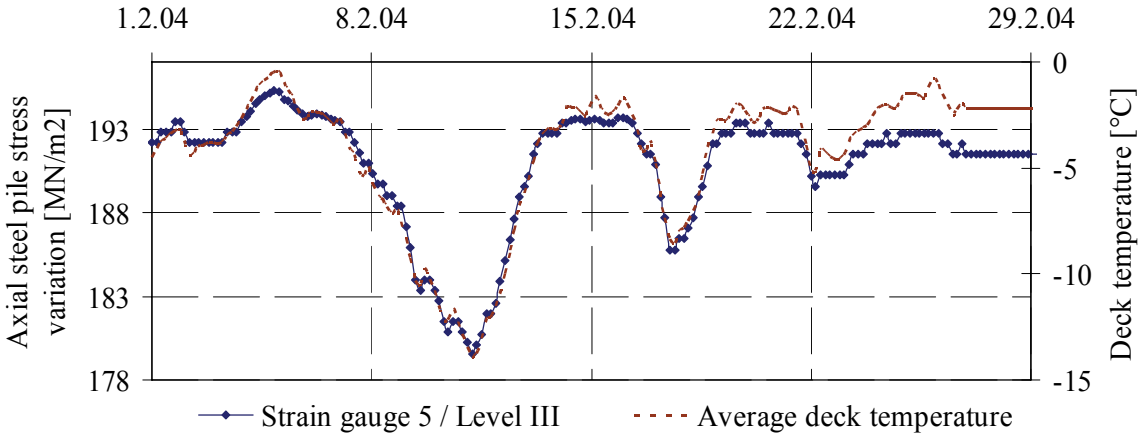

Figure 4.25 Strain variation on the surface of steel pipe pile during February 2004 and corresponding deck temperatures (Kerokoski et al 2005b).

The observed stress change in steel pipe pile at support T4, location 2, level II during 11.2.–15.2.2004 was $\Delta\sigma$ = 8 MPa. The pile was the southern one. Level II was located 6.35 meters under the abutment bottom. In spite of these logical observations, all strain gauges on piles did not function properly and large long-time drifts were observed. It is recommended that the strain gauges of subsequent field tests be installed within the piles near the main reinforcement bars.

The manually measured displacements during 18.9.2003.–22.4.2004 at support T4 are illustrated in Figure 4.26.

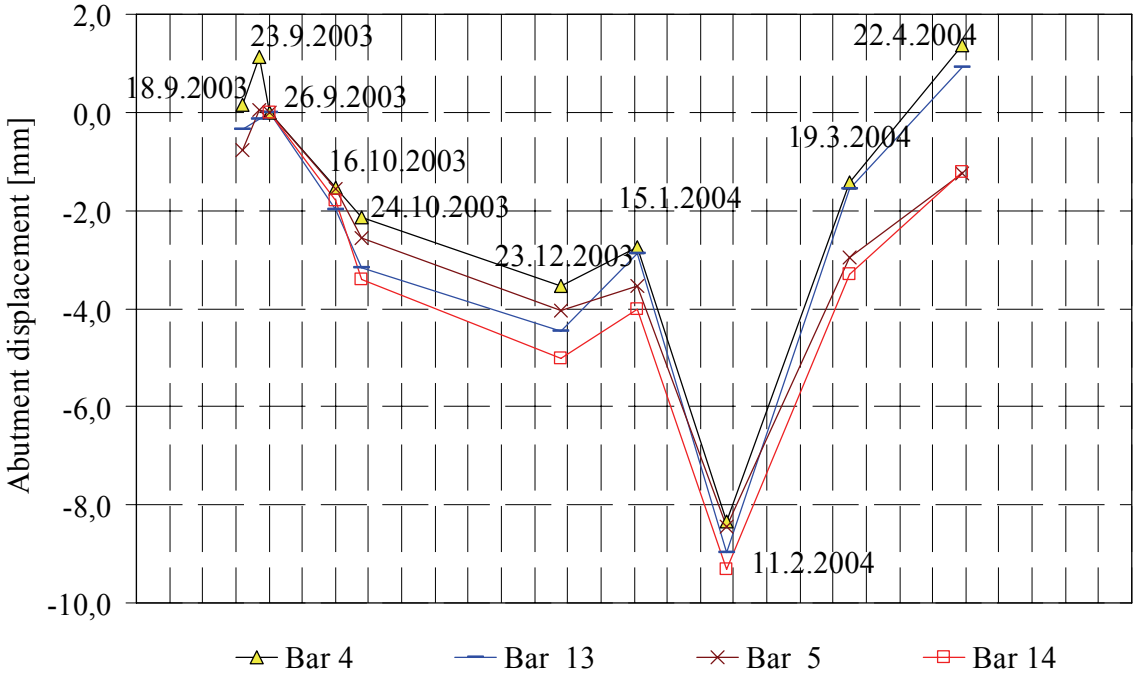

Figure 4.26 Measured displacements on two levels at support T4 during a seven-month observation period (Laaksonen 2004).

Bar 4 is located above bar 5 and bar 13 above bar 14; the vertical distance between them is 1210 mm.

Abutment displacement changes according to measuring bars 4, 5, 13 and 14, respectively:

- during 15.1.2004–11.2.2004: -5.6, -4.9, -6.1 and -5.3 mm.
- during 11.2.2004–19.3.2004: +6.9, +5.5, +7.4 and +6.0 mm.

Abutment rotations at locations 4 (5) and 13 (14), respectively:

- during 15.1.2004–11.2.2004 horizontal displacement changes were -0.7 mm and -0.8 mm and rotation changes were -1/1729 and -1/1513,
- during 11.2.2004–19.3.2004 the horizontal displacement change was +1.4 mm and the rotation change was 1/864.

Abutment rotations over long time periods have been observed also in field tests outside Finland (see App. 9 / Figure 0.2; Huang et al 2004). On the other hand, opposite observations and conclusions have also been presented. According to (Frosch et al 2005), the abutment primarily translates or "slides" longitudinally in response to thermal expansion and contraction of the bridge. Only minor rotations of the abutment occur and according to (Frosch et al 2005), these can be ignored in analyses. The slender piles were integrally connected with the abutment and bent in double curvature, and the horizontal response and structural stiffness of the piles were much smaller than those of the abutment.

The measured average deck temperatures at Haavistonjoki Bridge were:

- on 15.1.2004: -3.2 °C, on 11.2.2004: -12.2 °C, and on 19.3.2004: +2.5 °C
  - ⇨ temperature difference during 15.1.2004–11.2.2004 was -9.0 °C,
  - ⇨ temperature difference during 11.2.2004–19.3.2004 was +14.7 °C.

During 11.2.–15.2.2004 the average deck temperature increased 12°C, which should have caused the whole bridge structure length, about 50 meters, to increase 6 mm. Yet, the measured displacement 750 mm above the abutment bottom at support T4 was 5.4 mm. Thus, thermal expansion was not at all symmetrical, and displacements due to thermal expansion at opposite abutments varied remarkably. Abutment T1 was much stiffer than abutment T4, and occasionally the expansion length of a 50 m long bridge was more than 40 meters (see Figure 4.27). Accordingly, Haavistonjoki Bridge was an appropriate choice for field tests considering the abutment–soil behaviour, although the total length of the bridge was not large.

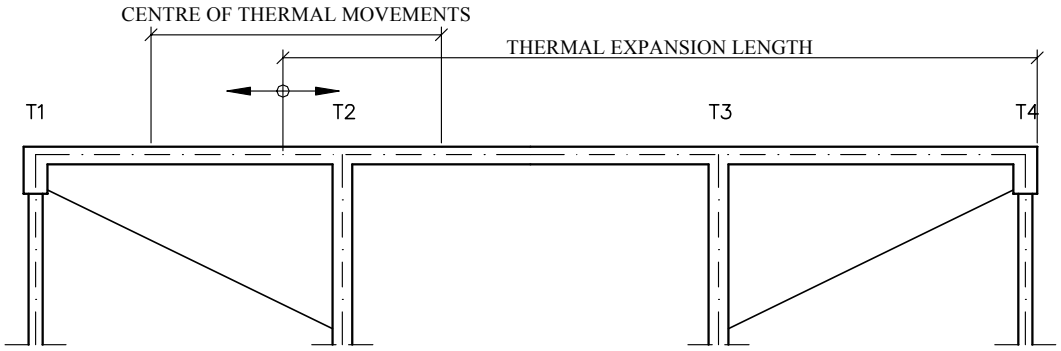

Figure 4.27 Variation of position of centre of thermal expansion.

Non-symmetrical thermal expansion of a symmetrical bridge superstructure has been observed also in field tests outside Finland (see e.g. App. 9 / Figure 0.10; Abendroth & Greimann 2005).

Stress changes in vertical reinforcement at intermediate support T3 are presented in Figure 4.28. Bars 2 and 17 are located 1.1 m below the deck bottom and bars 3 and 4 are 9.5 m below the deck bottom within surrounding soil. Bars 2 and 4 are at the eastern side of the pier and bars 3 and 17 at the opposite side (see Figure 4.8). The largest reinforcement stress variation based on deck temperature increase and consequent deck expansion occurred during 11.2.–15.2.2004, when also the tension and compression stresses corresponded to the typical bending moment in this kind of frame structure. During the observed smaller temperature changes, the effects of slow temperature changes at the pier intersection also have to be considered in pier behaviour evaluation.

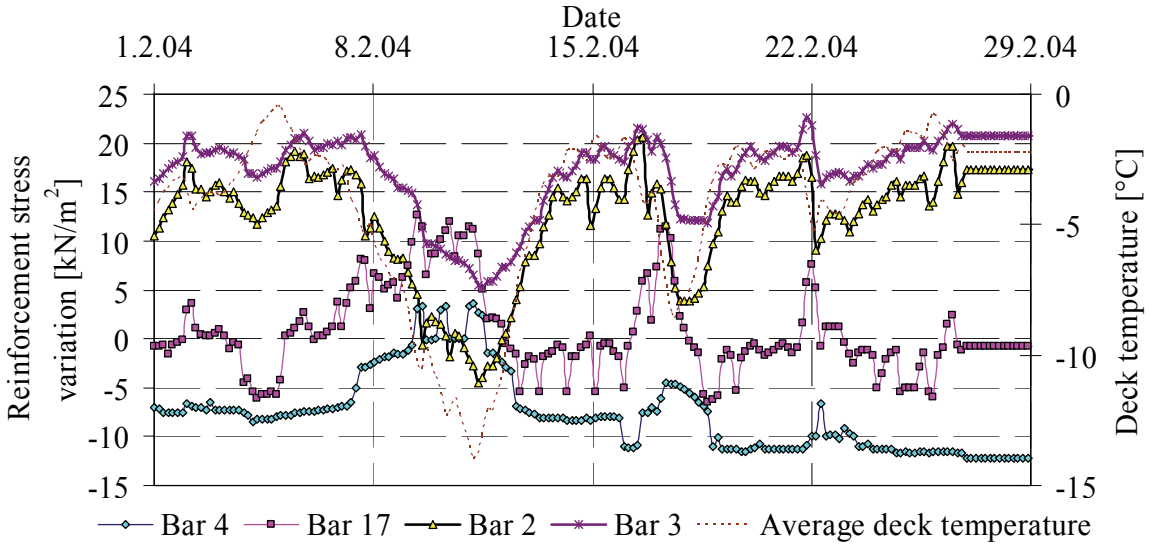

Figure 4.28 Variation in reinforcement bar stresses in northern pier at support T3 (Kerokoski et al 2005b).

During 11.2–15.2.2004 the measured stress changes in vertical reinforcement bars 1.1 m below the deck bottom within the piers at intermediate support T3 were:

- Bar 2: $\Delta\sigma_s = +18$ MPa,
- Bar 8: $\Delta\sigma_s = +10$ MPa,
- Bar 17: $\Delta\sigma_s = -14$ MPa,
- Bar 7: $\Delta\sigma_s = -12$ MPa.

Bars 2 and 8 are in adjacent piers on the abutment T4 side and bars 17 and 7 are in the same piers on the middle span side, respectively. The average of the absolute values was 13.5 MPa. The corresponding absolute concrete stress change near the reinforcement bars was $\Delta\sigma_c = 2.0$ MPa.

The comparison based on three separate 3D spring models and FEM software code is presented in the following chapter. The 2-dimensional modelling of Haavistonjoki Bridge, which also includes the transition slab, is presented in Chapter 6.3.2.

The transition slabs were connected to the abutments with dowels that permitted small horizontal movements. Based on the observed behaviour, the studied transition slab was an integral part of the approach embankment and did not move cyclically along with the abutment.

Stress changes in vertical reinforcement near the outer surface of eastern abutment, support T4, and corresponding deck temperatures are presented in Figure 4.29.

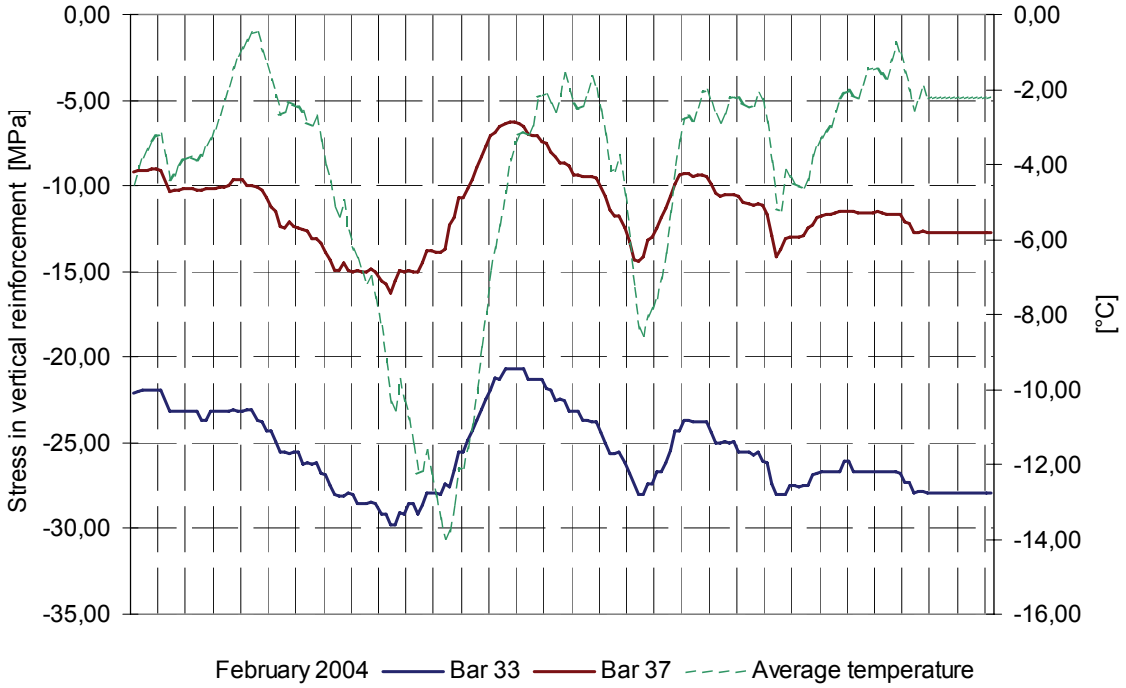

Figure 4.29 Stress changes in vertical reinforcement at eastern abutment in February 2004. Bar 33 (lower diagram in figure) is situated above a pile and bar 37 at the centre of abutment. Stresses began from zero on 3.10.2003 (Laaksonen 2005).

According to the above diagram, the observed stress change in the reinforcement bar during 11.2.–15.2.2004 was:

Average stress change = $\Delta\sigma_s$ = 7 MPa.

The stress change in concrete adjacent to the reinforcement bar is (E_c / E_s) * $\Delta\sigma_s$ = (31,623/210,000) * 7 MPa = 1.05 MPa. The corresponding bending moment at an uncracked concrete intersection would be M = σ_c*I_c/y_c = 1050 kN/m^2 *0.144 m^4/m /0.55 m = 280 kNm/m.

Conclusions

The Haavistonjoki Bridge was extensively instrumented in the summer of 2003. The data of most of the gauges was collected every 15 minutes after construction finished. Long-term follow-up of the bridge behaviour will continue at least until 2008.

Almost all the gauges were functioning correctly during shorter observation periods and many, for instance all earth pressure cells, functioned correctly throughout the entire observation period. The results of field test measurements were reliable and logical according to verifications based on several 3D and 2D FEM calculations (see Chs. 4.2.6 and 6.3.2), considering also the effect of the transition slab. According to observations and corresponding calculations, large and cyclic displacements at the bridge abutment create large and partly non-reversible deformations in the approach embankment fill. Although the bridge structures seem to be able to sustain the earth pressures, the decision on maximum expansion length should be based primarily on the long-term behaviour of the approach embankment.

During the coldest period, all earth pressures against the centre of the abutment were zero. The reason for the observed lack of earth pressure was the gap at the abutment–soil interface during the coldest winter days. The manually measured gap was about 0.5 mm.

The average earth pressure change during five days in February 2004, according to the five cells at the abutment centre, was 80 kPa. The measured earth pressures on the bridge abutments were quite high because the backfill was well compacted (cf. Chs. 4.2.6 and 6.3.2). The earth pressures were smaller at the cells near the wing walls than at the centre of the abutment (cf. App. 8).

The highest earth pressures were not observed in the middle of the summer but in May and in August – even in the middle of March – before the embankment had begun to get warm.

Displacements at opposite abutments due to thermal expansion varied remarkably because of different approach embankment stiffnesses. Occasionally, the longer expansion length of a 50 metre long bridge was more than 40 metres.

The bending moment of a large-diameter abutment pile was clearly related to the horizontal movement of the abutment. The stress changes in vertical reinforcement at an intermediate support supported the conclusions based on other observations.

The field test project is still unfinished (May 2006). The remaining field tests of the ongoing project will concern, for instance, skew abutments, long-term behaviour of an integral bridge, and bridge behaviour during vehicle braking (tested on Haavistonjoki Bridge in October 2005, report unpublished in May 2006).

4.2.6 Comparison based on 3D spring models and FEM

3D models with 1- and 2-dimensional structural elements

Three 3-dimensional calculation models of Haavistonjoki Bridge were made using either linear or non-linear springs to model both abutment–soil interaction and pile–soil interaction with Abaqus FEM software code (Abaqus 2001). The purpose of these conventional 3D calculations was to compare the results with measured values and with the results of a more advanced model (see Ch. 6.3.2).

The models were symmetrical in both horizontal directions and they comprised a quarter of the total bridge (see Figure 4.31). In the first case, the soil was modelled with linear springs (see Figure 4.30) using the same analysis principals as the bridge designer. In the other two cases non-linear springs were used (see App. 2); in Case 2 the approach fill soil

properties were determined according to typical dense non-cohesive soil and in Case 3 according to large-scale cyclic tri-axial test (see Figure 4.6).

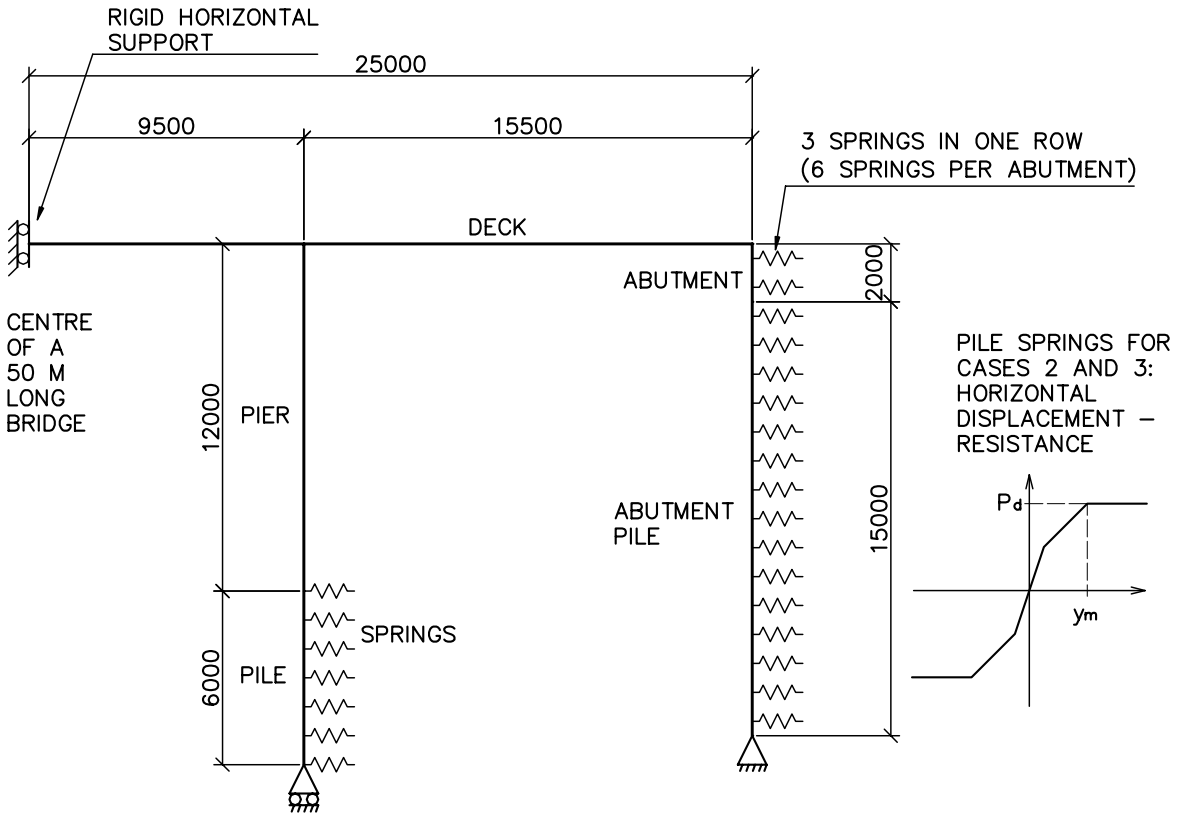

Figure 4.30 Structural model of Haavistonjoki Bridge with linear and non-linear springs. Transition slabs were not included. Side view.

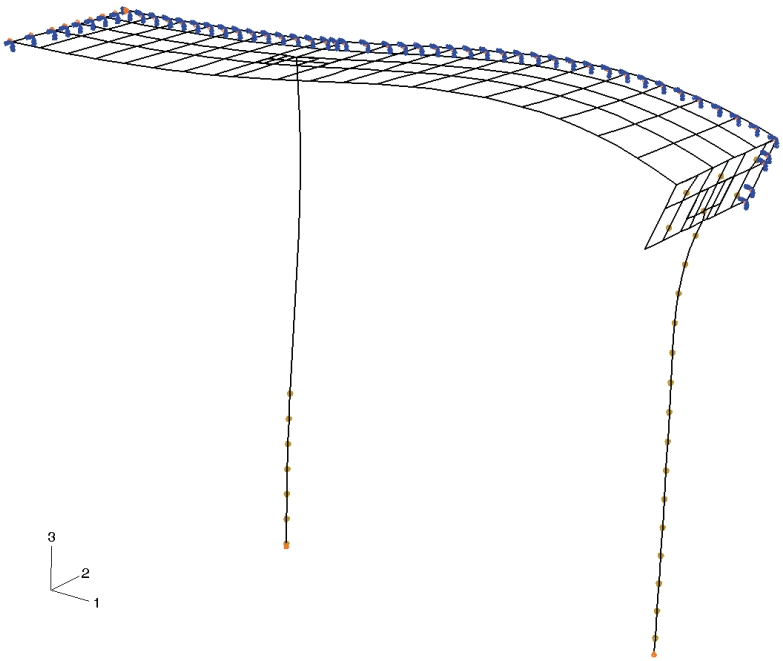

Figure 4.31 Structural model of Haavistonjoki Bridge with supports at both symmetric axles and connector elements at abutment and piles. The connector elements are special spring elements by Abaqus (Abaqus 2001). Deformations according to Case 2.

The deck slab temperature change was adjusted so that the abutment displacement at support T4 and depth 1.7 m was 5.4 mm corresponding to the displacement change measured during 11.2.–15.2.2004 at support T4. In Cases 1 and 2 the used deck temperature change was 31°C and in Case 3 it was 34.5°C. The used temperature changes were bigger than the measured value, for instance, because of the different location of the expansion centre. The temperature change in the pier was 12°C.

3D model analysis, Case 1

Case 1 is based on linear springs and a common Finnish design procedure. Accordingly, the lateral coefficient of subgrade reaction was n_h = 7.5 MN/m^3 and passive earth pressure coefficient was K_p = 4.2, both based on the friction angle ϕ = 38° taken from (Finnra 1999c). Hence, in Finnish practice lateral pile stiffness calculations are based on the soil strength parameter ϕ instead of the modulus of elasticity of soil. Below the ground water table, n_h is estimated to be 60 per cent of the standard value.

The effective unit weight of the soil around the piles and in the approach embankment was γ' = 21 kN/m^3. The soil was estimated to consist only of non-cohesive soil because of soil replacement. The material data on moraine were based on Finnish design guidelines.

The used modulus of lateral subgrade reaction was $k_s = n_h * z / d$. The corresponding pier pile spring constants were $k = k_s * d * s = n_h * (z / d) * d * s = 6.75*z$ [MN/m] down to depth $z = 10*d = 7$ m, as $n_h = 0.6 * 7.5 = 4.5$ MN/m^3 and s = 1.5 m. Displacements with these values were limited to $y_m/4 < 0.031$ m. The factor 0.6 was used because of the high groundwater level below the piers.

Abutment pile lateral spring constants were $k = n_h * (z / d) * d * s = 11.25*z$ [MN/m] down to depth $z = 10*d = 7$ m. Displacements were limited to $y_m/4 < 0.018$ m.

Passive earth pressure distribution against the abutment was estimated to be triangular with a total force:
$P = 0.5 * K_p * \gamma * H^2 * B = 0.5 * 4.2 * 21$ kN/m^3 * (2.4 m)^2 * 11.5 m = 2921 kN.

Passive earth pressure against the abutment was estimated to develop in dense non-cohesive soil after horizontal displacement $\delta = 0.002 * H = 0.002 * 2.4$ m = 0.0048 m (Finnra 1999a). Hence, the horizontal spring for the whole abutment was $k = P / \delta$ = 608 MN/m. Abutment height in these FEM calculations was 2 m. The modulus of lateral subgrade reaction used for the upper half of the abutment was k_s = 15.9 MN/m^3 and for the lower half k_s = 37.1 MN/m^3.

3D model, Case 2

In Case 2 the lateral subgrade reaction and ultimate resistance were evaluated according to design guidelines for non-cohesive soils and field survey results for cohesive soils.

The modulus of elasticity for the crushed rock was E_d = 80,000 kPa which was taken from Finnish guidelines (Finnra 1999a / Table 2) for very dense non-cohesive soil. In the case of cohesive soil layers, the proper soil springs for the piles were found by vane tests (see Ch. 4.2.2).

Lateral resistance next to piles and abutment was modelled with non-linear springs (see App. 2).

The ultimate values of lateral pile resistance and pressure p_m in cohesive soil can be estimated with the equation (Finnra 1999c):

$p_m = 6–9 * s_u$,

where s_u = undrained shear strength [kN/m^2]. In this case the used factor was 7.5 (Koskinen 1997).

In long-term loading, the approximation of the modulus of lateral subgrade reaction of the cohesive soil is $k_s = 50*s_u/d$ (Finnra 1999c), where the factor 50 corresponds to low displacement, in other words less than ¼ of the displacement at the beginning of ultimate lateral resistance.

The ultimate values of lateral pile resistance and pressure p_m in non-cohesive soil can be estimated with the equation (Finnra 1999c):

$p_m = 4.4 * \gamma' * z * K_p$,

where γ' = effective unit weight [kN/m^3],
z = depth [m],
K_p = passive earth pressure coefficient at studied depth.

The horizontal resistance of a pile in non-cohesive soil according to the Finnish practice is illustrated in Figure 4.32. Up to earth pressure level $p_m/2$, or displacement level $y_m/4$, the following linear relation is valid: $p_m/2 = k_s * y_m/4$.

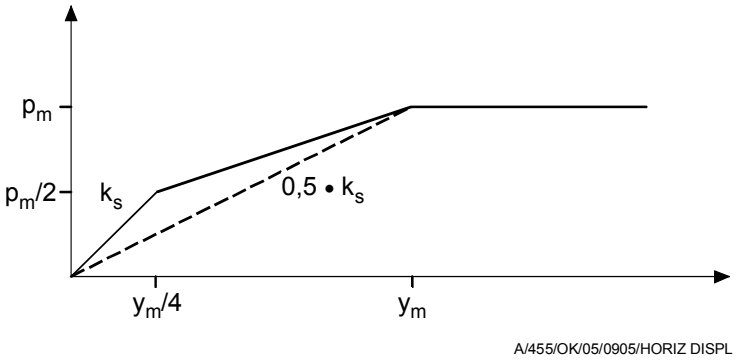

Figure 4.32 Horizontal displacement based on subgrade reaction to large-diameter piles. p_m = ultimate limit of horizontal resistance, y_m = corresponding displacement (Finnra 1999c).

The modulus of lateral subgrade reaction at a certain level for a pile was estimated by the equation $k_s = n_h * z / d$, and the corresponding pile spring constant was estimated by the equation $k = k_s * d * s = n_h * (z / d) * d * s$ down to depth $z = 10*d$ (Finnra 1999c).

In the case of small displacement, the lateral behaviour of the piles is defined by the modulus of lateral subgrade reaction, k_s, and in case of large displacement by the ultimate lateral resistance of piles, p_m.

The abutment pile spring values at support T4 (see App. 2) were based on equations $P_d = p_m * d$, $p_m = 4.4 * \gamma' * z * K_p$ and $d = 0.711$ m. The input values at the upper soil layers were based on internal friction angle $\phi = 42°$ which was taken from Finnish guidelines

(Finnra 1999a / Table 2) for very dense non-cohesive soil. Displacements corresponding to ultimate values of lateral resistance in non-cohesive soil were: $y_m = 2*p_m/ k_{s,\phi}$ and in cohesive soil: $y_m = 2.5*p_m/ k_{s,c}$.

The intermediate pier T3 pile spring values are also presented in Appendix 2. The presented values for the upper soil layers are also based on the internal friction angle ϕ = 42°. Ground water table is estimated to be above depth z = 3 m.

The lateral coefficient of subgrade reaction for the piles, n_h, could also have been estimated by the modulus of elasticity of drained soil, E_d (Finnra 1999c):

- $n_h = \alpha * E_d / z$, where $\alpha = 0.74$ (Terzaghi) or $\alpha = 1.0$ (Poulos) and z = depth.

- Thus, the modulus of lateral subgrade reaction (see Figure 4.32) can be calculated from: $k_s = n_h * z / d = \alpha * (E_d / z) * (z / d) = \alpha * E_d / d$, where E_d depends on the stress level within the soil, that is, from the depth.

- The spring constant, k, can also be estimated by E_d:
  $k = k_s * d * s = \alpha * E_d * s$ = (0.74 or 1.0) * E_d * s, where s is the distance between individual springs.

3D model, Case 3

In Case 3 lateral subgrade reaction and ultimate resistance were evaluated on the basis of laboratory tests for non-cohesive soils and field survey results for cohesive soils. The modulus of elasticity of crushed rock was E_d = 250,000 kPa which corresponds to resilient modulus in a large-scale cyclic tri-axial test at a low stress level (see Figure 4.6).

The abutment pile spring values based on friction angle ϕ = 45° are presented in Appendix 2. The friction angle was also a tested value (see Ch. 4.2.2).

The intermediate pier T3 pile spring constant values are the same as in Case 2.

Horizontal abutment spring properties

In Cases 2 and 3 the relation of half of the passive earth pressure to the abutment and the corresponding displacement were estimated by the equation (Bolton 1993; see App. 2):

$\delta_{0.5p} = 0.5*p_p/(E_d/H)$.

The horizontal abutment spring properties are presented in a table in Appendix 2 and in Figure 4.33.

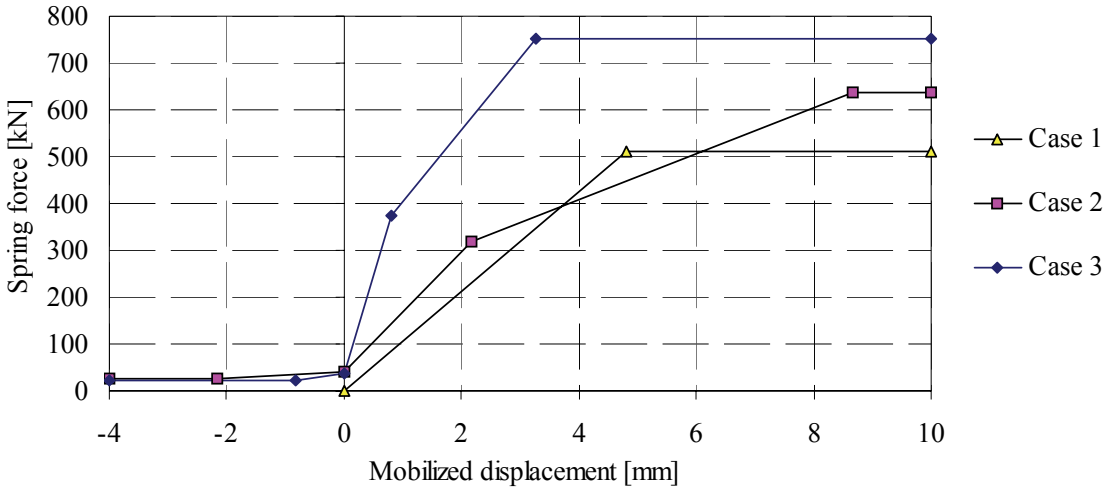

Figure 4.33 Abutment spring properties for breadth B = 1.833 m and total height H = 2.5 m. Displacement–force relations.

Calculation results

The main results from the three 3D models of Haavistonjoki Bridge are presented below. The comparisons are based on observed Haavistonjoki Bridge behaviour during 11.2.–15.2.2004.

Bending moments in abutment and deck

The bending moments in the abutment and deck in Case 2 are illustrated in Figure 4.34.

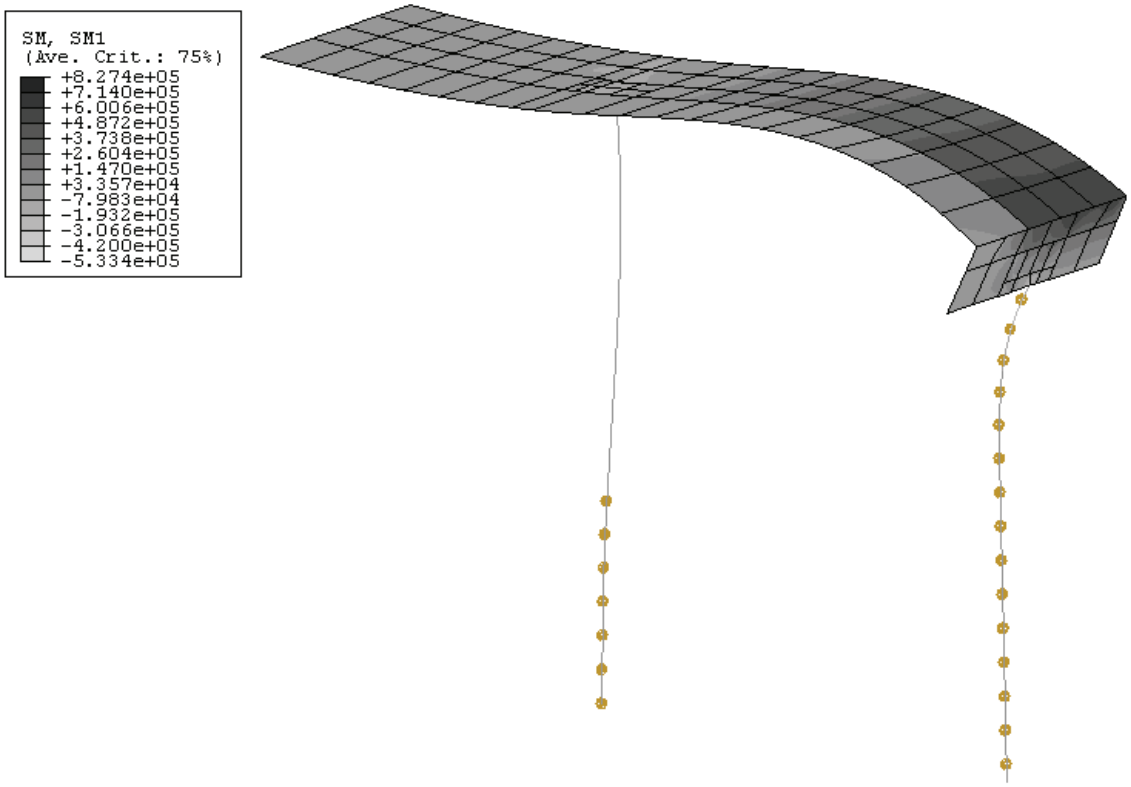

Figure 4.34 3D calculation model with non-linear springs (see dots at piles). Haavistonjoki Bridge bending moments in Case 2.

At the 860 mm thick deck–abutment joint, the average bending moments were:

- Case 1: M = 490 kNm/m,
- Case 2: M = 530 kNm/m,
- Case 3: M = 710 kNm/m.

At Haavistonjoki the bending moment at the deck-abutment joint was not measured.

The bending moment changed rapidly along the abutment height. In all three cases the moments were negative at the abutment–pile joint in contrast to the positive centre level values of Table 4.2.

Table 4.2 Bending moments at abutment centre level, i.e. 1.25 m from the abutment bottom [kNm/m].

Case 1		Case 2		Case 3	
Above the pile	Abutment centre	Above the pile	Abutment centre	Above the pile	Abutment centre
167	191	253	228	268	288

According to measurements, the corresponding average bending moment was 280 kNm/m. Consequently,stiff abutment springs, Case 3, modelled best the behaviour of Haavistonjoki Bridge in this respect.

Steel pipe pile stresses at depth z = 6.25 m

In Table 4.3 the calculated moments, resultant angles and vertical stresses at the steel pipe pile below the abutment at support T4 at depth z = 6.25 m are presented. The corresponding measured pile stress change was 14 MPa. Thus, Case 2 showed best correspondence. The other two cases were also quite close to the measured value considering the non-linear soil behaviour.

Table 4.3 Pile stress calculation results. Depth z = 6.25 m. Cases 1–3.

	Case 1	Case 2	Case 3
$M_{Longitudinal}$ [kNm]	162	150	122
$M_{Lateral}$ [kNm]	46	25	11
$M_{Resultant}$ [kNm]	168	152	122
Resultant direction angle [°]	16	9	5
Angle between resultant and gauge number 5 [°]	16	23	27
Gauge distance from perpendicular line to resultant through pile centre [mm]	341	327	316
Stress in pile at gauge 5 [MPa]	16	14	11

In Case 2, gauge number 5 was 23° off the bending moment resultant direction. The angle between the resultant and the bridge's longitudinal direction was 9°. The corresponding angles for other cases are presented in the previous table. The angle between gauge number 5 and the bridge's longitudinal direction is 32° according to Figure 4.35.

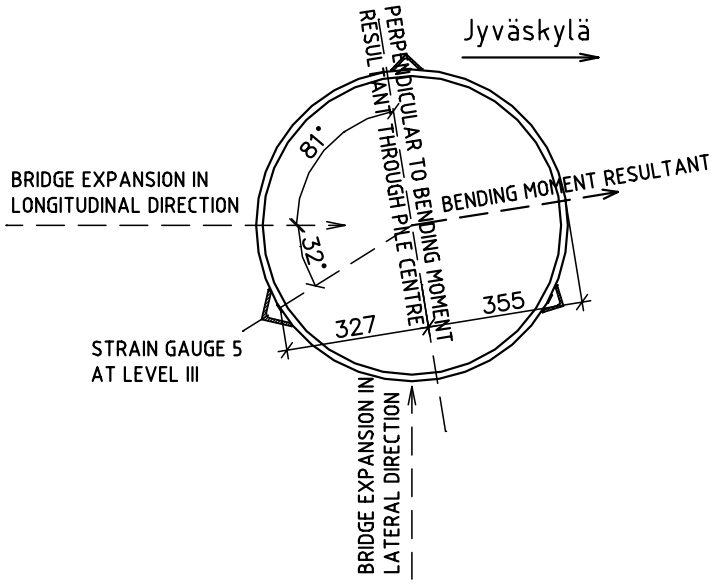

Figure 4.35 Pile cross section, bending moment resultant and strain gauge number 5. Bending moment resultant in Case 2.

The stresses due to the bending moment resultant and its direction in respect to the strain gauge location were calculated from the equation:

$\Delta\sigma_{steel} = M_{Resultant}*\delta_5*E_s/(EI_{total\ pile})$,

where $M_{Resultant}$ = bending moment resultant,
δ_5 = gauge distance from perpendicular line to resultant through pile centre,
E_s = modulus of elasticity of steel,
$EI_{total\ pile}$ = E*I of the steel pipe pile filled with reinforced concrete.

For example, in Case 2 at depth z = 6.25 m the stress in the pile at gauge 5 was $\Delta\sigma_{steel}$ = 152*0.327*210,000/754 = 14 MPa.

Steel pipe pile stresses at depth z = 8.75 m

In Table 4.4 the calculated moments, resultant angle and vertical stress at the steel pipe pile below the abutment at support T4 at depth z = 8.75 m are presented. The corresponding measured pile stress change was 8 MPa.

Table 4.4 Pile stress calculation results. Depth z = 8.75 m. Cases 1–3.

	Case 1	Case 2	Case 3
$M_{Longitudinal}$ [kNm]	54	8	-16
$M_{Lateral}$ [kNm]	5	1	-12
$M_{Resultant}$ [kNm]	54	8	20
Resultant direction angle [°]	5	6	38
Angle between resultant and gauge number 2 [°]	8	9	41
Gauge distance from perpendicular line to resultant through pile centre [mm]	352	351	270
Stress in pile at gauge 2 [MPa]	5	1	1

Case 1 corresponded best to the measured stress. Separate springs were too stiff compared to the real soil stiffness in the deep soil layers (see also Figure 4.36). In this kind of a 3-dimensional structure, the different soil layers do not support the pile separately from each other and independently of abutment behaviour. Consequently, the presented separate springs did not represent soil behaviour correctly, at least deep below the abutment (Cf. Figure 4.36).

Bending moments and shear forces

Bending moments (see Figure 4.36) and shear forces (see Figure 4.37) along the abutment pile are illustrated in the following two figures. The observed bending moments, calculated from the vertical strains on the steel pipe presented on previous pages, are also shown.

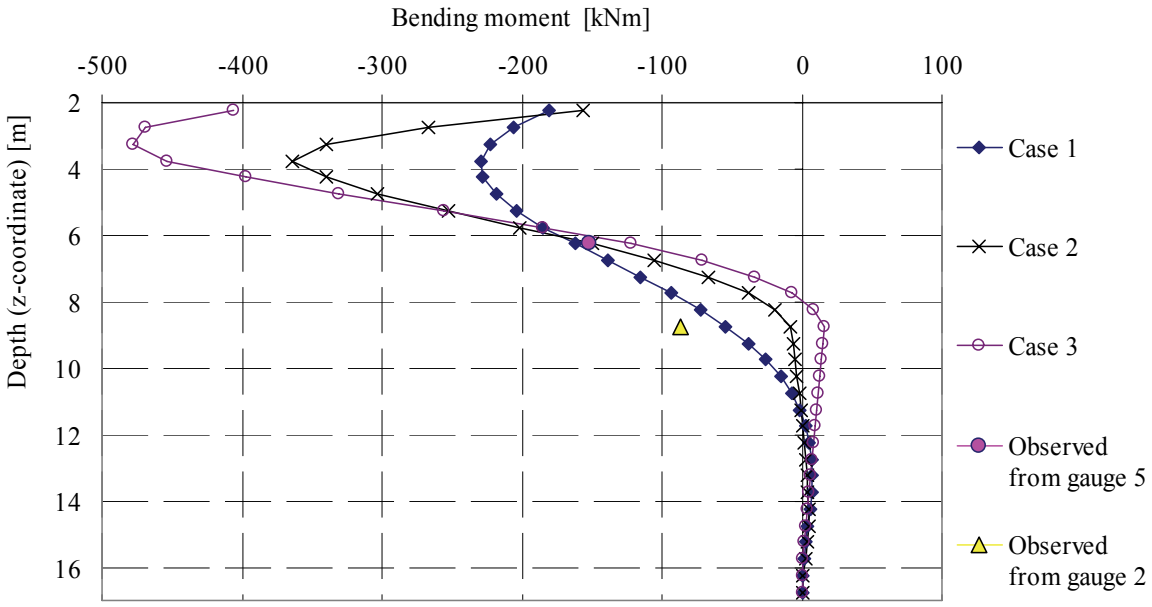

Figure 4.36 Bending moments at abutment pile in bridge longitudinal direction.

If the rigid soil spring model, Case 3, describes the soil behaviour correctly, the maximum bending moment at depth z = 3m is 480 kNm and the corresponding maximum stress change on the surface of the pile about 42 MPa. Accordingly, there would be no excessive stresses in these large-diameter piles. Furthermore, the large bending moments presented in Figure 4.36 just below the abutment are not likely (Cf. Ch. 6.3.2).

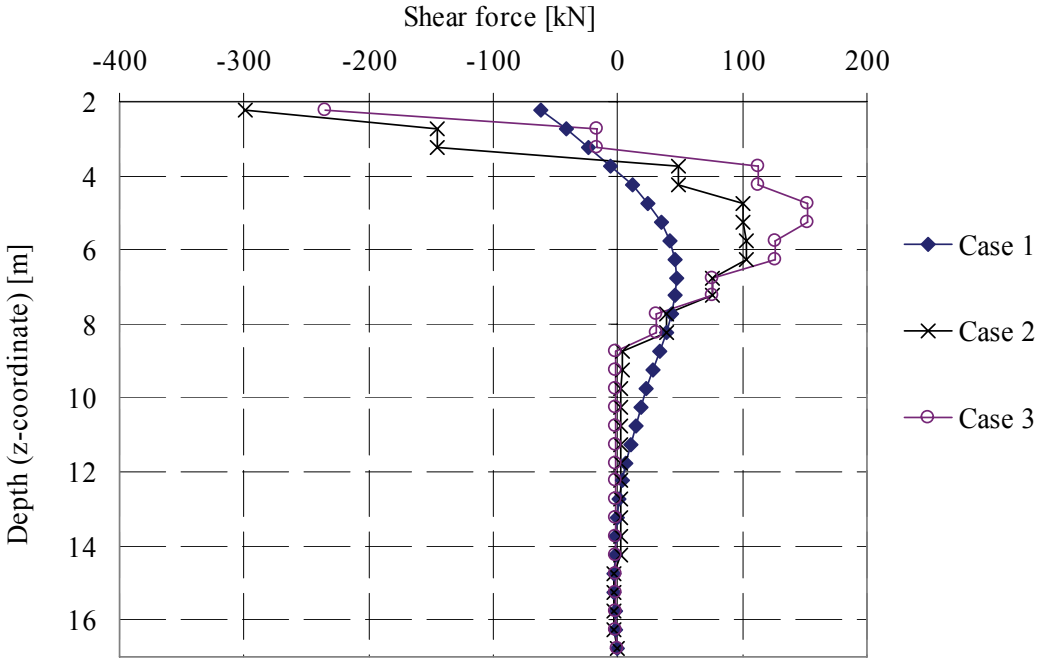

Figure 4.37 Shear forces at abutment pile in bridge longitudinal direction.

In non-linear Cases 2 and 3, the spring forces can be concluded from changes in shear forces (see Figure 4.37). Above the depth z = 9 m, the spring forces were large. Below the depth z = 9 m, they were negligible due to the very small horizontal pile displacements in the stiff soil represented by separate stiff springs.

Bending moments (see Figure 4.38) and shear forces (see Figure 4.39) in the pier and the pile are illustrated in the following two figures.

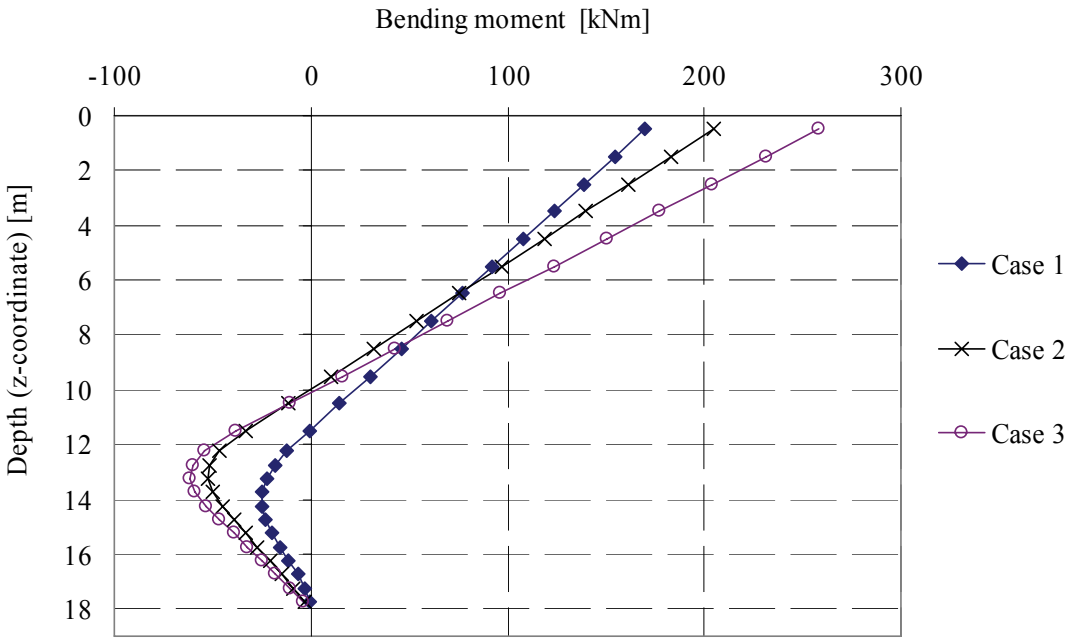

Figure 4.38 Bending moments at pier (z = 0 m–12 m) and underneath pile (z = 12–18 m) in bridge longitudinal direction.

Based on observed pier reinforcement strains (see Figure 4.8 and Figure 4.28), the horizontal support created by the surrounding fill during the coldest wintertime was located higher than concluded from Figure 4.38. Furthermore, the uppermost fill layer was stiffer than estimated in Cases 1–3.

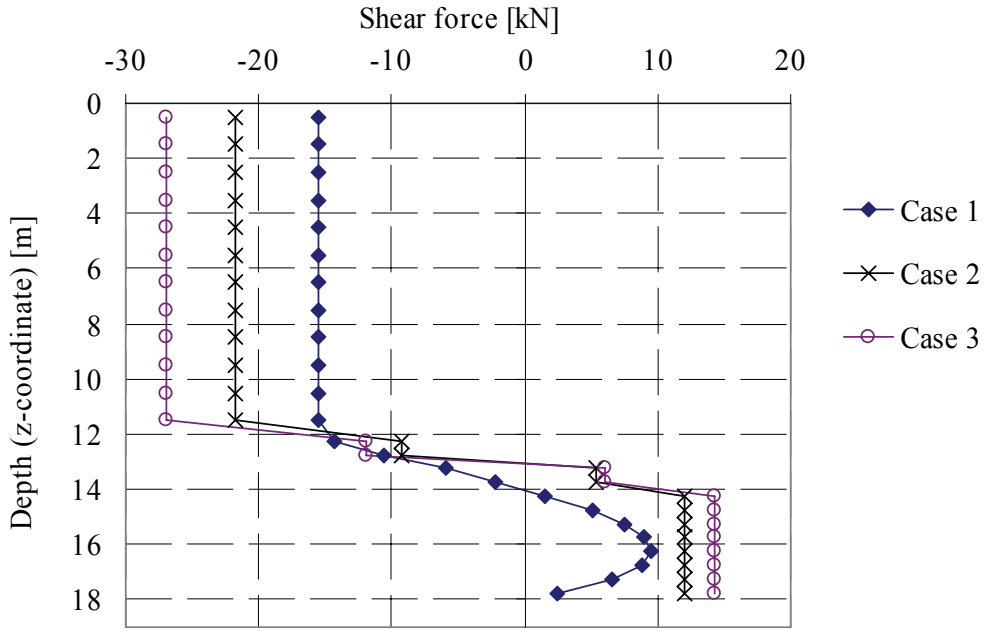

Figure 4.39 Shear forces at pier (z = 0 m–12 m) and underneath pile (z = 12–18 m) in bridge longitudinal direction. In Cases 2 and 3, the spring forces can be concluded from changes in shear forces.

The non-zero shear forces at pile tip are based on stiff horizontal supports.

Earth pressures against the abutment, Case 1

At depth z = 1.24 m from the road surface, the calculated horizontal displacement was 6.2 mm according to upper abutment springs. Thus, earth pressure had to be calculated as total passive pressure according to a displacement of 4.8 mm corresponding to maximum pressure => p_p = 76 kPa.

At depth z = 2.1 m from the road surface, the calculated horizontal displacement was 4.9 mm and earth pressure was p_p = 182 kPa.

The measured earth pressures near abutment centre at depth z = 1.6–2.2 m were 50–110 kPa. The calculated earth pressure at the upper half of the abutment was close to the measured average earth pressure. At the lower half, the measured earth pressure was smaller than the calculated value, probably because of the discontinuity of the structure at the abutment bottom (Cf. Figure 5.5) and the effects of the transition slab on the behaviour of the embankment soil at Haavistonjoki Bridge (Cf. Figure 6.9), which were ignored in the determination of horizontal abutment springs.

Earth pressures against the abutment, Case 2

At depth z = 1.24 m from the road surface, the calculated horizontal displacement was 6.6 mm and the spring force P_{upper} = 204 kN. Consequently, the earth pressure was p_{upper} = P_{upper} / (1.55 m*1.83 m) = 72 kPa. The calculated earth pressure corresponded to the average measured value, 50–110 kPa. The corresponding earth pressure coefficient due to the presented displacement was K = 3.4 without considering the effects of the transition slab. The spring force corresponding to passive earth pressure would have been P_p = 244 kN after a displacement of 8.7 mm (see Figure 4.33).

At depth z = 2.1 m from the road surface, the calculated horizontal displacement was 4.7 mm and the spring force P_{lower} = 271 kN. The corresponding characteristic earth pressure was $p_{lower} = P_{lower} / (0.95\ m * 1.83\ m)$ = 156 kPa. The measured earth pressure at the lower half, 50–110 kPa, was smaller than the calculated average earth pressure, probably because of the discontinuity of the structure at the abutment bottom and the effects of the transition slab on the behaviour of the embankment soil.

Earth pressures against the abutment, Case 3

At depth z = 1.24 m from the road surface, the calculated horizontal displacement was 7.0 mm and the spring force corresponding to passive earth pressure was P_{upper} = 289 kN. The passive earth pressure was p_{upper} = 102 kPa.

At depth z = 2.1 m from the road surface, the calculated horizontal displacement was 4.5 mm and the spring force corresponding to passive earth pressure was P_{lower} = 463 kN. The passive earth pressure was p_{lower} = 266 kPa.

The measured earth pressures were smaller than these calculated average earth pressures (Cf. Cases 1 and 2). Just using stiff abutment springs overestimated the development of earth pressure as both the soil and the transition slab structure were ignored.

Pile displacements and corresponding earth pressures below the pier

The displacements of the pile in the longitudinal bridge direction (see Figure 4.40) and the corresponding earth pressures (see Figure 4.41) below the pier are illustrated in the following figures. The calculation results for Cases 2 and 3 are based on an internal friction angle $\phi = 42°$ at the upper soil layers. The main cause for the different behaviour in Cases 2 and 3 is the difference in temperature change.

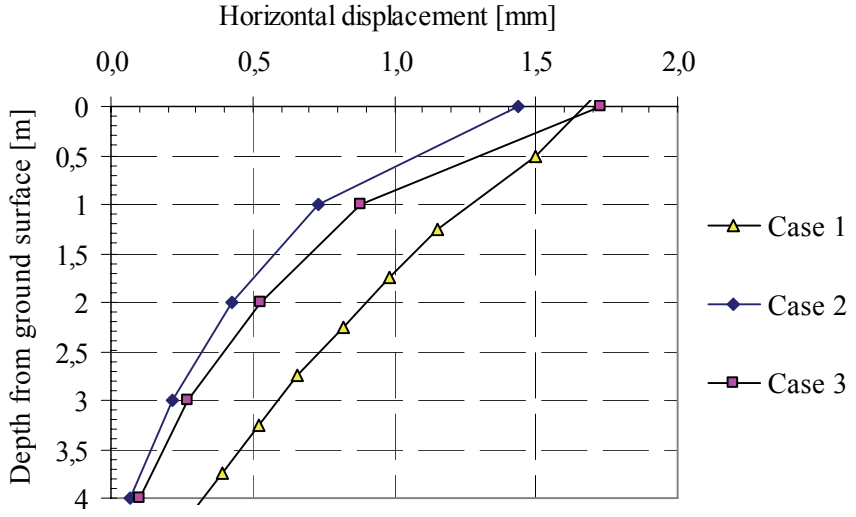

Figure 4.40 Calculated horizontal displacements of pile below pier.

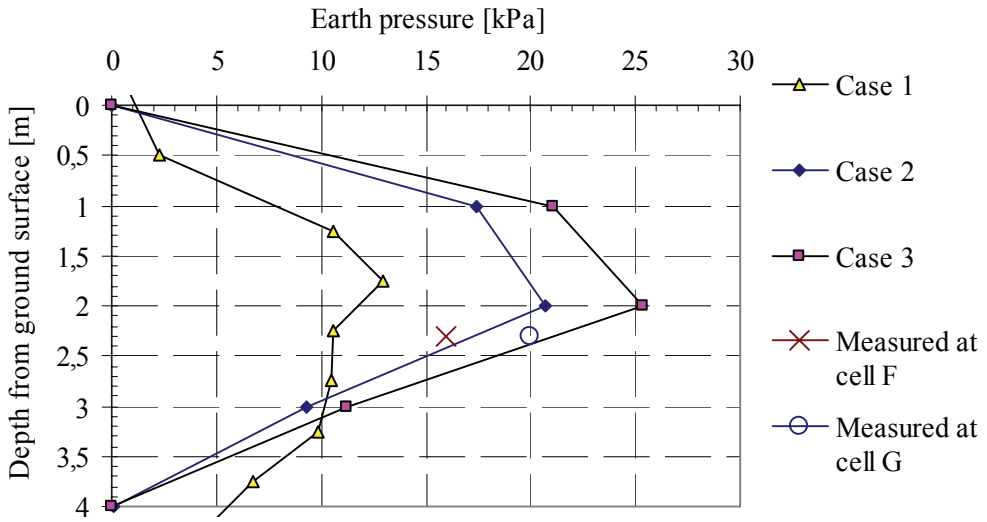

Figure 4.41 Calculated earth pressures of pile below pier and two measured values.

In the calculation model, the thermal expansion centre was at the centre of the bridge. In the real structure, based on observations, the thermal expansion centre was farther from support T3 than assumed in the model, and the measured horizontal displacement was about 4 mm compared to the average of 2.6 mm, which was used in calculations. Hence, the measured earth pressures were quite small compared to calculated earth pressures (Cases 2 and 3) and real horizontal displacement at support T3. The upper soil fill layers, above the observation depth and adjacent to the piers, must have been stiffer than the soil in front of the earth pressure cells.

The calculated displacement was small compared to the approximated displacement of about 40 mm required for passive earth pressure to develop at the observation depth.

During the coldest period of the winter there was no clear indication of frozen soil behaviour at the depth of the earth pressure cells.

Summary and recommendations

The presented 3D spring models omitted the transition slab in the analysis of the bridge and the embankment. The inaccuracy of the calculated results compared to measured values is mainly based on this fact. The model can be used to analyse earth pressures only in special cases considering this inaccuracy. Also, the nearness of the abutment bottom should be taken into account in the evaluation of earth pressures against the abutment and the behaviour of the soil next to the piles.

The traditional spring model overestimated the lateral subgrade reaction.

The calculation results corresponded satisfactorily to the observed values as regards:

- earth pressures against the lower part of piers
- abutment pile stresses at the higher observed points
- bending moment at the centre of the abutment

The presented 3D spring models can be recommended for the analysis of jointless bridges only if the presented limits are adhered to.

4.3 Tekemäjärvenoja Railway Bridge

4.3.1 Superstructure and substructure

Tekemäjärvenoja Railway Bridge is a continuous slab bridge with integral abutments. At the time of instrumentation in 2004, it was part of a railway track under construction between Kerava and Lahti in southern Finland. The total length of the jointless bridge is 34 meters and the spans are 8, 12 and 8 m long. The width of the bridge is 11.9 meters and the thickness of the reinforced concrete slab 930 mm. The ballasted slab carries a double-track structure. The ends are unskewed with 5 m long transition slabs according to Figure 4.42. The bridge is built on spread foundations, and the piers are connected to the slab rigidly without bearings.

The transition slabs were connected to the abutments with special equipment using either a rigid horizontal connection or a released horizontal connection.

The approach embankment adjacent to the abutment and the fill adjacent to all concrete structures are built of 0–64 mm crushed rock. The embankment subgrade fill is built of 0–300 mm crushed rock. The fills were constructed according to Finnish guidelines and construction practice.

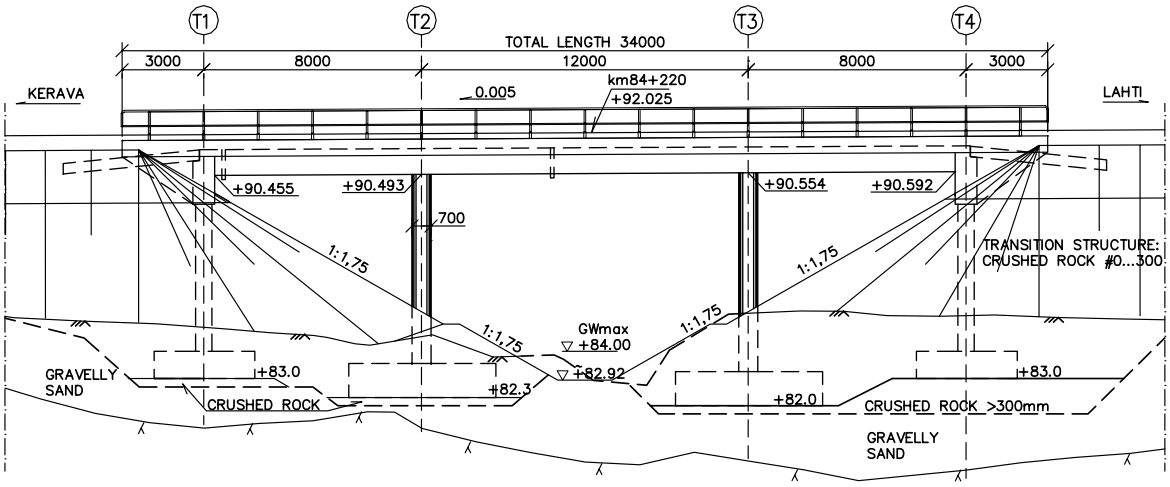

Figure 4.42 Main dimensions and elevation of Tekemäjärvenoja Bridge (Laaksonen 2005).

4.3.2 Field test programme

The field test programme for Tekemäjärvenoja Railway Bridge was drawn up at Tampere University of Technology under the name ‘Tekemäjärvenojan ratasilta: KOEOHJELMA 14.6.2004’. The designed research equipment were manufactured at the TUT laboratory by the staff of the Institute of Earth and Foundation Structures or at nearby engineering workshops. The staff of the institute also installed all the gauges and data loggers.

The northern rail strains were measured at 10 successive points under loading. The relative displacement between the deck and the rail was measured at 4 successive points labelled K1–K4 (see Figure 4.43).

Temperature was measured at various levels within the deck and the approach embankment at support T4.

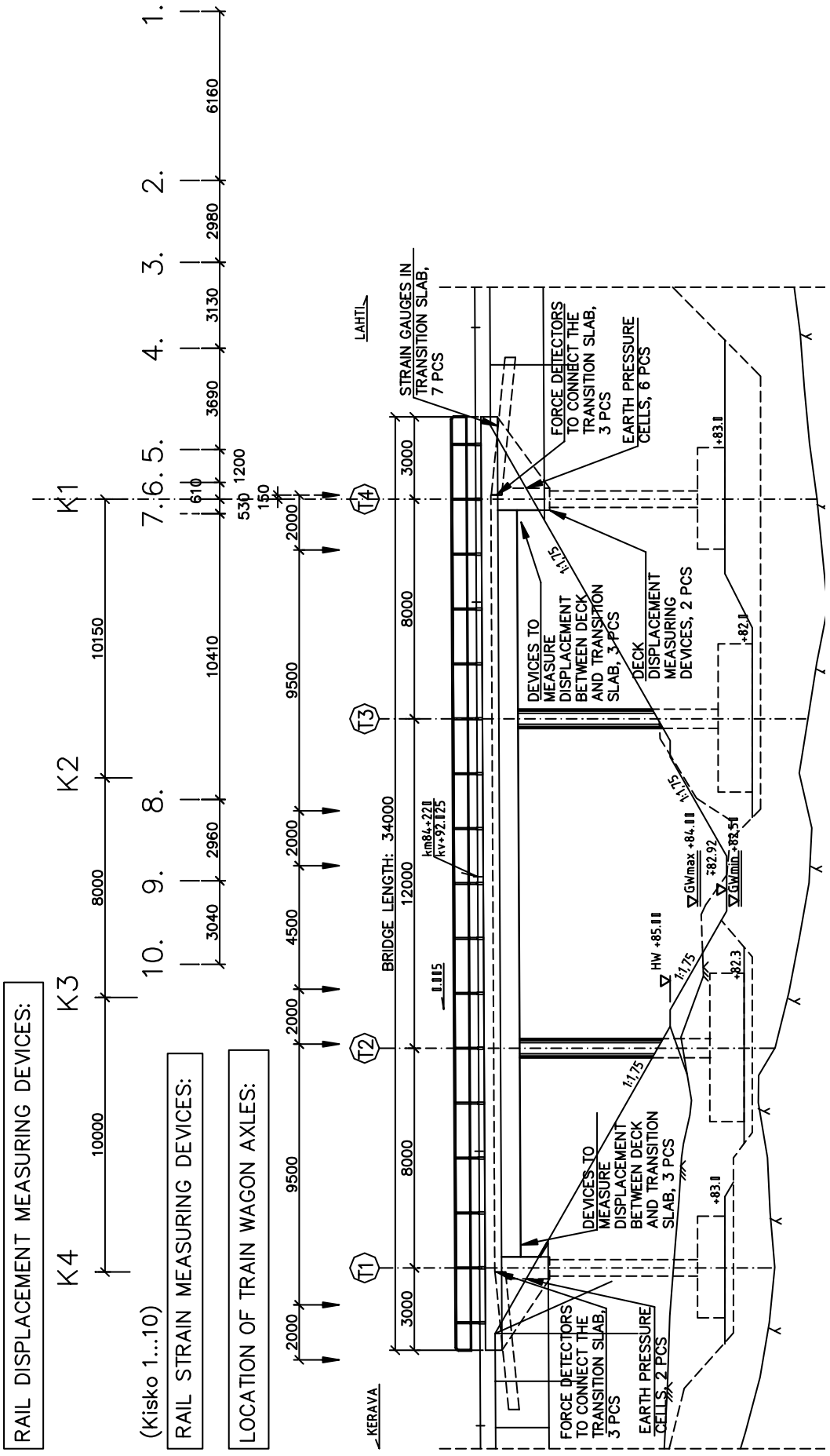

Figure 4.43 Location of measuring equipment (Laaksonen 2005).

At support T4 abutment displacement was measured with a long steel bar anchored inside the approach embankment. Earth pressure was measured with two cells at support T1 and with six cells at support T4 according to Figure 4.44. The cells were manufactured and calibrated at Tampere University of Technology.

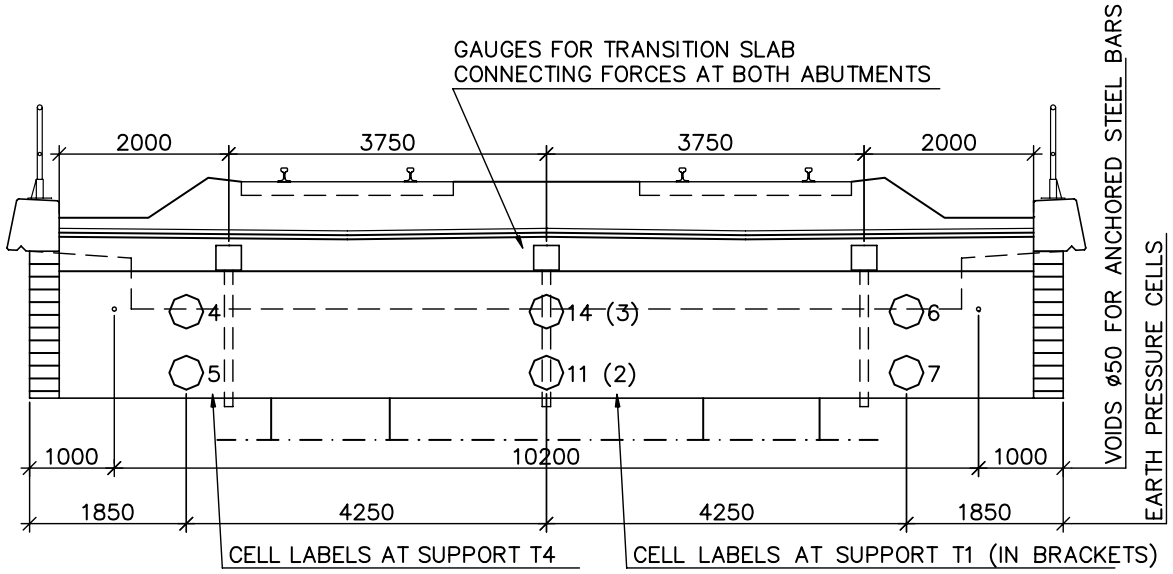

Figure 4.44 Instrumentation at support T4 or eastern abutment (Laaksonen 2005).

Horizontal connecting forces between the deck and the transition slab were measured with 3 gauges at both abutments. The gauges, called force detectors, acted simultaneously as force detectors and connectors. One of the force detectors and the situation before the construction of the transition slab are presented in Figure 4.45.

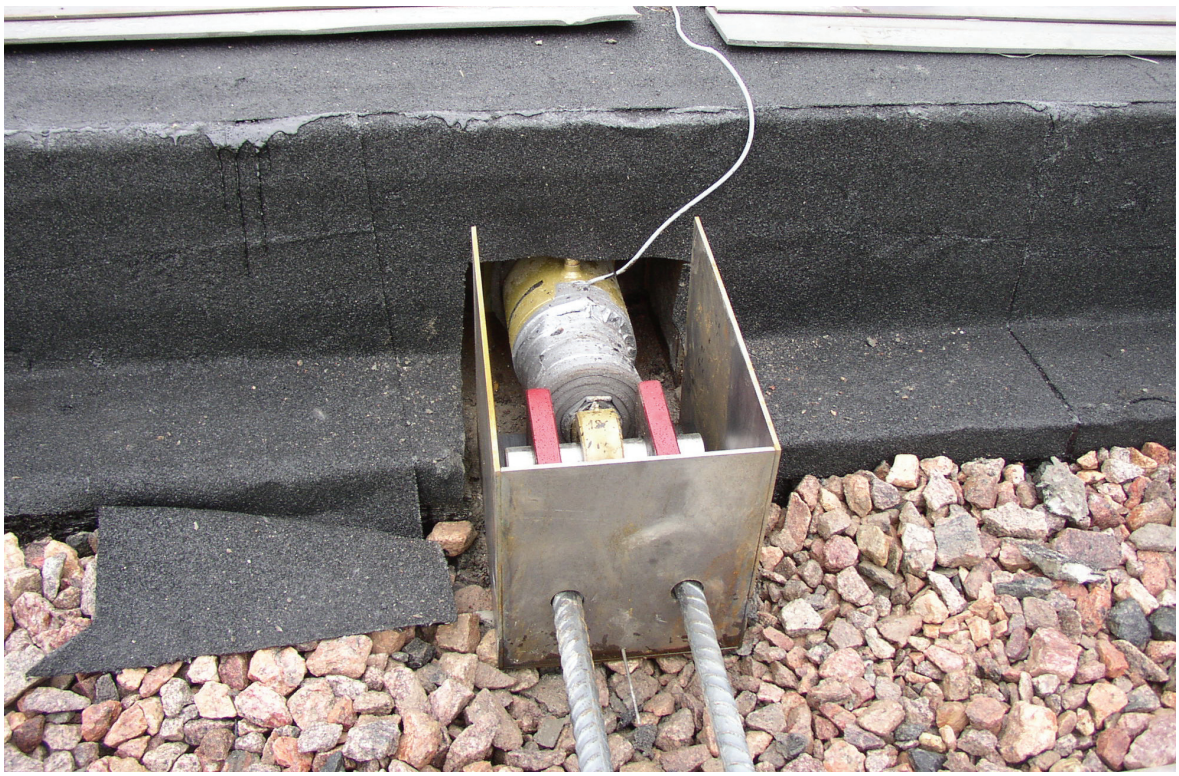

Figure 4.45 Force detector between transition slab and abutment.

The friction between the transition slab and support T4 was made minimal (see Figure 4.46). There was also a 50 mm wide horizontal gap to make transition slab movement possible.

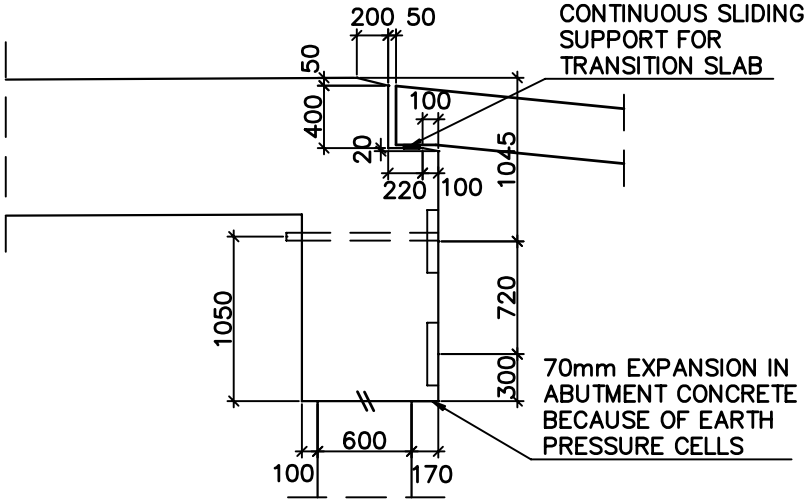

Figure 4.46 Tekemäjärvenoja Railway Bridge eastern abutment cross section (Laaksonen 2005).

4.3.3 Installation of gauges and field test arrangements

Rail displacement measuring devices and rail strain gauges were installed at the bridge site just before the loading tests.

Field test arrangements were made according to Figure 4.47. Four wagons loaded with ballast were parked on the bridge with their brakes on. The horizontal force to pull the

group of wagons in the direction of support T4 (towards Lahti) was transmitted through special equipment, for example, wire cables, steel pipes and connectors.

Figure 4.47 Field test arrangement at Tekemäjärvenoja Railway Bridge (Koskinen et al 2005).

Friction between the wagon wheels and rails was increased with a diamond paste. The first test measured maximum horizontal force. According to the preliminary calculations, the total maximum load was 0.6*750kN*4 = 1800 kN. However, the wagons began to move after a horizontal load of 550 kN because the brakes did not hold as well as anticipated.

In addition to being loaded with the wagons, force detectors were used to push or pull the transition slab in relation to the abutment, that is, to increase or decrease the gap between the transition slab and the abutment.

Altogether 12 separate tests were conducted. In tests 9–12 the force detectors were used as loading units. These tests were called transition slab push/pull tests.

Pre-processing of data

The data were collected with data loggers at the bridge site during individual loading instances and saved to a computer. The amount of data was very large and special software was needed to draw diagrams based on the measurements.

4.3.4 Field test results

Overview

From the test results it can be concluded that the forces from the wagons to the rails were not distributed evenly, mainly because of the uneven condition of the brakes. The total horizontal force of individual loading tests per track was 550 kN / 2 = 275 kN. The observed bridge deck displacements were small. Consequently, soil behaviour was almost

linear. Based on transition slab push/pull tests, the displacement size was remarkably larger and the soil behaviour was clearly non-linear.

The conditions before the tests influenced test results. The average bridge deck temperature during the tests on 30.10.2004 was 5°C and the embankment temperature was 9°C. In the morning, air temperature was -2ºC and in the afternoon 5ºC. The bridge had shortened due to the low air temperature before the first tests, which had an effect on earth pressures in the morning tests. At first, a small displacement was needed in order to reach the at-rest earth pressure state.

The effect of the vertical load from the wagons on the track was distinctive as displayed by the horizontal stiffness of the rails in the ballast. That could be concluded from the changes in horizontal rail stresses, even considering the differences in horizontal stiffness between the bridge and the embankment. Rail stresses changed clearly slower on the approach embankment than on the bridge.

When the horizontal load was kept steady for a certain period of time, some creep was observed in the soil. Consequently, the stresses in the rails increased according to some strain gauges. Creep in the soil and non-linear soil behaviour decreased after the first loadings. The reason was that the ballast and the embankment soil stiffened after the first loadings.

In transition slab push/pull tests the force changes indicated by force detectors corresponded to deck movement due to negative and positive changes in the transition slab–abutment gap width. However, according to Figure 4.48, for instance, at t = 32 seconds and at t = 51 seconds, the force returned to P = 0 kN, but the deck did not return to its original location.

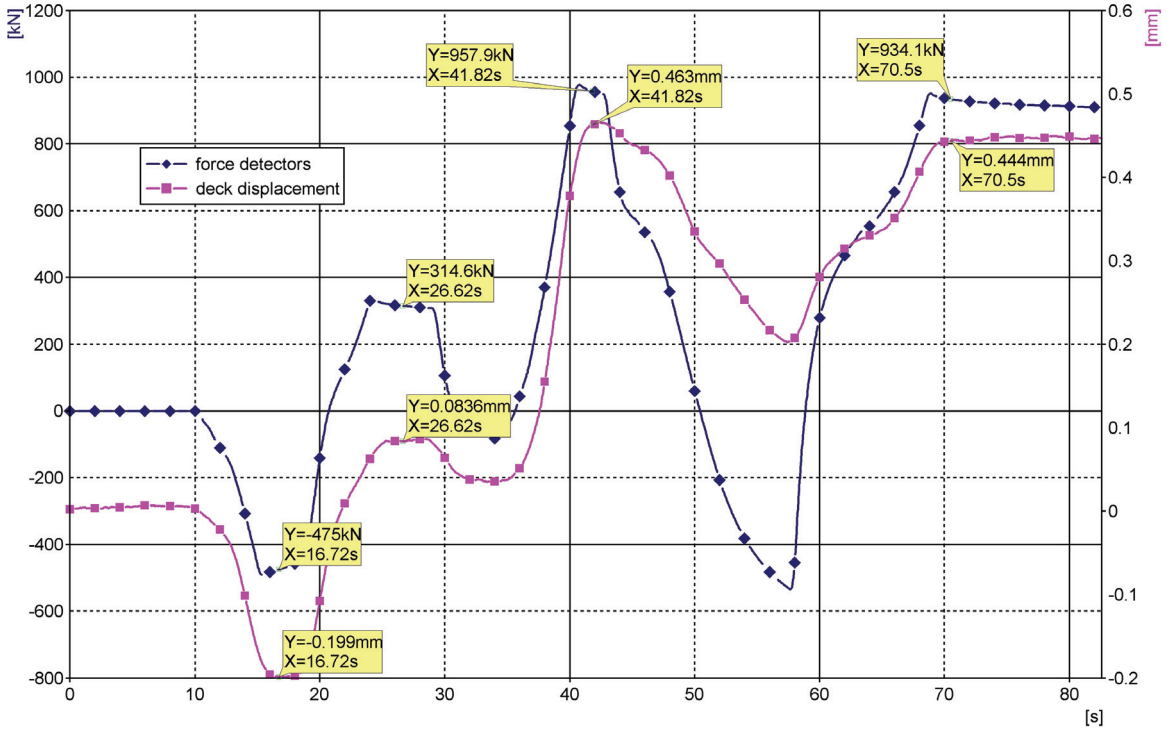

Figure 4.48 Deck displacements and forces indicated by force detectors during transition slab push/pull test (Laaksonen 2005).

Because of the rigid connection of the transition slab to the abutment, and because of the behaviour of the short bridge, the majority of the horizontal forces transferred to the embankment through the rails, ballast, and especially through the transition slab. The average shares in tests 1 and 4 were:

- rails: 29 %,
- transition slab: 35 %,
- embankment soil observed by earth pressure cells: 5 %,
- elsewhere: 31 % (includes columns, foundations, and ballast).

Stresses in rails

In the following diagrams, the negative rail stress and earth pressure changes correspond to compression. The force along the horizontal axles did not start from zero. Due to the loading arrangements, a small initial force was needed before starting an actual loading test.

The stresses of the fourth loading test are presented in Figure 4.49. Both rail forces [kN] and corresponding stresses [MPa] are presented. Right after the first wagon at location 'Rail stress 9' (Kisko 9 in Figure 4.43), the force in the rail was observed to be a tension force. At locations 'Rail stress 4, 5 and 6', that is, in front of the wagons a compression force was observed.

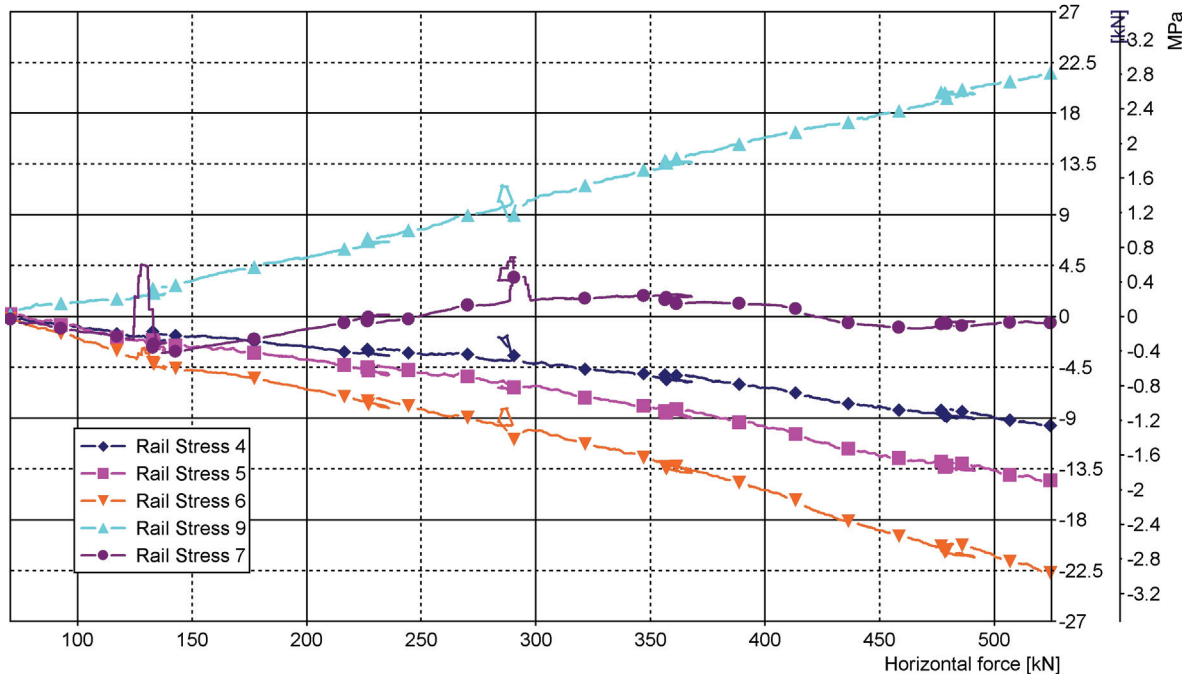

Figure 4.49 Horizontal force – rail stress relations at five locations along the track in fourth loading test (Laaksonen 2005).

Relative horizontal rail displacement and deck displacement

The greatest relative horizontal displacement between the rail and the deck was about 0.15 mm at location 'Relative rail displacement 1' or K1 (see Figure 4.43 and Figure 4.50). Next to support T1 at 'Relative rail displacement 4' relative horizontal displacement was insignificant.

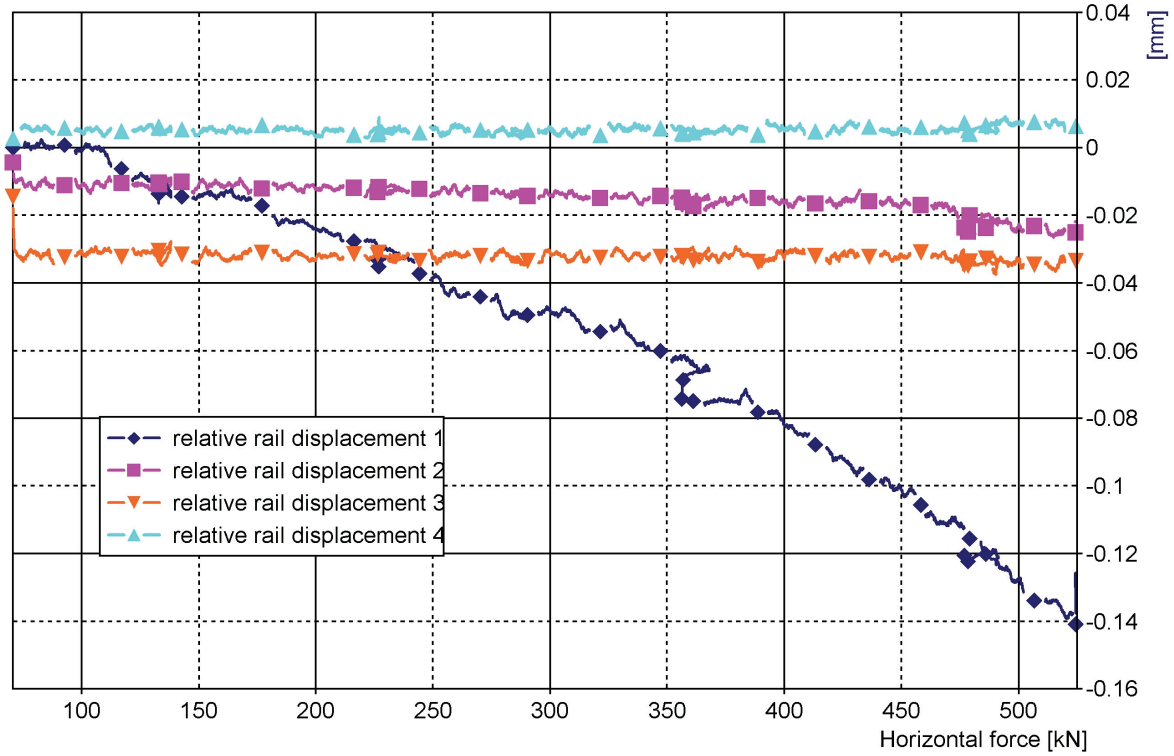

Figure 4.50 Relative horizontal displacements between rail and deck in fourth loading test (Laaksonen 2005).

The bridge deck displacements were quite small compared to the rail displacements, partly because of the non-stabilised ballast. For instance, in the fifth test the maximum deck displacement change was only 0.05 mm due to a total horizontal force of 550 kN.

Earth pressures and modulus of lateral subgrade reaction

Earth pressure changes below the transition slab in the fifth test are presented in Figure 4.51. Earth pressure changes were small because of the small deck displacement size. Earth pressures increased or decreased due to the deck movement at supports T4 and T1.

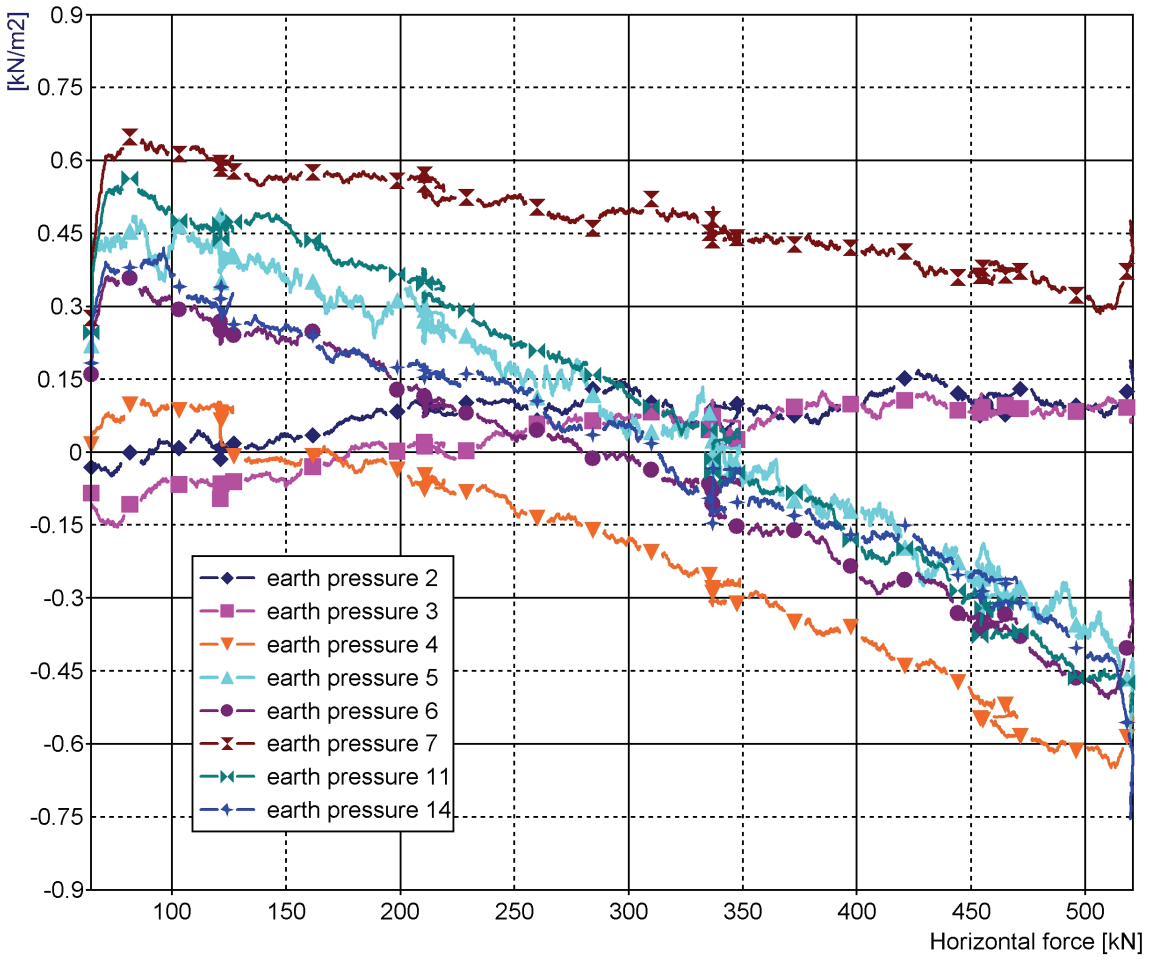

Figure 4.51 Earth pressure changes in fifth loading test indicated by some earth pressure cells. Cells 2 and 3 were at support T1, i.e. opposite to direction of displacement (Laaksonen 2005).

According to the 11th loading test, the transition slab push/pull test, the earth pressure indicated by cell number 5 (lower cell) increased 0.59 kN/m^2 while the deck moved 0.55 mm against the embankment. The movement corresponded to the return from the active earth pressure phase, and the calculated modulus of lateral subgrade reaction was k_{s1} = 0.00059 MN/m^2 / 0.00055 m = 1.1 MN/m^3 (see App. 4). At the beginning of the passive earth pressure phase, the modulus of lateral subgrade reaction was k_{s3} = 10 MN/m^3, while the movement against the embankment was about 0.05 mm. As the movement at the passive earth pressure phase was about 0.2 mm, the observed modulus of lateral subgrade reaction was k_{s2} = 25 MN/m^3. The average stiffness of the passive phase corresponded to the magnitude of observed average soil stiffnesses, for example in the first and the fourth loading tests with the wagons, which were k_s = 13 MN/m^3 and k_s = 19 MN/m^3, respectively. Also, the magnitude of the lateral subgrade reaction according to Haavistonjoki Bridge measurements during abutment displacement of 5.2 mm (see Ch. 4.2.5) corresponded to the measurements at Tekemäjärvenoja Railway Bridge.

According to the guidelines of Finnish Rail Administration, modulus of lateral subgrade reaction can be calculated from the equation (RHK 1997):

$$k_s = p_p / \delta_m = \gamma * z * K_p / (0.002 * H),$$

where δ_m is the displacement corresponding to horizontal abutment resistance.

Here, height is measured from the top of the ballast to the bottom of the abutment. From this equation we get the modulus of lateral subgrade reaction for the upper earth pressure cells k_s = 20kN/m^3 * 1.595m * 3.69 / (0.002 * 2.615m) = 23 MN/m^3 and the lower earth pressure cells k_s = 33 MN/m^3. Below the transition slab, observed lateral subgrade reactions were smaller than these calculated values, although the soil values proposed in guidelines were quite conservative. The effect of the transition slab on the stiffness of soil at low displacement level was distinctive also based on the results of the Tekemäjärvenoja Railway Bridge field tests.

Longitudinal track stiffness

The average longitudinal stiffness of the track, according to the transition slab push/pull test, can be calculated based on the observed relative rail displacement difference 0.366 mm at a distance of 28 meters (Laaksonen 2005):

$$\Delta\sigma = E * \varepsilon = 210000MPa * \frac{0{,}366mm}{28000mm} = 2.74MPa$$

$$\Delta P_{track} = \Delta\sigma * A = 2.74MPa * 7670mm^2 * 2 = 42000N$$

$$k_{average} = \frac{1}{0{,}366mm} * 42000N * \frac{1}{28000mm} = 4.1MN/m/m$$

A stabilised track is stiffer than the tested new track on Tekemäjärvenoja Railway Bridge. In general, the stiffness of a new and non-stabilised track is about 66 per cent of the final track stiffness (Noranta 2004). Consequently, the final track stiffness on Tekemäjärvenoja Railway Bridge will be about k = 6.2 MN/m/m. In Chapter 2.2.2, the general longitudinal resistance of a track is presented. Prior to the plastic phase, the stiffness of the sleeper in the ballast (well maintained) according to UIC is $k = k_r / u_0$ = 20 kN/m / 0.002 m = 10 MN/m/m. According to the Netherlands Railways (NS), with the same plastic resistance the corresponding resistance would have been $k = k_r / u_0$ = 20 kN/m / 0.0028 m = 7 MN/m/m. Thus, the estimated final track stiffness was close to the longitudinal stiffness applied in Central Europe.

4.3.5 Comparison with 3D FEM model

Calculation model

The 3D FEM model of Tekemäjärvenoja Railway Bridge is presented in Figure 4.52. It was constructed using 3D solid elements for the structures and the soil. Springs were used, for instance, to model the soil below the foundations and around the columns. The supports of the embankments and the track ends were also modelled with springs to describe the continuity of the track, ballast and the embankment. The wing walls were modelled by adding a rigid lateral support for the approach embankment at the location of the wing walls. Elsewhere the lateral support for the soil was modelled by linear springs. The total length of the model was 71 metres including the ballast at both ends of the bridge. The soil-structure interaction was paid special attention. The transition slabs and their connections to the abutment are part of the model. The symmetry was utilised in the lateral direction.

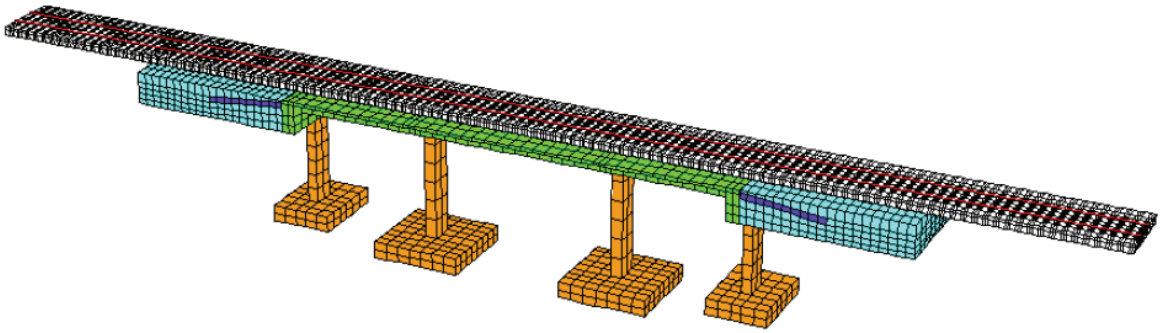

Figure 4.52 3D model of Tekemäjärvenoja Railway Bridge (Koskinen et al 2005).

The properties of the materials were evaluated on the basis of site investigations and typical behaviour of the used materials (Cf. Ch. 4.2.2).

Table 4.5 Input parameters for materials (Koskinen et al 2005).

Material	Modulus of elasticity E [MPa]	Poisson's ratio ν	Strength ϕ [º]
Concrete	30,000	0.22	-
Rails UIC 60	210,000	0.3	-
Backfill	200	0.3	42
Ballast	100	0.3	-

Calculation results

A 3D model was used to conduct horizontal loading tests of Tekemäjärvenoja Railway Bridge. The calculated average lateral subgrade reactions at the level of the upper earth pressure cells and lower earth pressure cells were k_s = 10 MN/m^3 and k_s = 15 MN/m^3, respectively. These values corresponded to the observed values (see Ch. 4.3.4). The distribution of horizontal forces in rails also corresponded to the measured values (see Figure 4.49).

The distribution of longitudinal stresses within the approach embankment is presented in Figure 4.53. The adjacent support was T4, and the results indicate the situation near the force detector, that is, 3.8 meters from the centre of the abutment. The total horizontal force representing the braking force was 550 kN. The compression stresses were small because of the small longitudinal deck displacement, the calculated value being about 0.15 mm. The highest stresses, about 7 kPa, were located at the end of the transition slab. Further from the abutment the stresses were smaller, about ±1 kPa. The calculated earth pressures against the abutment were 1.5 kPa at the upper earth pressure cell level and 1.9 kPa at the lower earth pressure cell level. The Abaqus code did not provide a "tension cut off" option for soil, which allowed some tension stresses to occur within the soil, mainly above and below the centre of the transition slab.

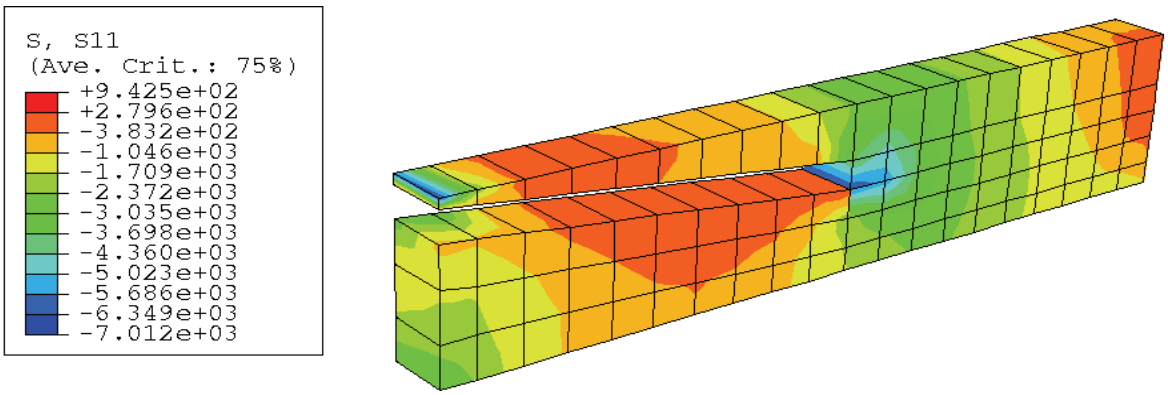

Figure 4.53 Distribution of longitudinal stresses within the approach embankment at Tekemäjärvenoja Railway Bridge (Koskinen 2005).

The main difference between the measured and the calculated values derived from the high stiffness of the ballast in the calculations. The used modulus of elasticity for the ballast was large, 100 MPa, which resulted in almost three times larger deck displacements compared to measured deck displacement. For that reason, and because the calculations concerning the variation of ballast soil parameters are not finished, further results and a more detailed comparison are not presented here. It is recommended that the presented 3D FEM calculations be revised by using, for instance, 40 MPa as the modulus of elasticity for the ballast.

A summary on the behaviour of Tekemäjärvenoja Railway Bridge is presented in Chapter 9.2.

5 WALL DISPLACEMENT–EARTH PRESSURE RELATION

5.1 Presentation of discussed phenomena

The most essential phenomena studied in Chapter 5 are presented in Figure 5.1. Both active and passive earth pressures are discussed as they concern non-cyclic and cyclic wall displacements. The wall movements consisted of horizontal displacement, rotation and upwards inclined movement. The moving wall was totally buried in the surrounding soil, but it had a finite height.

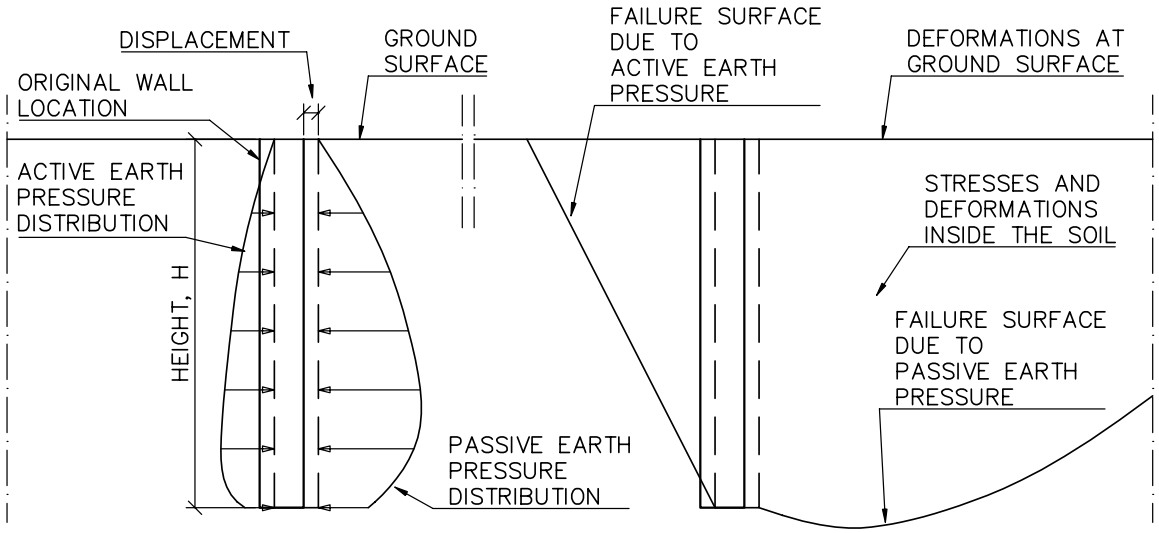

Figure 5.1 Studied phenomena of Chapter 5.

5.2 Earth pressure due to non-cyclic wall displacement

5.2.1 General earth pressure calculation theories

As a wall supporting earth moves horizontally towards the earth, earth pressure increases non-linearly from at-rest pressure to the ultimate pressure called passive earth pressure. If friction at the abutment–fill interface is substantial, Rankine's earth pressure theory gives too small passive pressures against the abutment. Rankine's theory is limited also in some other respects and cannot be generally recommended (e.g. Craig 1997).

Coulomb's earth pressure theory (e.g. Craig 1997) deals with the friction at the abutment–fill interface satisfactorily up to a wall friction angle $\delta = 0.4*\varphi$ (Duncan 2001). For larger wall friction angles, the earth pressure coefficients are excessive, for instance, for $\varphi = 40°$ and $\delta = 20°$ the earth pressure coefficient is $K_p = 12$ and for $\varphi = 43°$ and $\delta = 30°$ the coefficient is $K_p = 35$. The prerequisite for these large earth pressure coefficients is that the structure moving against the soil does not rise simultaneously. The resultant force according to coefficient K_p is inclined from the normal of the wall due to the wall friction angle, δ.

5.2.2 Earth pressure against shallow abutment due to finite displacement

The horizontal displacement required to mobilise passive earth pressure varies considerably according to different research reports and design manuals. Generally, it is estimated that a relative displacement magnitude of 0.005–0.050 times H is adequate, where H is the height of a retaining wall or a bridge abutment. According to a group of German researchers, a displacement of 0.025 x H is enough to mobilise passive earth pressure (FGSV 1994 / taken from Berger et al 2003, see Figure 5.2). A displacement of 0.0025 x H corresponds to earth pressure at $0.5*K_p$ and is also the recommended maximum displacement.

The German recommendation for the maximum top displacement of a wall rotating around its base is 4 times the maximum displacement of a horizontally moving wall. In many research reports the earth pressure distribution against the rotating wall is stated to be totally different from the 'horizontally moving wall' case. Because the real abutment of a jointless bridge rotates and translates simultaneously, the corresponding horizontal displacement in Figure 5.2 should be chosen from between the two presented values of δ_a, that is, δ_a = 0.0007–0.001 * H. Accordingly, δ_p may be estimated to be 0.007–0.01 * H.

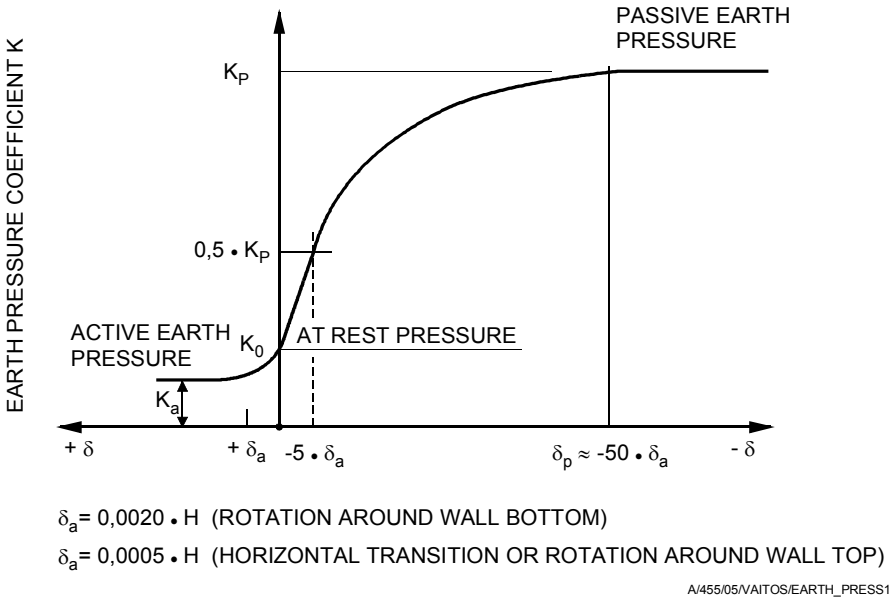

Figure 5.2 Earth pressure coefficient–horizontal displacement relation (FGSV 1994).

Various means to minimise earth pressure at the bridge abutment and the irreversible strains inside the approach embankment have been presented in several papers. An elastic vertical board behind the abutment and reinforcement of the backfill material seem to act satisfactorily together (Cf. Ch. 6.2.3).

5.2.3 Structural model for 2D calculations

The horizontal earth pressures against the continuous wall surrounded by soil on both sides were calculated with a 2 dimensional FEM model. The 2.5 m high wall was forced to transfer horizontally or rotate around its bottom. At the same time, its rising or sinking in the surrounding soil was prevented. The model was 40 meters wide and 15 meters high according to Figure 5.3. The groundwater level was z = 15 m at the bottom of the model.

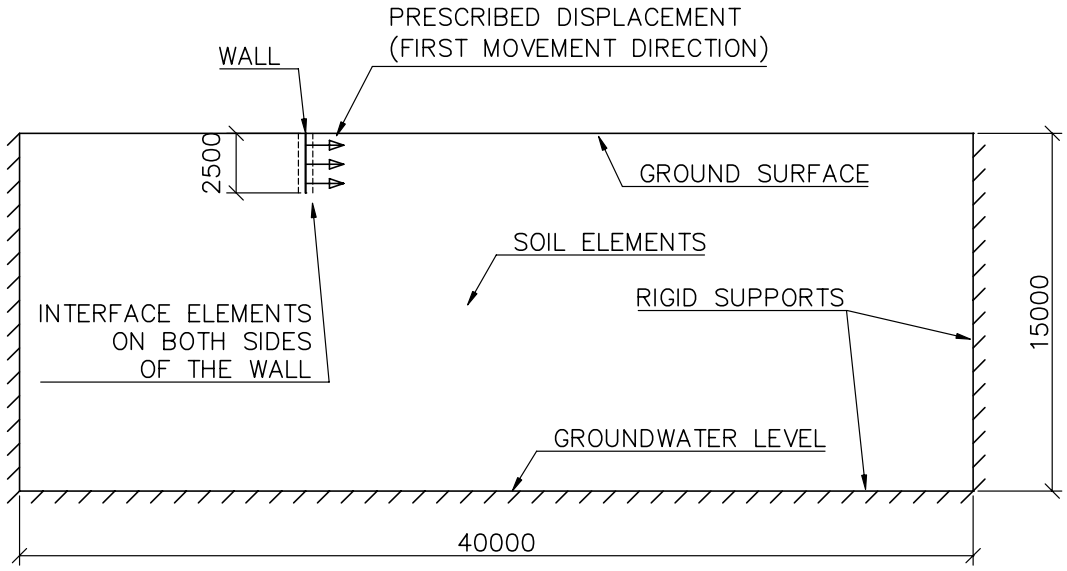

Figure 5.3 Structural model of an imaginary wall transferring horizontally. "First movement direction" refers to calculations in Chapter 5.3.

The model was built with 15-noded plain strain elements (see App. 1). It included interface elements at both sides of the vertical wall and also within the soil at a 500 mm distance under the wall.

The Mohr-Coulomb or MC soil model was used first. Comparisons were done with a Hardening-Soil or HS soil model.

Mohr-Coulomb soil model

The properties of the soil in MC soil model calculations are presented in Table 5.1.

Table 5.1 Soil material properties. MC soil model.

Type	γ [kN/m^3]	ν [-]	E_d [kN/m^2]	c [kN/m^2]	ϕ [°]	ψ [°]	R_{inter} [-]	G [kN/m^2]	M [kN/m^2]
Drained	21	0.3	80,000	1	38	3	0.5	30,800	108,000

Drained modulus of elasticity, E_d, depends on soil material and its density. The presented values correspond to an ordinary well-compacted non-cohesive soil. E_d, ϕ and γ were taken from (Finnra 1999a). Dilatancy angle, ψ, was roughly estimated on the basis of friction angle, ϕ, using the equation $\psi = \phi - 35°$ which produces a small value. The used wall friction angle, $\delta = \arctan(R_{inter}*\tan\phi) = \arctan(0.5*\tan 38°) = 21.3°$ is a typical ultimate friction angle, according to (California trenching and shoring manual 2001), between, for instance, form-faced concrete and clean gravel.

Hardening-Soil soil model

The properties of the soil in HS soil model calculations are presented in Table 5.2.

Table 5.2 Soil properties. HS soil model (see Ch. 4.1.1). The "dilatation cut off" option was used.

Type	γ [kN/m^3]	ν [-]	$E_d=E_{50ref}$ [kN/m^2]	c [kN/m^2]	ϕ [°]	ψ [°]	R_{inter} [-]	p_{ref} [kPa]	m [-]	e_{max} - e_{init} [-]
Drained	21	0.2	80,000	1	38	3	0.5	100	0.5	0.2

5.2.4 Calculation results and conclusions

The deformations in the soil after the prescribed displacement are illustrated in Appendix 1. Both the horizontally transferring wall case and the rotating wall case are presented.

The effective stresses based on calculations on a transferring wall are presented in Figure 5.4. The principal directions of the stresses show that the passive earth pressures against the wall tended to raise the wall upwards.

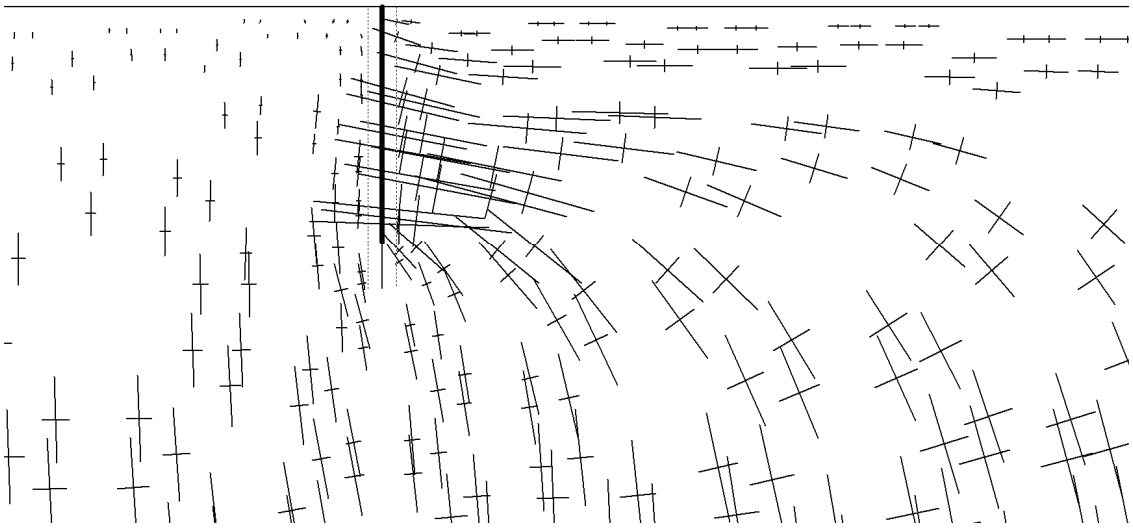

Figure 5.4 Effective stresses in soil next to the wall with 10 mm prescribed horizontal displacement.

The active earth pressures on the left side of the wall were almost negligible compared to the passive earth pressures on the right side.

Based on traditional passive earth pressure theories, earth pressures are assumed to increase linearly towards the bottom of the horizontally moving structure. According to the FEM calculations on an imaginary wall, earth pressure did not increase or even diminished along the lowest third of the wall after a displacement of 8 mm = 0.003 * H (see Figure 5.5) as the soil approached failure.

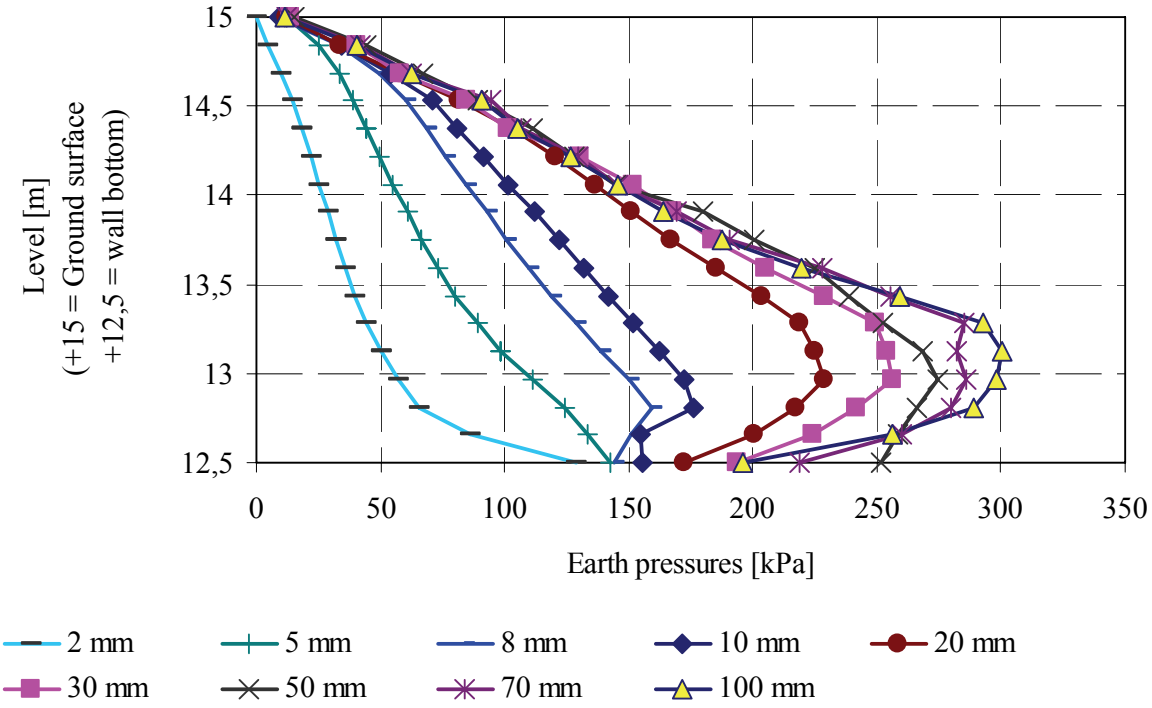

Figure 5.5 Earth pressures after some prescribed horizontal displacements. MC soil model.

The low earth pressure at the lowest part of the wall is explained by Figure 5.4. The principal directions are much more vertical than the upper principal directions while the size is not larger. Accordingly, the discontinuation of the structure within the soil affects earth pressures.

At Haavistonjoki Bridge the average measured earth pressure due to abutment movement δ = 5.2 mm at the centre of the abutment below the transition slab was 80 kPa (cf. Ch. 4.2.5 / Figure 4.20). The calculated value according to Figure 5.5 was 105 kPa, even though the used soil stiffness was not as high as indicated by the tests at Haavistonjoki which proves the significant impact the transition slab has on the magnitude of earth pressure. The significance of soil stiffness can be determined from Figure 5.12 where the stiffest soil corresponded to the measured soil stiffness at Haavistonjoki.

The rotating wall caused slightly greater earth pressures on its upper half than a horizontally transferring wall according to Figure 5.6. The earth pressures on the lower half were remarkably smaller in the case of the rotating wall, and near the bottom earth pressures were insignificant. Accordingly, earth pressures near the bottom were less than the earth pressure at rest. Maximum earth pressures occurred at depths 0.8 m–1.4 m or (0.32–0.56)*H when rotations were 8 mm–46 mm.

'Displacement 50 – Rotation' in Figure 5.6 means 50 mm top displacement and 25 mm bottom displacement. The smaller bottom displacement compared to even horizontal displacement of 50 mm resulted in 10–35 per cent smaller earth pressures on the lower half of the wall.

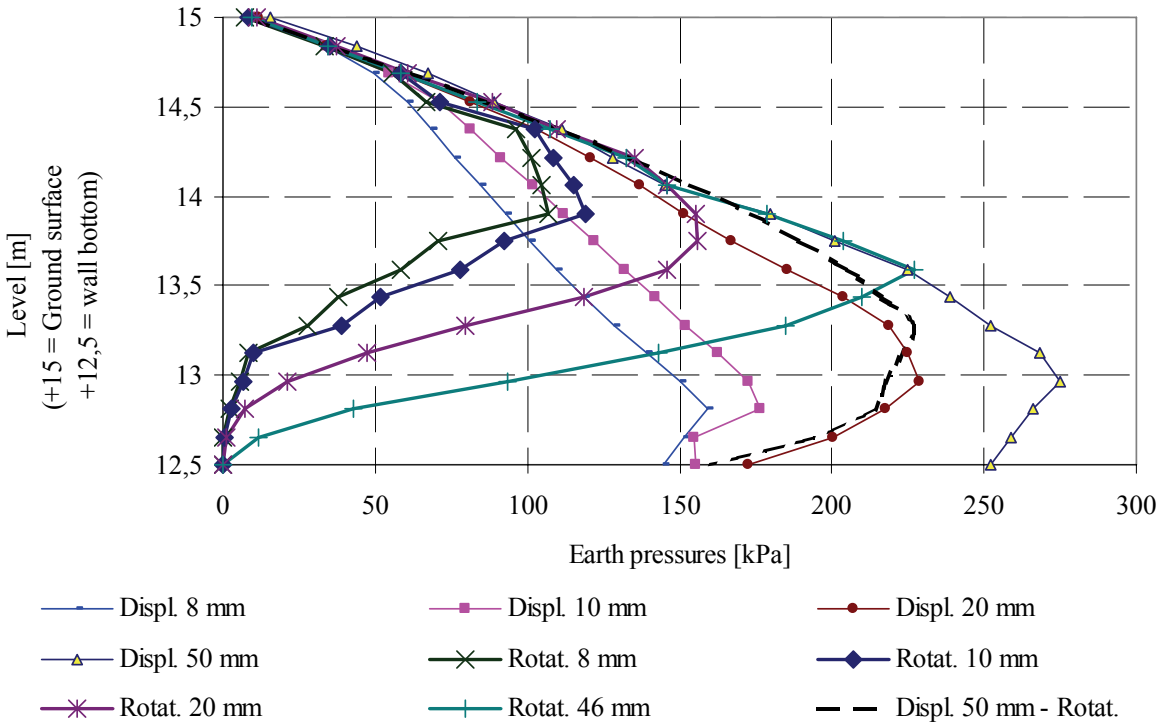

Figure 5.6 Comparison of earth pressures from different wall displacements or rotations around the bottom. Rotations were labelled according to the displacement of the top of the wall. 'Rotation 46 mm' was the maximum value. MC soil model.

A corresponding earth pressure distribution due to a rotating wall has been observed, for instance, in empirical small-scale tests on jointless frame bridges (Tsang et al. 2002).

After a displacement of 10 mm, as the wall was separating from the soil, the relative shear stresses along the wall were the highest possible: 1 or close to 1 along the entire wall height. Maximum absolute values of shear stresses occurred at levels where the highest active earth pressure acted at the same time. The Kerisel and Absi active earth pressures in Figure 5.7 were based on a wall friction angle $\delta = 21.3°$ with an active earth pressure coefficient $K_a = 0.23$ (Kerisel & Absi 1990 / taken from Craig 1997). The calculated shear stresses correspond to calculated active earth pressures against the 2.5 m high wall down to depth z = 2 m.

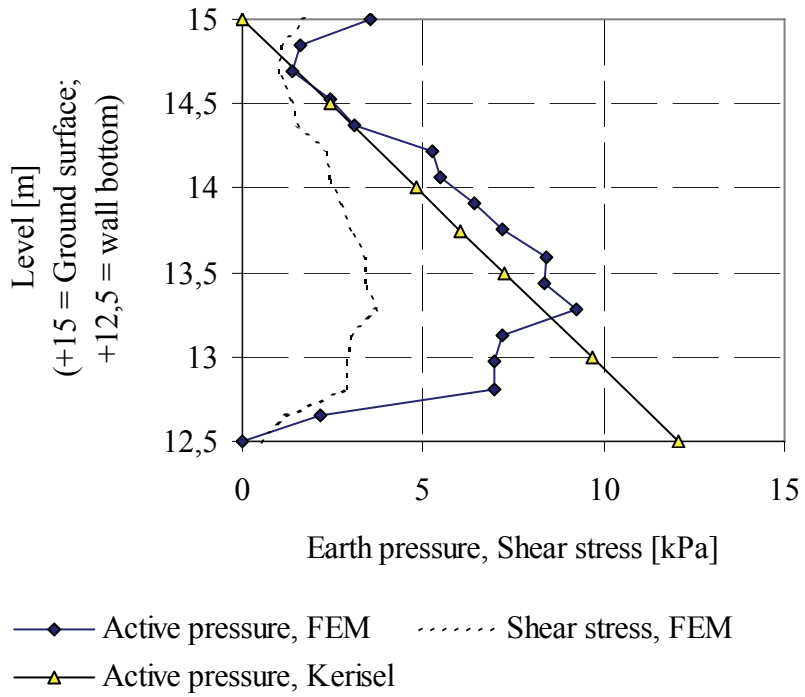

Figure 5.7 Active earth pressures according to FEM calculations after 10 mm displacement and corresponding Kerisel and Absi values. MC soil model.

The active pressure was much the same already after a horizontal displacement of 2 mm as after a displacement of 85 mm. Beyond that, the used software could not calculate. Thus, the ultimate active pressure after a really large displacement could not be analysed with the used software, but the used displacement level serves well in typical jointless bridge abutment calculations. The presented active pressures, 5–10 kPa, are small compared to previously presented passive earth pressures, less than 5 per cent, and may be ignored in most structural calculations related to jointless bridges.

Comparison with Hardening-Soil soil model and traditional earth pressure theories

The results from calculations with the Hardening-Soil model, and a comparison of the Hardening-Soil and Mohr-Coulomb models, are presented in the following figures. The pressure distribution calculated with the FEM model differed from the result based on the Kerisel and Absi theory, but the magnitude was quite close.

Due to the input value R_{inter} = 0.5, the wall friction angle in FEM calculations was δ = arctan(0.5*tan38°) = 21.3°. Based on the Coulomb earth pressure theory, the corresponding horizontal passive earth pressure coefficient was K_{ph} = cosδ*11 = 10.2, which was excessive according to Figure 5.8. According to Kerisel and Absi's earth pressure theory with values ϕ = 38° and δ = 21.3°, the passive earth pressure coefficient was K_p = 8 (e.g. Craig 1997).

Horizontal displacement of 50 mm corresponded to relative displacement of 0.02*H. At a depth of 1.25 m, the passive earth pressure is 268 kPa based on the Coulomb theory. Calculations with the HS or MC soil model yield an earth pressure of 177 kPa or 200 kPa, respectively.

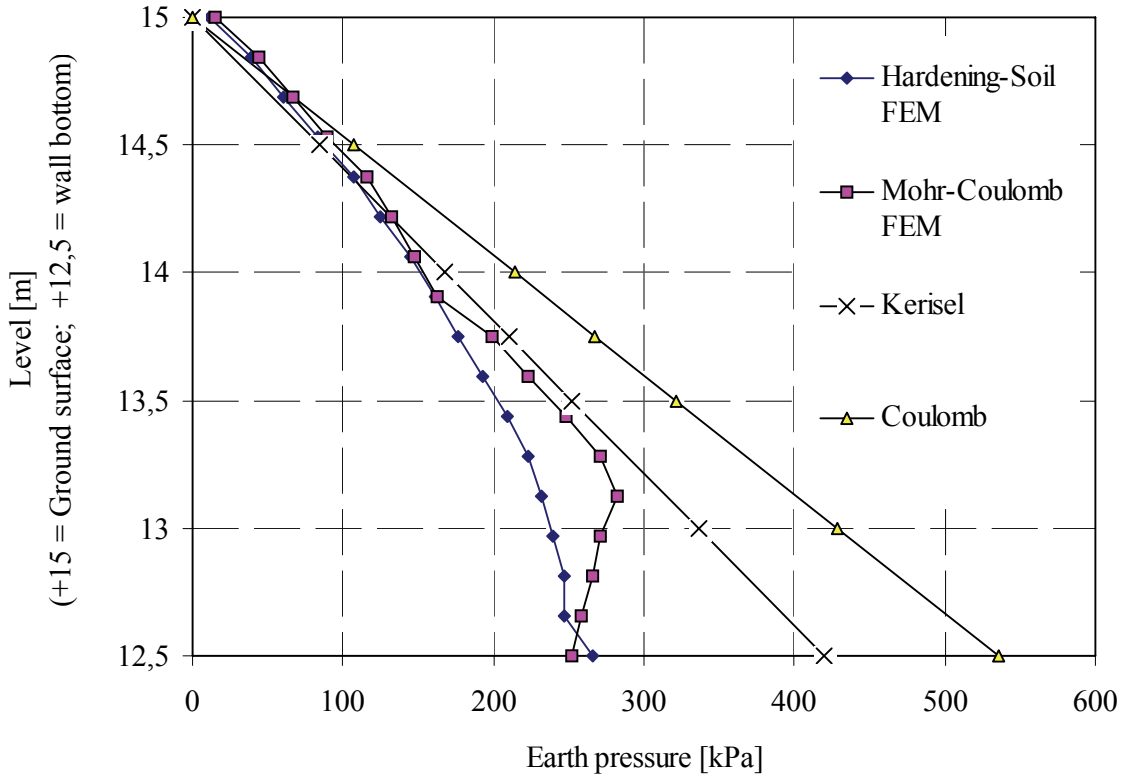

Figure 5.8 Calculated horizontal passive earth pressures with Hardening-Soil and Mohr-Coulomb soil models after 50 mm horizontal displacement. Comparison with Coulomb and Kerisel and Absi earth pressure theories using wall friction angle $\delta = 21.3°$.

Figure 5.9 allows determining the location of the failure surface. Next to the wall bottom, the failure surface on the passive earth pressure side was nearly horizontal while along the way to the soil surface its shape was circular. Below and above the failure surface the deformations within the soil were negligible. On the active earth pressure side, the failure surface was much more inclined and shorter.

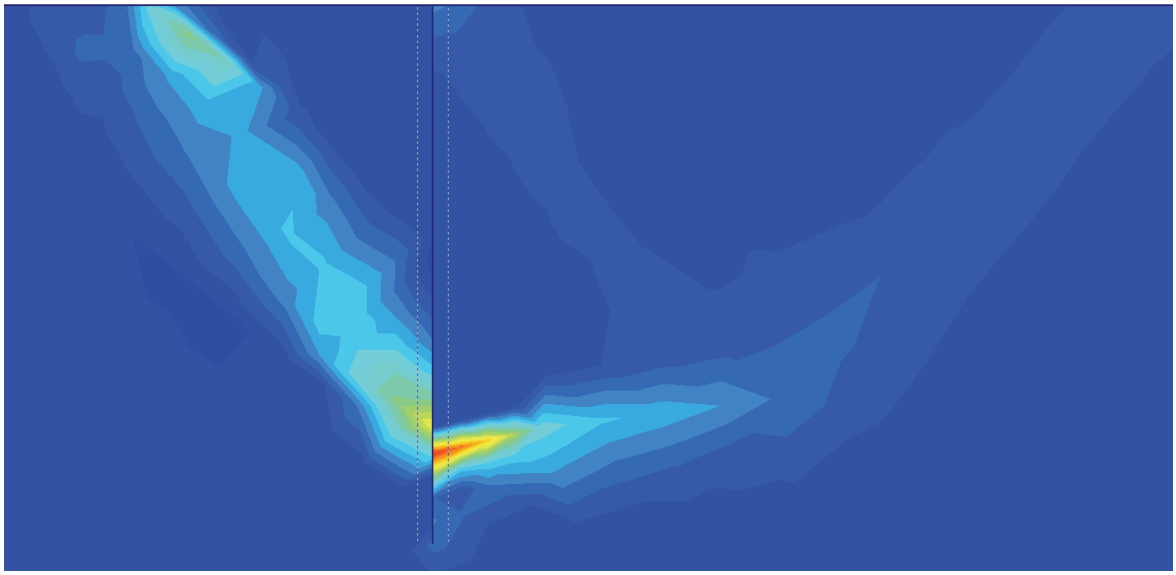

Figure 5.9 Shear strains after 50 mm horizontal displacement of wall calculated with the Hardening-Soil soil model.

The movement of separate soil zones can be concluded from the displacement increments at the end of the calculation phase (see Figure 5.10).

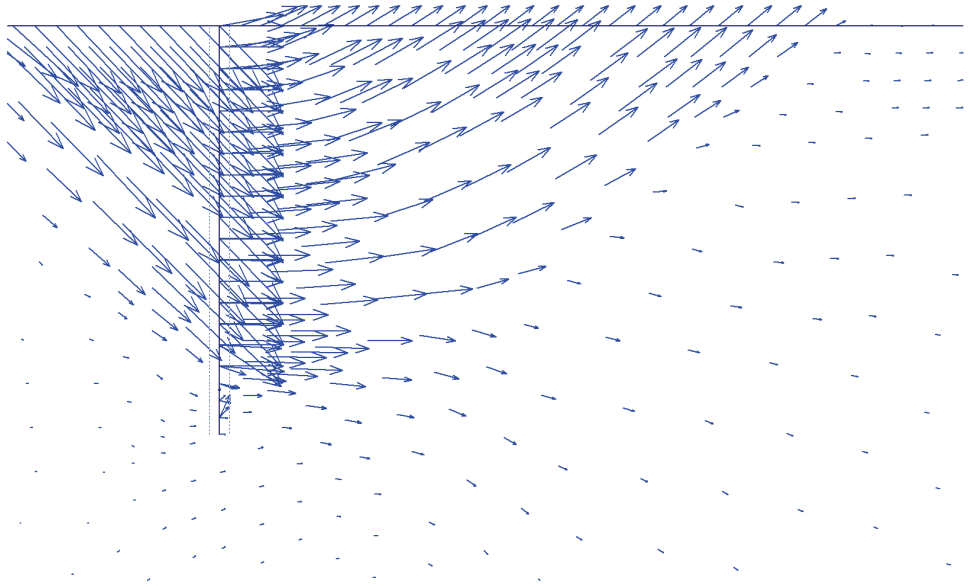

Figure 5.10 Displacement increments after 50 mm horizontal displacement of wall calculated with the Hardening-Soil soil model. The greatest increment, or the additional displacement, at the end of the last calculation phase was 0.3 mm.

From both Figure 5.9 and Figure 5.10 it can be concluded that the Coulomb theory failure surface, a plane, is not valid according to nonlinear FEM calculations.

Earth pressures were also calculated with wall friction angle $\delta = 4.5°$. With this small value the utilised FEM software yielded an ultimate result already after a displacement of 41 mm. After 10 mm displacement, the maximum earth pressure was 106 kN/m^2, which was remarkably smaller than with the wall friction angle $\delta = 21.3°$. Hence, the coarseness of the surface of the structure pushing against the soil has great significance considering the development of earth pressures.

For the sake of comparison, earth pressures were calculated also after an inclined prescribed displacement of 51 mm, that is, a combined 50 mm horizontal and 10 mm vertical displacement. The HS soil model was used, and the soil properties were the same as with the previous calculations. The total horizontal force after displacement was P_x = 366 kN compared to the total horizontal force P_x = 408 kN from a mere 50 mm horizontal displacement. Thus, the slightly larger displacement resulted in smaller earth pressures. The upward component of displacement diminished deformations within soil.

Horizontal displacement–earth pressure relation

The calculated earth pressures against the 2.5 m high wall at depth levels z = 1.25 m and z = 2 m are presented in Figure 5.11. The earth pressure corresponded to about 80 per cent of the maximum value already after a displacement of 30 mm or 0.012*H. The presented horizontal displacement–earth pressure relation supports the recommendation in Figure 5.2 (FGSV 1994).

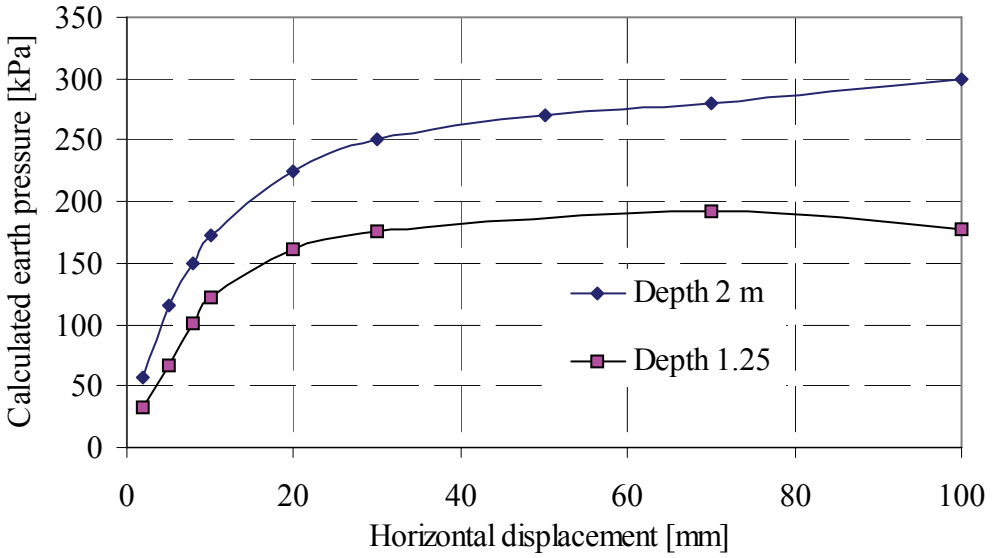

Figure 5.11 Displacement–earth pressure relation at two depths on 2.5 m high wall. E_d = 80,000 kPa. MC soil model.

At a depth of 2 m, the maximum earth pressure σ_h = 300 kPa corresponded to earth pressure coefficient K = 7.1 based on vertical pressure σ_v = 42 kPa. As the wall moved horizontally against the soil, the earth pressure increased almost linearly until a displacement of 15 mm or 0.006*H. As the displacement increased from 20 to 100 mm, the earth pressure increased only about 33 per cent.

A horizontal displacement of 50 mm or 0.02*H can be considered the limit value because thereafter earth pressure increased minimally (Cf. Figure 5.5). The limit value 0.02*H was much bigger than the current Finnish requirement of 0.002*H in dense sand or 0.006*H in loose sand. As a consequence, at the low displacement level of 5 mm or 0.002*H with the contemporaneous earth pressure coefficient K = 3, the lateral subgrade reaction was smaller than required by Finnish guidelines. Yet, the calculated maximum earth pressures were larger than those presented in Finnish guidelines.

Earth pressure against wall within various soils after 50 mm horizontal displacement

Comparison of various non-cohesive soils around the embedded wall was done according to Table 5.3 which shows the unit weight, stiffness moduli, internal friction angle and dilatancy angle of all the comparative cases. Wall friction angle was δ = 21.3°. The case with an internal friction angle ϕ = 38° corresponds to the previous HS soil model.

Table 5.3 Comparative cases. Properties of soil. HS soil model.

Property	Unit	Very loose	Dense	Dense to very dense	Very dense
γ	[kN/m^3]	17	21	21.5	23
E_{50ref}	[kN/m^2]	15,000	80,000	100,000	200,000
E_{urref}	[kN/m^2]	45,000	240,000	300,000	600,000
ϕ	[°]	32	38	42	45
ψ	[°]	0	3	7	10

The calculated earth pressures against the 2.5 m high wall after 50 mm horizontal displacement within various soils are presented in Figure 5.12.

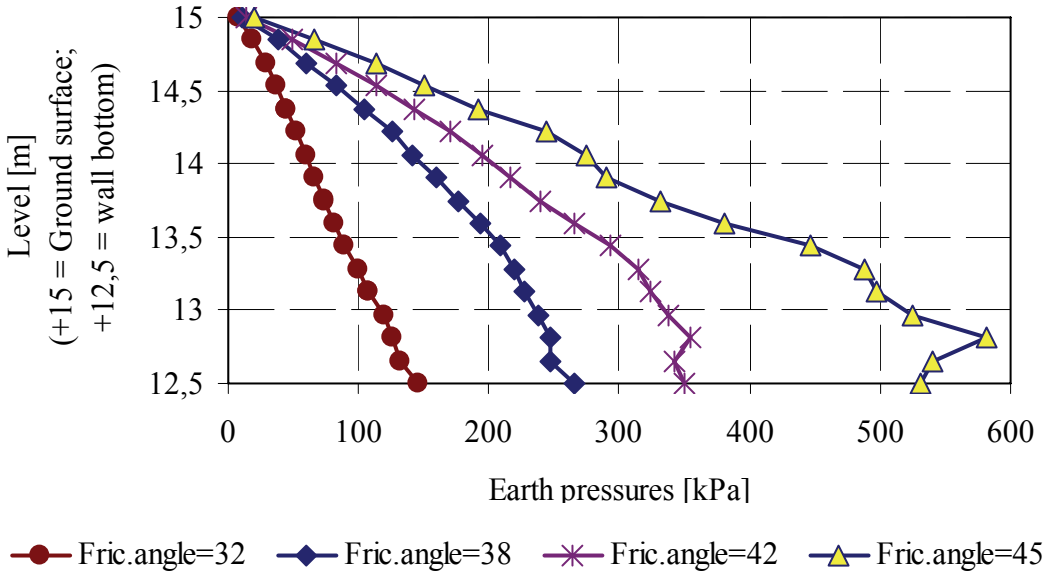

Figure 5.12 Earth pressure against wall within various soils after 50 mm horizontal displacement.

The effect of the variation in soil properties from very loose to very dense affects the intensity of the earth pressures against the whole height of the wall within the soil. With friction angles $\phi = 42°$ and $\phi = 45°$ and respective soil stiffnesses, the earth pressures were clearly higher than in the basic case with an internal friction angle $\phi = 38°$.

5.3 Influence of cyclic displacements on earth pressures and deformations

5.3.1 Structural model

The earth pressures, shear stresses and cumulative deformations from cyclic displacements of a wall constructed within soil were calculated with Plaxis 2D software (Plaxis 2002). The 40 m long and 15 m deep structural model is illustrated in Figure 5.3. The displacements were horizontal back and forth movements of a 2.5 m high wall. The size of the displacements was ± 15 mm or 0.006*H. During the 4 first cycles, calculation was stopped at the starting point, that is, the midpoint between the ultimate displacements. A displacement of +15 mm corresponds to the free thermal abutment displacement of a symmetric 120 m long bridge after a temperature change of +25 °C.

The mesh with triangular elements was dense near the wall (see App. 1). The elements were 15-noded plane strain elements. The calculation parameters for soil behaviour are presented in Table 5.4. The values were mainly based on typical dense gravel or crushed rock properties and were taken from (Finnra 1999a). The friction angle, ϕ, and coefficient R_{inter} were large. Also the wall friction angle calculated on the basis of these input values was large: δ = arctan (0.7*tan45°) = 35°. In Case 1, the unit weight of the soil, γ, was approximated on the basis of initial void ratio, e_{init}, and water content 4.5 %.

Table 5.4 Soil properties in Case 1. Hardening-Soil model (see Ch. 4.1.1).

γ	[kN/m³]	23
e_{init}	[-]	0,30
e_{max}	[-]	0.40
E_{50ref}	[kN/m²]	71,300
M_{ref}	[kN/m²]	69,706
Power (m)	[-]	0.5
c	[kN/m²]	1
ϕ	[°]	45
ψ	[°]	10
E_{urref}	[kN/m²]	285,200
ν_{ur}	[-]	0.2
p_{ref}	[kN/m²]	100
R_{inter}	[-]	0.7
E_{ur}/ E_{50}		4
Soil type		Drained
Interface permeability		Neutral

The dilatancy cut-off was used to stop the excessive volume increase of soil. The mobilised dilatancy angle, ψ_{mob}, was automatically set back to zero as soon as the volume change resulted in a state of maximum void, from e_{init} to e_{max}.

Comparative cases

In Cases 2–6 the void ratios and their difference, dilatation angle and the relation E_{ur} / E_{50} were changed. In Cases 7 and 8 a transition slab was added within the soil, and in Case 9 the wall bottom displacement was only half of the top displacement based on typical integral bridge abutment displacement. The exact values of various cases are presented in connection with the calculation results.

5.3.2 Calculation results and conclusions

The results of earth pressure calculations for Case 1 are illustrated in Figure 5.13. Earth pressure increased clearly after the first horizontal movement, and the increase was fastest during the first five cycles (see also Figure 5.18). The increase was distinct along the entire height of the wall, although near the bottom of the wall it was a little smaller. The increase in earth pressure was so evident that it should be recognised also in the estimation of earth pressures against the abutment of an integral bridge. The maximum value should be determined on the basis of the characteristic behaviour of the structure, not the traditional design based on non-cyclic behaviour. The nature of the abutment displacement, contemporaneous horizontal movement and rotation, also has to be considered in the evaluation of earth pressures (see also Figure 5.6 and Table 5.5/Case 9). In Case 1 with high non-cohesive soil strength and wall friction angle, the earth pressure coefficient down to depth z = 2 m was approximately K = 13 after 12th horizontal displacement.

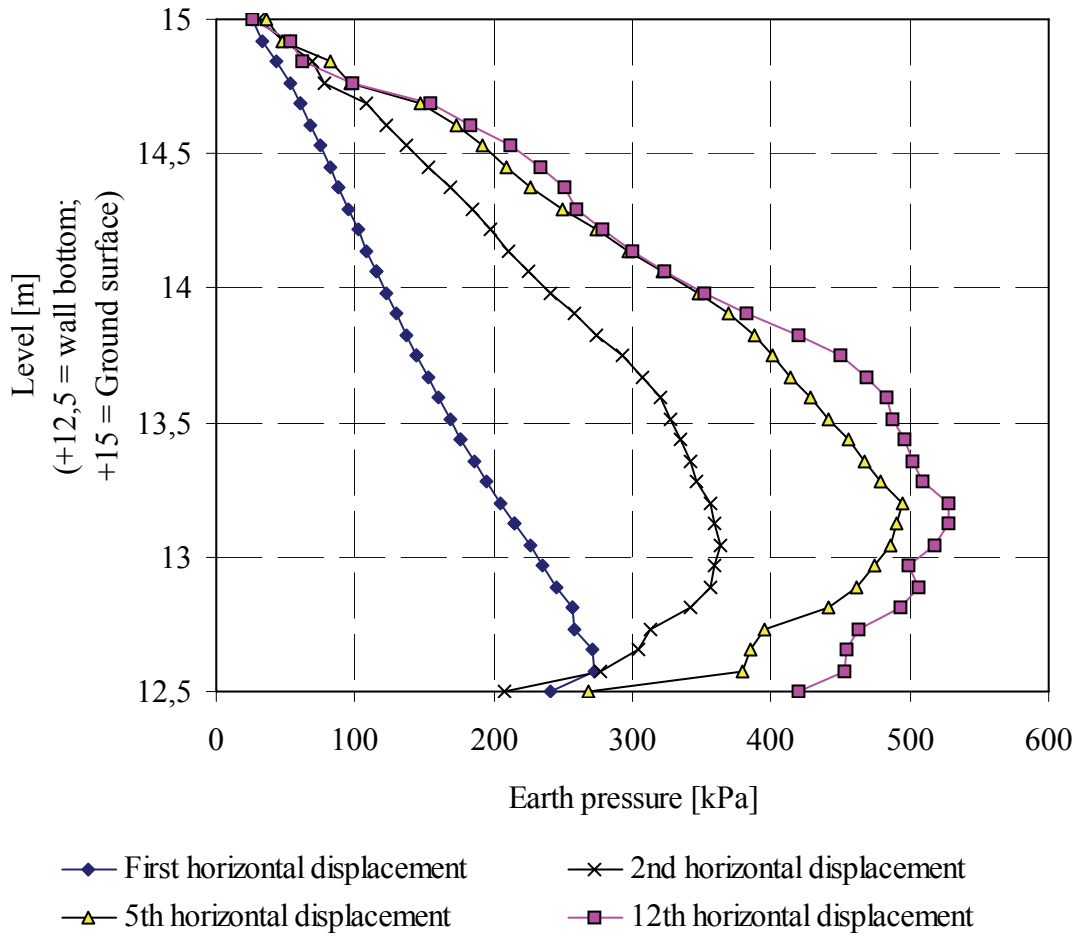

Figure 5.13 Earth pressures as effective normal stresses against the wall after first, 2nd, 5th and 12th horizontal displacement. Displacement magnitude was ±15 mm = 30 mm. Case 1.

The cyclically increasing earth pressures may result in a non-symmetrical movement of a bridge superstructure, which has been observed in field tests outside Finland (see e.g. App. 9 / Figure 0.4; Huang et al 2004).

The results of comparative study of cases

Table 5.5 shows the given values of all nine studied cases and the maximum positive (downward) and negative (upward) settlements at soil surface near the transferring wall after 12th positive movement. The plastic deformations on both sides of the wall were almost equal after 12 horizontal displacement cycles.

Table 5.5 Studied cases. Maximum positive and negative settlements at soil surface behind transferring wall. Displacement cycles were ±15 mm.

Case	Dilatation angle	Void ratio			Settlement		Note
	ψ [°]	e_{init} [mm]	e_{max} [mm]	E_{ur} / E_{50}	Upward [mm]	Downw. [mm]	
Case 1	10	0.3	0.4	4	122	105	
Case 2	10	0.13	0.13	4	130	210	
Case 3	10	0.13	0.18	4	122	170	
Case 4	5	0.13	0.18	4	130	170	
Case 5	10	0.13	0.18	2	37	55	
Case 6	10	0.13	0.4	3	117	95	
Case 7	10	0.13	0.4	3	100	60	*
Case 8	10	0.13	0.4	3	150	0	**
Case 9	10	0.13	0.4	3	55	65	***

* Transition slab was added above the cantilever support at the abutment.
** Transition slab was added and connected to the cantilever support at the abutment.
*** Prescribed horizontal displacement was only ± 7 mm at wall bottom.

According to the comparison with different input values, the most important cause for the size of deformations was the unloading–reloading modulus E_{ur}. Especially the smaller E_{ur} in relation to E_{50} gave remarkably smaller non-reversible deformations in Case 5 than the changes in dilatation angle or the changed dilatation cut-off performance from changing the difference between void ratios e_{max} - e_{init}.

In Case 9 the wall served as a model of a typical integral bridge abutment with a displacement at the bottom about half of the displacement at the abutment top. In that case the deformations near the wall bottom were clearly smaller than in other cases. Consequently, also the plastic deformations remained quite small.

Appendix 1 presents the displacements during the 12th horizontal movement for Case 6 from left to right. The largest total displacement was only 31 mm although the wall displacement was 30 mm. Hence, the directions of the movements near the wall were almost horizontal. Some other results for Case 6 are illustrated in the following figures.

The total displacements in the soil due to the horizontally moving wall after all 12 displacement cycles are presented in Figure 5.14. The largest total displacement was 169 mm, and the absolute values of the displacements were large over wide zones on both sides of the wall. The directions were almost vertical next to the wall and downward. Further from the wall, the direction of the overall displacement of soil was about 45 degrees from the horizontal soil surface.

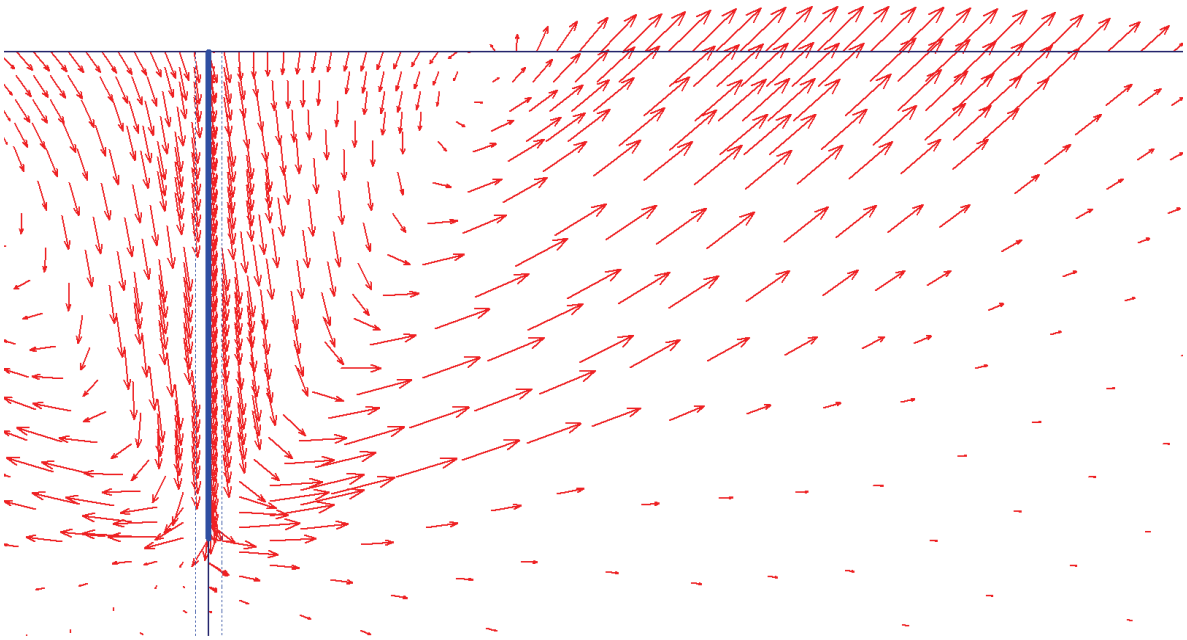

Figure 5.14 Total displacements in soil next to a horizontally moving wall after 12 displacement cycles and an extra positive wall movement. Total displacements were scaled up 2 times. Case 6.

The deformation increments in soil next to the horizontally moving wall at the end of the 12th positive displacement according to FEM calculations are shown in Figure 5.15. The largest soil particle increment was 0.12 mm. The triangular zones in the soil may be observed both on the left side (active pressure) and the right (passive pressure) side of the wall. On the passive earth pressure side, the soil movement direction was almost straight upward, which was the reason for the large soil surface upheave in the case of cyclic displacement and non-reversible soil movements (see also Table 5.5).

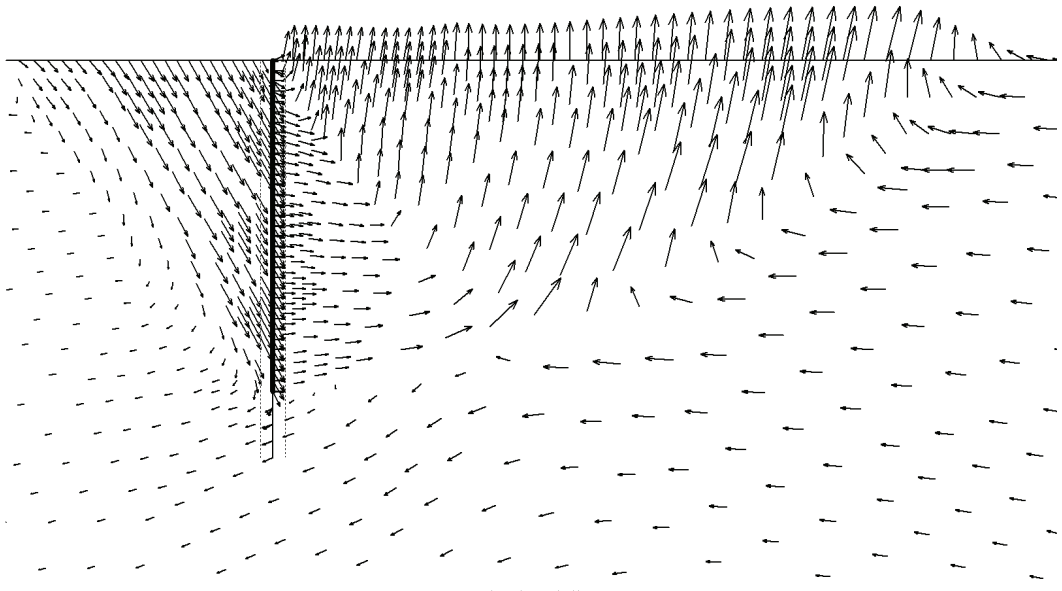

Figure 5.15 Deformation increments in soil next to a horizontally moving wall at the end of 12th positive displacement. Case 6.

The largest stress in soil was 855 kPa after the 12th positive displacement. On the active side of the wall, earth pressures against the wall were negligible. Yet, there were great residual stresses in the soil on the active side of the wall as can been seen on the left side of Figure 5.16. Although the wall had moved to the right, the horizontal stresses at depth z = 1.5–3 m were much bigger than normal at-rest earth pressures, which can be estimated from the horizontal line lengths in the lowest part of the figure.

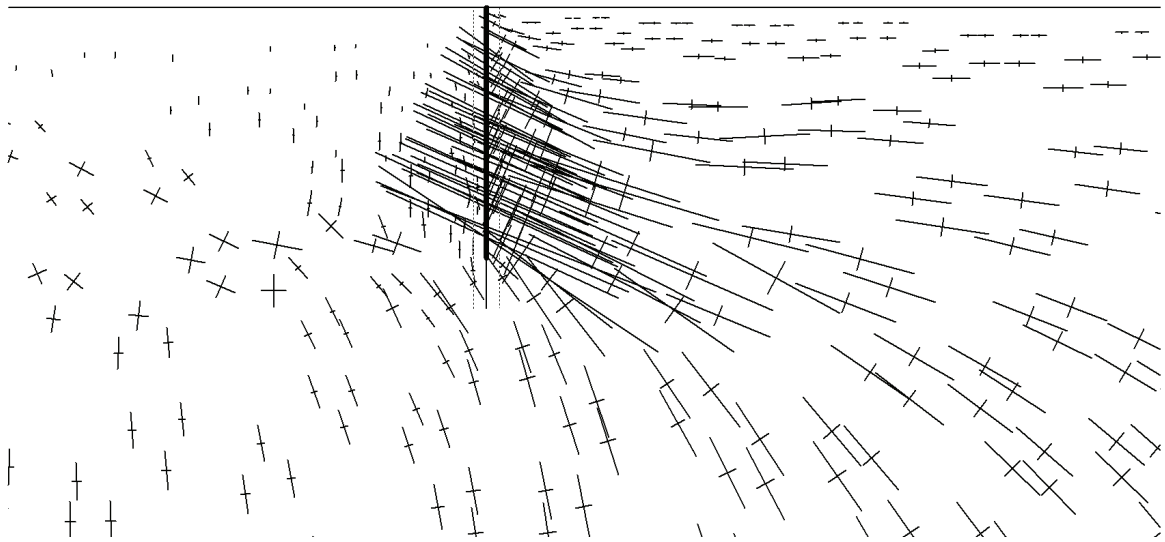

Figure 5.16 Effective stresses in soil next to a horizontally moving wall after 12th positive wall movement. Case 6.

The failure surface can be determined on the basis of maximum shear strains visualised in Figure 5.17 both at the active earth pressure phase and the passive earth pressure phase. The failure surface due to the passive earth pressure phase was a little curved and met the surface at a distance of about 2*H from the wall. That distance was less than calculated on the basis of the Coulomb earth pressure theory (e.g. Craig 1997) with the same wall friction angle.

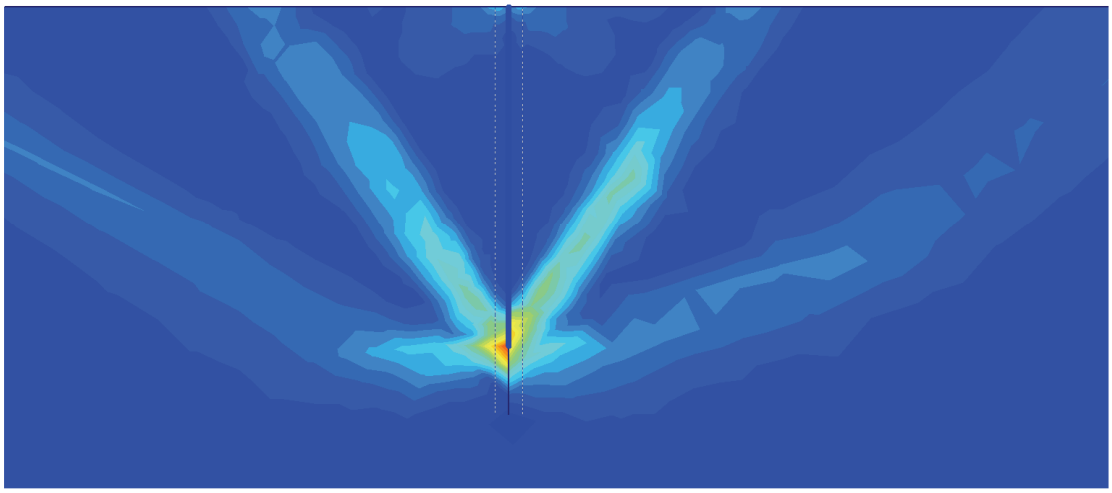

Figure 5.17 Shear strains in soil after 12th positive displacement. Case 6.

After 12 cycles, the maximum total horizontal force against the wall was 878 kN/m, and there was a 58 mm horizontal displacement in the soil 0.38 m from the wall at depth 1.86

m according to Figure 5.18. The average earth pressure corresponding to that total force was 351 kN/m^2, and the average earth pressure coefficient was K = 13.

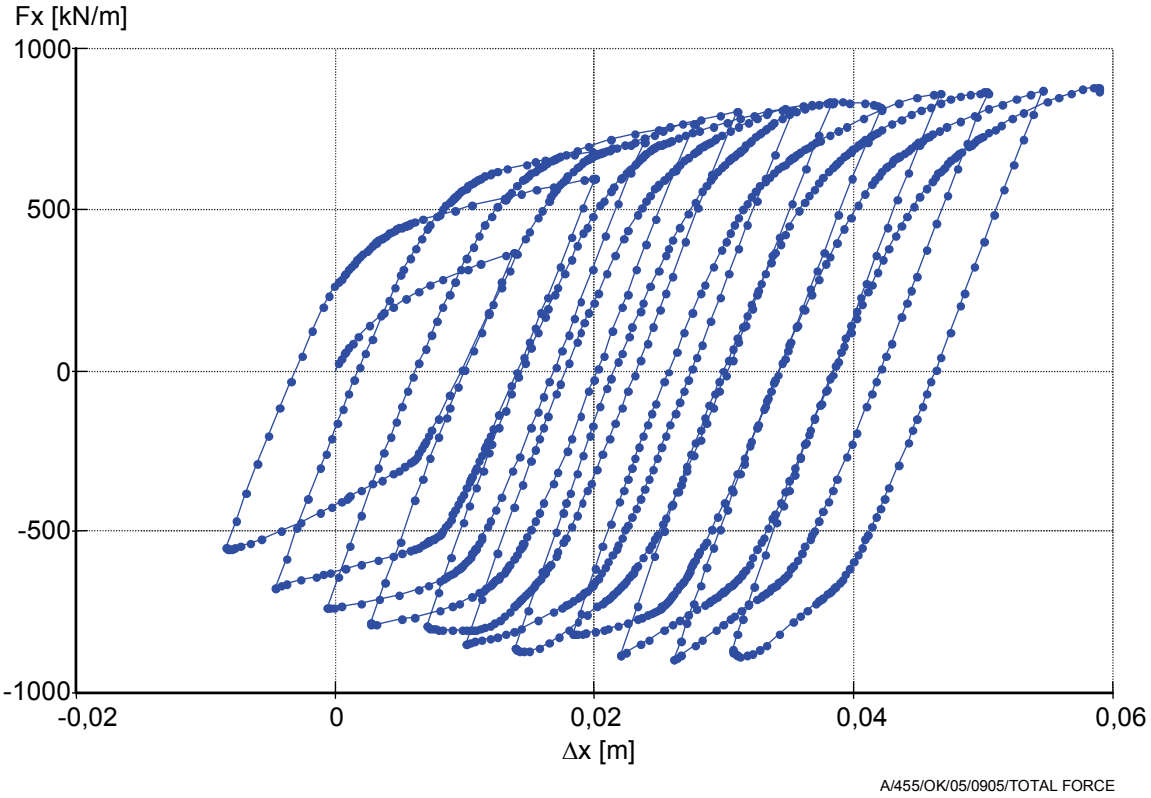

Figure 5.18 The total force against the horizontally moving wall related to a particle x-direction displacement at x = 12.380 m and y = 13.140 m during all twelve calculation cycles. Co-ordinate directions: positive x from left to right and positive y from bottom to top in Figure 5.3. Case 6.

The total force against the wall increased the most during the first five displacement cycles. During the last seven cycles, the force did not increase remarkably although the non-reversible deformations in the soil increased.

Above the observed particle in Figure 5.18, at depth 0–1.2 m, the non-reversible horizontal deformations were clearly smaller than the earlier presented non-reversible deformations. For instance, in soil 0.3 m from the wall at depth 1.06 m, a horizontal displacement of ±14 mm was completely reversible. In soil 0.33 m from the wall at depth 0.15 m, horizontal displacement was +14 to -22 mm and the studied particle moved slightly towards the wall along with each cycle.

As the wall returned after a full displacement cycle to its original position, the earth pressure on the left side of the model exceeded at-rest pressure while on the right side it was very small.

The earth pressure increase due to cyclic wall rotations has been observed, for instance, in empirical small-scale tests on jointless frame bridges (Tsang et al. 2002). The height of the test device was 600 mm. The initial void ratio of the Leighton Buzzard sand was e_0 = 0.58 and relative density was 94 % (England et al 2000). After 300 cycles of wall top movements of ± 0.0013*H, average earth pressure was approximately 2 times larger than after the first rotation and approximately 1.5 times larger than after the 10th rotation. These

observed values were smaller than the above-presented calculated values mainly because of the large soil calculation input parameters.

The effect of a transition slab on the settlement of the soil near the wall in Case 7 is illustrated in Appendix 1. The slab was not connected horizontally to the wall. The slab reduced settlement near the wall. Simultaneously, due to the progressive displacement cycles, it moved outwards from the wall and rose with each cycle. In Case 8 the transition slab was connected horizontally and vertically to the wall. The deformations in Case 8 are also illustrated in Appendix 1. The slab rotated around its connection and its free end rose. The case, where vertical dowels connect the transition slab only horizontally to the wall could not be modelled by the utilised software code.

As large deformations and settlements as presented here due to abutment displacements are not permitted on the surface of a bridge approach embankment. During maintenance the pavement will be repaired and levelled.

With a 2D model strains in the 3rd dimension are prevented, and the 3rd dimension is supposed to be extremely long. A bridge and a road embankment do not fulfil this prerequisite in the transverse direction. Consequently, 2D models should be used with caution in analysing jointless bridges and embankments. The wing walls are used to limit transverse strains in backfill adjacent to the abutment, which partly justifies use of the 2D models (Cf. Chs. 6.2.5 and 6.3.2).

5.4 Summary and recommendations

With the presented simple calculation model it is possible to verify the traditional earth pressure theories with varying soil properties, wall inclinations, earth surface inclinations, etc. in a non-cyclic 2D case. The results can also be presented based on a certain prescribed displacement level. This kind of easy-to-use special geotechnical software and the presented calculation model are recommended also for structural designers for earth pressure calculations. Earth pressure distribution can be analysed quickly and simply in various cases and in relation to various structure movements.

The use of the presented model was expanded to the evaluation of the deformations and earth pressures from cyclic wall displacement. The earth pressure increase calculated with the used soil model and the chosen soil properties were larger than the observed increase in small-scale tests in England. The calculated deformations after 12 displacement cycles were also quite large. Yet, the method performed satisfactorily in analysing the characteristic displacements and residual stresses within soil. The behaviour of transition slabs could also be analysed with the presented cyclic wall displacement model.

Figure 5.19 presents the recommended earth pressure coefficient-abutment movement relationship. The recommendation covers cyclic abutment displacement (quite high pressure after a small displacement), wall friction angle (Kerisel and Absi earth pressure theory) and makes the task of designers easier (linear during displacement 0–0.01*H). Compared to the present Finnish practice, the actual earth pressure does not increase dramatically on jointless medium length (40–70 m) bridges. Active earth pressure may be ignored in general jointless bridge earth pressure calculations.

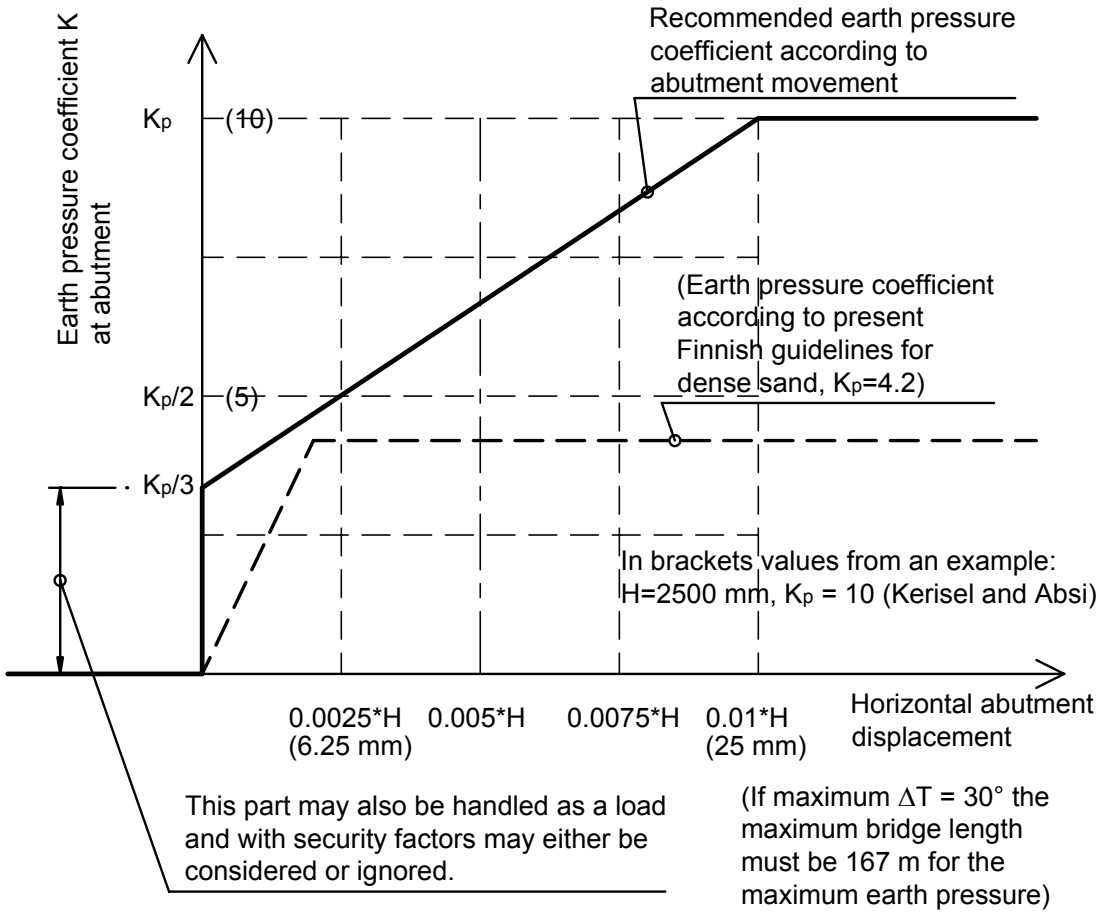

Figure 5.19 Recommended earth pressure coefficient based on abutment displacement.

The presented abutment displacement for full passive earth pressure, $\delta_p = 0.01*H$, is based on a typical abutment height, H = 2.5m, and the behaviour of typical approach embankment material, dense gravel or crushed rock.

Examples of estimation of earth pressure coefficients based on Kerisel and Absi´s earth pressure theory (Craig 1997):

- Example 1 (concrete–sand): $\phi = 38°$ and $\delta = 19°$ => $K_p = 8$ and $K_a = 0.22$.
- Example 2 (concrete–crushed rock): $\phi = 43°$ and $\delta = 21.5°$ => $K_p = 12$ and $K_a = 0.18$.

In Figure 5.19 the used passive earth pressure coefficient was the mean of these examples; it is clearly bigger than the value used in Finland at the present time. In any case, the bigger value is recommended due to the actual behaviour of the structure, that is, the interaction of the embankment soil and the abutment. Wall friction clearly increases earth pressure.

6 BEHAVIOUR OF INTEGRAL ABUTMENTS AND APPROACH EMBANKMENTS

6.1 Presentation of discussed phenomena

The most essential phenomena studied in Chapter 6 are presented in Figure 6.1. The calculated earth pressures, abutment rotations and the bending moment of piles after the forced displacement of 7 mm at the deck level were also used to verify the behaviour of Haavistonjoki Bridge.

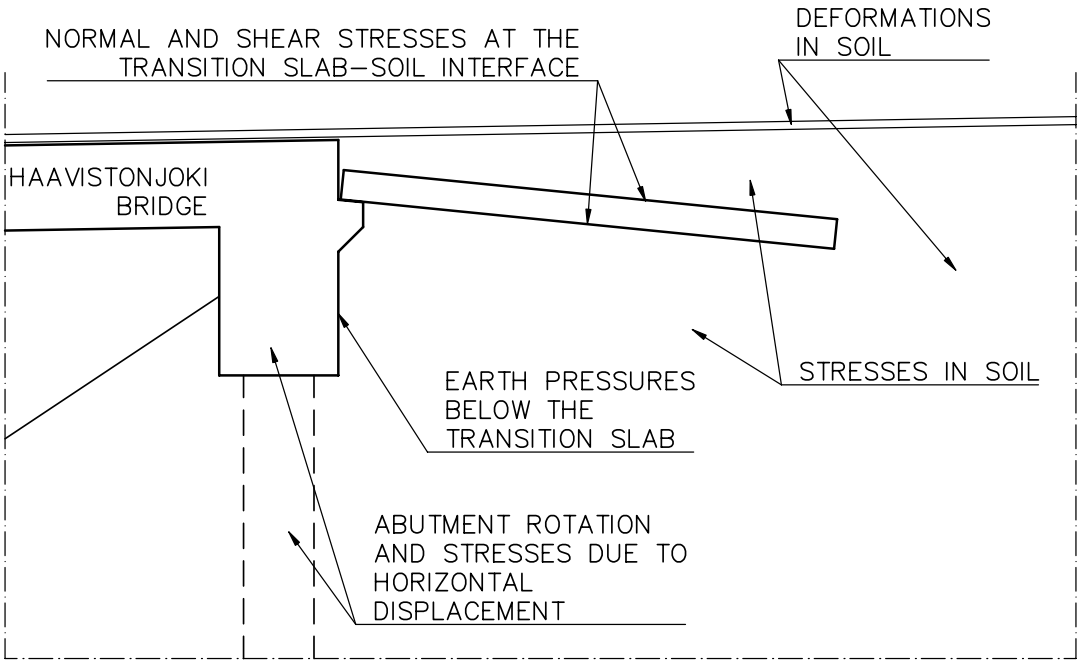

Figure 6.1 Phenomena studied in Chapter 6.

6.2 Performance of approach embankment and development of bump

6.2.1 Estimated maximum shear strain in backfill

Shear strain in the backfill near the abutment can be approximated by the equation (Bolton 1993):

$\gamma = 2 * \delta / H$,

where γ is shear strain, δ is horizontal displacement of abutment and H is height of abutment.

The maximum horizontal bridge abutment displacement from temperature change ΔT = 30°C in a 50 m long bridge, like Haavistonjoki Bridge, in a completely symmetrical case is:

$\delta = \alpha * \Delta T * L/2 = 10 * 10^{-6}$ 1/°C * 30 °C * 50,000 mm / 2 = 7.5 mm,

where L is bridge length and α is coefficient of thermal expansion.

The corresponding shear strain is

$\gamma = 2 * \delta / H = 2 * 7.5 \text{ mm} / 2500 \text{ mm} = 6 * 10^{-3}$.

Shear modulus at a certain shear strain level may be determined from the diagram in Figure 6.2. In a symmetrical 50 m long bridge the shear modulus of the backfill decreases from G_{max} to $G = (0.1–0.2)*G_{max}$ due to the large deformations during bridge thermal expansion according to the presented diagram. As a result, the plastic strains in a backfill material will be quite large. Longitudinal displacements due to a vehicle braking are much smaller, G/G_{max} is near 1, and the embankment is much stiffer than with large shear strains. Consequently, the horizontal stiffness of the embankment varies greatly according to the shear strain level.

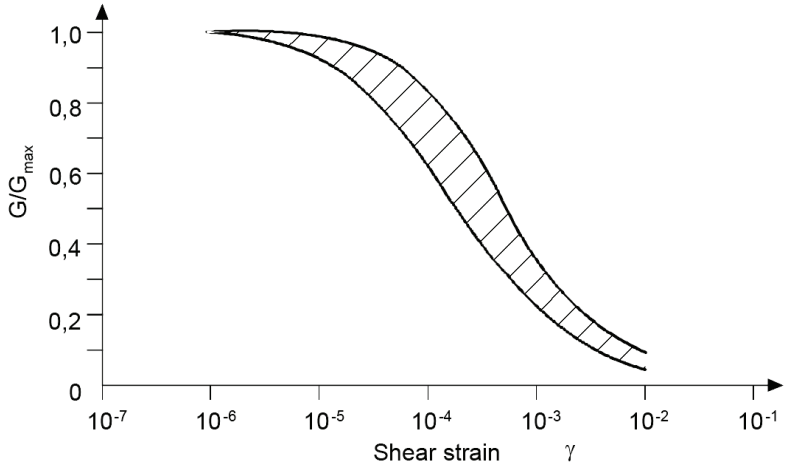

Figure 6.2 Typical variation in shear modulus according to shear strain level (Finnra 2001b).

6.2.2 Development of bump at approach embankment

According to a query, the bump at a bridge embankment causes problems in 25 per cent of all bridges in the United States of America (Briaud 1997). In many states the approach bump requires regular maintenance and causes high maintenance expenses. A jointless deck with integral abutment and large temperature changes increase the risk of a bump (see Figure 6.3). The co-operation of various specialists: the geotechnician, construction designer, constructor and maintenance chief has diminished the risk.

The most commonly reported causes of the bump are (Briaud 1997):

- Compression of the fill material
- Settlement of the natural soil under the embankment
- Poor construction practices
- High traffic loads
- Poor drainage
- Poor fill material
- Loss of fill by erosion
- Poor joints
- Temperature cycles

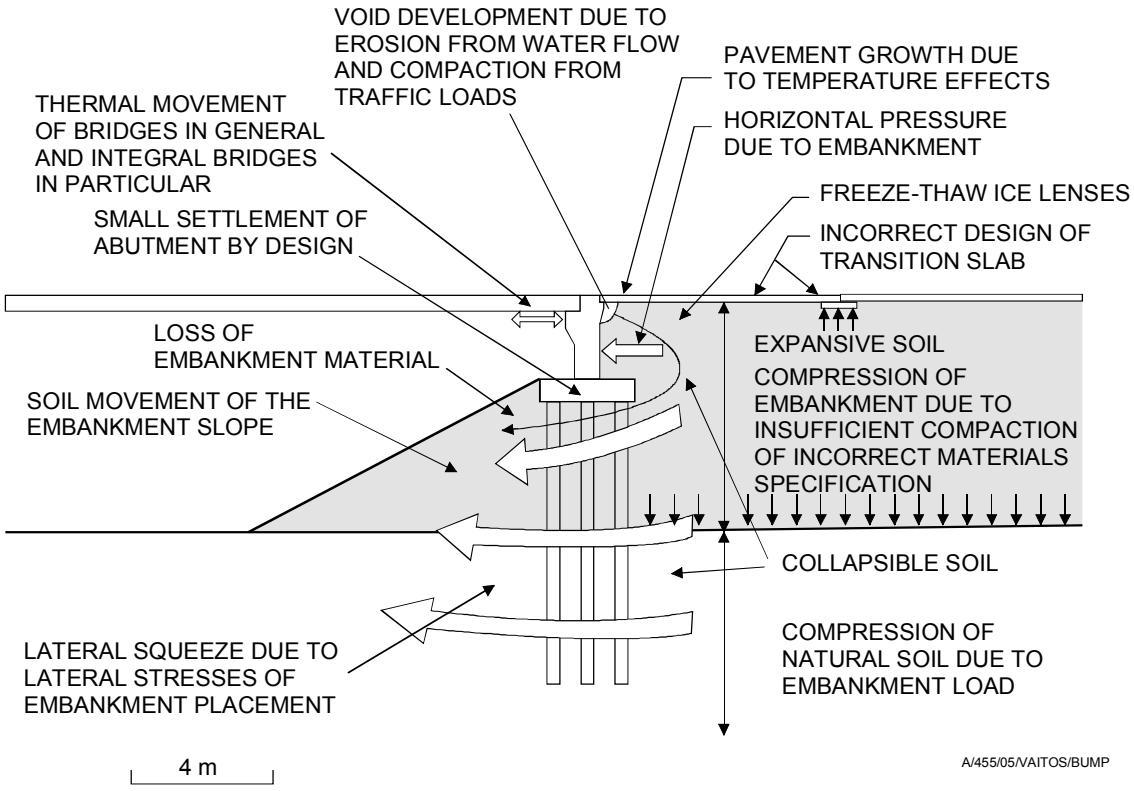

Figure 6.3 Main causes for the approach bump (Briaud 1997).

An excessively steep slope might lead to a loose approach embankment.

According to the query, the bump is minimised by the following factors (Briaud 1997):

- Abutment and embankment on strong natural soil
- Approach slab / transition slab (long and strong enough)
- Well-compacted or stabilised fills
- Good fill material
- Good drainage
- Low embankments
- Adequate interval between fill placement and paving
- Good construction practice and inspection
- Light truck traffic

Frost susceptible soil cannot be permitted in approach embankments.

The subsoil should be improved, for instance, with deep stabilisation methods, if necessary.

The use of a high coefficient of safety, for example 1.8, in slope design is needed to keep the horizontal displacements of the embankment within allowed limits. If the slope is 1:1.5 or steeper, the compaction of fill material cannot be completed properly. If the steepness of slope is, for example, 1:3, the slope can be compacted properly, but it also requires more space.

6.2.3 Improvement of abutment zone behaviour

The following measures have been found to be effective in preventing and mitigating approach settlement problems (Arsoy et al. 1999):

- Settlements should receive prime attention during design.
- An efficient drainage system should be incorporated in the design.
- Adequate compaction specifications and procedures should be employed. The denser the soil, the less vulnerable it is to settlement. One exception to this is soil in close proximity to the abutment. The cyclic nature of the abutment displacement will loosen dense backfill and densify the loose backfill. In other words, deformations induced by the abutment result in a density that is independent of the initial density of the backfill material. Therefore, very dense backfill is not likely to help reduce the settlement associated with moving abutments. This should be recognised and either adequate transition slabs or continuous pavement patching is required to compensate for the inevitable approach fill settlements.
- If the ground under the embankment is likely to settle significantly, soil improvement such as preloading, vertical drains, and other stabilisation techniques should be considered.
- It should be recognised that the traditional approach embankments of integral bridges are likely to require continuous maintenance in future.

Parallel use of a vertical elastic board behind the abutment and geotextiles within the approach embankment reduce horizontal earth pressures (see Figure 6.4). The problems with embankment settlement also diminish. The board provides an elastic horizontal support for the backfill while allowing abutment movements without excessive deformations within the backfill soil. Because of the support the vertical boards provide for the backfill, it is necessary that they remain elastic and preserve their original thickness after long-term use and cyclic thermal movement (see also App. 9; Hoppe 2005).

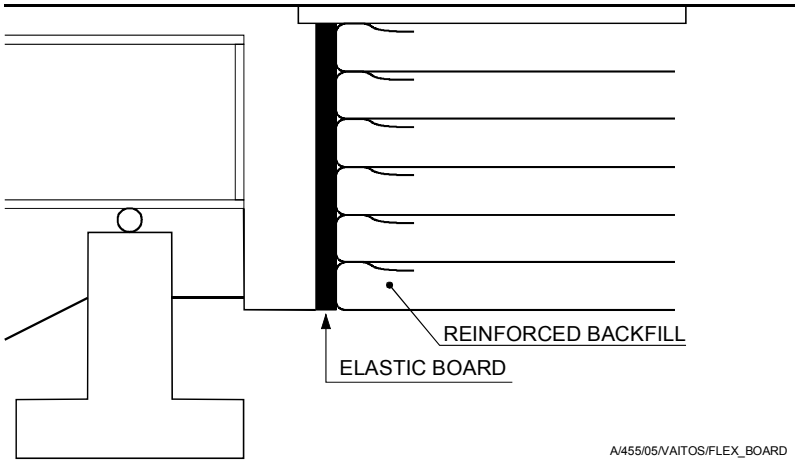

Figure 6.4 Vertical elastic board behind the abutment (Nielsen 1994).

6.2.4 Observed performance of approach embankment pavements in Finland

Finnra has monitored approach embankment performance during the years 1998 and 1999. In the case of the three monitored jointless bridges, where the asphalt pavement had a sealed expansion joint, bridge length was 64–76 meters and abutment height was 2–3 meters with ordinary transition slabs, the asphalt was in satisfactory condition (Finnra 2001a).

The joint seals in six observed long bridges were in order in only 50 per cent of the studied cases. Therefore, the researchers suggested that open pavement joints should be sealed immediately and authorities should consider certain recommendations and limiting values for the bridge design phase.

Wide joints filled with an elastic substance were found to serve better than mechanical joints and were recommended at least for motorway pavements.

6.2.5 Recommendation for wing walls

The wing walls cantilever horizontally from the back of the abutment wall, and must be designed to resist outward earth pressure. In classical soil mechanics, K_p is the largest possible ratio of soil pressures in the horizontal direction. This also applies to horizontal pressure against the abutment after a large displacement. If full passive pressure is used for the design of the abutment, this cannot exist without a pressure coefficient of at least one against the wing walls. Therefore, the wing walls should be designed for soil pressures based on K = 1 (Nicholson 1998, see Figure 6.5). The presented value is clearly larger than according to present Finnish practice. A calculation made to analyse earth pressures against the wing walls in one simple case is presented in Appendix 8.

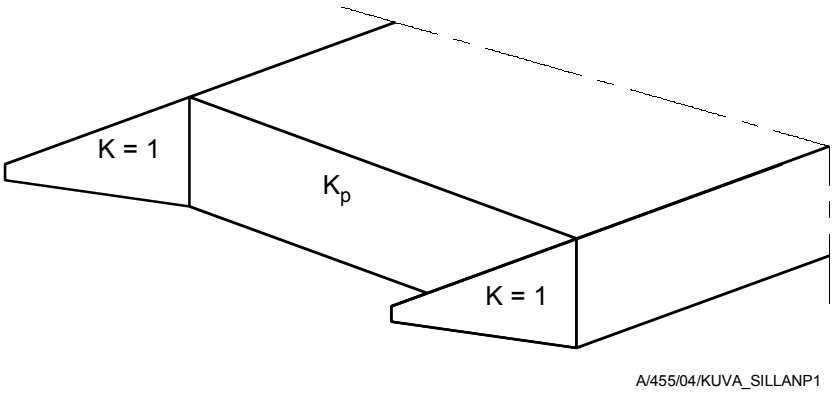

Figure 6.5 Earth pressure coefficients against the wing walls according to Nicholson (1998).

6.3 Behaviour of transition slabs

6.3.1 Overview

A transition slab constructed on top of the embankment is usually called an approach slab. Such slabs are used primarily in North America (see Figure 6.6). This research involves calculations on transitions slabs cast inside the embankment approximately 0.5 m–1 m deep.

The main reason for the use of transition slabs is to prevent the settlement of the embankment surface (Burke 1993).

Traditional transition slabs have to be attached to the abutment with reinforcement bars or dowels due to the continuous horizontal cyclic temperature movements at the bridge abutment. Otherwise, the slab will move slowly so far from the abutment that it might fall off its support (Cf. Ch. 5.3.2).

In order to increase designer confidence in integral abutment bridges, periodic and systematic visual inspections of structures built in the Province of Ontario were carried out to record their performance (Husain and Bagnariol 2000). The results of the observations were very encouraging. The structures were performing well and there were very few signs of deterioration or distress in any of the observed structures. The following observations are worth mentioning. The isolation joint detail shown in Figure 6.6 works well when the total length of the structure is less than 75 meters for a steel structure and 100 meters for a concrete structure. The gap widens in winter and the edges of the asphalt pavement appear to separate from the sealing compound. This gap, however, closes again in summer and does not result in any loss of riding quality. It was anticipated that after a few years of repeated movements it might become necessary to replace the rubberised joint sealing compound and carry out minor repairs to the edges of the asphalt pavement. In some cases where the total length of the structure exceeds the above limits, there is evidence of a wider gap at the joint location and distinct separation of sealant during the winter months.

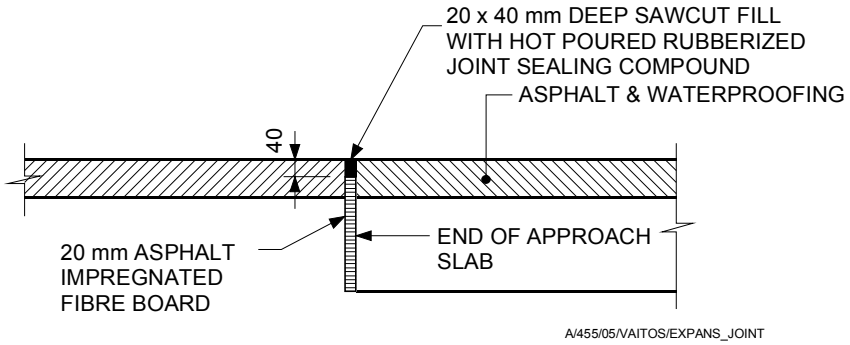

Figure 6.6 Expansion joint at end of approach slab. Maximum movement 25 mm according to Ministry of Transportation in Ontario, Canada (Husain and Bagnariol 2000).

A query in the U.S.A. revealed many construction problems with approach slabs in many states (Hoppe 1999). Approximately 50 per cent of respondents have had difficulty obtaining a specified degree of fill compaction in the proximity of bridge abutments. This is often cited as one of the main causes of approach slab settlement. Because of spatial limitations near the abutments, only small compaction equipment is normally used. A clear majority, 55 per cent, of respondents were convinced that approach slab settlement is a significant maintenance problem. Twenty-nine per cent of respondents consider it a moderate problem. Sixteen per cent do not view it as a problem.

According to Hoppe (1999), the pre-cambering of bridge approaches at up to a 1/125 longitudinal gradient for a minimum distance from the abutment equal to the length of the transition slab should be implemented where practical. The pre-cambering accommodates the differential settlement that will inevitably occur between a structure constructed on deep foundations and adjoining fill. Hoppe also prefers the underside of the transition slab to be placed at 700 mm below the surface and sloping away from the abutment.

According to the calculations presented in Chapter 5.3.2 (Cases 7 and 8), the importance of the transition slab is more pronounced when abutment movement is cyclic compared to non-cyclic abutment movement or traditional abutments. Large settlements and bumps may develop because of large non-reversible deformations in the backfill soil.

6.3.2 Evaluation of Haavistonjoki Bridge transition slab and approach embankment behaviour with a 2D FEM model

The structures of Haavistonjoki Bridge were presented in Chapter 4.2.1 while the results of field tests were presented in Chapter 4.2.5.

In a 2D FEM model of Haavistonjoki Bridge the columns and piles were modelled by calculating the real bending stiffness and sectional area and dividing the values by half the width of the bridge. The steel pipe piles are supposed to behave like a composite structure consisting of a pipe and the reinforced concrete within. In the model continuous walls like those in a frame structure have been used to model two isolated piles. Consequently, the modulus of elasticity, E, in the soil in the vicinity of the piles is reduced by a factor (3 times pile width/bridge half width) = 3 * 0.711 m / 5.75 m = 0.371. It must be emphasised that the behaviour of the reduced soil is the same in both directions, but during the last separate calculation stage, prescribed deck end displacement, the effect is minimal.

Wing walls and embankment slopes limit lateral embankment deformations. Yet, the real 3D stiffness of the embankment structure is smaller than an approximation with a 2D calculation model due to lateral deformations. The calculation model is illustrated in Figure 6.7.

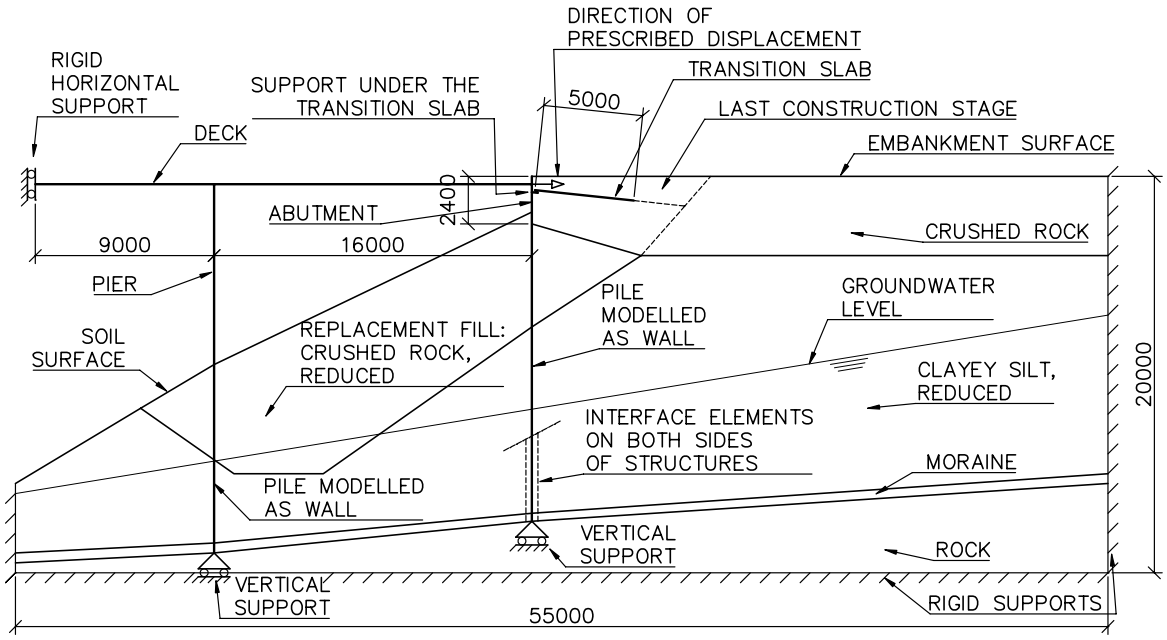

Figure 6.7 Plaxis 2D FEM model of Haavistonjoki Bridge (Kerokoski 2005d).

The model is designed to consider correctly also the fill area under the bridge slab. The transition slab is a 5 m long reinforced concrete slab within the approach embankment supported on a seat at the abutment. Vertical dowels to tie the transition slab to the abutment could not be modelled with the used software code.

The Plaxis 2D FEM code and Hardening-Soil soil model were used to calculate the Haavistonjoki Bridge deformations and stresses. The results of two separate modules of elasticity of crushed rock were compared, namely E_d = 80,000 kPa and E_d = 250,000 kPa. The lower value was taken from Finnish guidelines (Finnra 1999a) for well-compacted non-cohesive soil. The higher value was from the performed tests (see Ch. 4.2.2). The aim

was to compare the calculation results to observed values and to find out which corresponds more closely to them. Other soil parameters used are presented in Table 6.1.

The strength parameter, ϕ, for crushed rock was also from the tests. Other values were mainly taken from (Finnra 1999a) as typical values.

Table 6.1 Properties of soil.

Soil material	γ [kN/m^3]	γ_{sat} [kN/m^3]	E_d [kN/m^2]	ν	ϕ [°]	ψ [°]	R_{inter}
Crushed rock, embankment	22	23.1	80,000	0.3	45	8	0.5
Crushed rock, reduced	20	22.0	29,700	0.3	42	5	0.2
Clayey Silt, reduced	17	18.1	9,300	0.3	33	0	0.2
Moraine	23	23.0	80,000	0.3	45	4	0.7

Extra soil data:

- Cohesion c = 1 kPa ≈ 0 kPa,
- In crushed rock soil dilatation in embankment and around the piles ended when unit weight was reduced to 19 kN/m^3,
- Tension cut-off was on,
- Unloading-reloading modulus $E_{ur} = 3 \times E_{50}$,
- E_d (here) = E_{50} = Confining stress-dependent stiffness modulus,
- $E_{50} = E_{50ref} \times (-\sigma'_3 / p_{ref})^m$, if cohesion is c = 0,
- Level of stress dependency is given by power m = 0.5,
- Reference pressure in embankment soil p_{ref} = 30 kPa = minor principal stress σ'_3.

The calculations were done in nine stages according to real construction stages.

The R_{inter} factor for the reduced soil layers representing the soil around the piles was made as small as possible considering the software code's capacity to perform all the necessary calculation phases. Small R_{inter} factors describe soil behaviour best if the idea is to model two separate piles with one wall.

Comparison of various properties of crushed rock at the approach embankment level was done according to Table 6.2, which shows the unit weight, stiffness moduli, internal friction angle and dilatancy angle of the comparative cases. All the comparative cases were different from the basic case presented in the table above.

Table 6.2 Comparative cases. Properties of soil at abutment level. HS soil model.

Property	Unit	Very loose	Dense	Dense to very dense	Very dense
γ	[kN/m^3]	17	21	21,5	23
E_{50ref}	[kN/m^2]	15,000	80,000	100,000	200,000
E_{urref}	[kN/m^2]	45,000	240,000	300,000	600,000
ϕ	[°]	32	38	42	45
ψ	[°]	0	3	7	10

Calculation results

Because of the large deformations in the soft soil below the backfill, the average pressure at the bottom of the abutment was about 75 kPa before it moved according to a prescribed displacement. So the increase in earth pressure was only about 120 kPa - 75 kPa = 45 kPa with crushed rock with E_d = 80,000 kN/m^2.

At depth z = 2 m with crushed rock E_d = 250,000 kN/m^2, the increase was about 170 kPa - 80 kPa = 90 kPa, which corresponds to measured values. The same calculated earth pressure increase developed also just below the transition slab, which also corresponds to measured values. The measured values due to the same abutment movement are presented in Chapter 4.2.5 (Figure 4.20). The average measured earth pressure at the centre of the abutment was 80 kPa. Near the abutment bottom earth pressure did not increase remarkably despite the prescribed abutment displacement. The same phenomenon was discovered by the calculation presented in Chapter 5.2 (see e.g. Figure 5.5 and respective conclusions). The calculated earth pressures are presented in Figure 6.8 and Figure 6.9.

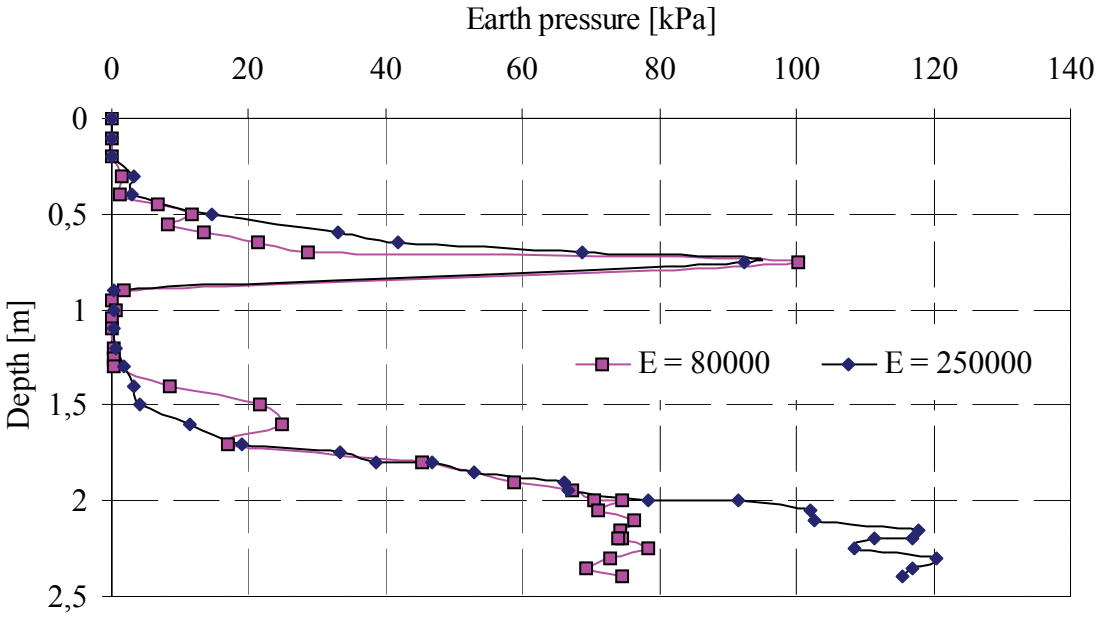

Figure 6.8 Earth pressures [kN/m^2] against the abutment after the construction stages, i.e. before prescribed displacement. E_d = 80,000 kPa or E_d = 250,000 kPa for crushed rock.

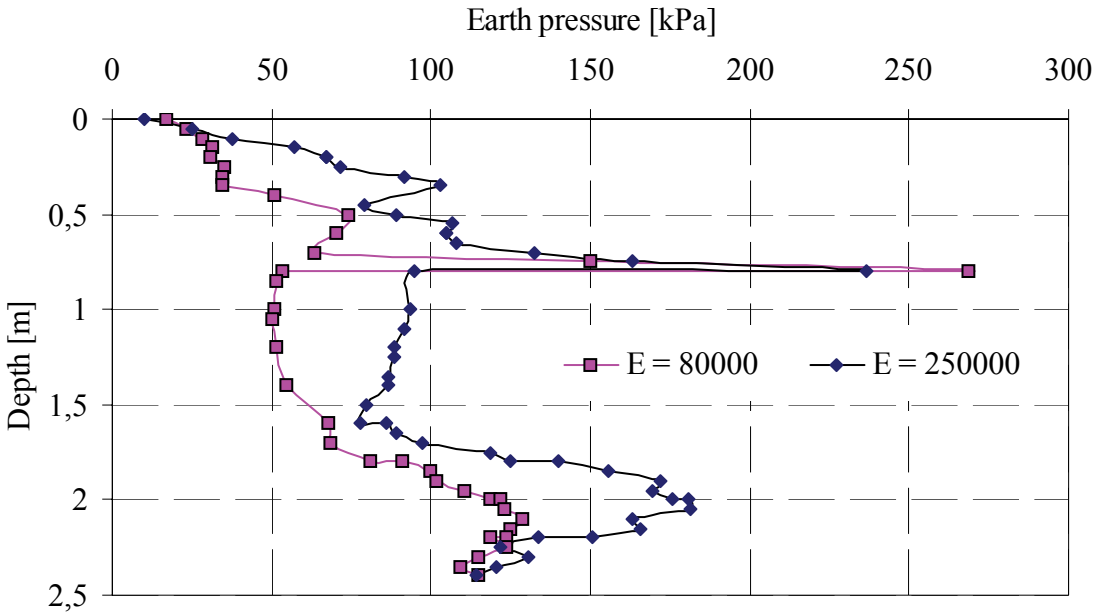

Figure 6.9 Calculated earth pressures [kN/m^2] on Haavistonjoki Bridge abutment after forced displacement of 7 mm at deck level. The transition slab at depth z = 0.8 m is clearly visible.

The calculated earth pressures on Haavistonjoki Bridge abutment after prescribed displacement of 7 mm at deck level according to various crushed rock properties are presented in Figure 6.10.

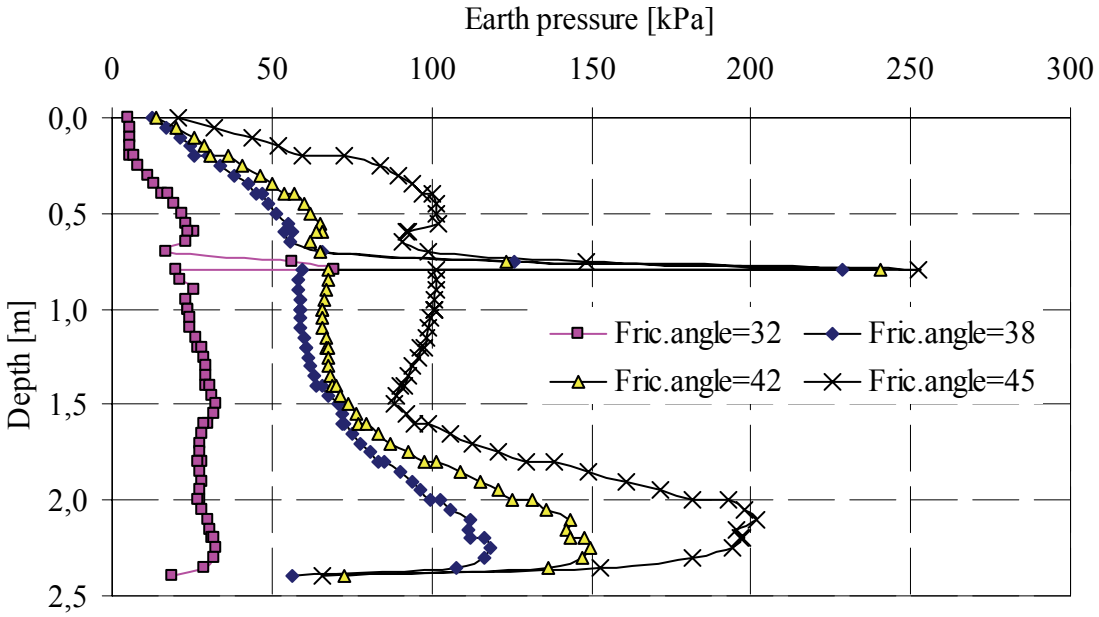

Figure 6.10 Earth pressures [kN/m^2] on Haavistonjoki Bridge abutment based on various crushed rock properties (see Table 6.2) after prescribed displacement of 7 mm.

The effect of the variation in soil properties from very loose to very dense affects the intensity of earth pressure against the abutment both above and below the transition slab. With friction angles $\phi = 42°$ and $\phi = 45°$ and respective soil stiffnesses, the earth pressures were higher than with a friction angle $\phi = 38°$, and much higher than with a friction angle ϕ

= 32°. The results of the case with a friction angle ϕ = 38° corresponded to the results of the basic case with E_d = 80,000 kPa presented in Figure 6.9, although the friction angle clearly differed.

Appendix 5 presents the total deformations (abutment rotation was 1/1570), the effective stresses and the relative shear stresses. The modulus of elasticity for crushed rock was E_d = 80,000 kPa. The vertical effective stresses in the soil above and below the transition slab centre zone were much smaller than corresponding horizontal stresses. The relative shear stresses next to the abutment are high above the transition slab and lower, about 0.5, under the transition slab.

Figure 6.11 illustrates the stresses at the upper soil–structure interface and Figure 6.12 the stresses at the lower soil–structure interface after 7 mm abutment displacement. Figure 6.13 shows the corresponding forces in the transition slab. The modulus of elasticity for crushed rock was E_d = 80,000 kPa.

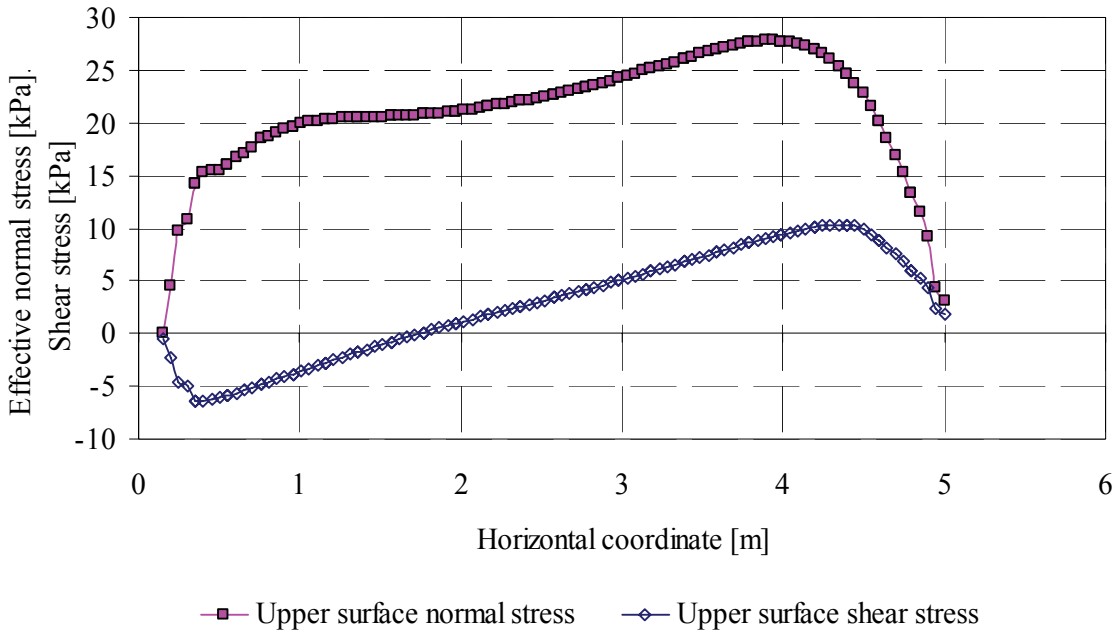

Figure 6.11 Effective normal stresses and shear stresses at the 5 m long transition slab upper surface.

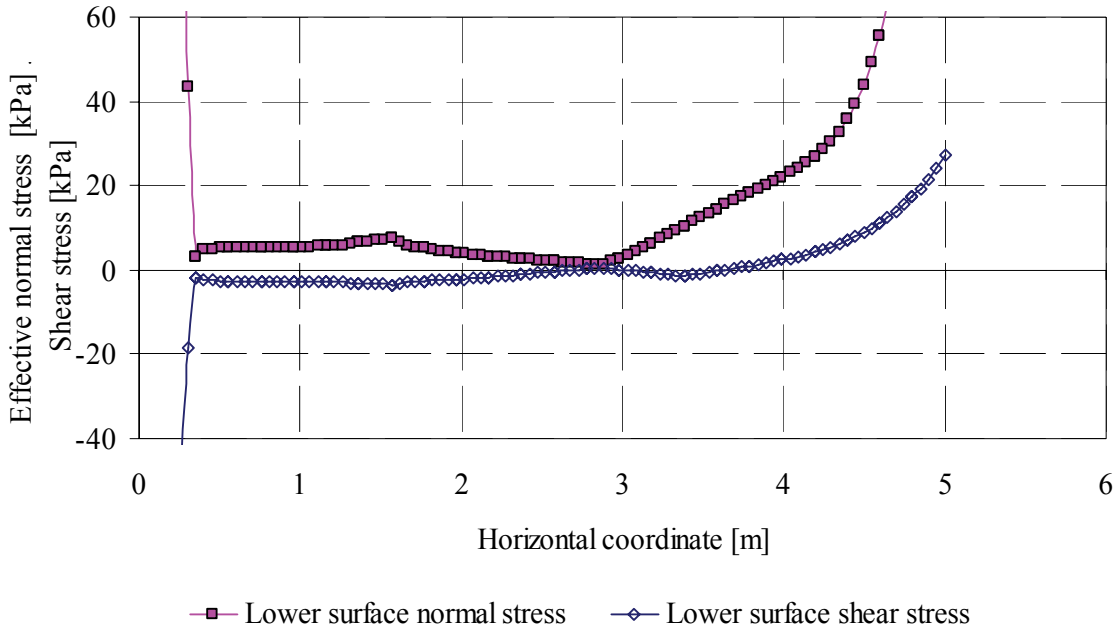

Figure 6.12 Effective normal stresses and shear stresses at the 5 m long transition slab lower surface. Maximum cumulative effective normal stress near the slab end was 160 kPa and at the slab support adjacent to the abutment 910 kPa. Maximum absolute value of the shear stress at the slab support was 114 kPa.

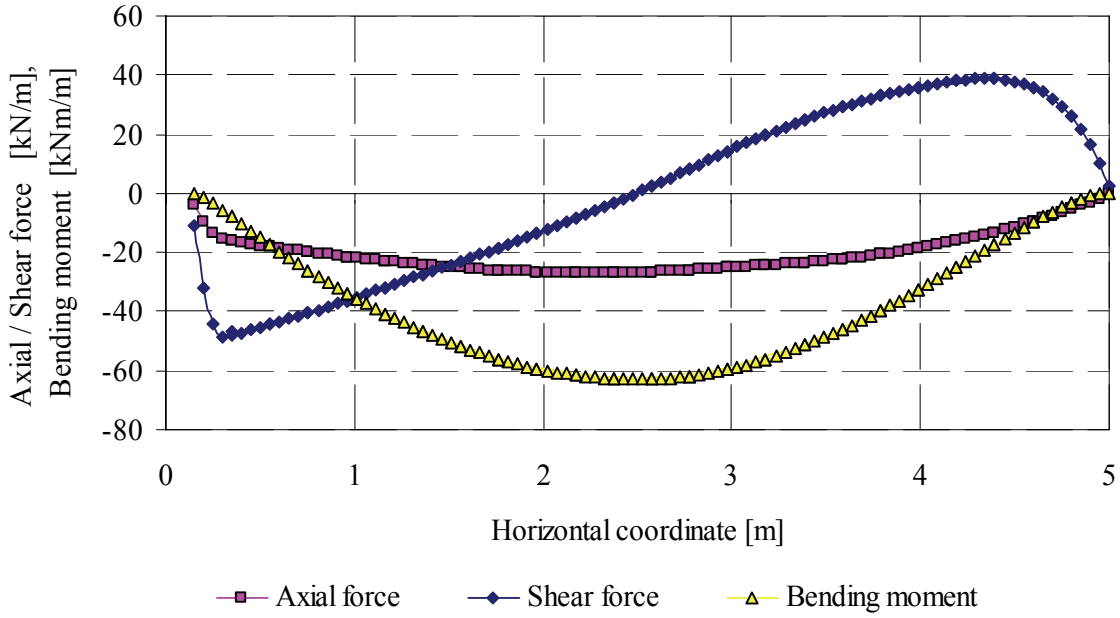

Figure 6.13 Axial forces, shear forces and bending moments in a 5 m long transition slab after 7 mm abutment displacement.

The observed bending moment change 2.5 meters from the abutment during 11.2.–15.2.2004 was smaller than the calculated value after all construction stages. According to subsequent calculations, the observed bending moment change was 21 kNm/m supposing an uncracked transition slab intersection (without reinforcement) and 7 kNm/m supposing a cracked transition slab intersection:

Observed concrete stress change during 11.2.–15.2.2004 at the bottom reinforcement level, 70 mm from the bottom of a 300 mm thick slab, was 0.75 MPa. The corresponding bending moment was about $M = \sigma_c * I_c / y_c = (0.75 MN/m^2 * 0.00225 m^4/m)/0.080m = 21$ kNm/m.

Observed steel bar stress change during 11.2.–15.2.2004 at the bottom reinforcement level, 70 mm from the bottom of a 300 mm thick slab, was 5 MPa. The corresponding bending moment was about $M = A_s * z_s * \sigma_s = 0.006702\ m^2/m * 0.220m * 5 MN/m^2 = 7$ kNm/m.

The bending moment in the transition slab from mere abutment displacement is difficult to analyse, and the results may be inaccurate. In any case, the influence of construction stages on bending moment before the 7 mm abutment displacement was distinct and can be determined, for instance, on the basis of the last figure in Appendix 5.

Using the HS soil model and E_d = 250,000 kPa for crushed rock, abutment rotation was (7.488-5.676)/2400 = 1/1320.

According to Figure 6.14, the calculated maximum abutment bending moment after just the prescribed displacement, $M_{difference}$, was close to the measured value 280 kNm/m. At depth z = 6.5 m the bending moment was only 1/3 greater than at depth z = 8.8 m. Respectively, pile-specific bending moments were M = 5.75m * 33kNm/m = 190 kNm and M = 5.75m * 25kNm/m = 144 kNm, which were only a little greater than the measured values (Cf. Table 4.3 and Table 4.4). According to measured steel pile strain changes, for example, the measured bending moment at depth z = 6.5 m was $M_{resultant}$ = 152 kNm.

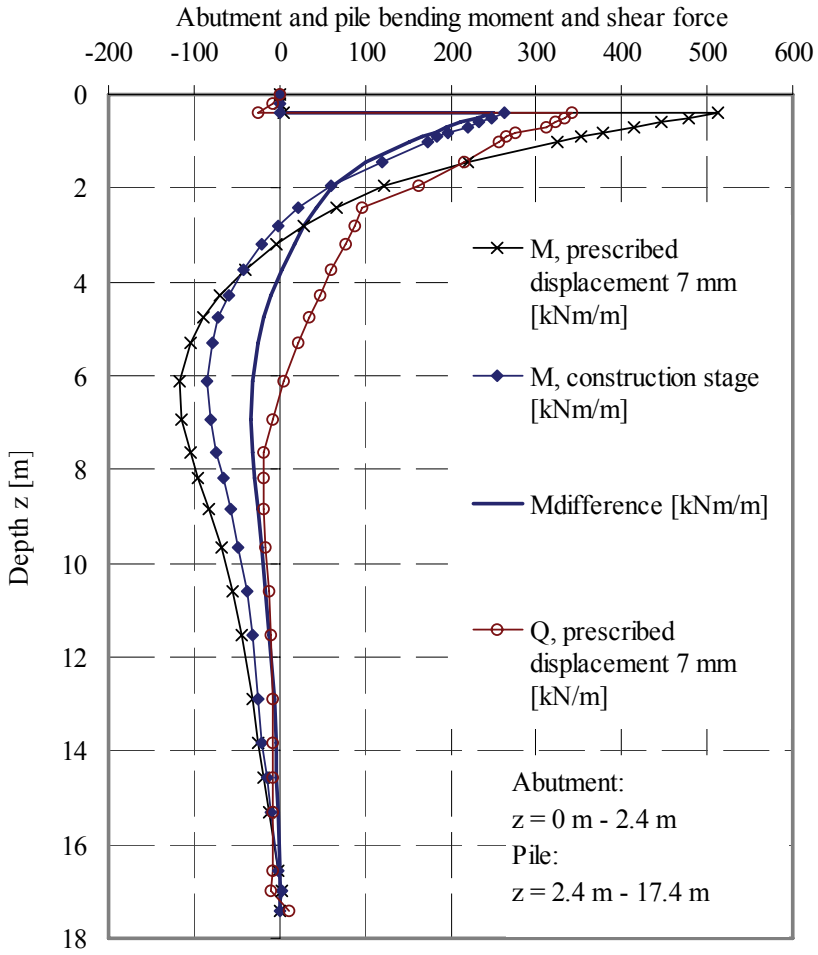

Figure 6.14 Bending moment, M, and shear force, Q, as a sum of all calculation stages and bending moment solely due to the construction stages and the difference between the two moments. As z = 6.5 m => $M_{difference}$ = 33kNm/m. As z = 8.8 m => $M_{difference}$ = 25kNm/m. The bending moment of an individual pile is calculated by multiplying the result by 5.75 m. HS soil model, E_d = 250,000 kPa for crushed rock.

The deformations illustrated in the last figure of Appendix 5 resulted solely from the construction of the crushed rock layer above the transition slab. Abutment rotation due to that stage was 1/2800. Vertical deformations were quite large because of the reduced soil properties of the thick silt layer. The gap below the transition slab support was visible because of the large scaling factor. A great part of the overburden on the transition slab was transferred to the support at the abutment.

Summary and conclusions on 2D calculations

Additional remarks and summary of the 2D calculations on Haavistonjoki Bridge:

- The transition slab is a stiff structural member in the longitudinal direction of the bridge structure compared to soil stiffness. The majority of high soil stresses and deformations occur several metres from the abutment. Earth pressures against the abutment are quite small under the transition slab. Consequently, actual abutment rotation is smaller than the rotation calculated with a 3D soil spring model without a transition slab (see Haavistonjoki Bridge 3D model, Cases 1–3, Ch. 4.2.6).
- The transition slab serves as a 1-span beam or slab carrying the overburden and the dead load of the transition slab.

- The shear stresses at the transition slab–soil interface reached the shear strength value within a 1 m zone near the slab end after a quite small displacement, about 10 mm, although the transition slab was not horizontally connected to the abutment. Hence, it can be concluded, that if this kind of a transition slab were horizontally connected to the abutment, there would be large tensile stresses both in the transition slab and the bridge superstructure in wintertime.
- Abutment displacement had a direct impact on soil deformations and stresses around the upper part of abutment supporting piles. The soil layer around the piles was not stationary and independent of abutment movement.
- The 2D model of 3D reality satisfactorily represents the real structure with the used assumptions.
- During 15.1.2004–11.2.2004 abutment displacement at the upper measuring bar level was about -5.9 mm while rotation was about -1/1600. During 11.2.2004–19.3.2004 abutment displacement was 7.2 mm and rotation 1/860, respectively. According to the calculation model with E_d = 250,000 kPa for crushed rock, the rotation after a deck level displacement of 7 mm was 1/1300 which corresponds quite closely to the measured value.
- With an increase in crushed rock modulus of elasticity, E_d, from 80,000 kPa to 250,000 kPa, earth pressure on the lower part of the abutment increased from 120 kPa to 170 kPa. With the modulus of elasticity E_d = 250,000 kPa for the crushed rock fill after all construction stages, earth pressure had already been about 80 kPa. So, the earth pressure increase of 90 kPa corresponded quite accurately to the observed values at the centre of the abutment.

The presented 2D calculation method served well in the evaluation of the behaviour of Haavistonjoki Bridge abutments, earth pressures and backfill including the transition slab.

6.3.3 Recommendation

According to a design manual for the German federal state Hessen, the integral bridge details of the abutment zone should be designed based on the transition slab illustrated in Figure 6.15.

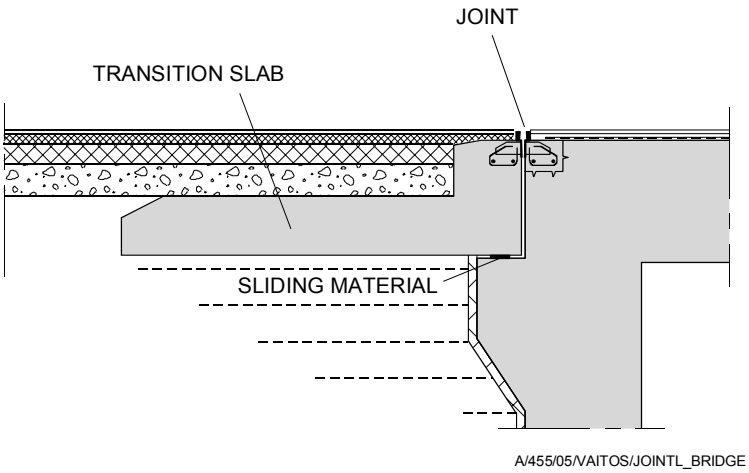

Figure 6.15 The end of a jointless bridge in Hessen, Germany. Bridge length is limited to 90 m with prestressed concrete structures and 105 m with reinforced concrete structures. The joint between the transition slab and the abutment must be 65 mm wide (Berger et al 2003).

The presented L-shaped transition slab type can be recommended as a jointless bridge end structure also in Finland. The abutment supports it vertically while the abutment can move horizontally in relation to the transition slab.

The benefit of the recommended structure is that it helps minimise the development of a bump near the abutment because the soil on the transition slab is supported both vertically and horizontally. The long horizontal section of the slab structure acts as part of the approach embankment and restricts the horizontal movement of the vertical section.

The length of the transition slab should be about 5 meters. The abutment–transition slab connection with dowels should be designed according to present Finnish practice in order to assure free transition slab movement in relation to the abutment. Also, the joint in the pavement between the abutment and the transition slab should be designed according to present Finnish practice considering, for instance, the benefits of wide joints filled with an elastic substance.

The presented L-shaped transition slab should be studied further, by calculations and field tests, in order to verify its performance in long jointless bridges, possibly longer than 120 meters.

7 BEHAVIOUR OF PILES BELOW PIERS IN FROZEN SOIL

7.1 Presentation of discussed phenomena

The most essential phenomena studied in Chapter 7 are presented in Figure 7.1. The longitudinal thermal changes in bridge length are behind the high stresses in vertical structural members. Piers cannot move freely in frozen soil.

The farthest piers may be quite short and rigidly connected to the deck, which exacerbates related problems.

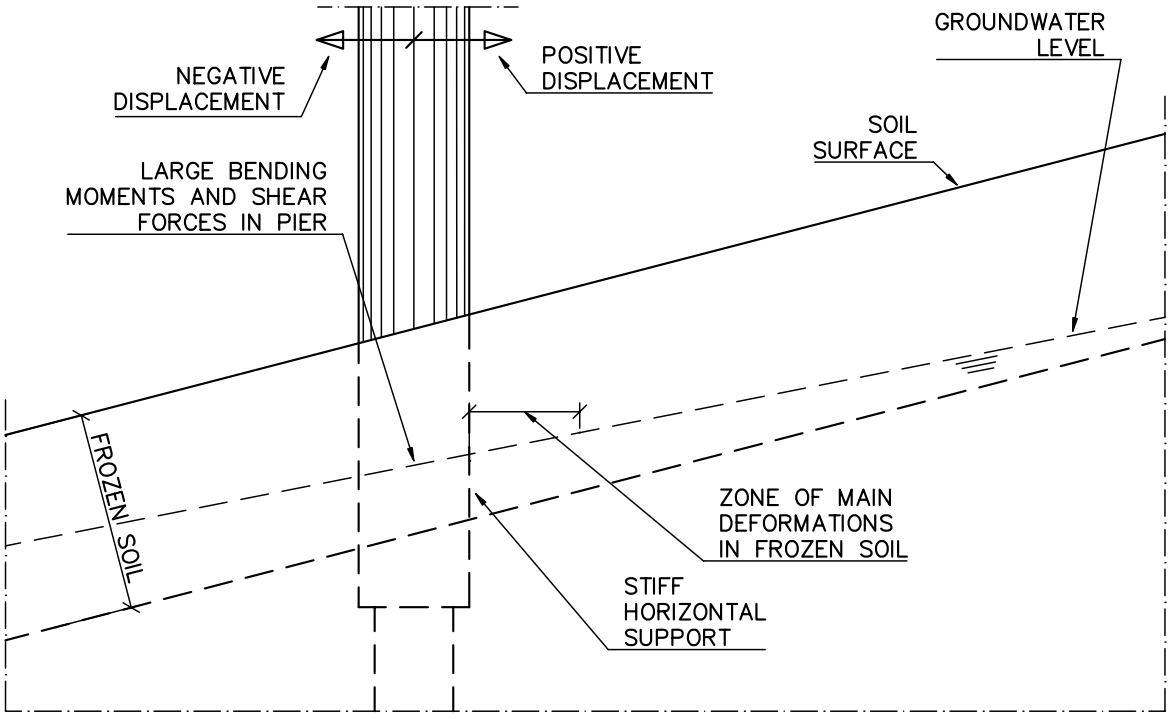

Figure 7.1 Phenomena studied in Chapter 7.

7.2 Mechanical properties of frozen soil

Frozen soil is a highly complex multiphase system consisting of components that differ in their properties and are in a variety of consistencies: solid, plastic, liquid and gaseous (Berggren 1983). Hence, each soil is specified as a unique ideal continuum, thus avoiding the heterogeneity problems.

Creep strength is defined as the stress level at which failure occurs after a finite time interval. The strength of frozen soil develops from cohesion, inter-particle friction, and particle interlocking. The strength magnitude may be compared with that of concrete. Due to ice cementation, cohesion is considerable, and tension strength may be more than 1/3 of compression strength.

Creep strength decreases with time. Instantaneous creep strength is about 5–15 times higher than limiting long-term strength (see Figure 7.2).

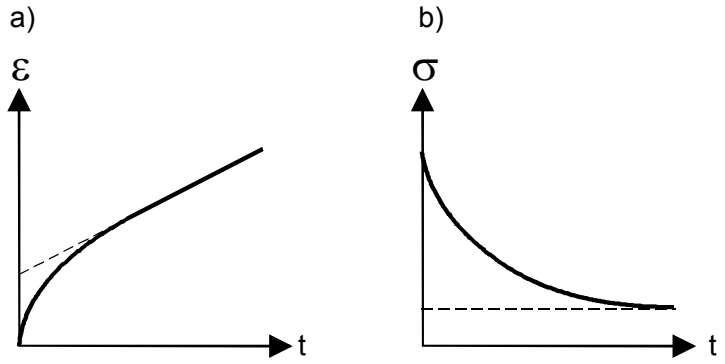

Figure 7.2 The time effect on a) strain ε and b) stress σ, when temperature and stress (Case a) or strain (Case b) are held constant (Berggren 1983).

An experimental investigation of the compressive strength of frozen soil versus strain rate showed that unconfined compressive strength of frozen soil usually depends on many factors (Li et al. 2001). These include temperature, strain rate, and water content. Some properties of the sample soils are listed in Table 7.1.

Table 7.1 Parameters of two quite similar sample soils (Li et al. 2001).

Classification	Water content [%]	Natural unit weight [kN/m^3]	Degree of saturation [%]	Liquid limit [%]	Plastic limit [%]
Silt with sand	31.1	17.3	89	24.5	20.8
Silty clay with sand	31.8	18.4	92	23.5	17.7

Figure 7.3 indicates that the compressive strength of the frozen soil increases with decreasing temperature for a given strain rate. The curves, marked from 1 to 5, refer to (1) strain rate = 9.9*10^{-6} 1/s, T = -20°C, σ = 5.05; (2) strain rate = 11.2*10^{-6} 1/s, T = -20°C, σ = 4.65; (3) strain rate = 25*10^{-6} 1/s, T = -10°C, σ = 2.77; (4) strain rate = 16.3*10^{-6} 1/s, T = -10°C, σ = 2.62; and 5) strain rate = 17.4*10^{-6} 1/s, T = -5°C, σ = 1.73, respectively.

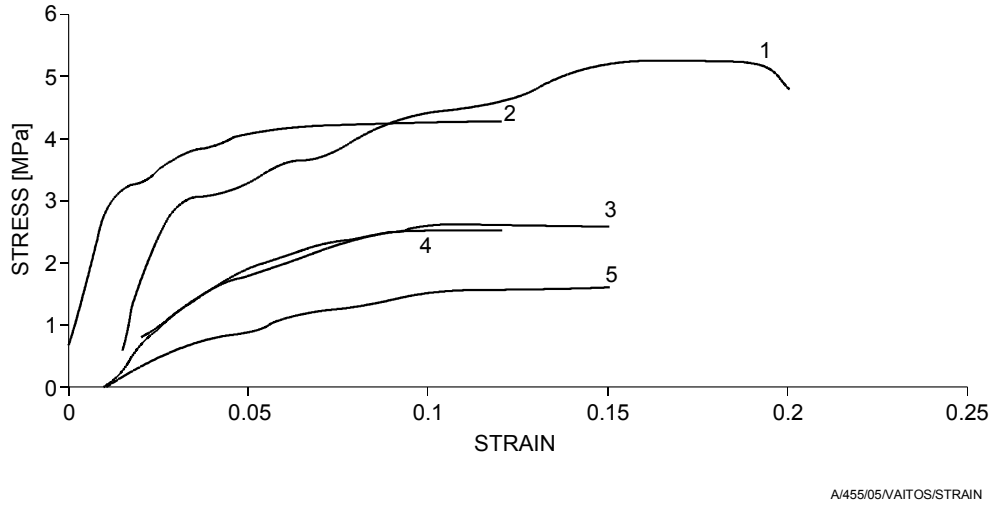

Figure 7.3 Stress–strain curves at different strain rates and temperatures. Unconfined compressive strength of frozen soil was 5.05–1.73 MPa (Li et al. 2001).

The modulus of elasticity, E, for frozen cohesive soil in the unconfined test can be calculated based on the beginning of the curves in the previous figure:

- Curve 5, T = -5°C: E = 0.56 MPa / 0.019 = 29 MPa,
- Curves 3 and 4, T = -10°C: E = 1.1 MPa / 0.019 = 58 MPa,
- Curves 1 and 2, T = -20°C: E = 2.1 MPa / 0.01 = 210 MPa.

The moduli of elasticity, E, for unfrozen cohesive soils are presented in various references and the values differ significantly. It can be stated that an average value for unfrozen silty clay is about E = 10–20 MPa. Thus, the ratio $E_{frozen}/ E_{unfrozen}$ is about 2–20.

According to Figure 7.4, strain rate has a great effect on the compressive strength of frozen soil.

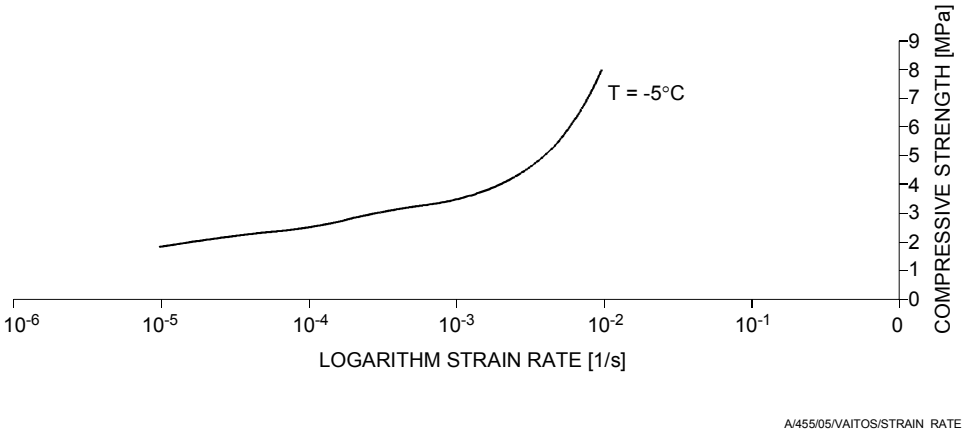

Figure 7.4 Compressive strength–logarithm strain rate relation (Li et al. 2001).

It is of vital importance whether the soil is coarse-grained and frictional with inter-particle contact or whether it contains large enough quantities of fine-grained particles to be classified as a cohesive soil. To distinguish between totally different behaviours, Tsytovich (1975) defined three categories of frozen soils: 1) coarse fragmented soils, 2) sands and 3) clayey soils (clays, loams, sandy loams). Frozen coarse fragmented soils may behave similarly as in their unfrozen state, except for their higher strength. Frozen clayey soils may display extreme plasticity. Frozen sandy soils will fall somewhere in between.

Figure 7.5 presents the Haavistonjoki Bridge embankment temperatures observed in February 2004. The lowest winter temperature seems to occur at the end of the month when at the depth of 1.8 m the lowest average temperature reaches 0°C. The temperatures observed during 1.3.2004–31.8.2004 are presented in Appendix 3.

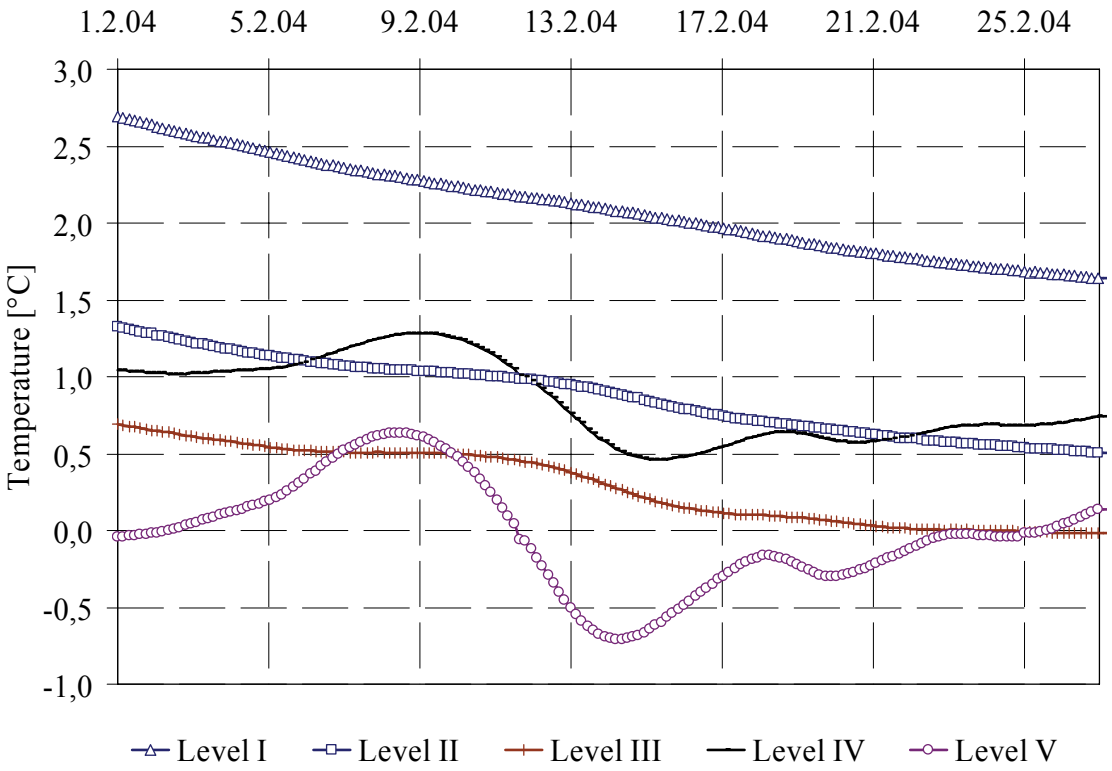

Figure 7.5 Observed temperatures within Haavistonjoki Bridge embankment at different levels. Level V is the highest at a depth of 1 m. Level I is the deepest at 2.5 m. The horizontal distance from abutment T4 is 2.4 m.

In laboratory tests $10*10^{-6}$ 1/s or 0.036 1/t has generally been regarded as a low strain rate. In the case of a large-diameter pier or pile, d = 1 m, it can be roughly estimated that most of the strain in the surrounding soil develops within a distance of about 1 meter which corresponds to the low strain rate 0.036 * 1000 mm / 1 t = 36 mm/t. In real bridge structures, horizontal pier displacement rate is not nearly that fast. During two days and nights between 11.1.2004 and 13.1.2004 the maximum observed average temperature change in Haavistonjoki Bridge was 11°C or 0.23°C per hour. In a 120 m long bridge the distance between the farthest piers can be about 80 meters. At the above temperature change rate they separate 0.184 mm from each other in an hour. At ground level the displacement rate is about half of the top displacement rate. Hence, the approximated displacement rate, based on measurements, 0.184/2/2 = 0.046 mm/t corresponds to 1/800 of a typical low strain rate in a laboratory test. The structure moves against the soil slowly and, consequently, deformations in the frozen soil develop so slowly that the soil behaviour can be regarded as plastic.

The nature of the behaviour of the frozen soil considering the time-dependency of the stiffness is somewhere between static and dynamic behaviour of soil.

In conclusion it can be stated that there is no need for a rigid horizontal support at ground water level. It can be replaced, for example, by a special spring depicting frozen soil behaviour.

7.3 Behaviour of a long integral bridge in frozen soil

7.3.1 Structural model

The analysis of a jointless bridge is performed with a spring model. The abutment with its piles and lateral springs as well as the deck are modelled on Haavistonjoki Bridge (see Ch. 6.3.2 / 3D model / Case 1). The temperature change of the deck is 30°C and the temperature change of the piers 12°C.

The structural model of an imaginary 120 m long jointless bridge is illustrated in Figure 7.6.

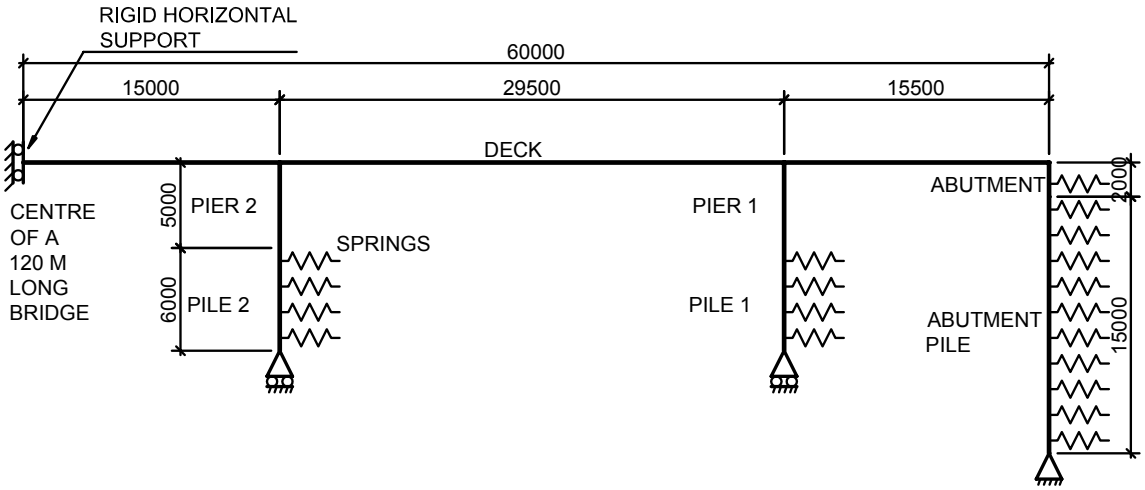

Figure 7.6 Structural model of an imaginary bridge.

Biggest stiffness growth is anticipated probably in connection with the freezing of cohesive soils. Yet, non-cohesive soils are generally the stiffest soils in the unfrozen state. Therefore, calculations are limited to non-cohesive soils.

Given soil properties, the typical values for well-compacted non-cohesive soil and abutment backfill material (Finnra 1999a), are the following:
$\phi = 38° \Rightarrow n_h = 7.5$ MN/m^3 and $K_p = 4.2$,
$\gamma' = 21$ kN/m^3.

Displacement corresponding to passive earth pressure or ultimate lateral resistance, p_m, is y_m, and it can be calculated from the equation (Finnra 1999c):

$$p_m/2 = k_s * y_m/4$$

Passive earth pressure against the pile is estimated to be 4.4 times greater than against the wall:

$p_m = 4.4 * \gamma' * z * K_p = 4.4 * 21 * z * 4.2 = 388.1 * z$ [kN/m^2] (Finnra 1999c).

7.3.2 Lateral springs for piles below piers

In the presented calculation models, the uppermost lateral soil spring is at 1 m depth under the ground surface, and it corresponds to the earth pressure in the 1.5 m zone along the

pile. The used depth, 1.75 m, may be regarded as a typical frost depth in Finland. The uppermost 0.25 m ground layer is ignored.

The only variable in the calculations are the properties of the uppermost spring at z = 1 m below the piers. In calculation model 2, the uppermost spring is 33 times as stiff as the unfrozen soil spring below groundwater level. The model is based on a literary review and a large safety factor. For example, the cohesive soil presented in Table 7.1 and Figure 7.3 is up to 20 times stiffer at -20 ºC than typical corresponding unfrozen soil. Consequently, a factor of 20 was used to account for the behaviour of a frozen non-cohesive soil in the following lateral spring stiffness calculations (see Calculation model 2).

As the extreme alternative, calculation model 3 has a rigid lateral support at depth z = 1 m.

Calculation model 1: Lateral springs corresponding to unfrozen soil

Below groundwater level the spring coefficients have to be reduced by multiplying them by 0.6. The spring coefficient is $k = k_s * d * s = n_h * (z / d) * d * s = 6.75 * z$ (see Table 7.2), as $n_h = 0.6 * 7.5 = 4.5$ MN/m^3 and s = 1.5 m.

Table 7.2 Pile springs of piers in unfrozen soil under groundwater level.

z	Spring coefficient k	$k_s*d = k/s =$ k/1.5m	Displacement limit $y_m/4$
[m]	[MN/m]	[MN/m^2]	[m]
1	6.8	4.5	0.031
2.5	16.9	11.3	0.031
4	27.0	18.0	0.031
5.5	37.1	24.8	0.031
7	47.3	31.5	0.031
8.5	47.3	31.5	0.037

Calculation model 2:

At depth z = 1 m, the lateral spring coefficient is 33 times the unfrozen soil spring coefficient or k = 33 * 6.8 MN/m = 225 MN/m. That spring coefficient corresponds to 0.6*33 ≈ 20 times the unfrozen spring coefficient above groundwater level in the same soil. The corresponding modulus of lateral subgrade reaction per 1 m along the pile is $k_s*d = k/s = k/1.5$ m = 150 MN/m^2.

Calculation model 3:

At depth z = 1 m lies a rigid lateral support.

7.3.3 Calculation results

Structural deformations and bending moments

Structural deformations at bridge end and adjacent pier of symmetrical calculation models 1–3 (see Ch. 7.3.2) are illustrated in Figure 7.7. In unfrozen soil the pile top moves horizontally about 6 mm more than in the case of a rigid lateral support.

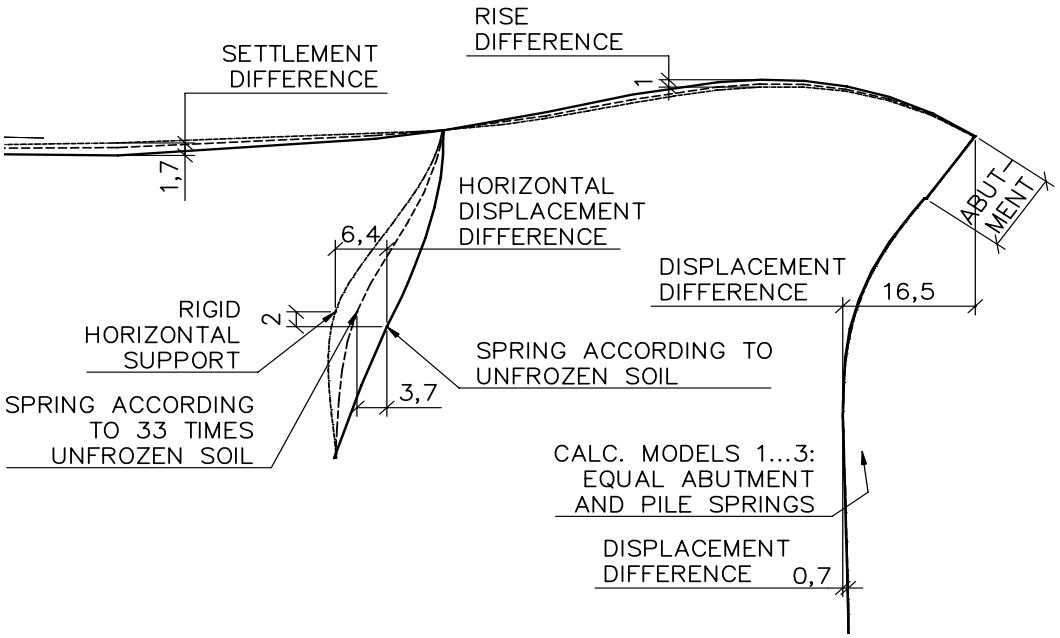

Figure 7.7 Structural deformations scaled up 250 times. Calculation models 1–3.

Horizontal displacements of the farthest pier and pile at 4 levels have been presented in Table 7.3. The variation in displacement is most marked at the pile top level 1 m higher than the highest spring.

Table 7.3 Horizontal displacements according to different calculation models [mm].

Level	Calculation model 1 Unfrozen soil	Calculation model 2 Frozen soil: 33 * unfrozen soil	Calculation model 3 Frozen soil: rigid lateral support
Pier top	11.8	11.5	11.4
Pile top	7.3	2.7	0
Pile bottom	-1.9	-1.7	-1.6
As bending moment = 0	4.8	6.2	4.1

The following figures present the bending moments (see Figure 7.8) and shear forces (see Figure 7.9) of the furthest piers.

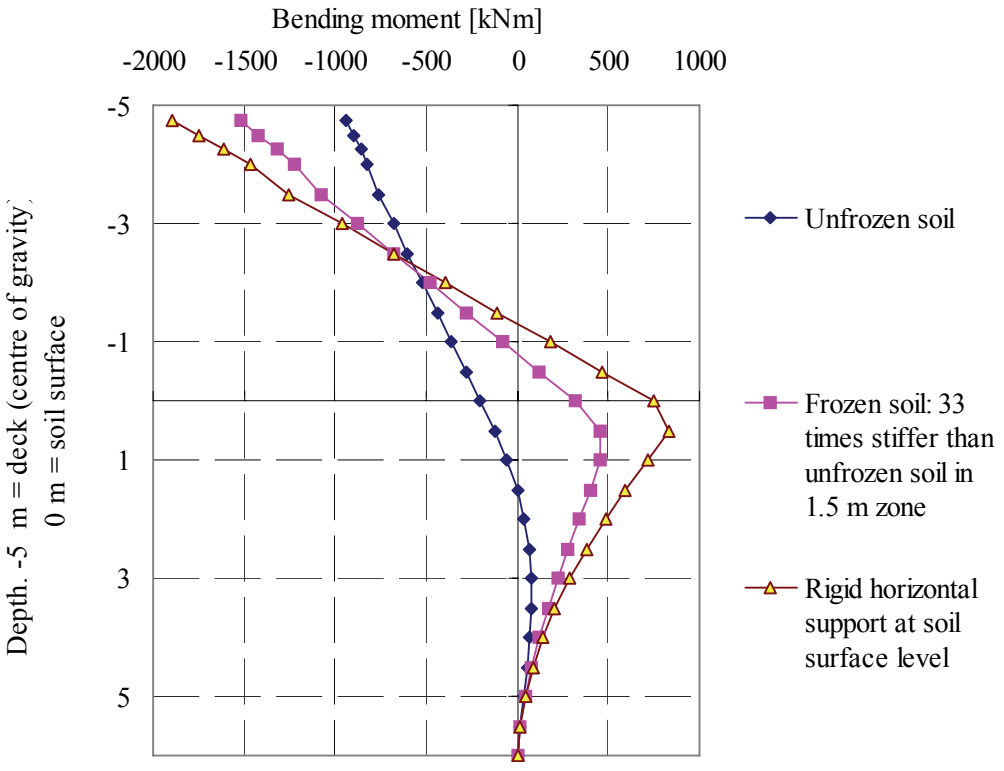

Figure 7.8 Bending moments along the pier and pile in the longitudinal direction.

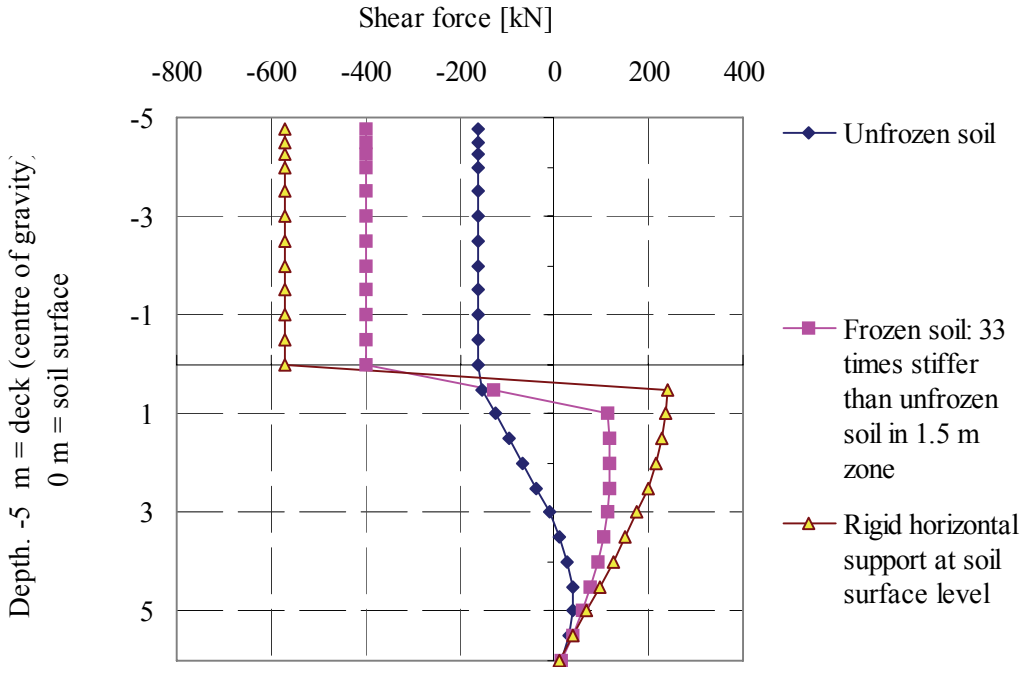

Figure 7.9 Shear forces along the pier and pile in the longitudinal direction.

Lateral bending moments and shear forces were much smaller than in the longitudinal direction.

7.3.4 Conclusions and recommendations for frozen soil springs

A single stiff spring at depth z = 1 m representing the horizontal resistance of frozen soil at depths z = 0.25–1.75 m corresponded to 33 times the unfrozen non-cohesive soil resistance below ground water level and to 20 times the resistance above ground water level at the same depth. In thermal expansion calculations, bending moment at pile top level was about half of the moment calculated with a model using a rigid horizontal support. Correspondingly, the greatest shear force change diminished from 810 kN to 510 kN. At the spring level, the horizontal displacement according to calculations was only 2.3 mm, which may be considered minor. Consequently, the supporting horizontal force against the pile top was P = k * y = 225,000 * 0.0023 = 510 kN.

The estimated frozen soil spring, k = 225 MN/m, is preferable for long jointless bridges, both above and below ground water level if level of ground water is not precisely defined, and should be made part of Finnish design practice. If ground water level is precisely defined, the frozen soil spring may be calculated according to the presented procedure (see Calculation model 2). In that case, soil stiffness should be based on a field survey and not less than suggested in Chapter 7.3.1.

8 LATERAL PILE DISPLACEMENT–FORCE RELATION

8.1 Presentation of discussed phenomena

The studied circular vertical pile within soil is presented in Figure 8.1. Its horizontal movement and the corresponding earth pressure are the most essential phenomena studied in Chapter 8. The relation between horizontal displacement and corresponding resistance and its changes in relation to size of displacement are important factors in the evaluation of the pile's capacity to carry both vertical and horizontal loads. The lateral pile displacement–force relation is examined by means of a 2-dimensional FEM model.

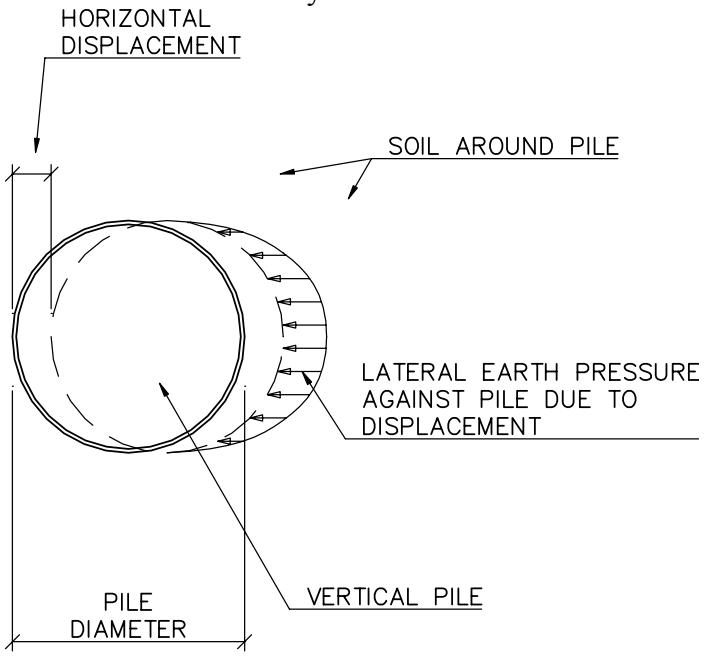

Figure 8.1 Structure studied in Chapter 8.

8.2 Structural model for lateral 2D FEM analysis

The size of the structural model is 20 m * 20 m. The vertical pile is located at the centre of the model according to Figure 8.2. A horizontal load of 16 kN/m^2 (Cf. Figure 8.4) is exerted against the soil at all four model edges. The load corresponds to earth pressure at 2 m depth as the at-rest pressure coefficient is $K_0 = 0.4$ and soil density is $\gamma' = 20$ kN/m^3. The mesh with triangular elements is presented in Figure 8.3.

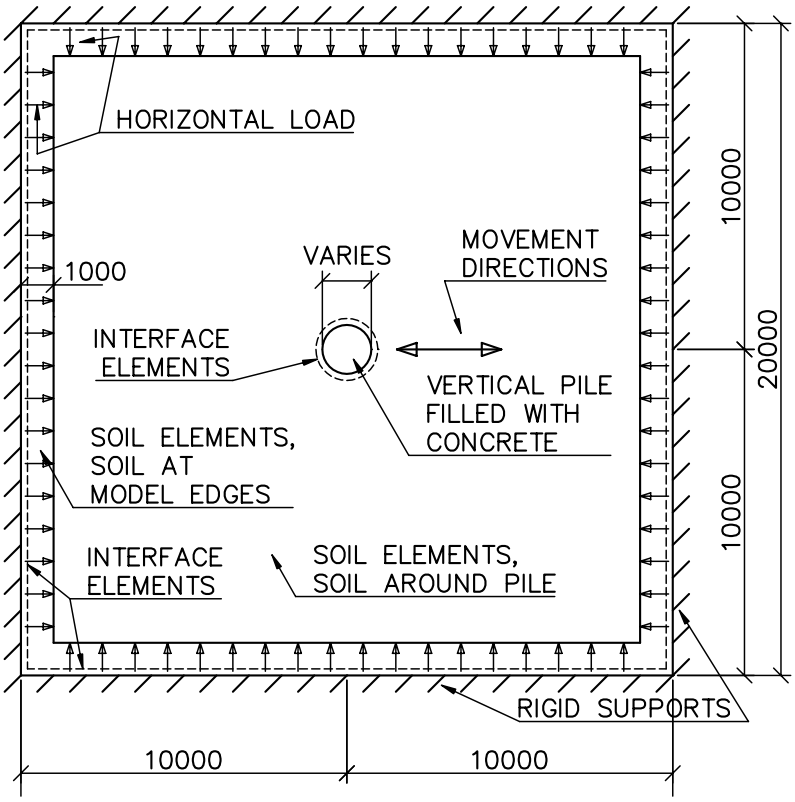

Figure 8.2 Structural model. At-rest earth pressure and pile displacement direction.

The soil was modelled with triangular elements according to Figure 8.3.

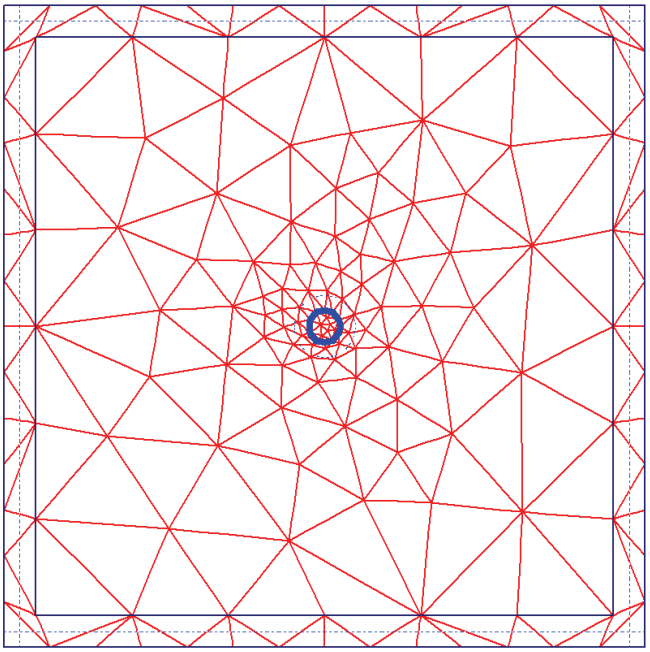

Figure 8.3 Triangular 2D elements.

The soil properties and pile fill properties are presented in Table 8.1. The soil near the edges was ten times stiffer than the soil around the pile in order to minimise deformations near the edges. Setting R_{inter} to the minimum at model edges eliminated the friction between the soil and the rigid supports.

Table 8.1 Soil and pile fill properties. Soil density is zero.

Soil model: Hardening-Soil	Unit	Soil around the pile	Concrete inside the pile	Soil at model edges
Type	[-]	Drained	Non-porous	Drained
γ	[kN/m³]	0	0	0
e_{max} - e_{init}	[-]	0.2	-	0.2
E_{50ref}	[kN/m²]	100,000	20,000,000	1,000,000
M_{ref}	[kN/m²]	100,000	22,000,000	1,000,000
power (m)	[-]	0.5	-	0.5
ϕ	[°]	42	-	45
ψ	[°]	5	-	0
E_{urref}	[kN/m²]	300,000	-	3,000,000
ν_{ur}	[-]	0.2	$\nu = 0.2$	0.2
p_{ref}	[kN/m²]	100	-	100
R_{inter}	[-]	0.45	1	0.01

The soil properties have been selected keeping in mind the typical properties of well-compacted non-cohesive soil (Finnra 1999a) at this depth and the results of the tests on Haavistonjoki Bridge fill material (see Ch. 4.2.2). The friction represented by the factor R_{inter} is also estimated to be a typical value between non-cohesive soil and steel. The wall friction angle calculated on the basis of these input values was: δ = arctan (0.45*tan42°) = 22°, which is a typical ultimate friction angle, according to (California trenching and shoring manual 2001), between steel sheet piles and clean gravel, gravel-sand mixtures or well-graded rock fill with spalls.

Wall thickness of the pile was t = 16 mm.

Comparison of properties of various non-cohesive soils with pile diameter d = 1000 was done according to Table 8.2.

Table 8.2 Comparative cases. Properties of soil around the pile.

Property	Unit	Very loose	Loose	Dense	Very dense a	Very dense b
E_{50ref}	[kN/m²]	15,000	50,000	100,000	200,000	200,000
E_{urref}	[kN/m²]	45,000	150,000	300,000	600,000	600,000
ϕ	[°]	32	37	42	45	45
ψ	[°]	0	2	5	5	10

8.3 Calculation results and conclusions

8.3.1 Stresses in soil before and after horizontal pile displacement at depth z = 2 m

There was a constant horizontal earth pressure of 16 kPa in the soil around the pile before the prescribed pile displacement (see Figure 8.4). Near the model edges the earth pressure was negligible.

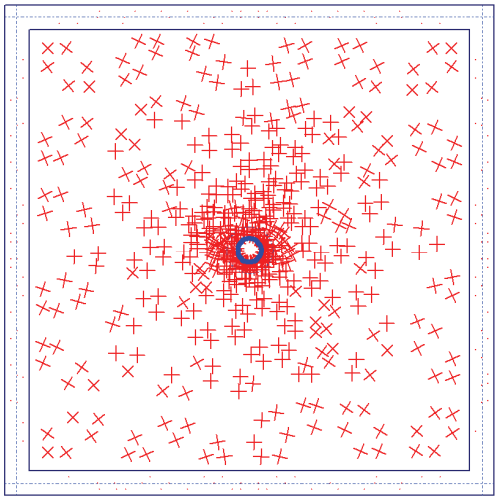

Figure 8.4 Horizontal earth pressure around the pile prior to pile displacement.

Before the prescribed displacement deformations, not stresses, were set back to zero. The effective stresses in the soil next to the pile after horizontal displacement y = 50 mm are presented in Figure 8.5. The extreme principal stress was 1200 kPa and it occurred on the surface of the pile in the direction of the displacement. Further from the pile stresses were clearly smaller. Only minor stresses transferred to the surrounding soil via the parts of the pile transversal to movement, although the wall friction angle was as large as $\delta = 22°$.

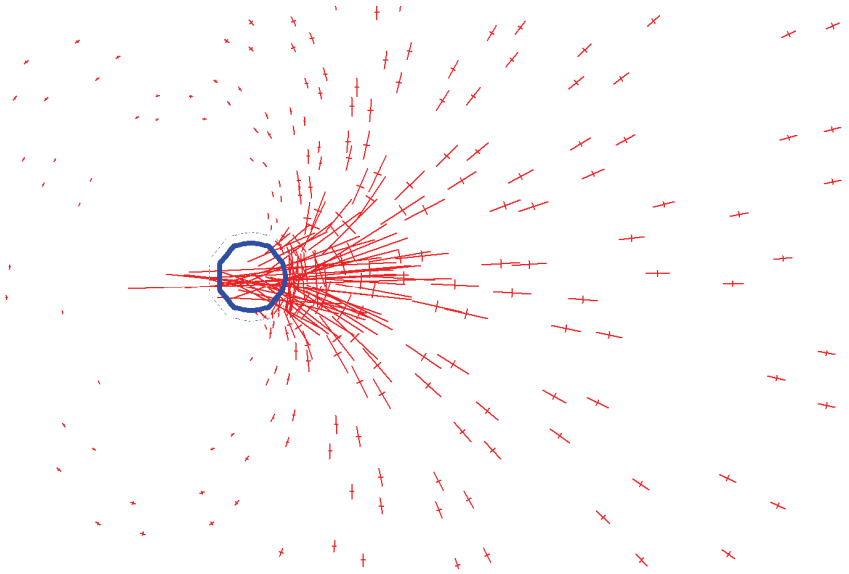

Figure 8.5 Effective stresses in principal directions. Depth z = 2 m. Pile diameter d = 1000 mm.

8.3.2 Displacement–force relation with pile diameters d = 500, 1000 and 1500

The horizontal displacement–force relation was studied with diameters d = 500, 1000 and 1500. The results of the three studied cases are presented in Figure 8.6 and Figure 8.7. The comparison diagram was calculated according to Finnish guidelines with soil internal friction angle $\phi = 42°$ (Finnra 1999c).

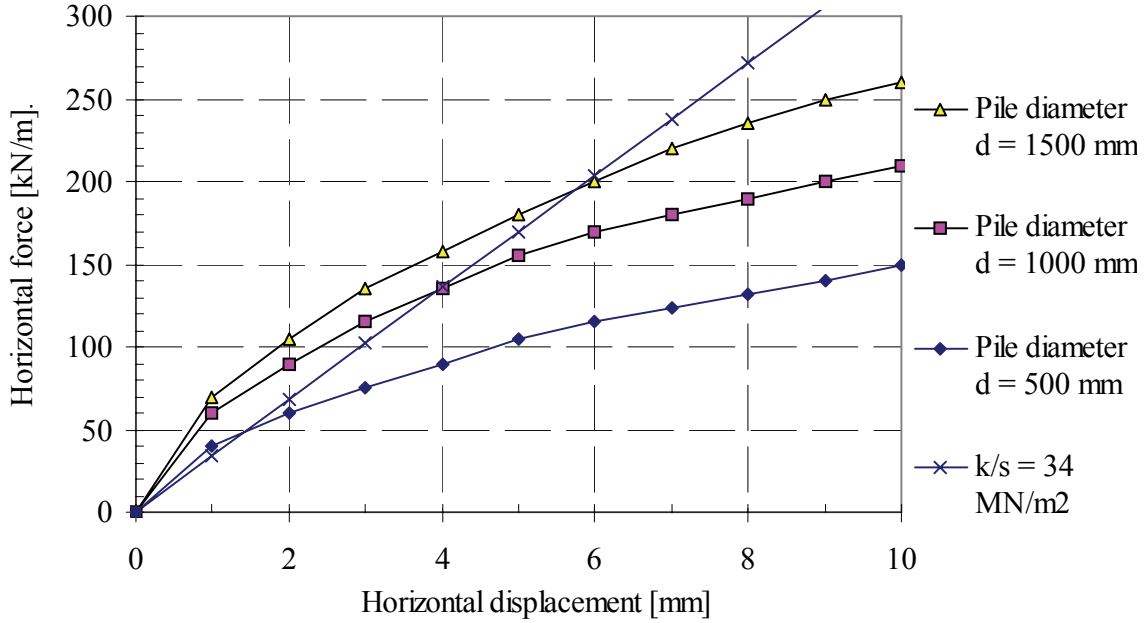

Figure 8.6 Displacement–force relations up to displacement y = 10 mm. Comparison with a linear line with k/s =34 MN/m^2.

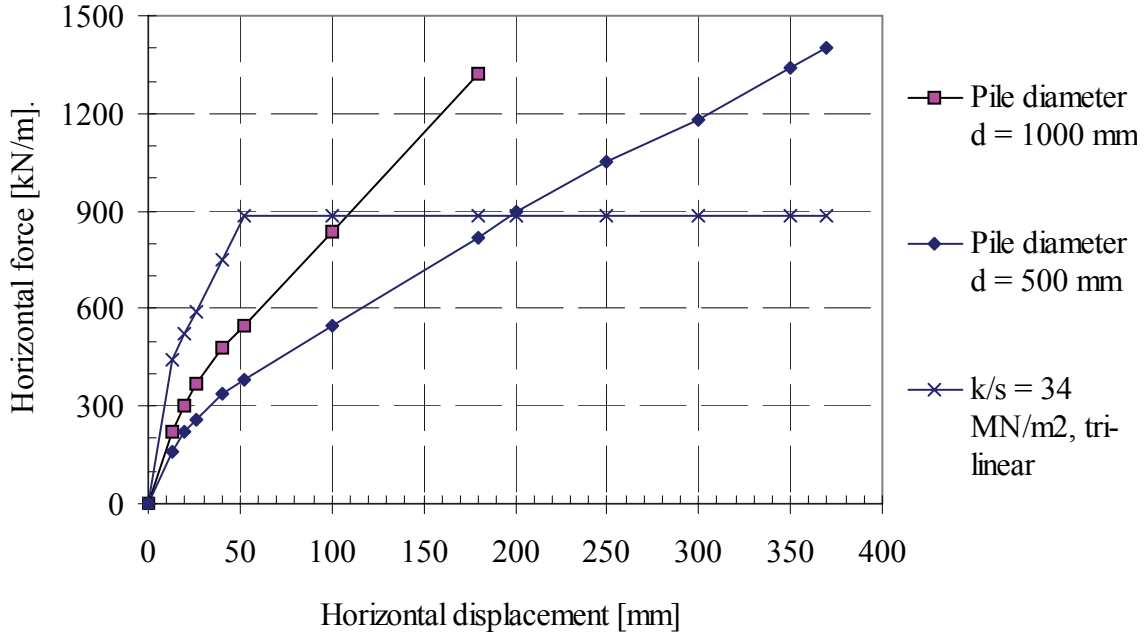

Figure 8.7 Maximum horizontal forces attained with pile diameters d = 500 and 1000 mm. Comparison with a tri-linear line with k/s = 34 MN/m^2 up to horizontal displacement y = 13 mm.

The maximum force attained for pile d = 1500 was P_x = 267 kN/m with displacement y = 10 mm. The used software code was unable to produce a result based on these input data after any larger displacement of this large-diameter pile.

Horizontal spring constants of piles

The spring constants of piles per pile length s = 1 m can be concluded from the presented displacement–force relations. For example, when horizontal displacement was y = 0–6 mm, the spring constants were:

$$d = 500 \Rightarrow \quad k/s = P_x/y = 112 \text{ kN/m} / 0.006 \text{ m} = 19{,}000 \text{ kN/m}^2,$$

$$d = 1000 \Rightarrow \quad k/s = P_x/y = 165 \text{ kN/m} / 0.006 \text{ m} = 28{,}000 \text{ kN/m}^2,$$

$$d = 1500 \Rightarrow \quad k/s = P_x/y = 199 \text{ kN/m} / 0.006 \text{ m} = 33{,}000 \text{ kN/m}^2.$$

The presented horizontal spring constants have been calculated as secant values from the presented diagrams. Consequently, they vary remarkably according to displacement level and pile diameter size.

Comparison of ultimate values

The ultimate value for lateral resistance according to Finnish guidelines can be calculated from the following equation (Finnra 1999c):

$$p_m = 4.4 * \gamma' * z * K_p = 4.4 * 20 * 2 * (\tan^2(45+\phi/2)) = 888 \text{ kN/m}^2.$$

Correspondingly, the lateral resistance per s = 1 m is $P_d = p_m * d = 888 \text{ kN/m}^2 * 1.0 \text{ m} = 888 \text{ kN/m}$, and the corresponding displacement $y_m = 2*p_m/ k_s = 2 * 888 / (34{,}000/1.0) = 0.052$ m (see also Figure 8.7).

According to FEM calculations, the total ultimate force against the pile with d = 1000 mm was 1313 kN/m after a large displacement y = 0.184 m (see Figure 8.7). The force corresponding to the horizontal displacement y = 0.052 m was $P_x = 531$ kN/m, which was less than in Finnish practice with the same displacement level.

The Finnish practice of calculating lateral spring constant and lateral resistance of standard large-diameter piles corresponds closely enough to the results of the presented calculations, although the practice does not at all consider the pile diameter in spring constant estimation. Yet, it should be noticed that in the displacement range 10 mm–100 mm, according to Finnish practice for common large-diameter pile diameters, the springs are stiffer than the calculated horizontal springs.

Comparison with various non-cohesive soils

Comparison of properties of various non-cohesive soils with pile diameter d = 1000 was based on a total of five different soil properties. The results of the comparison are presented in Figure 8.8 for a soil particle located 90 mm in front of the moving pile. The effect of the variation in soil properties affects the behaviour of the pile within the soil. Therefore, the properties of the soil at the bridge site should be determined before estimating pile behaviour and the consequent design of the structure.

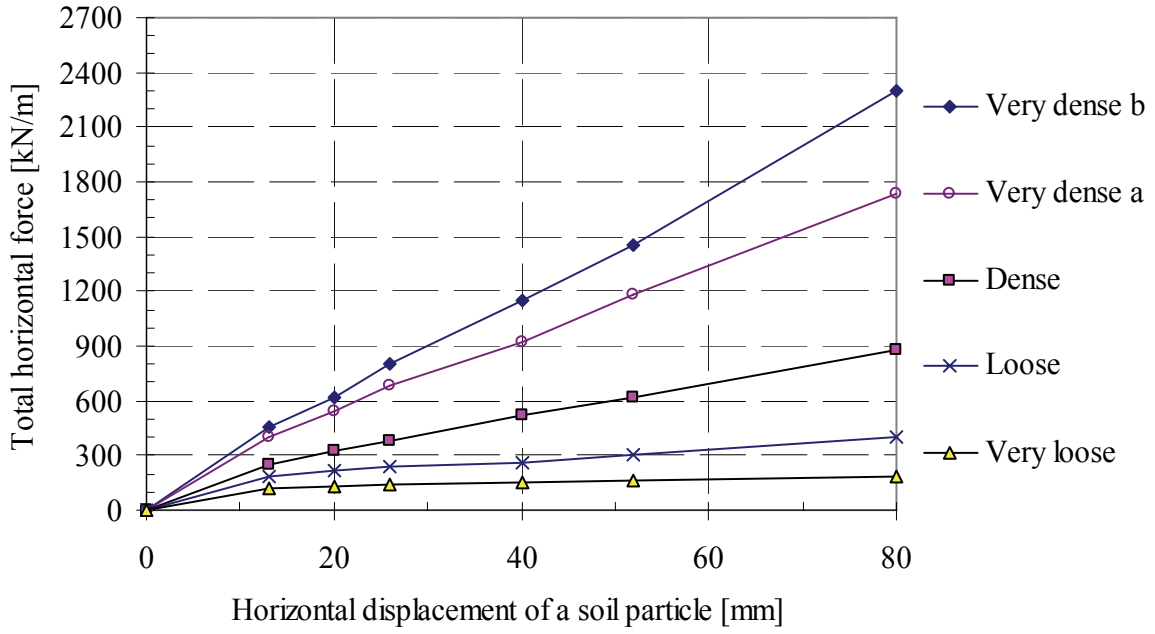

Figure 8.8 Comparative cases. Horizontal displacement v. total force against the pile, for pile diameter d = 1000.

8.4 Influence of cyclic pile displacements on lateral force and deformations

Cyclic pile displacement calculations were carried out with the model presented in previous chapters. The only difference was that pile movement was cyclic with an amplitude of ±10 mm = 20 mm. The first 10 mm movement according to Figure 8.2 was to the right. The diameter of the pile was d = 1 m. Soil properties were as in Table 8.1 with the exceptions: e_{max} - e_{init} = 0.27 and R_{inter} = 0.1.

Figure 8.9 presents the cyclic displacements of two particles in the soil around the pile. The displacements were proportional to the total horizontal force against the pile. The particles were 90 mm and 480 mm from the surface of the pile in the direction of the first movement. Initial displacements from the zero-position caused by the development of at-rest earth pressure are also presented.

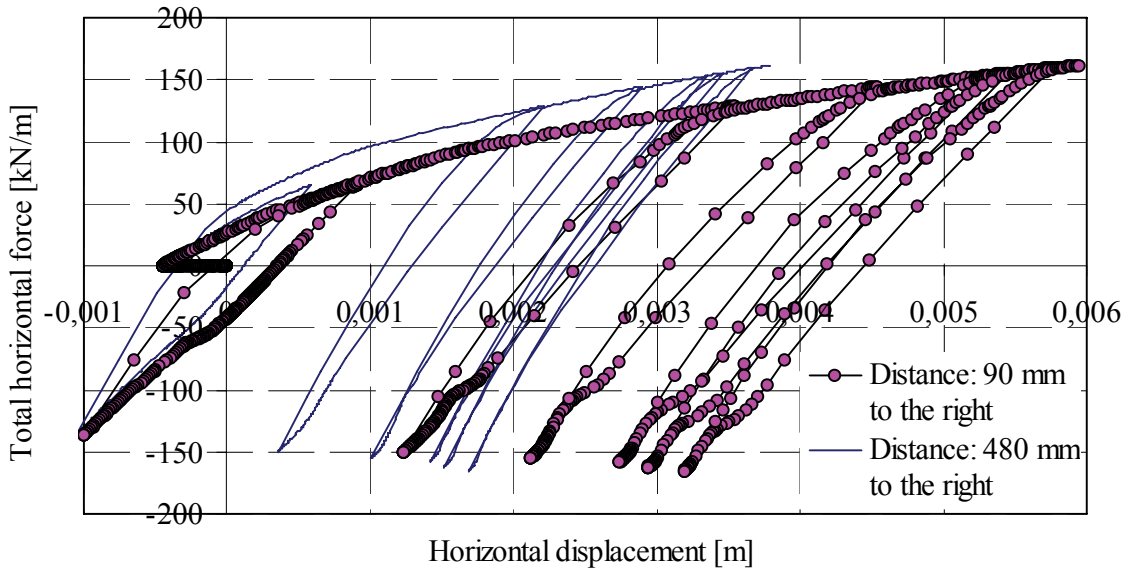

Figure 8.9 Horizontal displacements of two particles in soil around cyclically moving large-diameter pile.

The particle at a distance of 480 mm after, for example, the 6th pile movement did not return all the way but stayed more than 3 mm away from its original location although the pile returned and even moved an extra 10 mm in the opposite direction. The total movement of the particle was about 2.5 mm during the negative pile movement of 20 mm during the last cycle. Total displacements within soil, considering the whole zone around the pile, were less than 10 mm and mainly in the direction of pile movement or slightly inclined (see App. 6).

The total horizontal force developed clearly as a result of cyclic pile displacements although the pile wall friction angle was set to a small value. Because of low pile surface friction, the total force at y = 10 mm was clearly smaller, 65 kN/m, than the 210 kN/m yielded by non-cyclic calculations with typical pile surface friction (see Figure 8.6). The ultimate lateral force against the pile was also small, 164 kN/m. Thus, the wall friction angle was essential in the evaluation of the lateral forces due to both non-cyclic and cyclic pile movement.

With a typical pile surface friction, $R_{inter} = 0.45$, the horizontal force increased excessively along with each cycle, and both soil deformations and the resulting horizontal forces were unpredictable.

Non-symmetrically cyclic behaviour was also tested with one non-symmetrical cycle, where the 9th positive movement was 1 mm instead of 10 mm, which resulted in clearly non-symmetrical behaviour and a little higher negative displacement-phase earth pressures.

8.5 Summary and recommendation

The presented calculation model was used to evaluate the lateral displacement–force relation of circular piles of different diameters. The model served well, and the attained ultimate displacements and corresponding resistances were quite large. The significance of pile size could be also analysed. Wall friction angle was essential in the evaluation of lateral forces due to both non-cyclic and cyclic pile movement.

The Finnish practice of calculating lateral spring constant and lateral resistance of standard large-diameter piles corresponded closely enough to the results of the presented non-cyclic calculations. Thus, its use can be recommended also in the future, although the practice totally ignores pile diameter in spring constant estimation.

9 RAILWAY TRACK–BRIDGE–SOIL INTERACTION

9.1 Overview

Railway bridge end problems

Railway bridge ends are among the most complex details of railway tracks (see also Figure 2.6 and Figure 6.3). Next to the abutment the rails are subject to dynamic and cyclic forces from horizontal bridge movements, settlements, and traffic loads. The bump at the approach embankment usually develops over a long time. Therefore, costly maintenance has to be performed regularly and according to preliminary plans to avoid problems with traffic safety and comfort.

Effect of bridge deformations on rails next to an abutment with bearings

In central Europe the typical bridge superstructure consists of several consecutive and separate spans. In the warmth of a summer, the greatest compression in the railway track develops next to an abutment with a bearing (see right end of Figure 9.1).

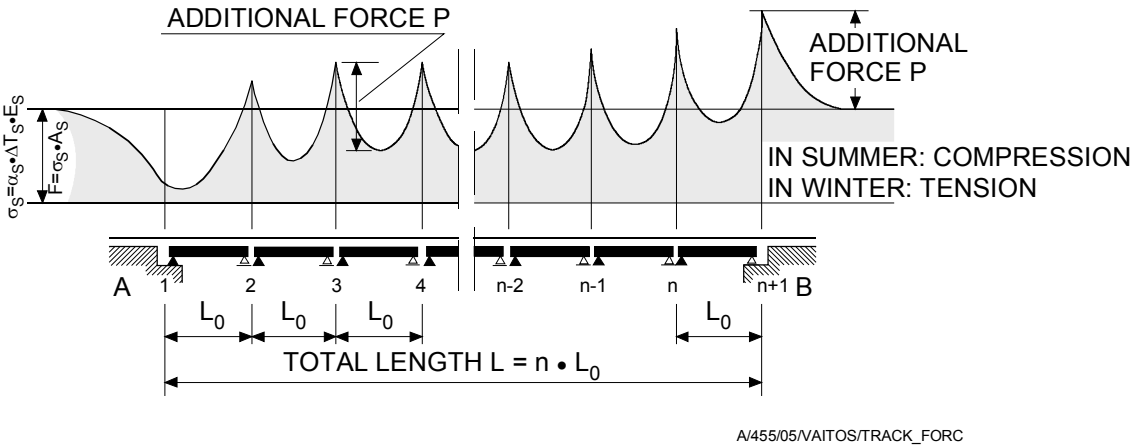

Figure 9.1 Track forces due to temperature change, ΔT (Gentz 2003).

The additional axial track force in Figure 9.1 can be roughly estimated from the equation (Gentz 2003):

$P = k_r * L_0 / 4$

As the stiffness of a rigid support increases, the track forces next to the freely moving bearing increase clearly. Figure 9.2 shows the forces in a 90 m long continuous bridge. The plastic part of the bilinear resistance between the track and the bridge was k_r = 20 kN/m as horizontal displacement was more than 2 mm.

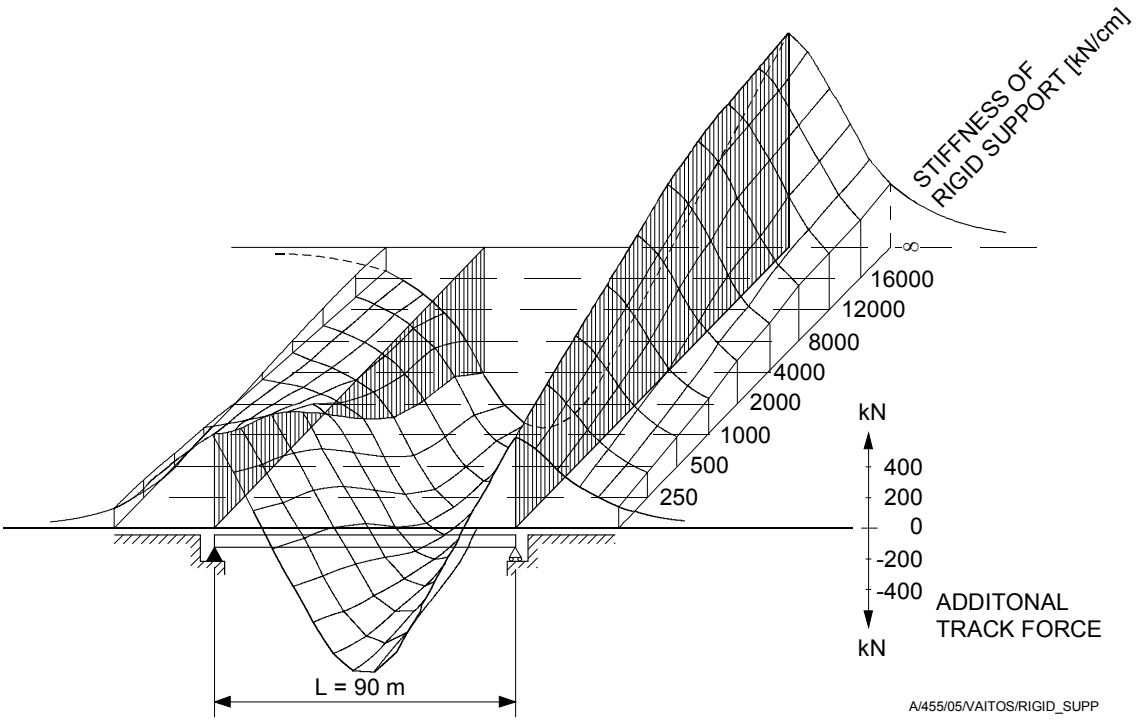

Figure 9.2 Sum of track forces as a function of temperature changes in a 2-track bridge with a rigid support on the left side. Horizontal stiffness at the left support varies between 0–∞ (Gerlich and Pahnke 1982).

9.2 Evaluation of Tekemäjärvenoja Railway Bridge track–bridge–soil interaction

Because of the rigid connection of the transition slab to the abutment and the behaviour of the short bridge, the majority of the horizontal forces in Tekemäjärvenoja Railway Bridge field tests transferred to the embankment through the rails, ballast and, especially, through the transition slab (see Ch. 4.3). The substructures including the abutment transferred less than 10 per cent.

The rigid transition slab–abutment connection increased the longitudinal stiffness of the bridge also as a result of the behaviour of the opposite abutment. At the abutment opposite to direction of the movement, earth pressures were small but the transition slab–abutment connection forces were large, and the transition slab resisted longitudinal bridge movement remarkably well.

Average embankment backfill stiffness at the earth pressure cell level in the transition slab push/pull test corresponded to average soil stiffness in loading tests with wagons. The observed lateral subgrade reaction according to Haavistonjoki Bridge measurements corresponded also to the observed lateral subgrade reaction at Tekemäjärvenoja Railway Bridge. However, below the transition slab, the observed lateral subgrade reactions were clearly smaller than the values calculated according to Finnish guidelines. The effect of the transition slab on the stiffness of soil in the case of low displacement was distinctive. Yet, earth pressures below the transition slab may be calculated according to present Finnish guidelines, but the designer should be aware of the real behaviour of the abutment and the backfill and in special cases use his own judgement in analysing the real behaviour (see Ch. 6.3.2 or Figure 4.52).

The effect of the vertical load from the wagons on the track was distinct as concerns the horizontal stiffness of the rails in the ballast.

The estimated final unloaded track stiffness according to measurements was close to the recommended horizontal stiffness used in Central Europe. The results of the Tekemäjärvenoja Railway Bridge field tests and verifying calculations support recommending the values given in UIC 774-3 (2001) concerning the track stiffness to be used also in Finland. However, the resistance, k_r, in the plastic zone could not be determined with the presented field tests because of the applied small horizontal force.

Finnish Rail Administration (RHK) has begun development of design guidelines for the real behaviour of a jointless railway bridge with continuously welded rails and its precise modelling in calculations. Continued development of the model presented in eurocode EN 1991-2:2003 is recommended (see also Figure 2.6).

10 CONCLUSIONS

10.1 Overview

Long jointless bridges with integral abutments can be adopted for use also in Finland. The limitations and guidelines presented in this thesis, and during the entire research project, must, however, be considered in Finnish practice. The maximum expansion length will be decided on the basis of the results of ongoing field tests and verifying calculations, the present estimation being 50–60 meters, which leads to 100–120 m long road bridges in a totally symmetrical case.

Stresses in the studied structures were not excessive, and the structural design of a superstructure and large-diameter piles can generally be performed based on present Finnish practice.

Large and cyclic displacements at the bridge abutment create large and partly non-reversible deformations in the approach embankment fill. Although the bridge structures are able to sustain the loads from earth pressures, the decision concerning the maximum expansion length should be made based on the behaviour of the approach embankment and particularly on the long-term behaviour of the approach embankment after several displacement cycles of the abutment.

A horizontal wall displacement of 0.0025 x H corresponds to earth pressure based on a coefficient of $0.5*K_p$ according to the performed calculations and the results of the performed literature review. The presented displacement is recommended as maximum displacement, if large non-reversible deformations must be avoided. However, the presented limitation leads to short bridges, about 40 meters in the case of a 2.5 m high abutment, which can be exceeded depending on the real behaviour of the bridge end. Yet, in such cases regular pavement maintenance cannot be avoided.

Frozen soil behaviour is plastic, and the mechanical properties of the soil depend, for instance, on loading rate, temperature and stress state. Horizontal displacement of bridge piers based on temperature change is very slow compared to general strain rates measured in tri-axial and compression tests. However, frozen soil is much harder and stiffer than unfrozen soil.

On the basis of studied UIC and ERRI research projects, researchers have not found a simple and valid solution to railway bridge end behaviour problems. For example, the risk of bump development still exists in spite of many trials and alternatives in design and maintenance.

A remarkable share of test results were verified with calculations, and several calculations were verified by performed tests. Thus, the field tests formed the basis for the presented conclusions and recommendations.

10.2 Conclusions and recommendations based on presented key points

Wall displacement–earth pressure relation

The presented calculation model allows verifying traditional earth pressure theories incorporating varying soil properties, wall inclination, earth surface inclination, etc. in a non-cyclic case. The results can also be presented based on a certain prescribed displacement level. This type of easy-to-use special geotechnical software and the presented calculation model are recommended also for structural designers as an earth pressure calculation method. Earth pressure distribution can be analysed quickly and simply in different cases and for various structure movements.

In traditional passive earth pressure theories earth pressures are considered to increase linearly towards the bottom of the horizontally moving structure. According to the calculations on an imaginary wall, earth pressure does not increase or even diminishes along the lowest third of the wall.

A rotating wall causes slightly greater earth pressures than a horizontally moving wall on the upper half of the wall. Earth pressures on the lower half are remarkably smaller in the case of a rotating wall, and near the bottom earth pressures are insignificant.

The presented model was expanded to evaluate the deformations and earth pressures accompanying cyclic wall movement. The earth pressure increase calculated with the used soil model and the chosen soil properties was larger than the observed increase in small-scale tests in England. Earth pressures increased the most during the first five cycles. Calculated non-reversible deformations after 12 displacement cycles were quite large. Yet, the method worked satisfactorily in analysing the characteristic displacements and residual stresses within soil. The behaviour of transition slabs could also be analysed with the presented cyclic wall displacement model.

Calculated maximum earth pressures were larger than those presented in Finnish guidelines, and they depended greatly on used wall friction angle and type of the movement. The Kerisel and Absi theory corresponded to the calculated behaviour much better than the theories of Coulomb or Rankine. The presented horizontal movement–earth pressure relation should also be considered in the development of Finnish guidelines.

Behaviour of integral abutments and approach embankments

According to Haavistonjoki Bridge 2D FEM calculations, a transition slab is a stiff structural member in the longitudinal direction of a bridge structure compared with soil stiffness. The majority of high soil stresses and deformations occur several metres from the abutment. Earth pressures against the abutment are quite small under the transition slab. The transition slab serves as a 1-span slab carrying the overburden. If this type of transition slab were to be horizontally connected to the abutment, large tensile stresses would occur both in the transition slab and the bridge superstructure in wintertime.

Abutment displacement had a direct impact on soil deformations and stresses around the upper part of the piles supporting the abutment. The soil layer around the piles was not stationary nor independent from abutment movement. As the integral abutment and the embankment moved simultaneously, the horizontal resistance of the piles was smaller than the resistance of individual piles would have been. Consequently, the bending moments in

the upper part of the piles were quite small. The traditional spring model used in Haavistonjoki Bridge 3D analysis overestimated the lateral subgrade reaction.

The presented 2D calculation method worked well in the evaluation of the behaviour of the Haavistonjoki Bridge abutments, earth pressures and backfill including the transition slab. The earth pressure increase due to a prescribed displacement corresponded to the observed values at the centre of the abutment. The best correlation was achieved with high soil strength and stiffness parameters. Similar earth pressure behaviour has been observed also at the instrumented railway bridge, Tekemäjärvenoja Railway Bridge, during load tests with small displacements.

The highest observed earth pressures at the Haavistonjoki Bridge abutment–soil interface due to thermal abutment displacements did not develop in the middle of the summer 2004 but in May and August –even in the middle of March before the embankment started to warm up.

According to the observed Haavistonjoki Bridge abutment displacements and verifying calculations, displacement at the bottom of the abutment was 60–75 per cent of the displacement at the top of the 2.4 m high abutment. Consequently, the earth pressure distribution against the abutment can be concluded partly according to a horizontally transferring wall and partly according to a rotating wall.

The transition slabs at Haavistonjoki Bridge were connected to the abutments with dowels that permitted small horizontal movements. According to the observed behaviour, the studied transition slab was an integral part of the approach embankment and did not move cyclically along with the abutment.

The presented L-shaped transition slab type that is recommended in Hessen, Germany is recommended as a jointless bridge end structure also in Finland. The abutment supports it vertically while horizontally the abutment can move in relation to the transition slab. The L-shaped transition slab limits deformations in the upper soil and pavement and tolerates abutment movements better than the typical Finnish counterpart. This may lead to even longer jointless bridges being built.

In countries, where integral bridges are constructed, various means for minimising earth pressures and non-reversible deformations within approach embankments have been presented. Some of them are referred to in Chapter 6, but detailed analysis is not part of this study. Nevertheless, it may be stated that, for instance, the placement of an elastic vertical board behind the abutment could possibly increase the maximum allowable length from what was suggested at the beginning of Chapter 10.

Behaviour of piles below piers in frozen soil

At ground water level, there is no need for a rigid horizontal support. It can be replaced, for example, by a special spring depicting frozen soil behaviour. A frozen soil spring, $k = 225$ MN/m at depth $z = 1$ m, is recommended for long jointless bridges and should be made part of Finnish design practice.

Lateral pile displacement–force relation

The presented calculation model was used to evaluate the lateral displacement–force relation of circular steel piles of different diameters. The model worked well and the

calculated ultimate displacements and corresponding resistances were quite large. The significance of pile size and soil strength could also be analysed. Wall friction angle was essential in the evaluation of lateral forces from non-cyclic or cyclic pile movement.

The Finnish practice of calculating lateral spring constant and lateral resistance of standard large-diameter piles corresponded closely enough to the results of the presented non-cyclic calculations. Thus, its use can also be recommended in the future, although the practice totally ignores pile diameter in spring constant estimation. Accordingly, also other large-diameter piles, for instance, drilled steel pipe piles, can be used in accordance with the related design manuals at the discretion of the designer to support jointless bridges.

Railway track–bridge–soil interaction

Because of the rigid connection of the transition slab to the abutment and the behaviour of the short bridge, the majority of the horizontal forces in Tekemäjärvenoja Railway Bridge field tests transferred to the embankment through the rails, ballast and, especially, through the transition slab. The share of the substructures including the abutment was less than 10 per cent.

Finnish Rail Administration has begun development of design guidelines for the real behaviour of a jointless railway bridge with continuously welded rails and its precise modelling in calculations. Continued development of the calculation model and parameters presented in eurocode EN 1991-2:2003 is recommended.

10.3 Need of further research

Further studies during the ongoing project will focus on, for instance, skewed abutments, the long-term behaviour of an integral bridge, and bridge behaviour during vehicle braking. These areas were excluded from this dissertation but are important issues contributing to the real behaviour of jointless bridges. The results of ongoing temperature change observations and consequent conclusions will be written into another dissertation at TUT.

A reinforced embankment with an elastic layer between the abutment and the embankment may be an excellent construction considering the reduction of earth pressures and non-reversible deformations within the approach embankment. The construction deserves thorough research with a focus on the long-time behaviour of the vertical elastic layer.

The presented L-shaped transition slab should be studied further in order to verify its performance in long jointless bridges, possibly longer than 120 meters.

Long frame bridges were not discussed in this dissertation, but are widely used, for instance, in the U.K. It could be an alternative for sites where space is limited.

The fatigue strength of the jointless structure should be verified in another research project. Some data of relevant studies in Europe and the USA on the subject could be found through a brief literature review.

The horizontal stiffness of a railway track on a bridge should also be tested with stabilised ballast after a period of regular train traffic.

REFERENCES

Abaqus. 2001. Abaqus manual. Pawtucket, U.S.A. Hibbitt, Karlsson, & Sorensen, Inc.

Abendroth, Robert E. & Greimann, Lowell F. 2005. Field Testing of Integral Abutments. Report No. HR-399. Center for Transportation Research and Education, Iowa State University. Internet 12.5.2006 http://www.ctre.iastate.edu/reports/hr399.pdf

Arsoy, S. & Barker, R.M. & Duncan, J.M. 1999. The behaviour of integral abutment bridges. FHWA/VTRC 00-CR3. Virginia Transportation Research Council.

BA 42/96. 1996. The design of integral bridges. Design manual for roads and bridges. United Kingdom.

Banverket. 2002. Banverkets ändringar och tillägg till Vägverkets Bro 2002. (Amendments and additions by Swedish Railway Administration to publication 'Bridge 2002' by Swedish Road Administration.) Standard BSV 583.10. 6th edition. Sweden, BV Bro. (In Swedish)

Berger, Dieter & Graubner, Carl-Alexander & Pelke, E. & Zink, M. 2003. Fugenloses bauen (Jointless construction). Entwurfshilfen für integrale Straßenbrücken. (Sketches for integral road bridges). Heft 50-2004 der Schriftenreihe der Hessischen Strassen- und Verkehrsverwaltung. Germany. (In German)

Berggren, Anne-Lise. 1983. Engineering creep models for frozen soil behaviour. Ph.D. thesis. Norway, Trondheim, Norwegian University of Science and Technology (NTNU). 174 p. + 183 app.p.

Bolton, M. D. 1993. What are partial factors for? Limit state design in geotechnical engineering. Copenhagen. Danish Geotechnical Society for ISSMFE TC 23, Proc. International Symposium on Limit State Design in Geotechnical Engineering, Vol. 3. pp. 565-583.

Briaud, Jean-Louis. 1997. Settlements of bridge approaches. Washington D.C. National Academy Press, National Cooperative Highway Research Program. 75 p.

Burke, Martin P. Jr. 1993. Steel bridges. News and information on the steel bridge from the U.S.A.

California trenching and shoring manual. 2001. Earth pressure theory and application. Internet 20.4.2006:
http://www.dot.ca.gov/hq/esc/construction/Manuals/TrenchingandShoring/TrenchingandShoring.htm

Card, G.B. & Carder, D.R. 1993. A literature review of the geotechnical aspects of the design of integral bridge abutments. TRL Project Report. (Pr 52). 53p.

Craig, R.F. 1997. Soil mechanics. 6th edition. Great Britain. ISBN 0415327032.

Duncan, J. Michael & Mokwa, Robert L. 2001. Passive earth pressures: theories and tests. Journal of Geotechnical and Geoenvironmental Engineering. Vol. 127, No. 3, pp. 248-257.

EN 1991-2:2003. 2003 Eurocode 1. Actions on structures. Traffic loads on bridges. Brussels, CEN - European committee for standardization. 170 p. ISBN: 0 580 42879 6.

Engelsmann, Stephan. 1998. Integrale Betonbrücken – Entwerfen und Bemessen von Brücken ohne Lager und Fugen (Integral concrete bridges – Design and calculation of bridges without bearings and joints). Dissertation. Universität Stuttgart (University of Stuttgart, Germany).

England, George L. & Tsang, Neil C.M. & Bush, David I. 2000. Integral Bridges. A fundamental approach to the time–temperature loading problem. Thomas Telford Ltd, London. 152 p. ISBN 0727728458

Finnra. 1999 a. Pohjarakennusohjeet sillansuunnittelussa. (Guidelines for foundations of bridges.) TIEL 2172068-99. Helsinki, Tiehallinto (Finnish Road Administration). 51 p. + 18 app.p. ISBN 951-726-583-2 (In Finnish) Internet 24.7.2006: http://alk.tiehallinto.fi/sillat/julkaisut/prakos99.pdf

Finnra. 1999 b. Siltojen korjaus. Kuivatuslaitteet. (Bridge repair. Drainage devices.) Sillan ja siltapaikan kuivatus. TIEL 2230095 - SILKO 1.601. Tiehallinto (Finnish Road Administration).

Finnra. 1999 c. Teräsputkipaalut. (Steel pipe piles. Code of practice.) Helsinki, Tiehallinto (Finnish Road Administration). 77 p. + 3 app.p. ISBN 951-726-523-9 (In Finnish) Internet 7.10.2005: http://alk.tiehallinto.fi/sillat/julkaisut/steelpipepiles1999.pdf 2000. Third edition. 81 p. + 3 app.p. ISBN 951-726-617-0 (In English)

Finnra. 1999 d. Sillan osat. Tyyppipiirustusluettelo ja piirustuspienennökset: Siirtymälaatta. (Type drawing: Transition slab 5 m.) R15/DL 2. Siirtymälaatta 5,0 m, elementtirakenne. 26.8.1999 (In Finnish) Internet 24.1.2006: http://alk.tiehallinto.fi/sillat/tyyppipiirustukset/sillanosat/siirtymalaatta/dl.pdf

Finnra. 2001 a. Siltojen rakentamisen ja korjaamisen seuranta. (Monitoring of bridge construction and repair) Seurantaraportti, osa 1. Tiehallinnon selvityksiä 7/2001. TIEH 3200645. Helsinki, Finnish Road Administration. 116 p. ISBN 951-726-709-6 (In Finnish)

Finnra. 2001 b. Teiden pohjarakenteiden suunnitteluperusteet. (Foundation structures of roads. Background for design.) TIEH 2100002-01. Helsinki, Finnish Road Administration. 59 p. + 54 app.p. ISBN 951-726-743-6 (In Finnish)

Finnra. 2002. Sillansuunnittelun täydentävät ohjeet (Supplementary bridge design instructions). Vaasa, Multiprint Oy. Helsinki, Finnish Road Administration. 23 p. + 67 app.p. ISBN 951-726-749-5 (In Finnish)

FGSV (Forschungsgruppe für Strassen- und Verkehrswesen, Arbeitsgruppe Erd- und Grundbau) (Research group for road and traffic administration). 1994. Merkblatt über den Einfluss der Hinterfüllung auf Bauwerke (Brochure about influence of backfill soil to structures). FGSV Heft 526. (In German)

Frosch, R. & Wenning, M. & Chovichien, V. 2005. The In-Service Behavior of Integral Abutment Bridges: Abutment-Pile Response. The 2005 FHWA Conference, March 16–18, 2005: Integral Abutment and Jointless Bridges (IAJB 2005). Baltimore, Maryland. pp. 30-

40. Internet 26.5.2006: http://www.engineering.manhattan.edu/civil/faculty/horvath/publications/ProceedingsIAJB2005.pdf

Gentz, Eberhard. 2003. Zur Problematik an Überbauenden von Eisenbahnbrücken (About problems involved in superstructures of railway bridges). Eisenbahningenieur. 54. (In German)

Greimann, L.F. & Yang, P. & Wolde-Tinsae, A.M. 1986. Nonlinear analysis of integral abutment bridges. Journal of Structural Engineering. Vol. 112, No. 10. pp. 2263-2280.

Harvey, David I. & Kennedy, Don W. & Ruffo, Gordon W. 2001. Integral Abutment Bridges - Design and Constructibility.
Internet 30.12.2004: http://www.ae.ca/files/integralabutmentbridges.pdf .

Hoppe, Edward J. 1999. Guidelines for the use, design, and construction of bridge approach slabs. VTRC 00-R4. Charlottesville, Virginia. Virginia Transportation Research Council. 19 p. + 20 app.p.

Hoppe, Edward J. 2005. Field Study of Integral Backwall with Elastic Inclusion. Virginia Transportation Research Council. The 2005 FHWA Conference, March 16–18, 2005: Integral Abutment and Jointless Bridges (IAJB 2005). Baltimore, Maryland. pp. 257-269. Internet 26.5.2006: http://www.engineering.manhattan.edu/civil/faculty/horvath/publications/ProceedingsIAJB2005.pdf

Huang, Jimin & French, Catherine & Shield, Carol. 2004. Behavior of Concrete Integral Abutment Bridges. Report No. MN/RC - 2004-43. University of Minnesota, Department of Civil Engineering. p. 349. Internet 12.5.2006 http://www.lrrb.org/pdf/200443.pdf

Husain, Iqbal & Bagnariol, Dino. 2000. Performance of integral abutment bridges. Ontario. Report BO-99-04. The Queen's Printer for Ontario. Bridge Office, Ministry of Transportation. ISBN 0-7778-9265-0.

Jernbaneverket. 2002. JD 525. Bruer. (Bridges.) Regler for prosjektering og bygging (Guidelines for design and construction). (In Norwegian)

Kerisel, J. & Absi, E. 1990. Active and passive earth pressure tables. Swets & Zeitlinger Publishers. 234 p. ISBN 9061918863.

Kerokoski, Olli. 2003. Soil–structure interaction of jointless bridges. Research plan. Institute of Earth and Foundation Structures, Tampere University of Technology. 2 p. (In Finnish, unpublished)

Kerokoski, Olli. 2005 a. Soil–structure interaction of jointless bridges. Literarture research. Institute of Earth and Foundation Structures, Tampere University of Technology. 150 p. ISBN 952-15-1352-7 Internet 25.7.2006: http://alk.tiehallinto.fi/sillat/julkaisut/silta_ja_maa_kirj_05.pdf (In Finnish)

Kerokoski, Olli. 2005 b. Soil–structure interaction of jointless bridges. Calculations. Institute of Earth and Foundation Structures, Tampere University of Technology. 126 p.

Internet 7.10.2005: http://alk.tiehallinto.fi/sillat/ julkaisut/silta_ja_maa_lask_05.pdf (In Finnish)

Kerokoski, Olli. 2005 c. Soil–structure interaction of jointless railway bridges. Literature search. 101 p. (In Finnish, unpublished)

Kerokoski, Olli. 2005 d. Approach Embankment Behaviour of Jointless Bridges with Transition Slab: Field Test and 2D-FEM Calculations. Institute of Earth and Foundation Structures, Tampere University of Technology. 18 p. (Paper submitted for Baltic Geotechnics X, Riga, October 12-14, 2005. Published)

Kerokoski, Olli & Laaksonen, Anssi. 2005 a. Soil–structure interaction of jointless bridges. The 2005 FHWA Conference, March 16–18, 2005: Integral Abutment and Jointless Bridges (IAJB 2005). Baltimore, Maryland. pp. 323-336. Internet 26.5.2006: http://www.engineering.manhattan.edu/civil/faculty/horvath/publications/ProceedingsIAJB 2005.pdf

Kerokoski, Olli & Laaksonen, Anssi. 2005 b. Monitoring of Haavistonjoki Bridge Abutment Performance. 19 p. (Paper submitted for 85th TRB Annual Meeting, January 22–26, 2006 in Washington, DC. Published on TRB CD-ROM)

Kolisoja, Pauli. Tampere 1997. Resilient deformation characteristics of granular materials. Doctoral thesis. Publication number 223, Tampere University of Technology. 216 p.

Koskinen, Mauri. 1997. Soil–structure interaction of jointless bridges on piles. Doctoral thesis. Publications 200, Tampere University of Technology. 184 p.

Koskinen, Mauri & Sinisalo, Ilkka & Kerokoski, Olli & Laaksonen, Anssi. 2005. Ratasillan ja maan yhteistoiminta. (Soil–structure interaction of railway bridges). Rakennustekniikka 2, pages 16-19. (In Finnish)

Koskinen, Mauri. 2005. Sillan ja maan yhteistoiminta. (Soil–structure interaction of bridges). Tekemäjärvenojan sillan (Oikorata S70) numeerinen analyysi. (Numerical analysis of Tekemäjärvenoja Bridge, Bridge S70 on direct line from Kerava to Lahti. Research Report.) Raportti 31.1.2005. (In Finnish, unpublished on 23.1.2006)

Laaksonen, Anssi. 2004. Soil–structure interaction of jointless bridges. Instrumentation of Haavistonjoki Bridge. Master's thesis. Tampere University of Technology. 160 p. + 76 app.p. ISBN 952-15-1338-1. (In Finnish) Internet 11.5.2006: http://alk.tiehallinto.fi/sillat/julkaisut/liikuntasaumattoman_sillan_maan_%20yhteistoimint a.pdf

Laaksonen, Anssi. 2005. Field tests on Tekemäjärvenoja Railway Bridge. Research report. Institute of Earth and Foundation Structures, Tampere University of Technology. (In Finnish, unpublished on 13.10.2005)

Li, H. & Yang, H. & Chang, C. & Sun, X. 2001. Experimental investigation on compressive strength on frozen soil versus strain rate. Journal of Cold Regions Engineering. Vol. 15, No. 2, pp. 125-133.

Mourad, S. & Tabsh, S. W. 1999. Deck slab stresses in integral abutment bridges. Journal of Bridge Engineering. Vol. 4, No. 2, pp. 125-130.

NBS I19 (Nordiskt bantekniskt samarbete). 1988. Spår på broar. (Railway tracks on bridges.) Information från NBS-gruppen. (Information from 'Nordic Co-operation on Railway Technology' Group.) 9 p. + 23 app.p. (In Swedish)

NBS I25 (Nordiskt bantekniskt samarbete). 1991. Föreskrifter för spårkonstruktion på broar med genomgående ballast. (Guidelines for railway track on ballasted bridges.) Information från NBS-gruppen. (Information from 'Nordic Co-operation on Railway Technology' Group.) 6 p. (In Swedish)

Nicholson, B. A. 1998. Integral abutments for prestressed beam bridges. Uniskill Ltd. Leicester. Prestressed Concrete Association (PCA). 84 p. (Internet 8.3.2004)

Nielsen, Anders. 1994. Ändskärmbro, sammanverkan mellan bro och motfyllning. (Bridge with end screen abutments, bridge–backfill interaction.) Examensarbete 1994:097. (Graduation Work.) Högskolan i Luleå & Vägverket. (Luleå University of Technology & Swedish Road Administration.) 45 p. + 27 app.p.

Noranta, V. 2004. Tiivistelmä kirjasta Plasser&Theurer, kohta AA-16a (Abstract from Plasser&Theurer book, Chapter AA-16a). Helsinki, VR-Rata. (VR-Track Ltd.) (In Finnish)

Pètursson, Hans & Collin, Peter. 2002. Composite bridges with integral abutments minimizing lifetime cost. Melbourne, Iabse symposium. 9 p.

Plaxis Manual. 2002. 2D - Version 8. Netherlands, A.A. Balkema publishers.

Pötzl, M. & Schlaich, J. & Schäfer, K. 1996. Grundlagen für Entwurf, die Berechnung und konstruktive Durchbildung lager- und fugenloser Brücken (Basics of design, calculation, and construction of bridges without joints and bearings). DAfStb Heft 461. Berlin, Beuth Verlag. 125 p. (In German)

RHK. 1997. Rautatiesiltojen suunnitteluohjeet. Osa 4 (RSO 4) (Railway bridges, Code of practice). Rautatiesiltojen perustusten erityiskysymyksiä (Foundations). Ratahallintokeskus. (Finnish Rail Administration.) 17 p. (In Finnish)

RHK. 2000. RAMO 8, Ratatekniset määräykset ja ohjeet (Technical regulations and guidelines for railway tracks). Osa 8 (Part 8). Sillat (Bridges). Ratahallintokeskus (Finnish Rail Administration). 43 p. + 32 app.p. (In Finnish)

RHK. 2002. RAMO 11, Ratatekniset määräykset ja ohjeet (Technical regulations and guidelines for railway tracks). Osa 11 (Part 11). Radan päällysrakenne. (Railway track superstructure.) Ratahallintokeskus (Finnish Rail Administration). (In Finnish)

RHK. 2003. SYL-R, Rautatiesiltojen yleiset laatuvaatimukset. (General quality requirements for railway bridges). Ratahallintokeskuksen julkaisuja D 13., Ratahallintokeskus (Finnish Rail Administration), Helsinki. 55 p. + 9 app.p. ISBN 952-445-087-9. Internet 17.10.2005: http://www.rhk.fi/maaraykset/SYL-R.pdf (In Finnish)

Rosell, Ebbe. 2003. Special information by e-mail. Borlänge, Sweden. Swedish Road Administration.

SGY. 1980. Kairausopas I, Painokairaus (Weight sounding test), tärykairaus, heijarikairaus (Ram sounding test). ISBN 951-676-1275.

Statens vegvesen. 2000. Bruhåndbok Number 4 (Bridges Manual no. 4). Plassproduserte platebruer (Cast-in-Place Slab Bridges). Nr. 100 i Vegvesenets håndbokserie. Norway, Trykkpartner A/S. ISBN 82-7207-535-0. (In Norwegian)
Internet 10.10.2005: http://www.vegvesen.no/vegnormaler/hb/100_4/index.html

Thippeswamy, Hemanth K. & GangaRao, Hota V. S. & Franco, Jason M. 2002. Performance evaluation of jointless bridges. Journal of Bridge Engineering. Vol. 7, No. 5. pp. 276-289

Tsang, N. C. M. & England, G. L. & Dunstan, T. 2002. Soil/structure interaction of integral bridge with full height abutments. 15th ASCE Engineering Mechanics Conference, June 2-5 2002. New York, Columbia University. 10 p.

Tsytovich, N. A. 1975. The mechanics of frozen ground. McGraw-Hill Book Company. 426 p.

UIC Code 774-3 R. 2001. Track/bridge interaction. Recommendations for calculations. 2nd edition. International Union of Railways (UIC). 70 p. + 37 app.p. ISBN 2-7461-0257-9

Vägverket. 2002. Bro 2002. (Bridge 2002. Code of practice.) BY 20 A 2001:17114. Publication number 2002:47. Borlänge, Sweden. Swedish Road Administration.

Vägverket. 1996. Broprojektering - En handbok (Bridge design manual). Publication number 1996:63. ISSN 1401-9612. Borlänge, Sweden. Swedish Road Administration. 132 p.

APPENDICES

Appendix 1 Some extra results on wall displacement–earth pressure relation calculations

Appendix 2 Some input data tables for the comparison of Haavistonjoki Bridge with 3D spring FEM models

Appendix 3 Observed temperatures within the Haavistonjoki Bridge embankment at different levels during 1.3.2004–31.8.2004

Appendix 4 Observed earth pressure changes in transition slab push/pull test

Appendix 5 Calculated total deformations, effective stresses and relative shear stresses in Haavistonjoki Bridge abutment zone after forced displacement of 7 mm at deck level

Appendix 6 Total displacements within soil after 7th lateral pile movement

Appendix 7 Soil properties based on soil samples and soundings

Appendix 8 Abutment with wing walls: structural model for longitudinal 2D FEM analysis

Appendix 9 Field tests outside Finland:
- Behaviour of concrete integral abutment bridges (Huang et al 2004)
- Field Testing of Integral Abutments (Abendroth & Greimann 2005)
- Field Study of Integral Backwall with Elastic Inclusion (Hoppe 2005)

Appendix 1 Some extra results on wall displacement–earth pressure relation calculations

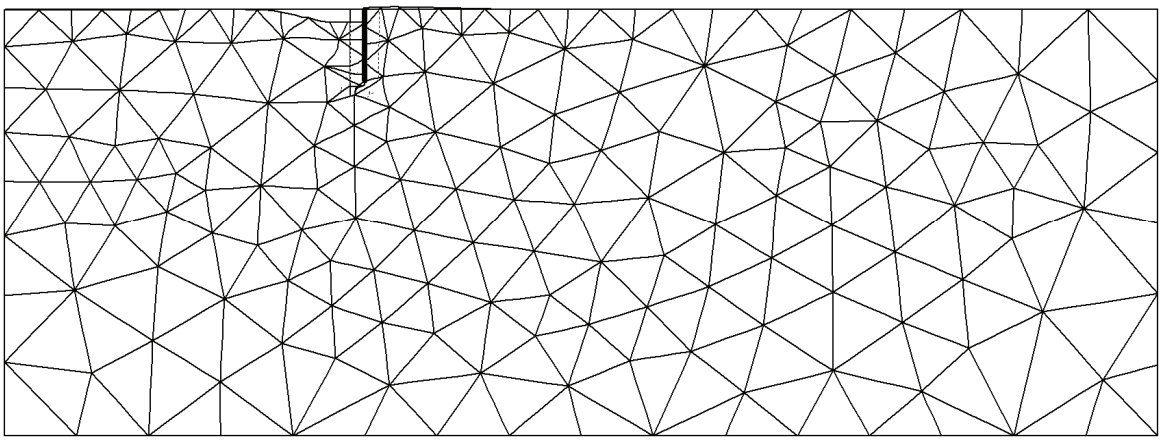

A 2.5 m high wall that moves horizontally in soil. The structural model presents the mesh used in non-cyclic calculations. Displacement was 10 mm. Deformations were scaled up 50 times.

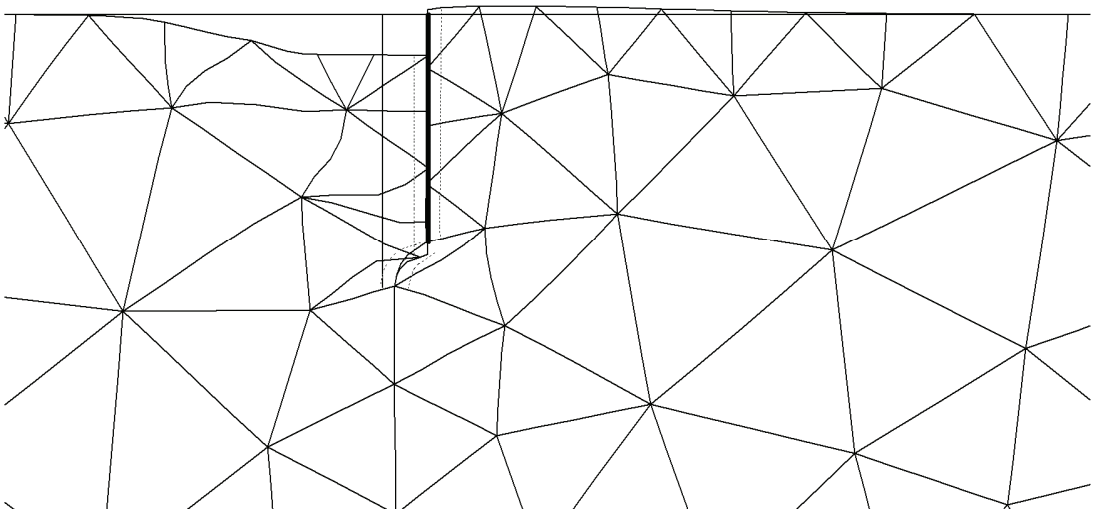

Deformations near the wall after 10 mm displacement. The greatest displacement was 14.2 mm. Displacements were scaled up 50 times.

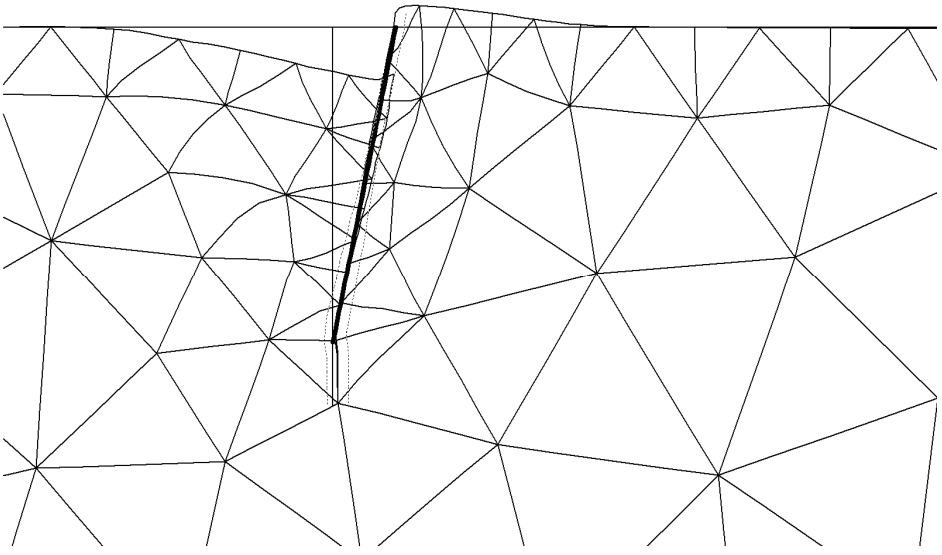

Calculated deformations after rotation caused by 10 mm wall top displacement. Deformations were scaled up 50 times.

Appendix 1 Some extra results on wall displacement–earth pressure relation calculations

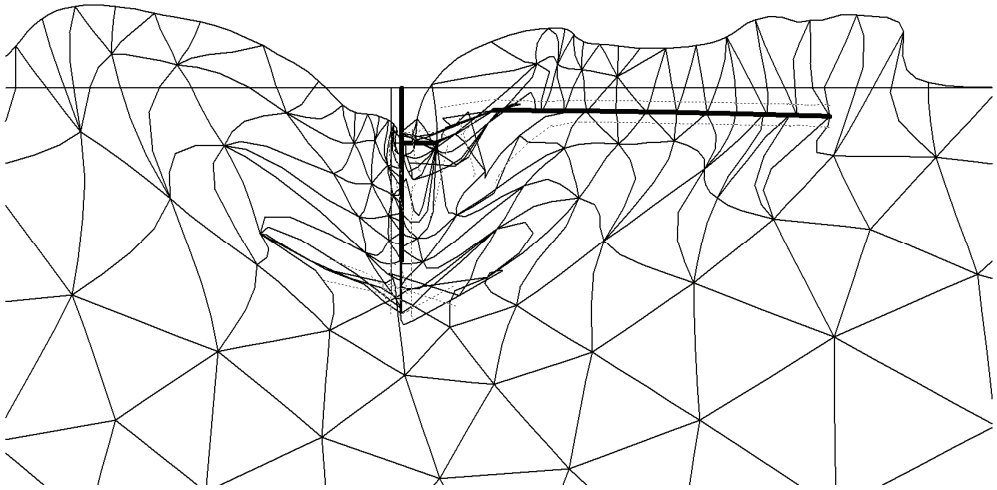

Deformations in soil next to the wall after 12 displacement cycles ±15 mm. The greatest displacement was 185 mm. Displacements were scaled up 10 times. Case 7.

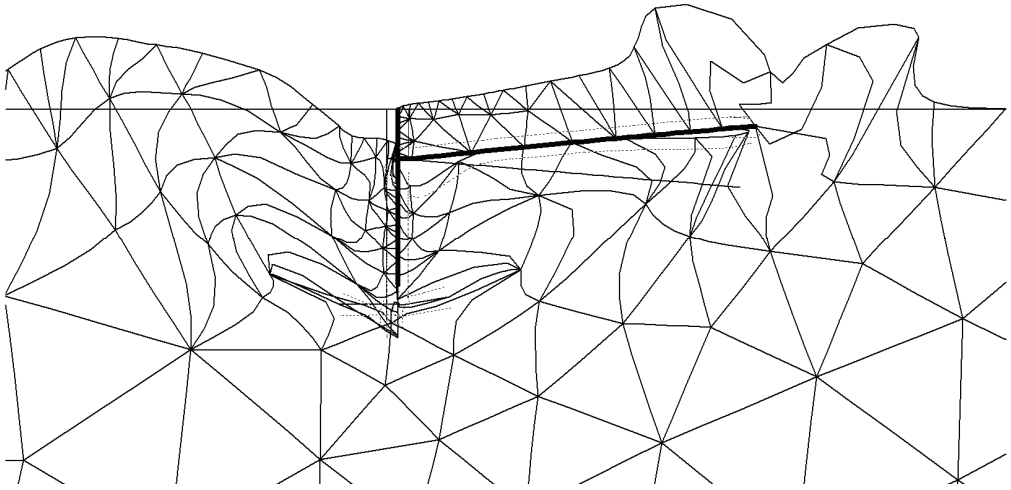

Deformations in soil next to the wall after 12 displacement cycles ±15 mm. The greatest displacement was 160 mm. Displacements were scaled up 10 times. Case 8.

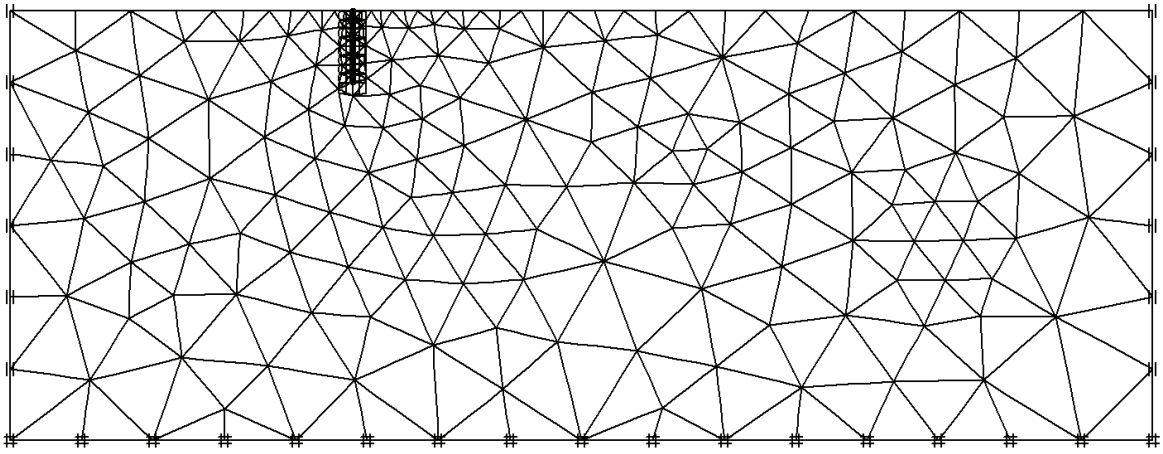

The mesh representing soil and horizontally moving wall. Cyclic calculations.

Appendix 1 Some extra results on wall displacement–earth pressure relation calculations

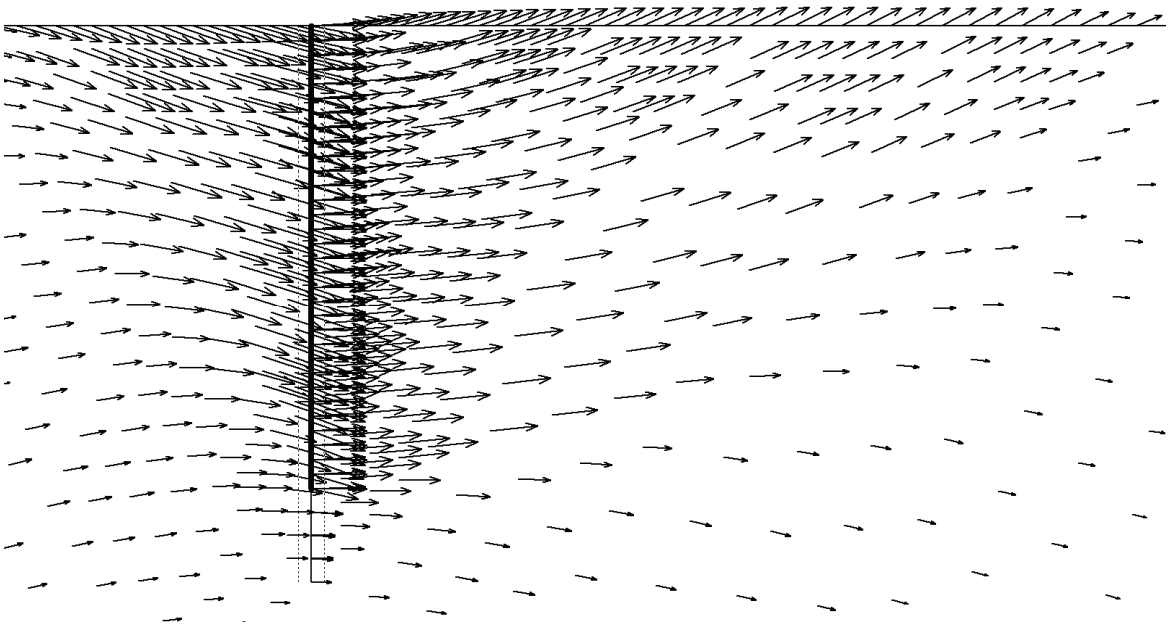

Cyclic calculations. Displacements during 12th horizontal movement from -15 mm to +15 mm. Displacements were scaled up 10 times. Case 6.

Appendix 2 Some input data tables for the comparison of Haavistonjoki Bridge

Haavistonjoki Bridge vane test results [kPa] on cohesive soil and corresponding lateral resistances and subgrade reactions of pile d = 711 mm. s_s = shear strength, s_{sh} = shear strength after soil disturbance.

				Pile d = 711 mm	
Coordinates (Point 16 at site): X: 6844570.693 Y: 2524486.002 Ground surface level: + 90.1			Lateral resistance [kN/m^2]	Lateral resistance [kN/m]	Lateral subgrade reaction [kN/m^3]
Depth from ground surface [m]	s_s	s_{sh}	p_m	p_m	k_s
4.3	20.7	5.6	155	110	1456
5	23.9	4	179	127	1681
Coordinates (Point 21 at site): X: 6844574.329 Y: 2524500.999 Ground surface level: + 94.7		[kN/m^2]	Lateral resistance [kN/m]	Lateral resistance [kN/m^3]	Lateral subgrade reaction [kN/m^3]
Depth from ground surface [m]	s_s	s_{sh}	p_m	p_m	k_s
7.5	44.6	8	335	238	3136

Lateral subgrade reactions, ultimate values of lateral resistance and corresponding displacements at abutment or support T4 steel pipe piles. Case 2.

Soil material	γ' [kN/m^3]	Depth z [m]	ϕ [°]	K_p	n_h [MN/m^3]	$k_{s,\phi}$ [kN/m^3]	$k_{s,c}$ [kN/m^3]	p_m [kN/m^2]	P_d [kN/m]	y_m [mm]
Crushed rock	22	2.9	42	5.0	17	69,339		1416	1007	40.8
Crushed rock	22	3.9	42	5.0	17	93,249		1904	1354	40.8
Crushed rock	22	4.9	42	5.0	17	117,159		2393	1701	40.8
Crushed rock	22	5.9	42	5.0	17	141,069		2881	2048	40.8
Crushed rock	22	6.9	42	5.0	17	164,979		3369	2396	40.8
Crushed rock	22	7.9	42	5.0	17	170,000		3858	2743	45.4
Crushed rock	22	8.9	42	5.0	17	170,000		4346	3090	51.1
Clayey silt	10.2	9.9					3136	335	238	266.9
Clayey silt	10.2	10.9					3136	335	238	266.9
Clayey silt	10.2	11.9					3136	335	238	266.9
Clayey silt	10.2	12.9					3136	335	238	266.9
Clay	10.2	13.9					1000	141	100	351.6
Moraine	13.2	14.9	45	5.8	18	180,000		6666	4740	74.1
Moraine	13.2	15.9	45	5.8	18	180,000		7004	4980	77.8
Moraine	13.2	16.9	45	5.8	18	180,000		7343	5221	81.6

Appendix 2 Some input data tables for the comparison of Haavistonjoki Bridge

Lateral subgrade reactions, ultimate values of lateral resistance and corresponding displacements at intermediate pier T3 steel pipe piles. Cases 2 and 3.

Soil material	γ' [kN/m^3]	Depth z [m]	ϕ [°]	K_p	n_h [MN/m^3]	$k_{s,\phi}$ [kN/m^3]	$k_{s,c}$ [kN/m^3]	p_m [kN/m^2]	P_d [kN/m]	y_m [mm]
Crushed rock	20	1	42	5.0	17	23910		444	316	37.1
Crushed rock	20	2	42	5.0	17	47820		888	631	37.1
Crushed rock	20	3	42	5.0	10.2	43038		1332	947	61.9
Clayey silt	10.2	4					1456	155	110	265.6
Clayey silt	10.2	5					1681	179	127	265.6
Clay	10.2	6					1000	141	100	351.6
Moraine	13.2	7	45	5.8	18	177215		2661	1892	30.0

Lateral subgrade reactions, ultimate values of lateral resistance and corresponding displacements at abutment or support T4 steel pipe piles. Case 3.

Soil material	γ' [kN/m^3]	Depth z [m]	ϕ [°]	K_p	n_h [MN/m^3]	$k_{s,\phi}$ [kN/m^3]	$k_{s,c}$ [kN/m^3]	p_m [kN/m^2]	P_d [kN/m]	y_m [mm]
Crushed rock	22.5	2.9	45	5.8	27	110,127		1673	1190	30.4
Crushed rock	22.5	3.9	45	5.8	27	148,101		2250	1600	30.4
Crushed rock	22.5	4.9	45	5.8	27	186,076		2827	2010	30.4
Crushed rock	22.5	5.9	45	5.8	27	224,051		3404	2421	30.4
Crushed rock	22.5	6.9	45	5.8	27	262,025		3981	2831	30.4
Crushed rock	22.5	7.9	45	5.8	27	270,000		4558	3241	33.8
Crushed rock	22.5	8.9	45	5.8	27	270,000		5135	3651	38.0
Clayey silt	10.2	9.9					3136	335	238	266.9
Clayey silt	10.2	10.9					3136	335	238	266.9
Clayey silt	10.2	11.9					3136	335	238	266.9
Clayey silt	10.2	12.9					3136	335	238	266.9
Clay	10.2	13.9					1000	141	100	351.6
Moraine	13.2	14.9	45	5.8	18	180,000		6780	4821	75.3
Moraine	13.2	15.9	45	5.8	18	180,000		7119	5061	79.1
Moraine	13.2	16.9	45	5.8	18	180,000		7457	5302	82.9

Appendix 2 Some input data tables for the comparison of Haavistonjoki Bridge

Horizontal abutment spring properties of Case 2 (E_d = 80,000 kPa) and Case 3 (E_d = 250,000 kPa).

			Case 2			Case 3		
Symbol	Definition	Unit	Abutment spring for breadth 1.833 m	Abutment spring at depth 2.1 m	Abutment spring at depth 1.0 m	Abutment spring for breadth 1.833 m	Abutment spring at depth 2.1 m	Abutment spring at depth 1.0 m
Breadth B (per spring)	Given value	[m]	1.833			1.833		
Height H	Given value	[m]	2.5			2.5		
Average earth pressure depth z	Given value	[m]	1.25	62 %	38 %	1.25	62 %	38 %
γ	Given value	[kN/m^3]	22	Two horizontal springs to substitute for one stiffer spring		22.5	Two horizontal springs to substitute for one stiffer spring	
ϕ	Given value	[aste]	42			45		
E_d	Given value	[kN/m^2]	80,000			250,000		
σ_h	=z*γ	[kN/m^2]	27.5			28.125		
K_p	=tan^2(45+ϕ/2)		5.04			5.83		
K_0	=1-sinϕ		0.33			0.29		
K_a	=1/K_p		0.20			0.17		
p_p average	=K_p*σ_h	[kN/m^2]	139			164		
p_0 average	=K_0*σ_h	[kN/m^2]	9.1			8.2		
p_a average	=K_a*σ_h	[kN/m^2]	5.5			4.8		
Force P_p	=B*H*p_p	[kN]	636	391	244	751	463	289
Force $P_{0,5p}$	=0,5*P_p	[kN]	318	196	122	376	231	144
Force P_0	=B*H*p_o	[kN]	42	26	16	38	23	15
Force P_a	=B*H*p_a	[kN]	25	15	10	22	14	9
δ_p	= 4* $\delta_{0,5p}$	[mm]	8.67			3.28		
$\delta_{0,5p}$	=0.5*p_p/(E_d/H)	[mm]	2.17			0.82		
δ_o	Starting point	[mm]	0			0		
δ_a	= - $\delta_{0,5p}$	[mm]	-2.17			-0.82		

δ_p = 8.67 mm corresponds to relative abutment displacement 0.0035 * H.
δ_p = 3.28 mm corresponds to relative abutment displacement 0.0013 * H.

Appendix 3 Observed temperatures within the Haavistonjoki Bridge embankment

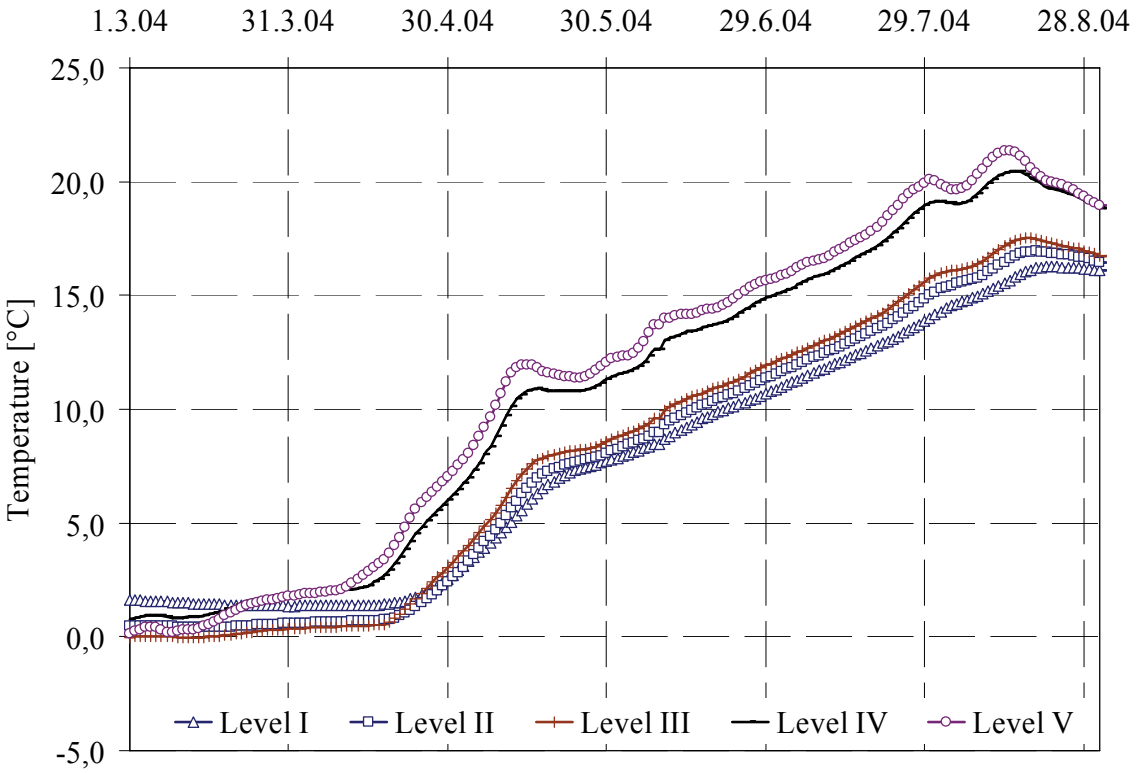

Observed temperatures within the Haavistonjoki Bridge embankment at different levels during 1.3.2004–31.8.2004. Level V is the highest and its depth is 1 m. Level I is the deepest and its depth is 2.5 m. The horizontal distance from abutment T4 is 2.4 m.

Appendix 4 Observed earth pressure changes in transition slab push/pull test

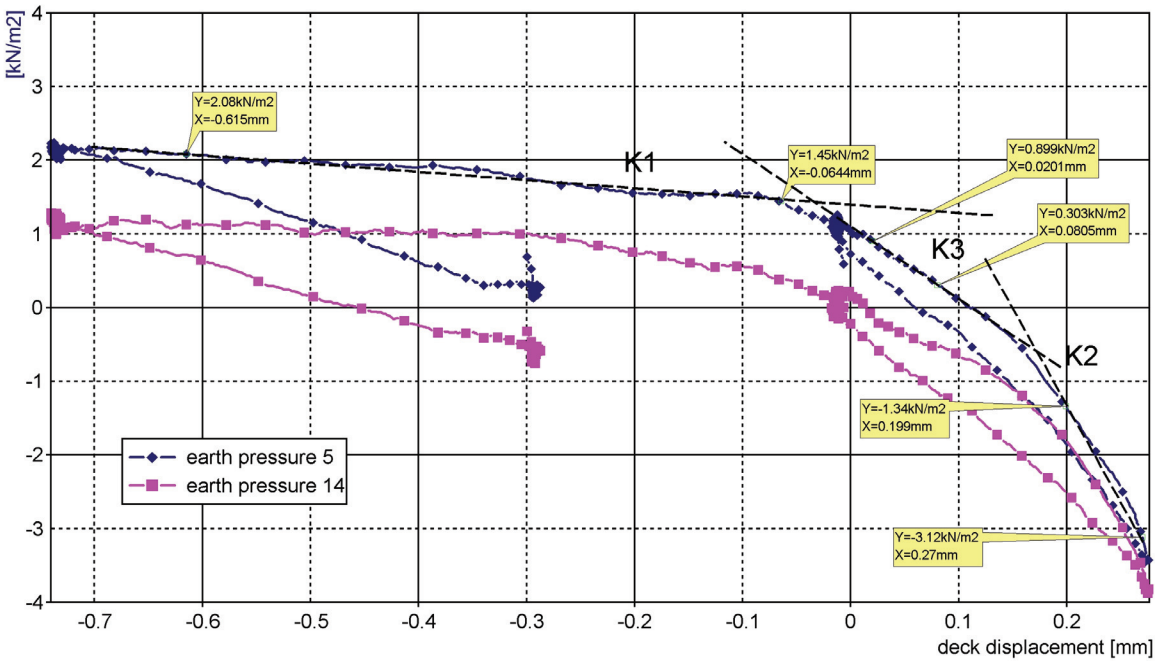

Observed earth pressure changes in 11th loading test, i.e. transition slab push/pulltest, according to earth pressure cells 5 and 14 (Laaksonen 2005).

Appendix 5 Calculated total deformations, effective stresses and relative shear stresses in Haavistonjoki Bridge abutment zone after forced displacement of 7 mm at deck level

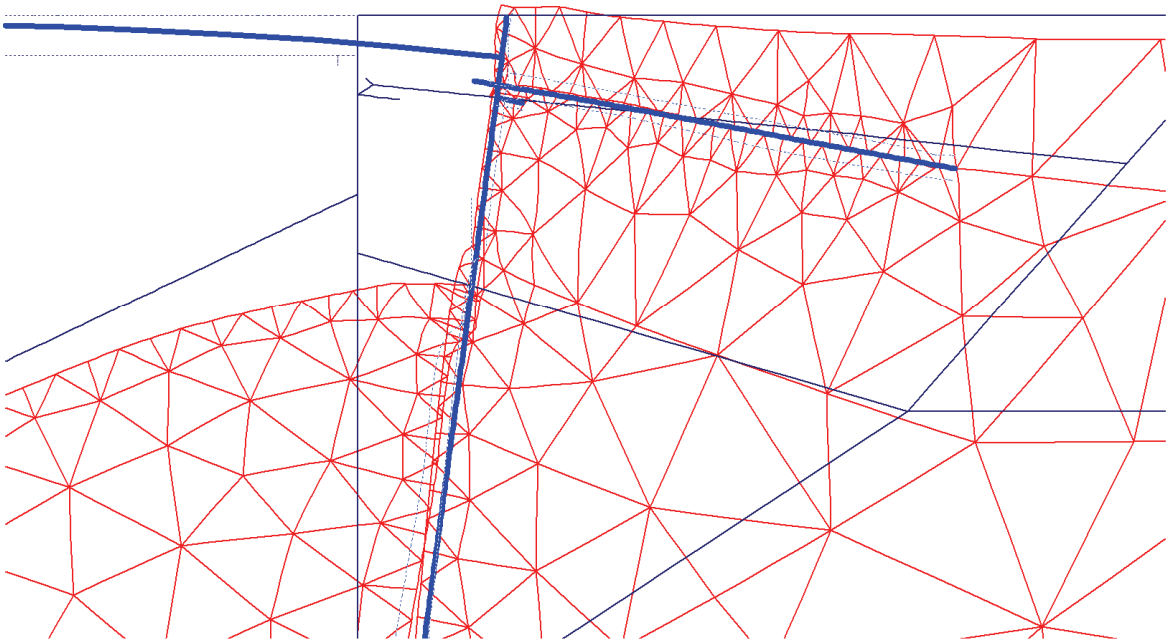

Deformed mesh of Haavistonjoki Bridge 2D FEM model. Displacements are scaled up 200 times. Extreme displacement is 7.7 mm. Abutment rotation is (7.44 mm - 5.91 mm) / 2400 mm = 1/1570. E_d *= 80,000 kPa for crushed rock.*

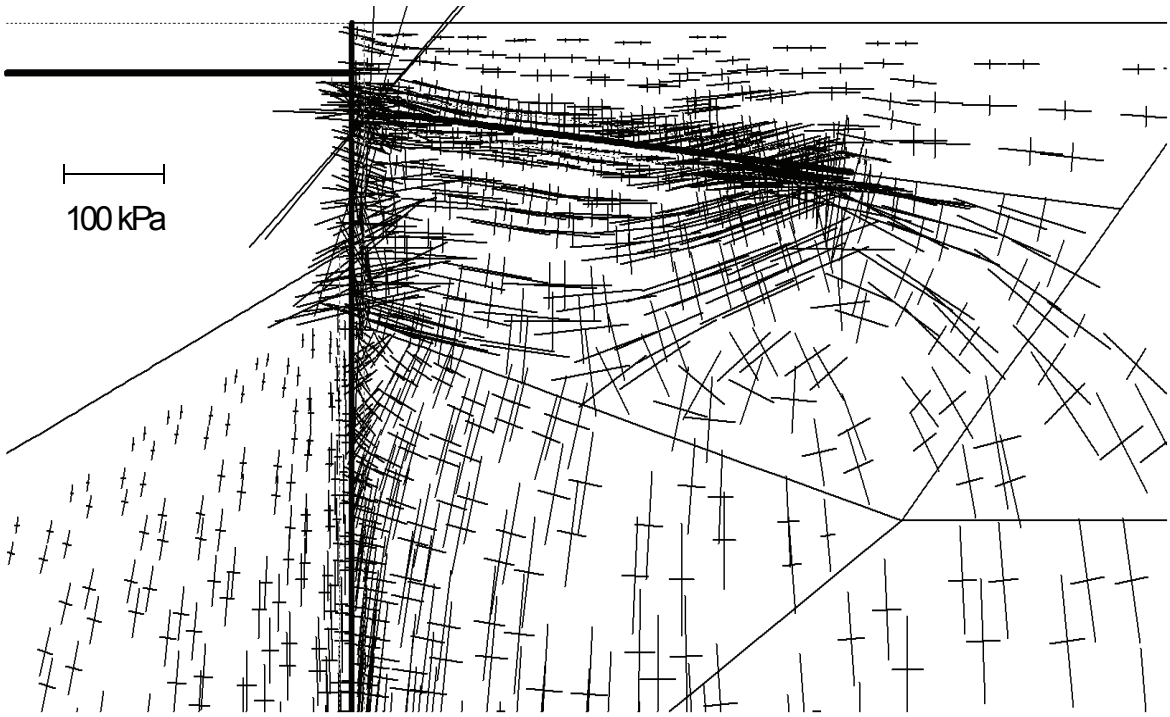

Effective stresses in soil around Haavistonjoki Bridge abutment. E_d *= 80,000 kPa for crushed rock.*

Appendix 5 Calculated total deformations, effective stresses and relative shear stresses in Haavistonjoki Bridge abutment zone after forced displacement of 7 mm at deck level

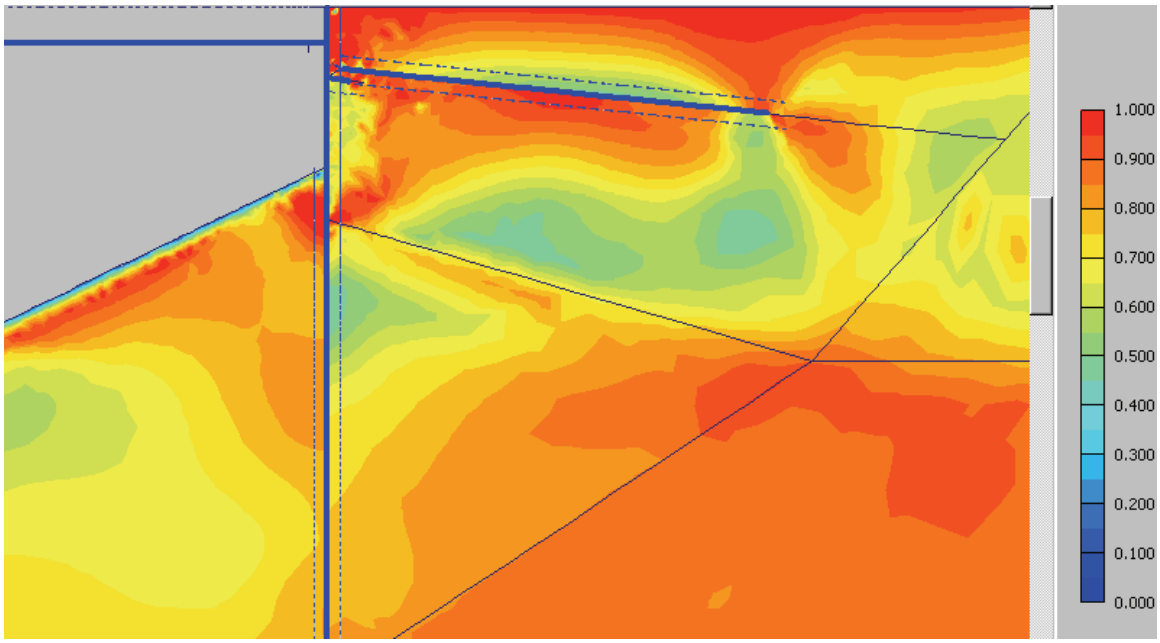

Relative shear stresses next to Haavistonjoki Bridge abutment. The interface elements between the structures and soil are also presented. E_d = 80,000 kPa for crushed rock.

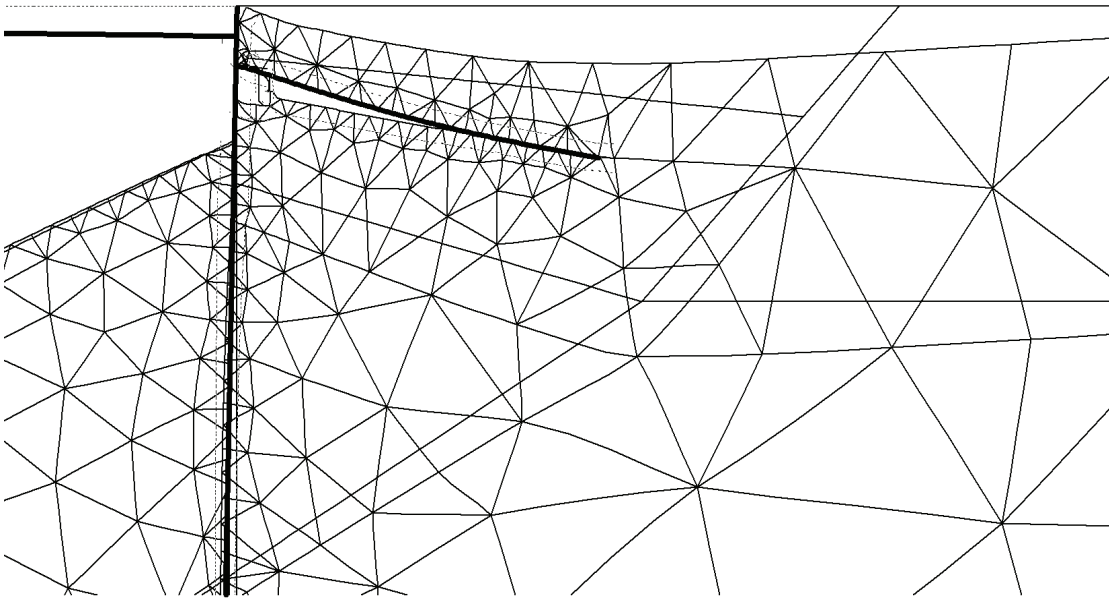

Deformations solely due to the construction of a crushed rock layer above the transition slab. Deformations were scaled up 50 times. HS soil model, E_d = 250,000 kPa for crushed rock.

Appendix 6 Total displacements within soil after 7th lateral pile movement

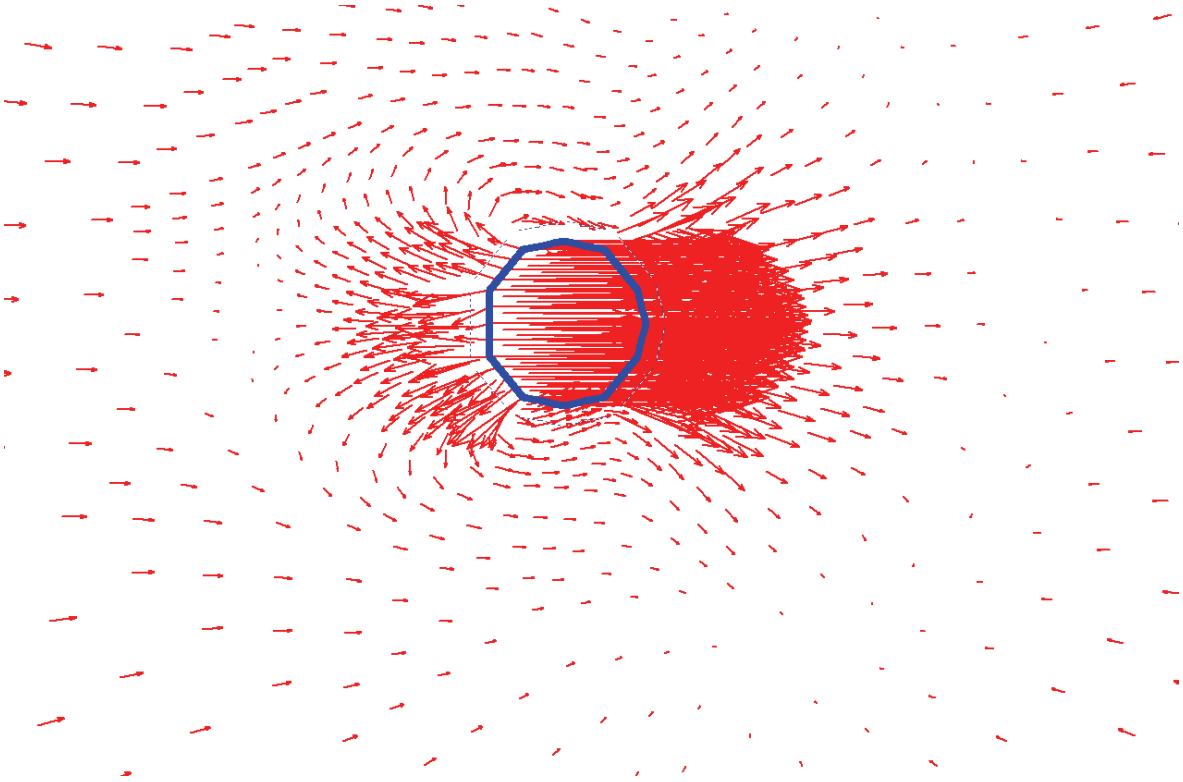

Total displacements within soil after 7th lateral pile movement. The displacements were less than 10 mm and mainly in the direction of pile movement or slightly inclined. Friction on the pile surface was small.

Appendix 7 Soil properties based on soil samples and soundings

The tables below present the measured water content, w, and remoulding index, F, values at three locations on Haavistonjoki Bridge.

Water content w [%] and remoulding index F [%] values measured from soil samples at Haavistonjoki Bridge site locations 17, 20 (eastern embankment) and 101 (western embankment) (see site investigation plan).

Site location 17	Ground surface +89.661		
Located at (X,Y): 6844568.45, 2524485.63			
Depth [m]:	Water content [%]	Remoulding index [%]	Soil
2	24	50	Clayey Silt
3	25	39	Clayey Silt
4	36	35	Clayey Silt
5	33	33	Clay

Site location 20	Ground surface +93.471		
Located at (X,Y): 6844577.04, 2524498.74			
Depth [m]:	Water content [%]	Remoulding index [%]	Soil
2	21	39	Clayey Silt
3	23	37	Clayey Silt
4	24	36	Clayey Silt
5	24	35	Clayey Silt
6	26	29	Clayey Silt
7	28	28	Clayey Silt
8	11	-	Moraine

Site location 101	Ground surface +90.154		
Located at (X,Y): 6844566.77, 2524458.36			
Depth [m]:	Water content [%]	Remoulding index [%]	Soil
1	3.4	-	Moraine
2	9	-	Moraine

No undisturbed soil samples were analysed.

Appendix 7 Soil properties based on soil samples and soundings

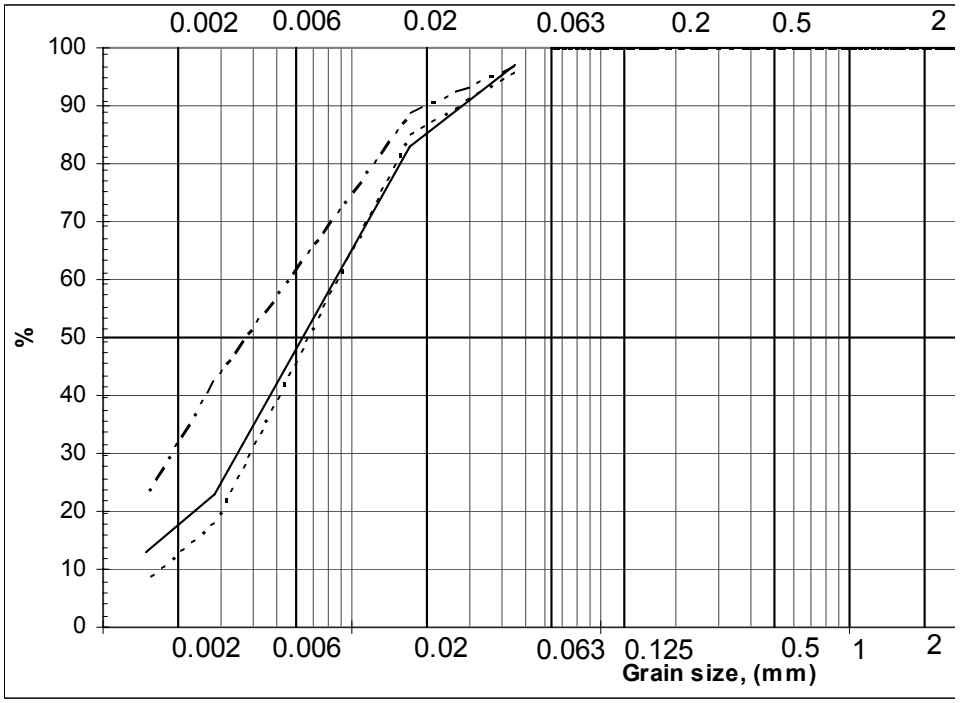

Grain size distribution curve. Haavistonjoki Bridge. Site location 17. Depths 2m (continuous line), 3m (dotted line) and 4m + 5m.

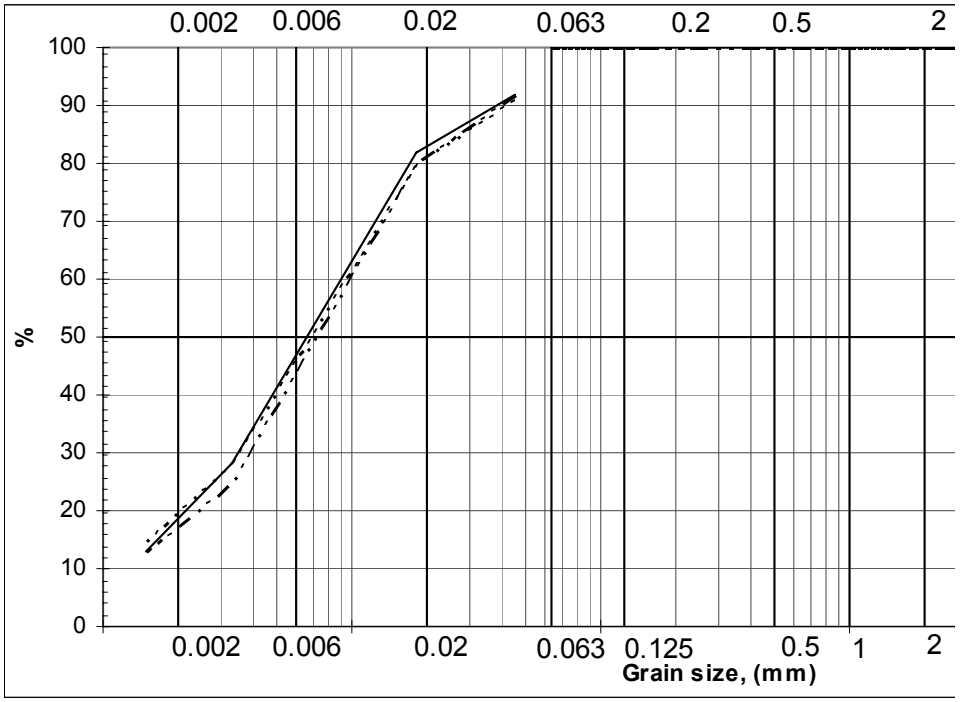

Grain size distribution curve. Haavistonjoki Bridge. Site location 20. Depths 2m + 3m (continuous line), 4m + 5m (dotted line) and 6m + 7m.

Appendix 7 Soil properties based on soil samples and soundings

Soil properties based on weight sounding test results

Part of the weight sounding test (SGY 1980) results are presented in the following seven figures: eastern embankment site locations 16 and 21 and one about 17 meters from the eastern abutment below the proposed road embankment.

Estimated soil properties according to the test results:

- At site location 16, the sounding ended at depth 5.8 m from ground surface. Between 1.2–4 meters the average number of half rounds was 45 and the soil was estimated to be silt. According to design manual "Pohjanrakennusohjeet sillansuunnittelussa" (Finnra 1999a), Table 2, with the reduced number 45 / 1.3 = 35 for silt, relative density is medium and friction angle 36º–3º = 33º, and modulus of elasticity E_d = 25 MPa. The saturated density of silt is about 20 kN/m^3. Below the silt there is a 1 m thick layer of clay. The weight sounding penetrated almost 1 meter into the moraine layer. According to the ram sounding test (SGY 1980), the thickness of the bottom moraine layer is about 3.5 m.
- At site location 21 the sounding ended at depth 9 m from soil surface. The upper 4 meters was a fill layer. Between 4.2m–7m the average number of half rounds was 45 and the soil was estimated to be silt. Consequently, the results for the silt layer are the same as at site location 16. Also, the layers below silt are the same as at site location 16.
- Below the proposed road embankment the sounding ended at depth 8.4 m from ground surface. Between 0.6m–2.2m the average number of half rounds was 16 and the soil was estimated to be silt. With the reduced number 16 / 1.3 = 12 for silt, relative density is loose and friction angle 32º–3º = 29º, and modulus of elasticity E_d = 11 MPa. Between 2.4m–5.8m the average number of half rounds was 116 and the soil was estimated to be silt. With the reduced number 116 / 1.3 = 89 for silt, relative density is very high and friction angle 41º–3º = 38º, and modulus of elasticity E_d = 65 MPa.

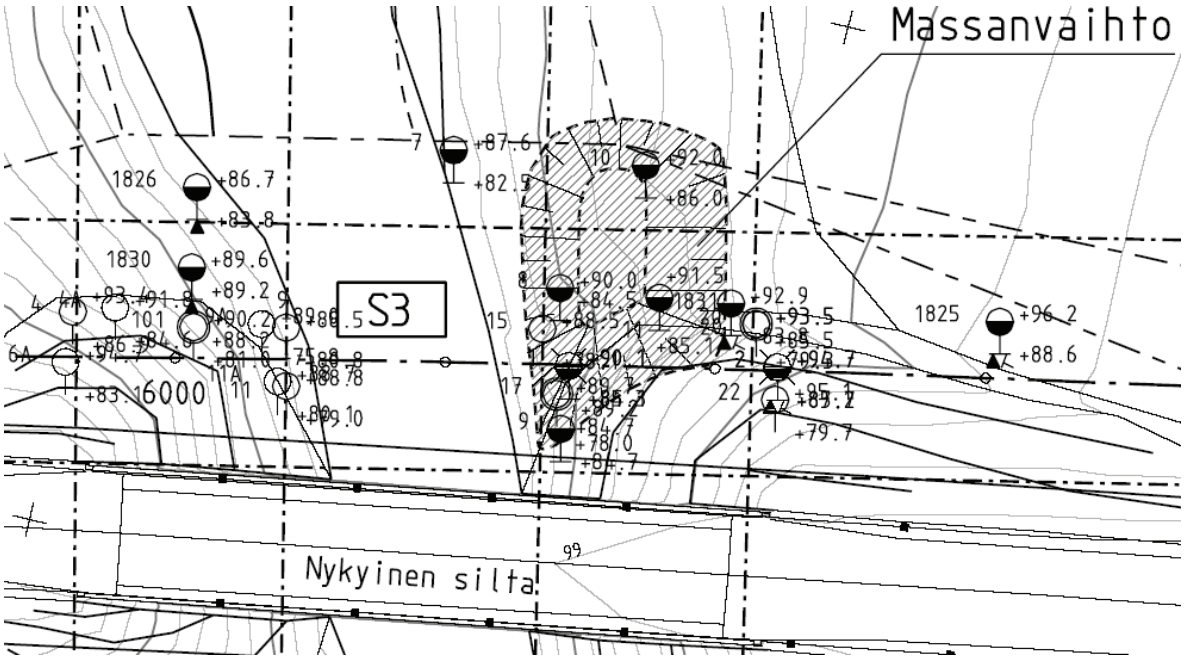

Site investigation plan. Nykyinen silta = replaced old bridge. Massanvaihto = replacement fill area located close to the old bridge embankment. S3 = proposed Haavistonjoki Bridge.

Appendix 7 Soil properties based on soil samples and soundings

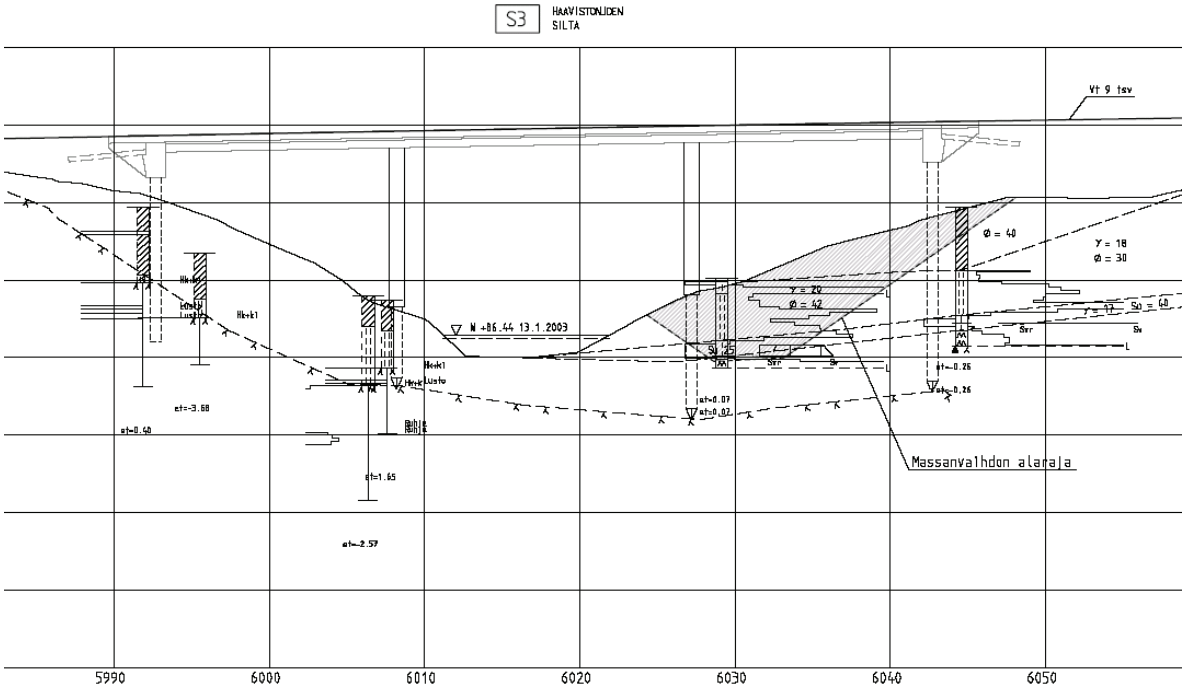

Site investigation. Longitudinal section along the bridge length. Massanvaihdon…= replacement fill with proposed γ = 20 kN/m^3 and ϕ = 42°. At western abutment the proposed drilled steel pipe piles were not used.

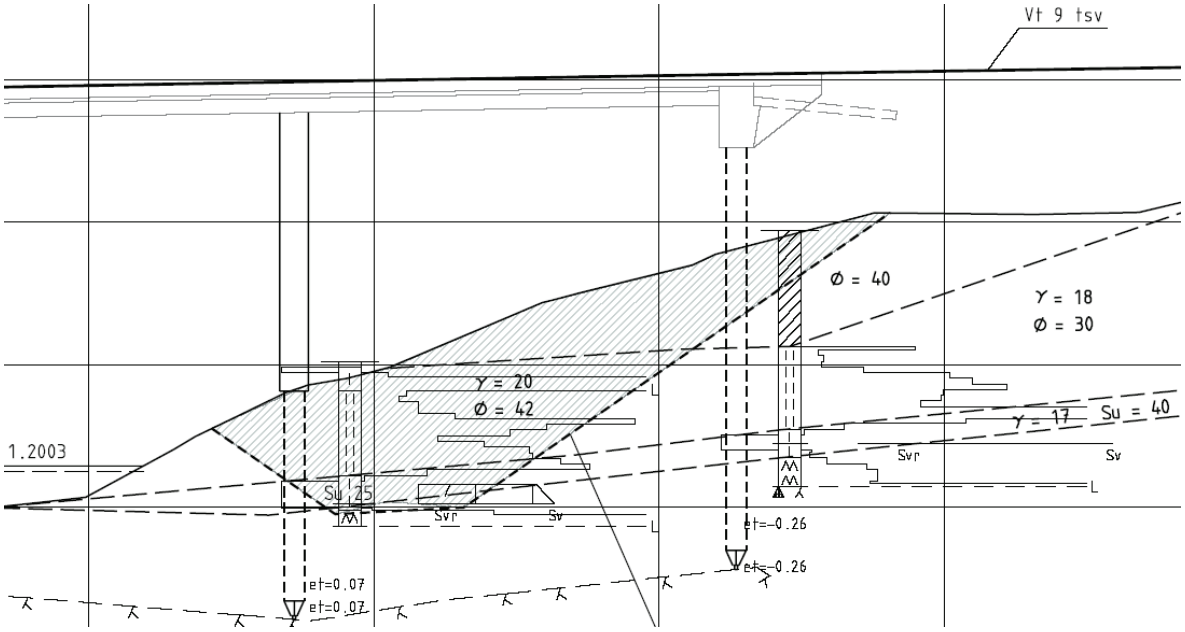

Site investigation. Longitudinal section. Details of eastern abutment.

Appendix 7 Soil properties based on soil samples and soundings

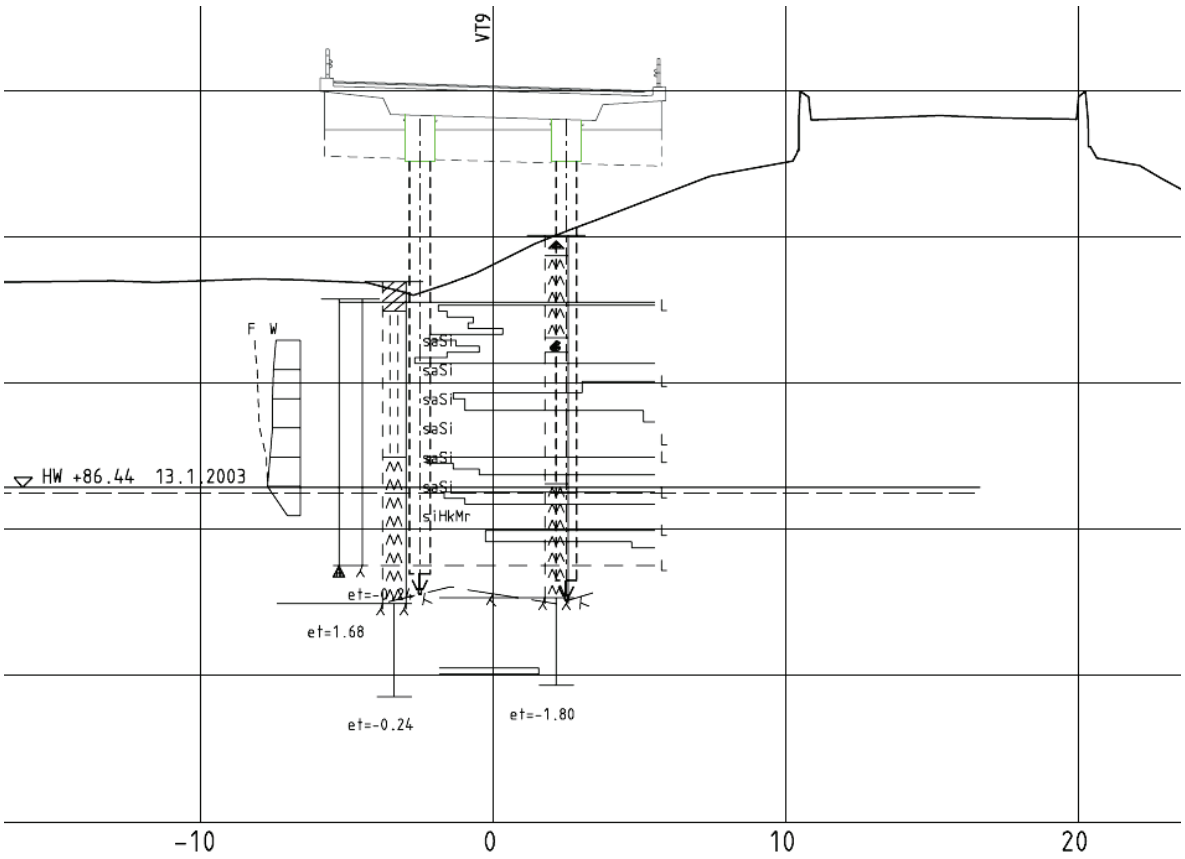

Site investigation. Transverse section near eastern abutment. The old bridge with its embankment is also shown.

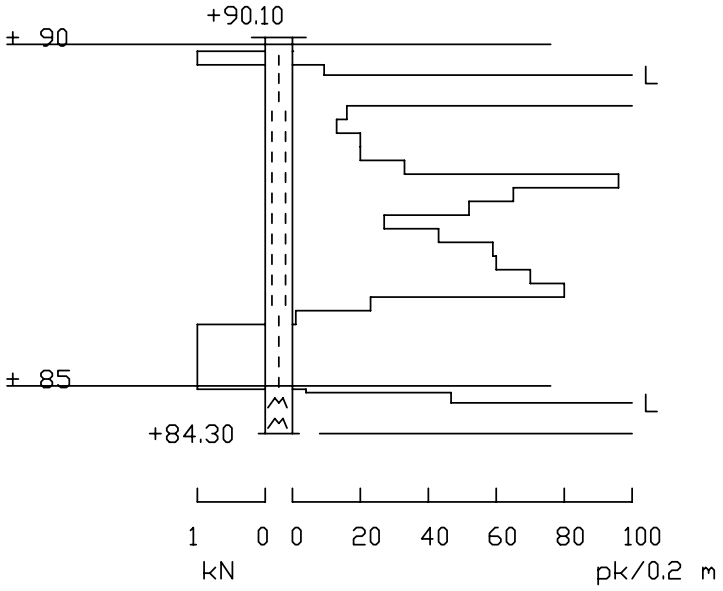

Site investigation. Weight sounding test results at site location 16. pk/0.2m = number of half circles per 0.2 m depth. X = 6844570.693, Y = 2524486.002, Ground surface +90.10.

Appendix 7 Soil properties based on soil samples and soundings

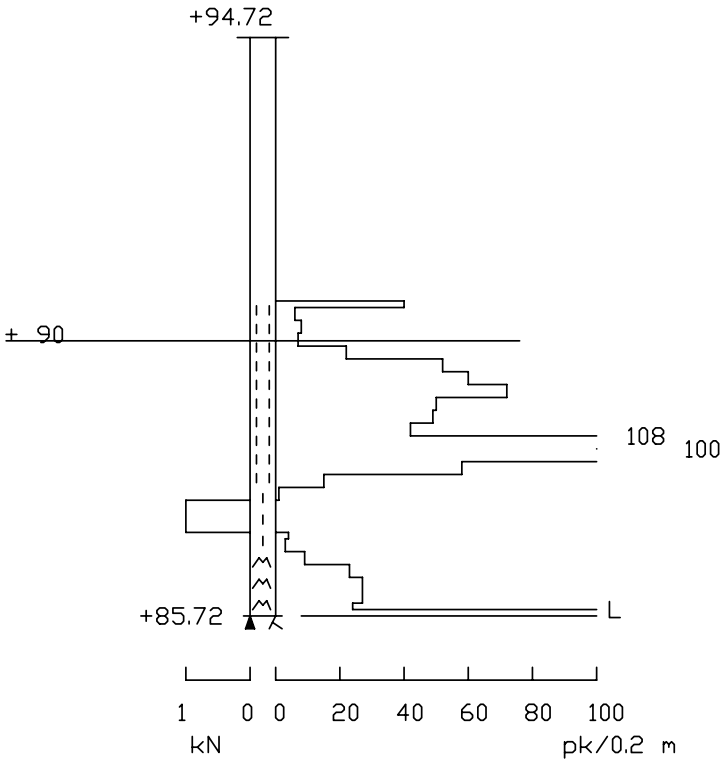

Site investigation. Weight sounding test results at site location 21. pk/0.2m = number of half circles per 0.2 m depth. X = 6844574.329, Y = 2524500.999, Soil surface +94.72.

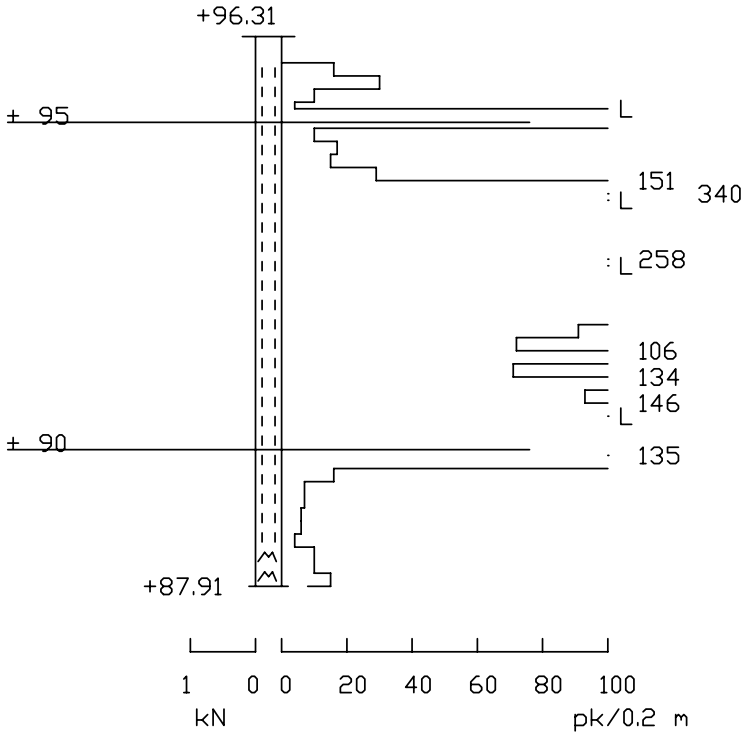

Site investigation. Weight sounding test results. Location about 17 m from the eastern abutment below the proposed road embankment. pk/0.2m = number of half circles per 0.2 m depth. X = 6844577.664, Y = 2524517.397, Ground surface +96.31.

Abutment with wing walls: a simple structural model for longitudinal 2D FEM analysis

The size of the structural model was 20 m * 30 m. The abutment with wing walls was located close to the centre of the model. A horizontal load of 16 kN/m^2 was exerted against the soil at all four model edges. The load corresponded to earth pressure at 2 m depth as the at-rest pressure coefficient was about $K_0 = 0.4$ and soil density was $\gamma' = 20$ kN/m^3.

The prescribed displacement in longitudinal bridge direction was 12 mm.

The structural model and the mesh with triangular elements are presented in the figures below.

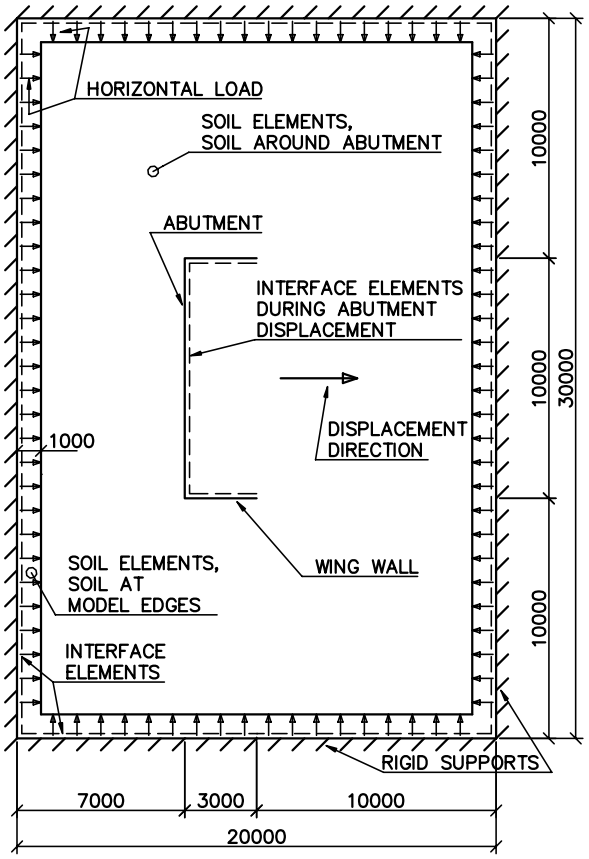

Structural model. At-rest earth pressure and pile displacement direction.

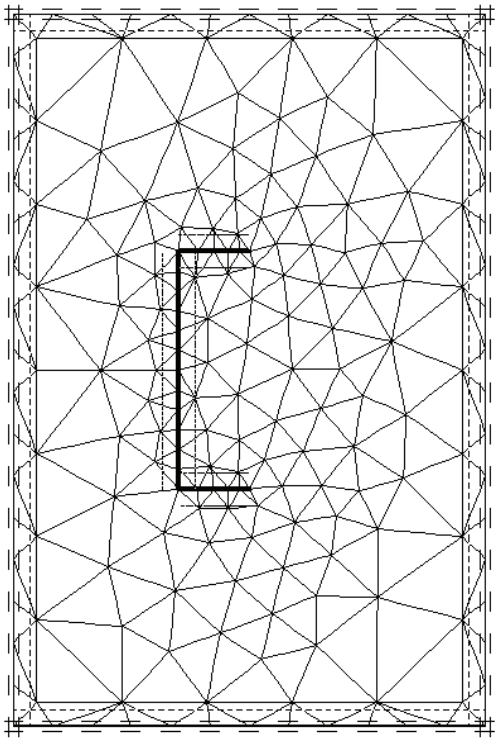

Triangular 2D elements.

The soil properties are presented in the table below. The soil near the edges of the model was ten times stiffer than the soil around the abutment in order to minimise deformations near the edges.

The soil properties have been selected keeping in mind the typical properties of well-compacted non-cohesive soil (Finnra 1999a) at this depth.

Appendix 8 Abutment with wing walls: structural model for 2D FEM analysis

Soil properties. Soil density is zero.

Soil model: Hardening-Soil	Unit	Soil around the abutment	Soil at model edges
Type	[-]	Drained	Drained
γ	[kN/m³]	0	0
e_{max} - e_{init}	[-]	0.2	0.2
E_{50ref}	[kN/m²]	100,000	1,000,000
M_{ref}	[kN/m²]	100,000	1,000,000
power (m)	[-]	0.5	0.5
ϕ	[°]	42	45
ψ	[°]	5	0
E_{urref}	[kN/m²]	300,000	3,000,000
ν_{ur}	[-]	0.2	0.2
p_{ref}	[kN/m²]	100	100
R_{inter}	[-]	0.45	0.01

Results

This calculation concentrated only on earth pressures against the abutment and the wing walls. Thus, the results are presented only in the following two figures.

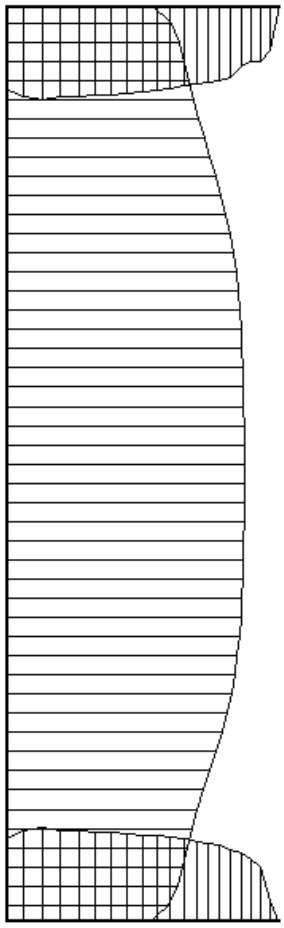

Effective normal stresses against abutment and wing walls. Extreme stress 88 kPa.

Appendix 8 Abutment with wing walls: structural model for 2D FEM analysis

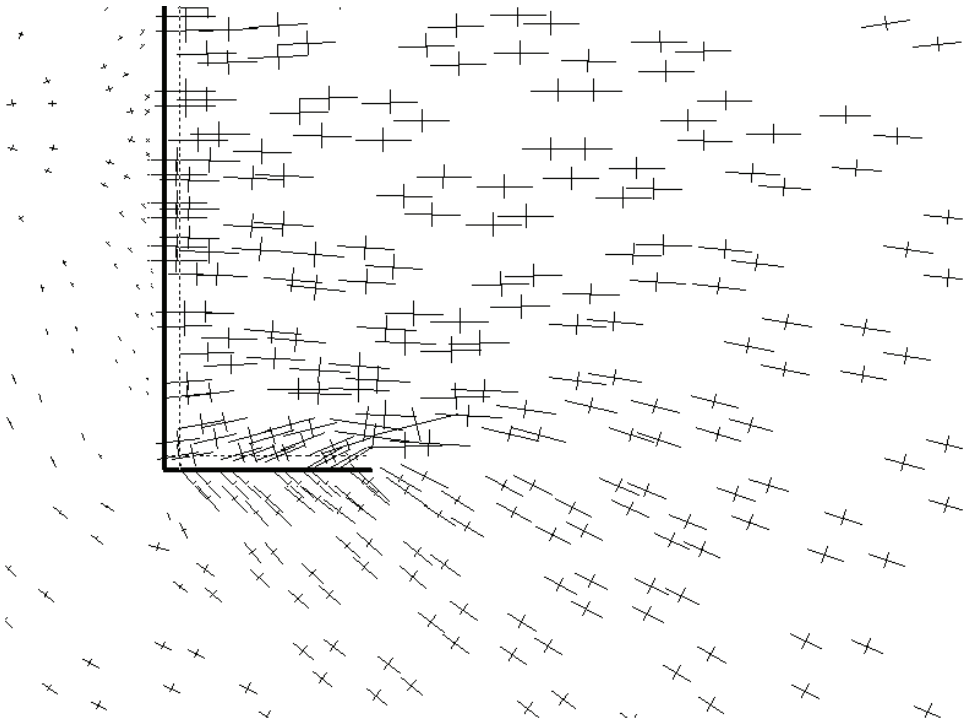

Effective stresses within soil close to the abutment and a wing wall.

0 FIELD TESTS OUTSIDE FINLAND

0.1 Behaviour of concrete integral abutment bridges (Huang et al 2004)

Description of the test bridge

The bridge in Minnesota was a three-span pre-stressed concrete bridge with a total length of 66 meters (216.6 ft, see Figure 0.1). Each span consisted of four 22 m long pre-stressed girders with a centre-to-centre spacing of 3.35 m. The total bridge width was 12 m. At the piers, the girders were supported by a curved plate-bearing assembly to achieve a simple support. A 50 mm gap was set between the adjacent girders. The continuity of the superstructure over the piers was provided by a 230 mm thick reinforced concrete deck. A single row of six piles was driven at each support of the bridge. Wingwalls were oriented at 45^{o} to the abutment centreline.

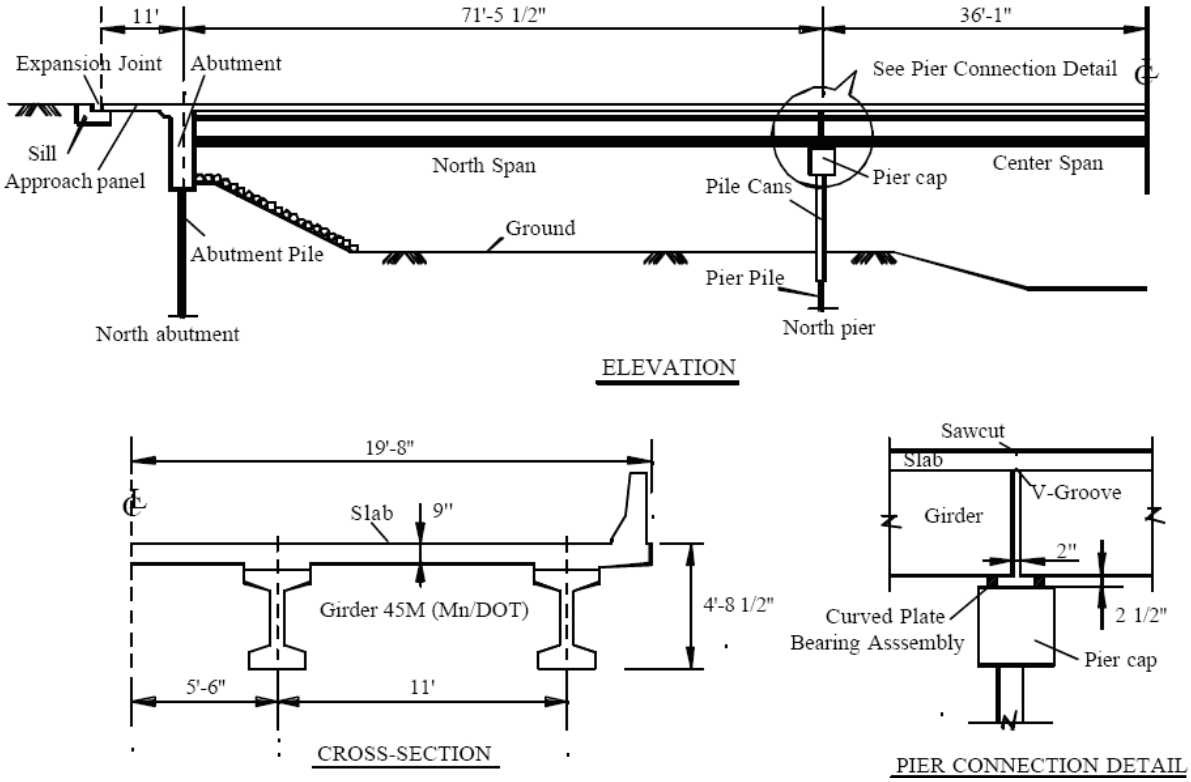

Figure 0.1 Bridge elevation and cross section. Bridge #55555 in Olmsted County, Minnesota, USA over the Zumbro River (Huang et al 2004).

Temperature and solar radiation

The temperature difference between the girder and deck was very small in winter and could be nearly neglected, indicating that the thermal gradient was nearly zero during winter. During summer, positive thermal gradients developed and reached the maximum during the months of July and August. The structural temperature and thermal gradients are closely related to ambient air temperature and solar radiation.

Seasonal abutment movements

Figure 0.2 shows the abutment rotation for 1998, which was obtained from tiltmeters installed on the front surface of the north abutment. The range of the abutment rotation was approximately 0.095 degrees (1/603) for the entire year. A general tendency for the abutment to rotate away from the river was observed in summer. The rotation of the abutment may have been caused by the effects of thermal gradients, the pile constraints and the passive backfill soil pressure. The positive thermal gradient existed for most of the time in summer days. Positive thermal gradients may have put the girder into a negative curvature, which forced the abutment to rotate outward. The pile constraints limited the lateral movement of the pile cap, resulting in a rotation of the abutment. The passive backfill soil pressure, induced by the expansion of the superstructure due to the average temperature rise and the pile constraints, caused the abutment to rotate in the same direction as that caused by the effect of thermal gradients in girders and pile constraints. In addition to the rotation of the abutment, seasonal average temperature caused the abutment to slide. Abutment rotation and sliding are associated with each other due to the same source of driving temperature rise and solar radiation.

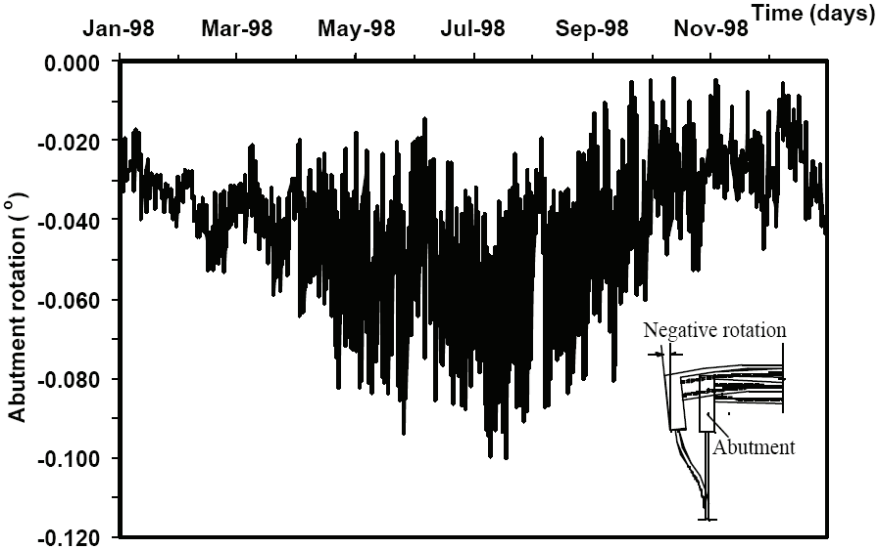

Figure 0.2 North abutment rotation in 1998 (Huang et al 2004).

Seasonal backfill soil pressure against abutment backwall

A good similarity between the deck temperature and the soil pressure was observed. The earth pressure changed corresponding to the change in the deck temperature. The reason is that the backfill soil pressure was affected by the abutment movement which was potentially driven by the bridge elongation related to the deck temperature. During summer, due to the larger expansion of the bridge superstructure, a larger passive soil pressure was caused. The changes in pressure during the summer at the pressure cells behind the abutment backwall and wingwalls were found to be bounded by 79 kPa and 102 kPa, respectively. Accordingly, earth pressures against the 45º oriented wing walls (see Figure 0.5) were a little higher than against the abutment.

Longitudinal pile curvatures

The pile curvatures (5.11.1996–22.2.2004) measured from the gages of Row A (150 mm below bottom of abutment) for the exterior pile under the north abutment are given in Figure 0.3. The longitudinal pile curvatures increased during each winter (temperature fall)

and decreased during each summer (temperature rise). The average longitudinal pile curvatures increased significantly over the past seven years. The total amount of time-dependent change in pile curvature was approximately 3540 με/m (90 με/in). The average yearly increase in pile curvature was approximately 590 με/m (15 με/in), corresponding to a flange stress of 15 MPa.

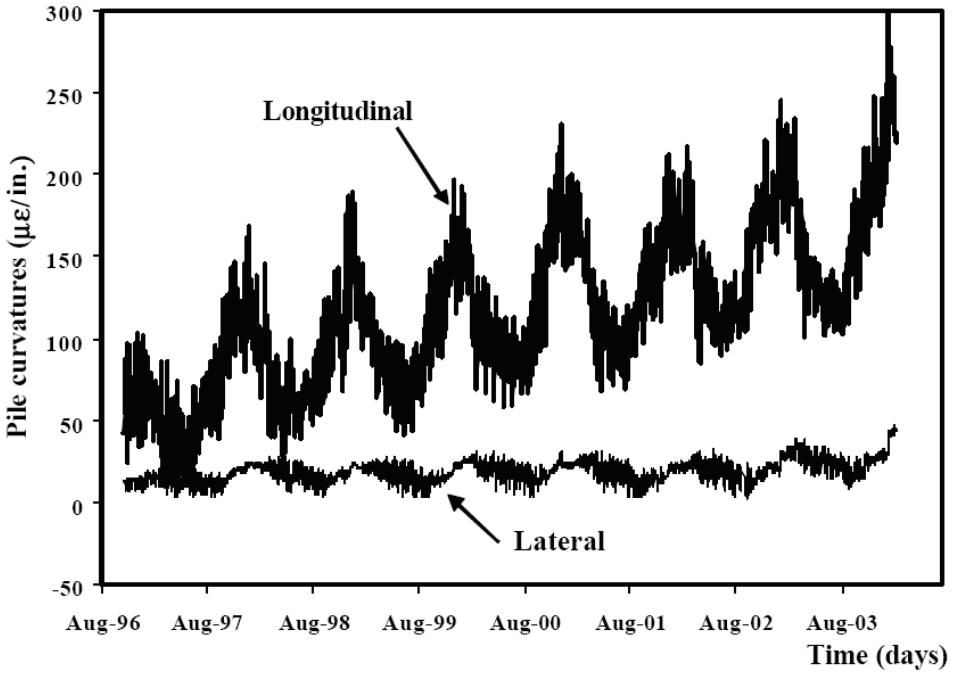

Figure 0.3 Abutment pile longitudinal and lateral curvatures (North abutment, exterior pile, Row A) (Huang et al 2004).

Horizontal extensometer measurements

The measured abutment movements from the southeast horizontal extensometers over the past seven years are given in Figure 0.4. Four curves are shown corresponding to four rods with different lengths, 1.52, 3.05, 4.57, 6.10 meters (= 5, 10, 15, and 20 ft). The abutment movement measured by the southeast horizontal extensometer was approximately 39 mm to 45 mm, and the readings of southwest horizontal extensometer showed an abutment movement of approximately 48 mm to 55 mm (= 1.90 in to 2.18 in). The movement of the south abutment was larger than that of the north abutment according to the extensometers (see Figure 0.5). West parts of the abutments had larger movements than those of the east parts.

Soil movement may also have occurred during summer due to the movement of the abutment toward the backfill. Such soil movements would have carried the soil anchors of the horizontal extensometers away from the abutment, resulting in larger apparent bridge shortenings than the real ones.

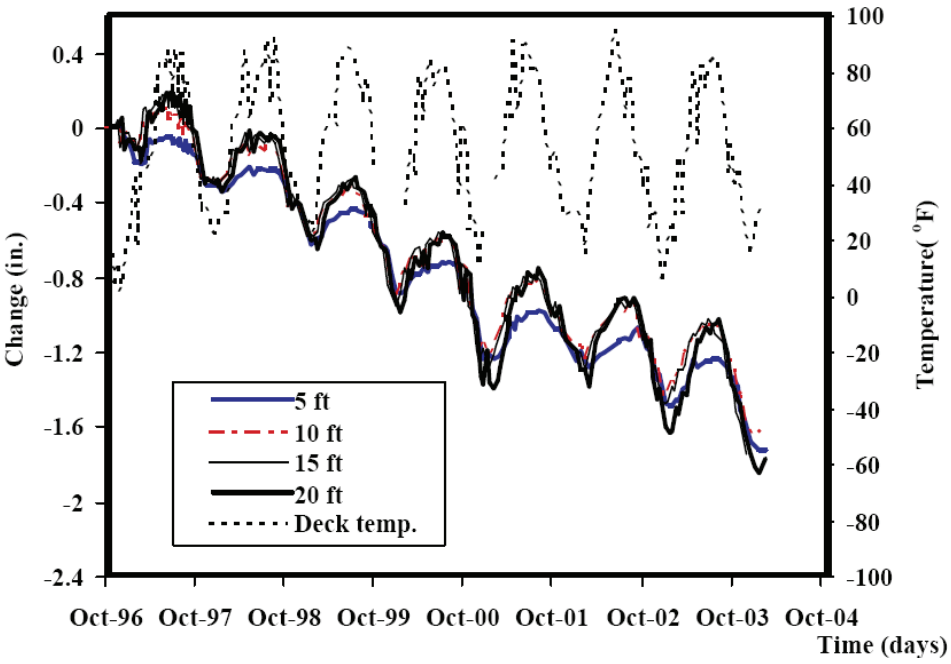

Figure 0.4 Abutment movements measured by the southeast horizontal extensometer (Huang et al 2004).

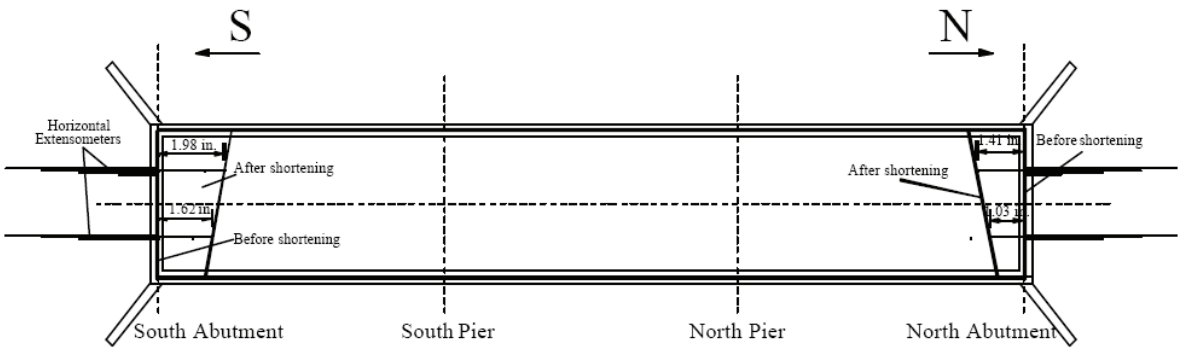

Figure 0.5 Illustration of bridge shortening according to average readings for all extensometer rods (February 1997 to February 2004) (not to scale) (Huang et al 2004).

The abutment movements and rotations resulted in the abutment piles bending in double curvature. Bridge shortening was observed from the readings of different sensors (i.e., horizontal extensometers and crackmeters) and the survey data.

From observed pile curvatures and pile axial strains, nearly 20 % of the flange cross section of the piles under the abutment yielded. The piles in the test bridge would not be expected to fail due to low-cycle fatigue under the daily and seasonal displacement cycles unless the steadily increasing tendency in average pile curvatures continues over the next 40 years.

0.2 Field Testing of Integral Abutments (Abendroth & Greimann 2005)

Description of the test bridge

The selected bridge is a county-road bridge on the secondary-road system. The bridge, which will be referred to as the Guthrie County Bridge, is located in Guthrie County, just south of the Town of Panora, Iowa on Route P28, where the highway crosses the Middle Raccoon River.

The bridge is a three-span-continuous, 97 m long, PC girder bridge with a right-side-ahead 30-deg. skew angle. The bridge has a U-shaped abutment with a single row of ten HP 10 x 42 steel piles under the reinforced-concrete (RC) backwall, and an HP10x42 pile under each wingwall. The piles under the RC backwall are oriented with their webs parallel to the abutment face. The wingwall piles are oriented with the webs perpendicular to the longitudinal axis of the bridge. The piles were driven to a depth of at least 13.7 m into shale bedrock at the south abutment and to a depth of at least 12.2 m into shale bedrock at the north abutment. Pre-bored holes that were filled with bentonite slurry were specified for the piles at this bridge. A spread footing that is keyed into the shale bedrock supports each Tee-shaped pier. At the south pier, which is an expansion pier, the bridge girders bear on 95 mm thick steelreinforced neoprene pads. The RC diaphragm at this pier does not extend down to the top of the pier cap. At the north pier, which is a fixed pier, the RC pier diaphragm is cast into keyways in the top of the pier cap. The keyways are lined along their sides and bottom with an expansion-joint filler. Between the keyways the pier diaphragm is cast against a continuous neoprene pad. The bridge girders bear on 25 mm thick neoprene pads at this pier.

The plan of the bridge and displacement transducer locations are shown in Figure 0.6.

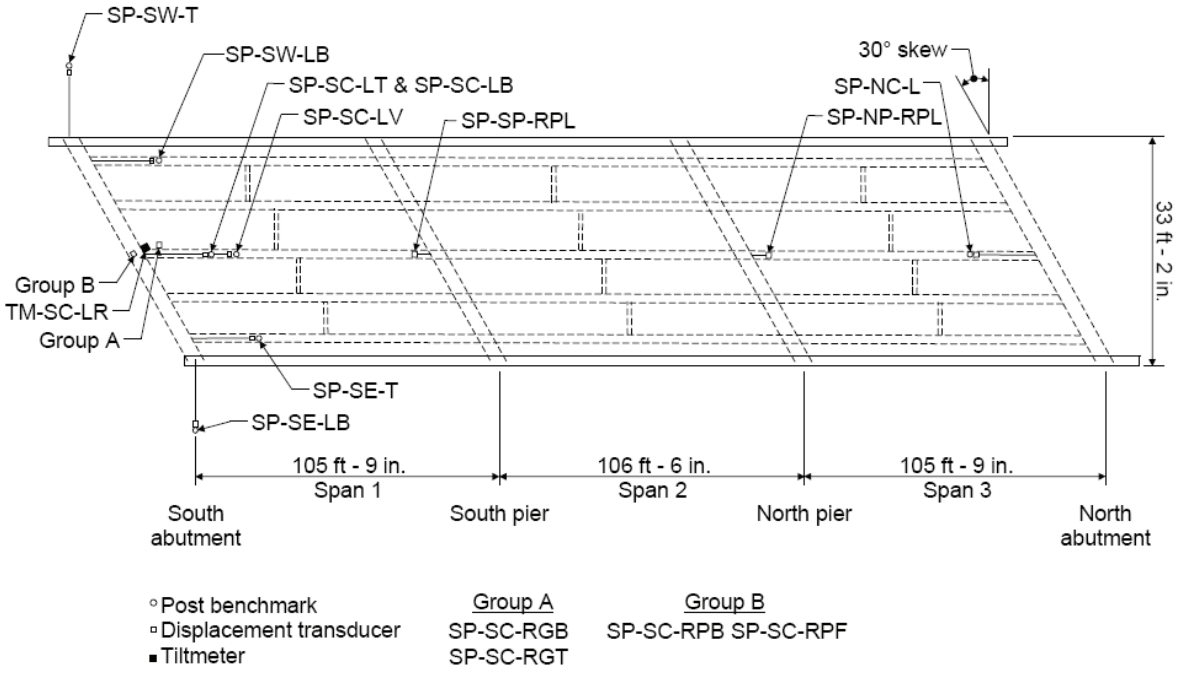

Figure 0.6 Displacement transducer locations at the Guthrie County Bridge (not to scale) (Abendroth & Greimann 2005).

Appendix 9 Field tests outside Finland

Bridge monitoring program

One of the objectives of the research was to monitor an integral-abutment bridge for temperature-induced displacements and strains. The instrumentation installed at the bridge site consisted of displacement transducers and a tiltmeter to measure bridge movements, strain gages to measure longitudinal strains in members, and thermocouples to measure air and concrete temperatures.

Pile strain gages

The strain gages on the abutment piles required a more in-depth filtering process to determine their reliability than that for the other instrumentation devices because the weldable strain gages had a higher rate of failure than that for the other instrumentation devices. The strain measurements for each of the monitored piles were plotted versus time and compared for similar patterns to graphs of the longitudinal displacements versus time for the abutment that was supported by the pile. After applying this filtering process for the upper cross section for the pile near the mid-width of the north abutment for the Guthrie County Bridge, the strain-component plots are shown in Figure 0.7 and in Figure 0.8.

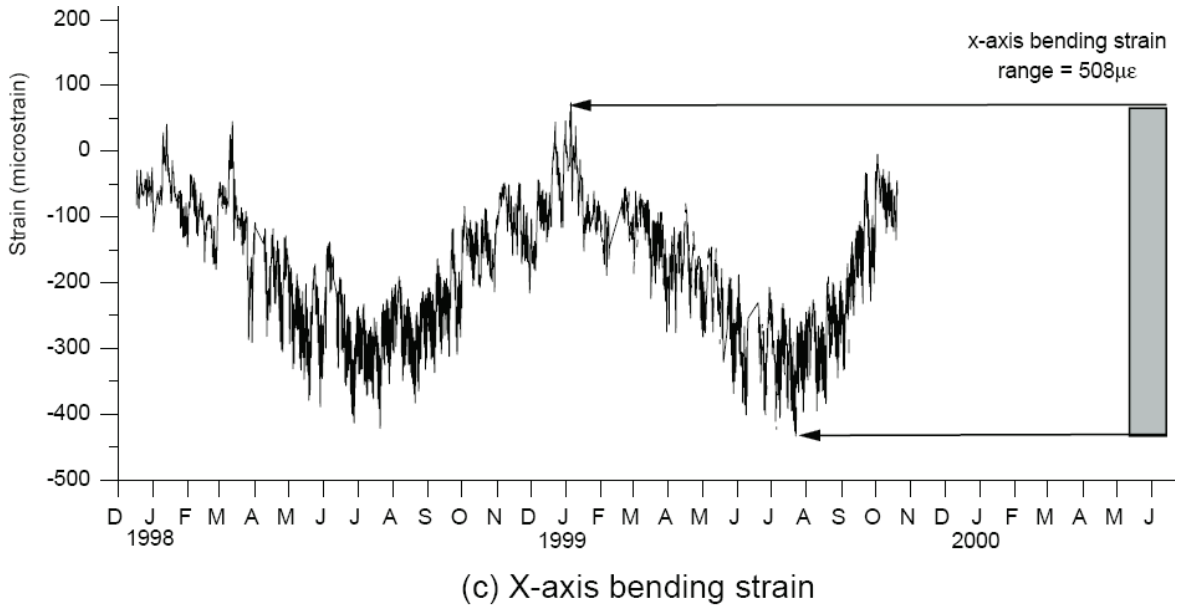

Figure 0.7 Final strain components after the filtering process for the upper cross section of the pile near the mid-width of the north abutment at the Guthrie County Bridge, X-axis (Abendroth & Greimann 2005).

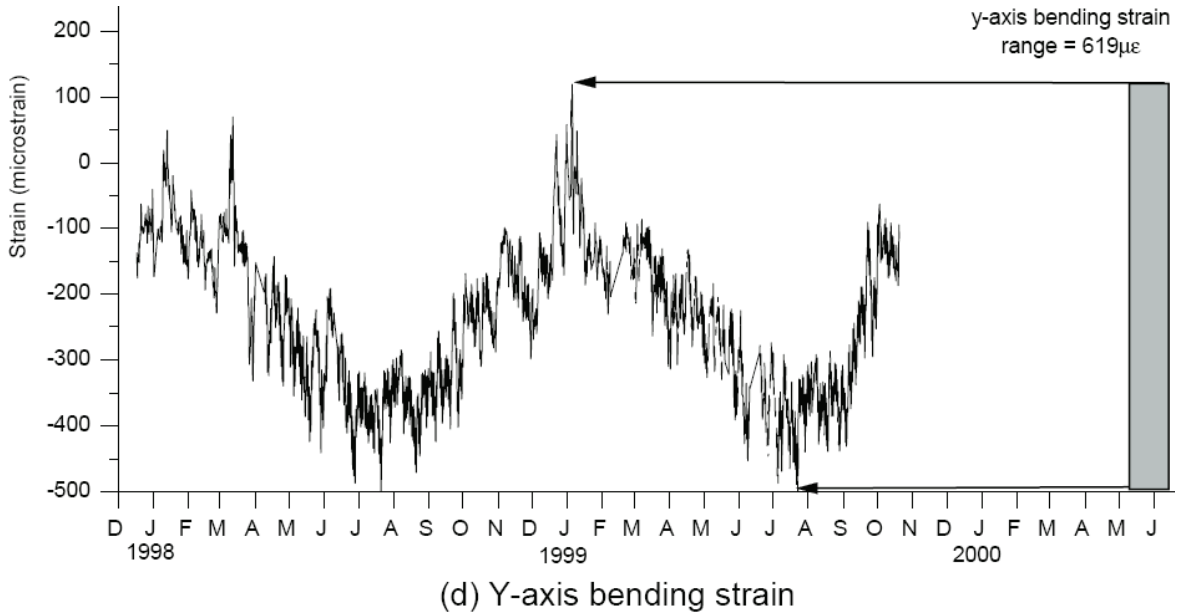

Figure 0.8 Final strain components after the filtering process for the upper cross section of the pile near the mid-width of the north abutment at the Guthrie County Bridge, Y-axis (Abendroth & Greimann 2005).

Bridge temperatures

The temperatures that were measured with the thermocouples, which were embedded in the concrete superstructure for each bridge, were analyzed to establish an average bridge temperature and the thermal gradients in each bridge. The average bridge temperature is the weighted average of the temperatures that were measured by all of the thermocouples, which were embedded in a bridge superstructure.

Graphs of the average bridge temperatures versus time for the Guthrie County Bridge and the Story County Bridge are shown in Figure 0.9.

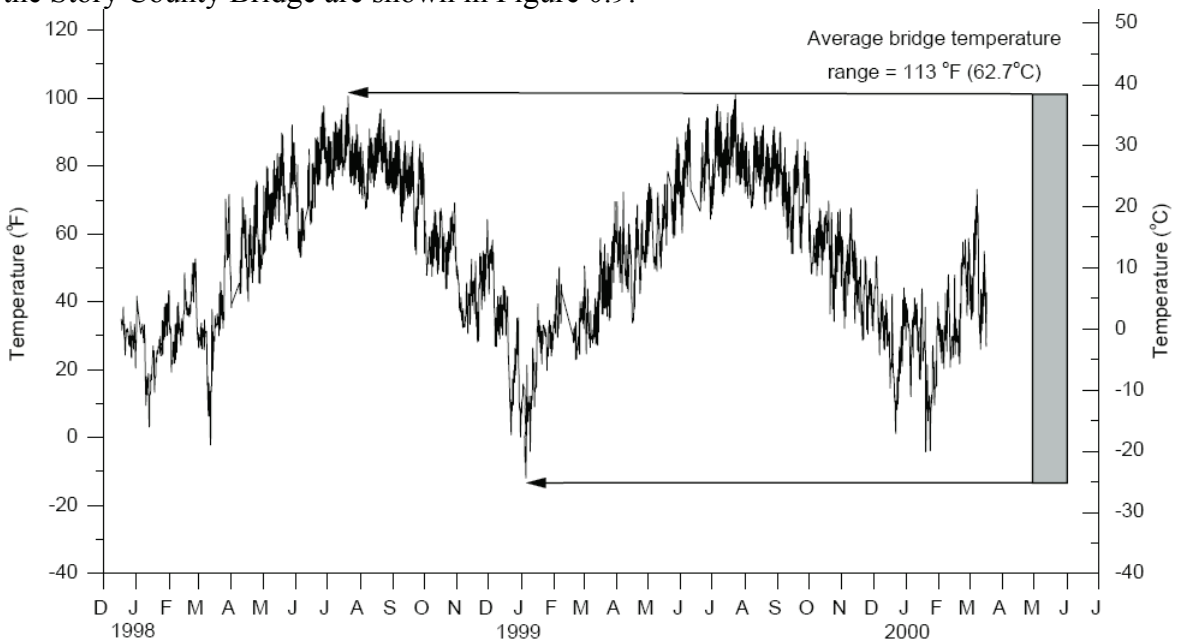

Figure 0.9 Average bridge temperature for two monitored bridges (Abendroth & Greimann 2005).

At the Guthrie County Bridge, the maximum average bridge temperature of 38.3 °C occurred in the early evening hours of July 20, 1998 and July 22, 1999. The highest slab temperatures were also recorded at these times. The minimum average bridge temperature measured at the Guthrie County Bridge was -24.4 °C, which occurred before sunrise on January 5, 1999. The maximum ranges in average bridge temperature for two monitored bridges are shown in Figure 0.9.

The maximum average bridge temperature was warmer than the air temperature measured by a thermocouple placed under the bridge.

Bridge displacements

The longitudinal displacement data correlated well with the recorded change in the average bridge temperature. Regardless, equal abutment displacements in the longitudinal direction of the bridge did not occur at the ends of the Guthrie County Bridge. The longitudinal displacements measured at the north abutment were approximately twice as large as those measured at the south abutment. Except for the pier details, the bridge geometry is symmetric. The relationship between the displacements in the longitudinal direction of the bridge for each abutment and the average bridge temperature at the bridge is shown in Figure 0.10.

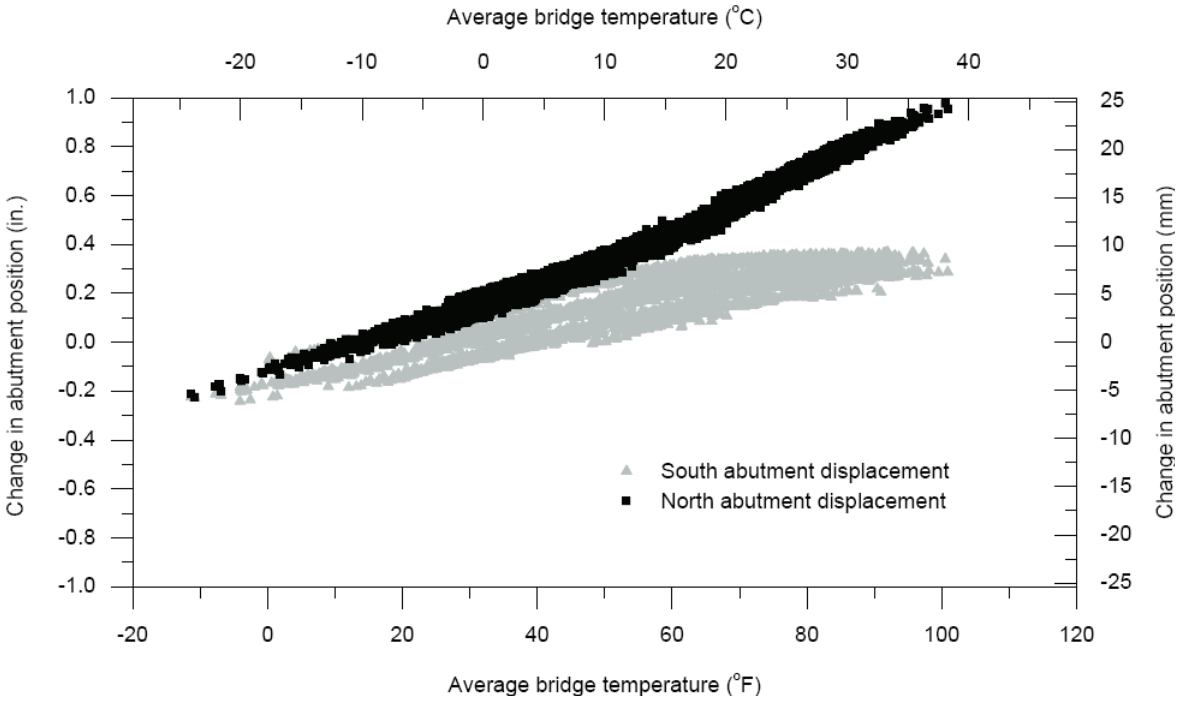

Figure 0.10 Change in the longitudinal displacements of the north and south abutments versus the average bridge temperature at the Guthrie County Bridge (Abendroth & Greimann 2005).

Relative displacements at the bridge piers

Relative longitudinal movements of the bridge superstructure over the pier caps were measured between the bottom of the center PC girder and top of the RC pier cap. The south pier is an expansion pier and the north pier is a fixed pier. Therefore, less longitudinal restraint for relative displacement exists between the superstructure and the south pier than that between the superstructure and the north pier. The relative displacements of the superstructure over the south and north piers of the Guthrie County Bridge were

approximately 4.2 mm and 1.8 mm, respectively. The relative magnitudes of these measured displacements are in agreement with the types of pier that were used at these locations. The daily ranges for the relative displacements of the superstructure over the fixed pier were smaller during the winter than during the summer.

0.3 Field Study of Integral Backwall with Elastic Inclusion. (Hoppe 2005)

Description of the test bridge

The project involved a replacement bridge situated on Route 60 over the Jackson River in Alleghany County, Virginia. The integral backwall (semi-integral) bridge is 100 meters long and 16.6 meters wide (overall), with three-span continuous steel plate girders, and no skew. Fixed bearings were provided over two piers, and expansion bearings were installed at abutments. There were no approach slabs constructed at the bridge.

The bridge was constructed with a layer of elasticized expanded polystyrene (EPS) 0.25 m thick attached to the backwall. The instrumentation of the bridge backwall is presented in Figure 0.11.

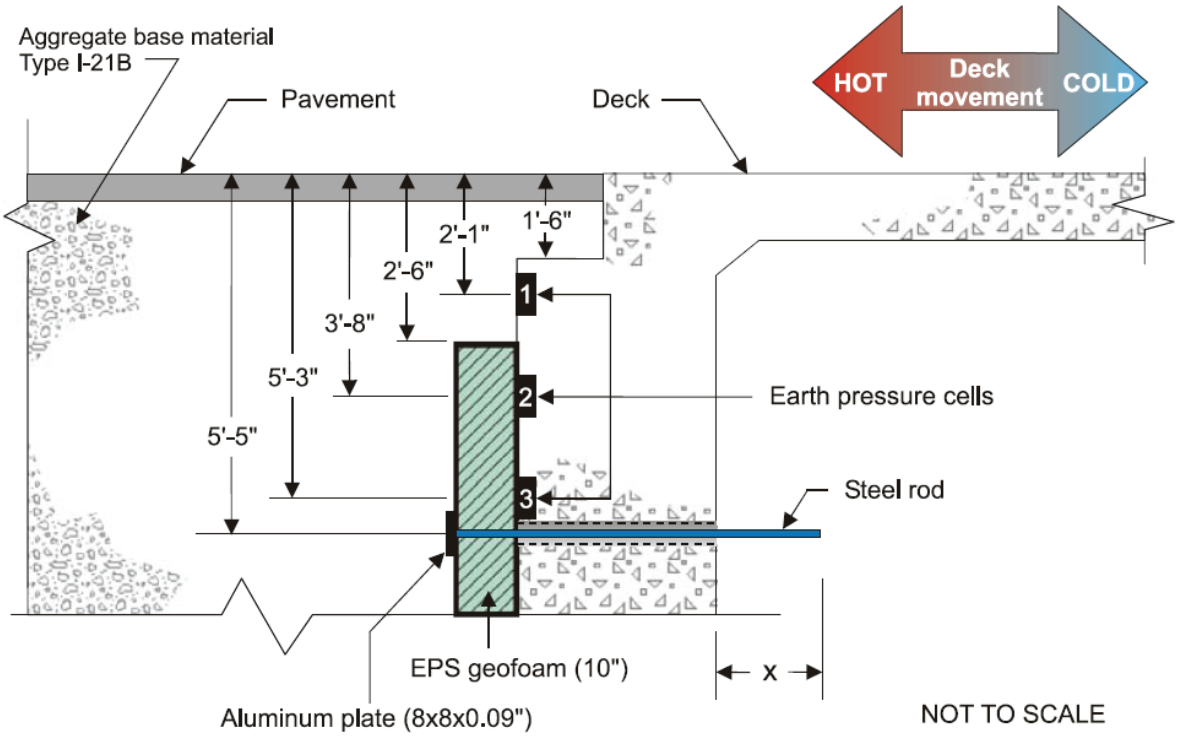

Figure 0.11 Integral backwall instrumentation (Hoppe 2005).

Results

The elastic inclusion consisting of a layer of elasticized EPS 0.25 m thick has performed effectively during the 5 years of field monitoring, which started in October 1999. The material remained elastic in the observed working strain range of 4 % to 13 %. Anyway, long-term creep of the material is still of primary concern, because bridges have to perform well for a longer period than only five years.

Appendix 9 Field tests outside Finland

Field tests indicated reduced earth pressures and approach settlements at the integral bridge. The elasticized EPS layer was functioning effectively in allowing the superstructure to interact with the adjoining backfill material. The bridge under study performed well without approach slabs.

Tampereen teknillinen yliopisto
PL 527
33101 Tampere

Tampere University of Technology
P.O. Box 527
FIN-33101 Tampere, Finland